Biogrout

Ground Improvement

by

Microbially Induced Carbonate Precipitation

Leon van Paassen

Biogrout

Ground Improvement

by

Microbially Induced Carbonate Precipitation

PROEFSCHRIFT

ter verkrijging van de graad
van doctor aan de Technische Universiteit Delft,
op gezag van de Rector Magnificus Prof.dr.ir. J.T. Fokkema,
voorzitter van het College voor Promoties,
in het openbaar te verdedigen

op dinsdag 20 oktober 2009 om 15:00 uur

door

Leon Andreas VAN PAASSEN

mijnbouwkundig ingenieur
geboren te Rijswijk

Dit proefschrift is goedgekeurd door de promotor

Prof.dr.ir. M.C.M. van Loosdrecht   Technische Universiteit Delft

Samenstelling promotie commissie

Rector Magnificus	Technische Universiteit Delft, voorzitter
Prof.dr.ir. M.C.M. van Loosdrecht	Technische Universiteit Delft, promotor
Prof.dr. J. Bruining	Technische Universiteit Delft
Prof.dr.ir. F.B.J. Barends	Technische Universiteit Delft
Prof.dr.ir. K. van Breugel	Technische Universiteit Delft
Prof. M. Hassanizadeh, PhD, M.E.	Universiteit Utrecht
Prof. K. Soga, PhD, M.E.	University of Cambridge, United Kingdom
Mr. S. Borel, PhD	Soletanche-Bachy, France

"Leon giet heel voorzichtig wat zand in het bakje.
De korreltjes zand glippen altijd weer weg.
Poeh! Vormpjes van zand maken is moeilijk.
Maar het lukt wel!. Kijk maar eens naar dat schildpadje…"
Het kliederboek van kleine Leon, Linne Bie, 2006

Voor Marja, Naima en haar kleine zusje….

Table of contents

1

Introduction

Ground improvement

In many regions around the world the mechanical properties of soils are insufficient for the desired land use: Roads and railways undergo settlement and require continuous maintenance. Dikes, dunes and slopes can become unstable and slopes, coasts and rivers are subject to erosion. Earthquakes can cause liquefaction of loose sediments and consequently damage to constructions on top of it. Water and oil production wells in loosely cemented sediments often produce sand, of which removal is a costly process and in land reclamation projects the compaction of the recovered land is sometimes a major concern.

Stabilization of soil (ground improvement) can be desirable for these applications. Before and during construction, soil stabilization is often applied at or from the surface by using constructive approaches like compaction, installing nails, sheets or piles, or mixing the soil with lime or cement (Karol, 2003). When stabilization of a soil mass is required deeper in the underground these surface techniques are insufficient and strengthening techniques, like deep mixing, cement or chemical *grouting* (Figure 1) or ground freezing are being used.
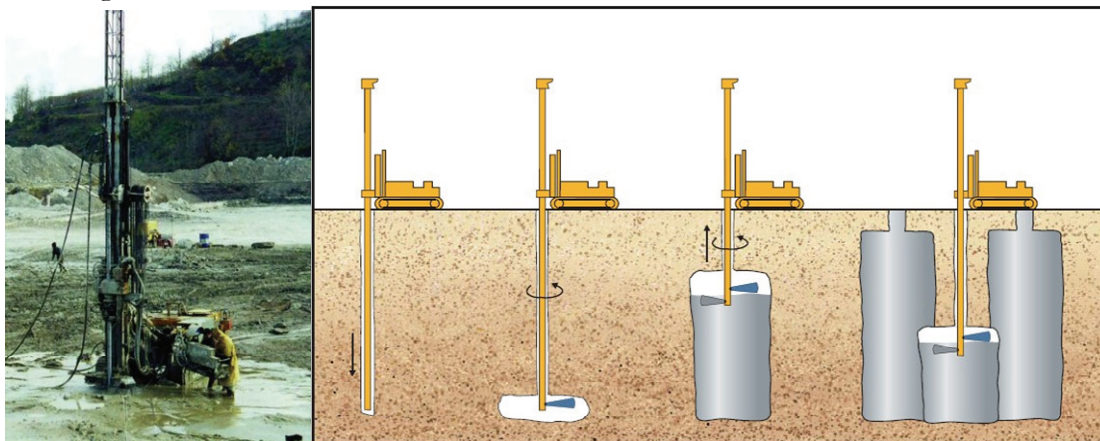
Figure 1 Conventional ground improvement by "jetgrouting": A mixture of cement, water and/or air is injected in the ground under high pressure, through a rotating injection rod. While the rod is pulled upwards, the native soil is eroded and replaced by a soil/cement mixture, which hardens out in time. By overlapping the jetgrouted columns walls of cemented soil can be formed in the subsurface (www.haywardbaker.com).

Traditional ground improvement methods have several limitations. The action radius is limited to the proximity of the mixing equipment. High pressures are often required to inject the grouts due to their high viscosity or fast hardening time. Freezing is only a temporal solution during construction. Next to that most of these methods are expensive, require heavy machinery, disturbing urban infrastructure and involve chemicals with significant environmental impact. Finally, these methods significantly reduce the permeability of the strengthened soil, which hinders groundwater flow and limits long distance injection. Consequently, these conventional methods are not suitable for treating large volumes of soil.

Natural "ground improvement"

In order to address the disadvantages of current ground improvement techniques one could look at natural alternatives. Natural lithification of sediments, *diagenesis*, occurs as a result of physical, chemical and biological processes. After deposition, sediments are compacted as they are buried beneath successive layers of sediment and cemented by minerals that precipitate from groundwater. In general, these natural transitions from soil to rock are slow processes, but in some cases natural diagenesis can be relatively quick. For example in arid coastal areas loose beach sediments can turn into hard "*beachrock*" within years due to tide related sea level changes and evaporation. Biological processes can accelerate cementation even further as they actively induce biochemical conversions in the subsurface, changing the chemistry of the pore water which could result in precipitation (or dissolution) of inorganic minerals. E.g. In sandy soils of which the mineral composition mainly comprises calcium carbonate (calcarenites), biochemically induced dissolution and reprecipitation of calcium carbonate, have lead to significant cementation of unconsolidated sand (Figure 2). Water uptake or putrefaction of tree roots is considered to play a major role in this process.

Figure 2: Biochemically induced dissolution and reprecipitation of calcium carbonate in the surroundings of plant roots, have led to significant cementation of loose carbonate sands. After the loose sands were eroded by wind forces these cemented sands were exposed and form The Pinnacles in Nambung National Park, Western Australia (Lipar, 2009).

Microbially induced carbonate precipitation (MICP)

When supplied with suitable substrates, micro-organisms can catalyze chemical reactions in the subsurface resulting in precipitation (or dissolution) of inorganic minerals, which change the mechanical soil properties. This study focuses on microbially induced precipitation of calcium carbonate.

Most of the inorganic carbon on the earth surface is present as layers of limestone of which a significant portion is of biogenic origin (Ehrlich, 1996). Many organisms can induce the precipitation of calcium carbonate, but not all can be used for ground improvement. Precipitation of calcium carbonate occurs when a solution is oversaturated, the amount of calcium and carbonate ions in solution exceeds the solubility product, i.e. the solution gets oversaturated. The role of micro-organisms in calcium carbonate precipitation is attributed to:

1. producing carbonate (e.g. by hydrolysis, respiration, etc.).
2. producing alkalinity (increasing the pH locally, which causes the dissolved inorganic carbon which is mainly present as bicarbonate to dissociate causing an increase in carbonate concentration).
3. acting as nucleation sites in an already oversaturated solution.

For example, autophototrophic micro-organisms, like algae or cyanobacteria can induce precipitation of $CaCO_3$ in open water by consuming CO_2, causing the pH to rise locally which in the presence of calcium would lead to precipitation (Figure 3).

Other organisms, such as foraminifera, corals and shells, use $CaCO_3$ to build their skeleton, resulting in large limestone structures, such as coral reefs. Although these two biological processes are considered the main sources of biogenic calcium carbonate precipitation (Ehrlich, 1996), they cannot be induced in the underground due to the lack of space, oxygen and light. Conditions in the subsurface are in general anaerobic, without light and with limited space, as the biochemical conversions occur mainly in water, which is restricted to the pore space.

To stimulate microbially induced calcium carbonate precipitation in the subsurface, micro-organisms or substrates have to be injected and transported over a substantial distance into the porous material. Transport of bacteria (and hence bacterial activity) is limited in fine grained soils. As bacteria have a typical size of 0.5 to 5 μm, they cannot be transported through silty or clayey soils, nor can their activity be used to induce carbonate precipitation in these layers (Mitchell & Santamarina, 2005).
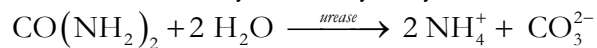
Figure 3: An intrusion of ground water enriched in calcium and bicarbonate on the eastern shore of Lake Clifton, Yalgorup national park, Western Australia, combined with metabolism of a benthic microbial community of algae (rich in Scytonema), provide a chemical environment conducive to the formation of calcified stromatolites (Moore, 1987)

MICP by urea hydrolysis

Hydrolysis of urea is one of the first processes associated with microbially induced carbonate precipitation in the late nineteenth century (Ehrlich, 1996). Although it is now considered as one the least important sources of biogenic carbonate, due to the limited abundance of urea, the process has gained increased attention since the late twentieth century for several industrial applications, such as restoration of calcareous stone materials (Tiano et al., 1995; Castanier et al., 2000; Stocks-Fisher et al., 1999; Rodriguez-Navarro et al., 2003), bioremediation (Ferris, 2003; Fujita et al., 2000; Warren et al., 2001), wastewater treatment (Hammes et al., 2003), strengthening of concrete (Ramachandran et al., 2001) and selective plugging for enhanced oil recovery (Ferris & Setehmeir, 1992; Gollapudi et al., 1995; Nemati & Voordouw, 2005). Most studies on bio-mediated ground improvement –*Biogrouting*- are also based on urea hydrolysis. They use micro-organisms containing the enzyme urease and in particular the bacteria *Sporosarcina pasteurii* DSM33 (DSMZ, FRG). These micro-organisms are cultivated in the laboratory (Whiffin et al. 2007), introduced in the soil and supplied with a solution of urea and calcium chloride (Nemati & Voordouw, 2003; DeJong et al., 2006; Whiffin et al., 2007).

The microbial urease catalyzes the hydrolysis of urea into ammonium and carbonate.

$$CO(NH_2)_2 + 2\,H_2O \xrightarrow{\text{\textit{urease}}} 2\,NH_4^+ + CO_3^{2-}$$

The produced carbonate ions precipitate in the presence of calcium ions as calcite crystals, which form cementing bridges between the existing sand grains.

$$Ca^{2+} + CO_3^{2-} \rightarrow CaCO_3(s)$$
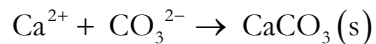
The remaining ammonium chloride solution is removed. Once precipitated the calcium carbonate will only dissolve very slowly, either when continuously flushed by acidic groundwater or as a result of acidifying processes in the pores (e.g. degradation of biomass). When sufficient calcium carbonate is precipitated, durable soil stabilization can be achieved.

Biogrout process, its requirements and limitations

This study focuses on the Biogrout process based on microbially induced precipitation of calcium carbonate by urea hydrolysis and its potential for strengthening sandy soils. A general Biogrout procedure would involve the following steps:

1. Cultivate suitable micro-organisms in the laboratory (or in the subsurface).
2. Inject micro-organisms (and nutrients) in the ground and transport them to the desired location.
3. Supply the micro-organisms with suitable substrates to induce a biochemical conversion resulting in precipitation of calcium carbonate.
4. Remove the remaining products.

The application of Biogrout is assumed to be limited to fine sands or coarser material, due to pore size constraints. To enable commercial application of Biogrout, the process should be reliable and competitive with alternative ground improvement methods. In order to be a competitive ground improvement method and to allow strength improvement for large volumes in the shallow subsurface without disturbing the serviceability of urban infrastructure present in the vicinity, the following requirements for Biogrout were identified:

- Limited volume to be injected, which implies high concentrations of urea and calcium chloride to achieve sufficient cementation.
- Limited treatment time, which implies high reaction rates and hence high concentrations of catalyzing bacteria.
- Long injection distance and low injection pressure, which implies that permeability should be maintained to enable multiple treatments and limit the number of required injection wells.
- Low costs
- Low environmental impact

In order to be reliable, the results of Biogrout treatment should be predictable, controllable, reproducible and homogeneous.

Research goal

This research aims at creating the knowledge, which is required to determine the potential of MICP by urea hydrolysis for ground improvement applications and enable scale up for

practical applications. The research should identify the limitations of the technology and provide the engineering tools, which are required to design treatment procedures. The engineering tools should enable to relate the operational process variables like, flow rate, pumping time and volume, amount of reagents and bacteria, and injection (and extraction) strategy to the required process results, such as the engineering parameters strength, stiffness, permeability, porosity and eventually also costs.

Research approach

To establish a relation between operational variables and process results two approaches can be used:

- An empirical approach in which experiments are performed at increasing scale, providing a proof of principle of the method, experience for the executors and empirical correlations, which are essential for engineering design.
- A fundamental approach in which all relevant phenomena are identified and implemented in a mathematical model, providing explanations for the experimental observations and a means for process prediction.

In this study the empirical and fundamental approaches are combined in order to investigate the relevancy of different phenomena within the Biogrout process, which take place at different scales in time, space and concentration.
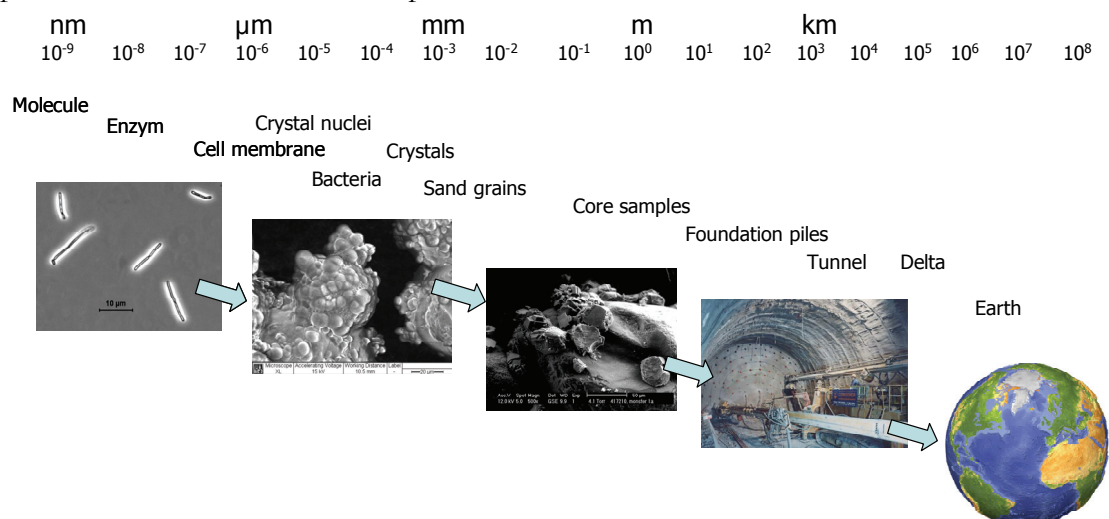

Figure 3 Different spatial scales encountered during the research on Biogrout.

Outline of the thesis

Initially the Biogrout process was studied using liquid experiments, in which bacteria were mixed with urea and calcium chloride under the intended conditions for field applications, i.e. high conversion rates (order of moles of $CaCO_3$ per liter per day) and high concentrations (order of moles per liter). Factors affecting the rate of combined urea hydrolysis and calcium carbonate precipitation, were evaluated in **chapter 2**.

During the experiments a wide variety of crystal properties was observed, using different kinds of microscopy, which are described in **chapter 3**. Using the results of the previous

chapter the occurrence of the various crystals was explained, while factors, which could influence the crystal properties were evaluated considering that these properties would affect the resulting engineering properties of the treated soil.

To induce urea hydrolysis and calcium carbonate precipitation in the soil bacteria and reagents need to be injected and transported to the desired location preferably at a long distance. When bacteria, urea and calcium chloride are mixed before injecting them in the ground the Biogrout process would immediately start and bacteria tend to form flocks, which could result in a high concentration of bacteria close to the injection well, and consequently a limited injection distance, especially in fine sands. In **chapter 4** a method is described in which bacteria and reagents are flushed sequentially through the soil in order to achieve a more efficient use and homogeneous distribution of the bacteria and the resulting precipitation rate over a long distance.

After several small sand column experiments the procedure was applied in a five-meter sand column experiment, which is described in **chapter 5**. This experiment provided the first evidence that significant strength increase could be achieved at low injection pressure, within 3 days of treatment and 5 flushed pore volumes (including placement of bacteria and removing the remaining ammonium chloride), at a long distance and without reducing the permeability significantly.

Further scale up experiments, using conditions and techniques which are used in the field, are described in **chapter 6**. First experiments were performed in a $1m^3$ container set-up simulating a spherical injection from a single point and secondly the results are presented from a $100 m^3$ field scale experiment.

While analyzing the results of these scale-up experiments, empirical relations could be established between the amount of $CaCO_3$ and engineering parameters, like density, strength, stiffness, porosity and permeability, which are described in **chapter 7**. These correlations enabled to determine the required parameters and to design treatment procedures for several emphasized applications.

In **chapter 8** the results of the field scale experiment (partly overlapping with chapter 6) are used to determine the feasibility of a typical application: increasing the stiffness of railroad embankments in order to minimize maintenance, which is required to counteract the compaction due to dynamic loading of passing trains.

Another potential application is presented in **chapter 9**, in which the feasibility of using Biogrout for the in-situ reinforcement of calcarenite room and pillar mines was investigated, showing that Biogrout can also be used to increase the strength in already lightly cemented rocks.

Remaining issues in the Biogrout process based on urea hydrolysis include the required removal of ammonium chloride and the use of axenically cultivated aerobic organisms

with consequent decaying urease activity in time due to a lack of oxygen in the subsurface. To avoid both these issues the suitability of other possible MICP processes for ground improvement is evaluated in **chapter 10**. The feasibility of the best alternative, in which calcium acetate (or another fatty acid) and calcium nitrate are converted to induce calcium carbonate precipitations is evaluated experimentally.

As this thesis is structured as a paper dissertation, i.e. it consists of a number of scientific articles, some repetitions in the individual chapters were unavoidable.

2

Kinetics of microbially induced calcium carbonate precipitation by urea hydrolysis

Abstract

Ground improvement by microbially induced hydrolysis of urea and precipitation of calcium carbonate requires high urea and calcium chloride concentrations and high hydrolysis rates to minimize the treatment time and number of flushes required for sufficient soil stabilization. In this study the factors affecting the kinetics of combined urea hydrolysis and calcium carbonate precipitation by the ureolytic bacteria, *Sporosarcina pasteurii*, are evaluated using experiments and mathematical modelling. The urea hydrolysis rate is mainly affected by the amount of bacteria and the conditions during growth, storage, hydrolysis and precipitation. This study showed that for fast hydrolysis of urea (>1 M-urea day^{-1}) in a highly concentrated equimolar solution with calcium chloride (>0.25 M) the solubility product of $CaCO_3$ is exceeded within a short period (less than 30 minutes). The supersaturation remains high for longer periods, resulting in prolonged periods of nucleation and crystal growth and extended growth of metastable mineral phases. The pH, being a result of the speciation, quickly rises until critical supersaturation is reached and precipitation is initiated. Then pH drops (sometimes showing oscillating behaviour) to about neutral where it stays until all substrates are depleted. Higher hydrolysis rates lead to higher supersaturation and pH and relatively many small crystals, whereas higher concentrations of urea and calcium chloride mainly lead to lower pH values. The conversion can be reasonably monitored by electrical conductivity and reasonably predicted, using a simplified model based on a single reaction as long as the urea hydrolysis rate is known. More complex models including acid-base equilibria and precipitation kinetics do not differ significantly from the simplified model, but enable calculation of supersaturation, pH, and the number, size and type of crystals. Quantitative prediction to a level at which the pH and conductivity are simulated accurately was not yet possible with the developed models.

1 Introduction

The potential of microbial induced calcium carbonate precipitation (MICP) is being investigated for many applications, including soil stabilization (DeJong et al. 2006; Whiffin et al. 2007). Most studies on MICP for soil stabilization, use micro-organisms containing the enzyme urease and in particular the bacteria *Sporosarcina pasteurii*. These micro-organisms are cultivated under axenic, aerobic conditions. The suspension containing the bacteria is mixed with or injected in the soil and supplied with a solution of urea and calcium chloride. Urease catalyzes the hydrolysis of urea into ammonium and carbonate. The produced carbonate ions precipitate in the presence of calcium ions and form calcium carbonate crystals. The remaining ammonium chloride has to be removed. Once precipitated, the calcium carbonate might dissolve as a result of acidifying processes (e.g. degradation of biomass or ammonium oxidation) and removal by groundwater flow. However, as these dissolution processes are slow, durable precipitation can be achieved, when sufficient calcium carbonate is precipitated. Whiffin et al. 2007 indicated at least 60 kg precipitated $CaCO_3$ per m^3 of soil is needed to obtain a measurable increase in soil strength. To produce such an amount of precipitate within limited time and flushed volume, high hydrolysis rates (in the order of 1 M urea/day) and high concentrations of urea and $CaCl_2$ (in molar range) are desired.

Control and prediction of the time and place of calcium carbonate precipitation is required when designing procedures for engineering applications. For this purpose understanding the active (bio-)chemical reactions and their kinetics is essential. Figure 1 gives an overview of these reactions.

In this study the factors which influence the kinetics of combined urea hydrolysis and calcium carbonate precipitation are described and evaluated under similar conditions as for the intended application as ground improvement method (i.e. high concentration, high rate). A theoretical evaluation is performed using a numerical model for which the level of detail (and complexity) is stepwise increased. The model results are compared with results from experiments. The differences between theoretical and experimental results are explained. The required level of detail in models to be useful in process prediction is discussed.
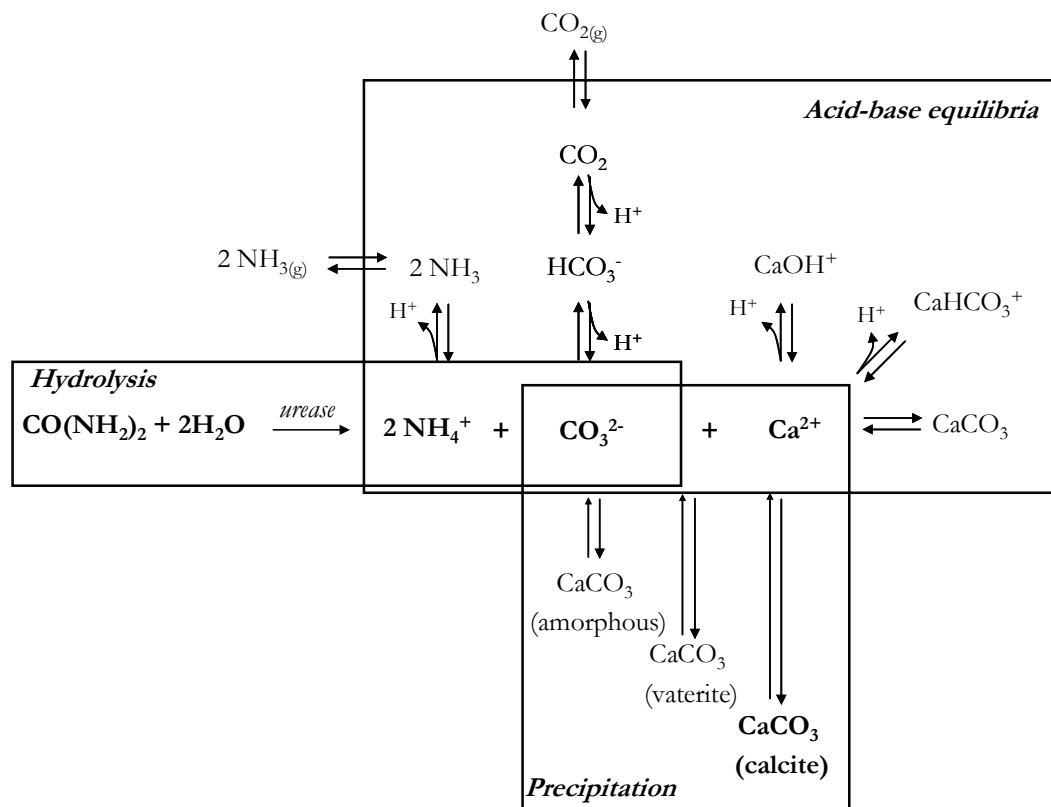
Figure 1 Chemical reactions involved in combined microbial induced urea hydrolysis and calcium carbonate precipitation. The reactions are divided in three groups: hydrolysis, acid-base equilibria and precipitation, which are described below. In bold are the initial substrates and end products of the two reactions considered in a simplified system. Gas exchange with the atmosphere is indicated in this figure but neglected for the application in water saturated soil systems..

2 Theory

2.1 Urea hydrolysis

Hydrolysis of urea is an irreversible reaction in which urea reacts with water to form ammonium and carbonate.

$$CO(NH_2)_2 + 2\,H_2O \xrightarrow{\;urease\;} 2\,NH_4^+ + CO_3^{2-} \tag{1}$$

At neutral pH, bicarbonate (HCO_3^-) is the dominant carbonate species rather than carbonate (CO_3^{2-}), causing a rise in pH to maintain charge balance. As a result of the increasing pH, ammonium (NH_4^+) starts to dissociate to ammonia (NH_3) until equilibrium is reached between NH_4^+/NH_3 and HCO_3^-/CO_3^{2-} at a pH of about 9.3 (see paragraph 2.2). Chemical (uncatalyzed) hydrolysis of urea is a very slow process. The enzyme urease (urea amidohydrolase EC 3.5.1.5) catalyzes the reaction significantly (up to 10^{14} times faster, (Benini et al. 1999)). Urease is a commonly found enzyme in many organisms, including many bacteria, some yeasts and several higher plants (Whiffin 2004). The specific urease activity, which is defined as the rate at which urea in aqueous solution is hydrolyzed per gram of dried biomass, differs from species to species (Hammes et al. 2003; Whiffin 2004). Jack Bean (*Canavalia ensiformis*) is the most common source of commercially available urease (Whiffin 2004). The urease is available in different qualities

varying from grinded bean meal to a purified powder, with specific activities ranging from 6 up to 1200 mol-urea L^{-1} min^{-1} gDW^{-1}. The mostly used bacterial source of urease is *Sporosarcina pasteurii*. This micro-organism, formerly known as *Bacillus pasteurii*, is also well known for its high ureolytic activity and is also the subject in this study. Specific urease activities have been obtained of 12 mol-urea L^{-1} min^{-1} gDW^{-1} (Whiffin 2004). The total urease activity in suspension is the specific urease activity multiplied by the concentration of biomass.

Different units are used in literature to express the specific and total urease activity, depending on the type of measurement. Whiffin (2004) e.g. measures the urease activity of a bacterial suspension by electric conductivity (mS cm^{-1} min^{-1}) and the amount of biomass using a spectrophotometric method, in which the optical density (OD) i.e. the absorbance (or scattering) of light of 600 nm wavelength is an indicative measure for the amount of cells per mL suspension. Consequently, urease activity and specific urease activity are presented in the units mS cm^{-1} min^{-1} mL^{-1} and mS cm^{-1} min^{-1} OD^{-1}. These units are converted to mol L^{-1} min^{-1} and mol L^{-1} min^{-1} gDW^{-1} by multiplying with respective factors of about 11 and 19 (Whiffin, 2004).

2.1.1   The effect of cultivation and storage conditions on urease activity

Even when using a single species, like *Sporosarcina pasteurii*, the conditions during growth and storage of the bacteria affect the specific urease activity significantly. Different nutrient compositions result in different values for the specific urease activity and different specific growth yields. The nutrient concentration determines the overall growth yield and hence the total urease activity of the suspension. Whiffin (2004) optimized growth media in order to get the highest specific urease activity for the lowest costs of nutrients.

Sporosarcina pasteurii are cultivated aerobically, mostly under axenic conditions starting from a freeze dried sample of the type species from a culture collection (DSM 33 (DSMZ)/ ATCC 11859, renamed from *Bacillus pasteurii*). Limited supply of oxygen during cultivation can result in lower growth yield. When the bacteria are cultivated in batch the highest growth yield is obtained when cultivation ends and the bacterial suspension is stored at the late exponential or early stationary growth phase (figure 2). With a doubling time of about 2 hours (at a temperature of $30^{o}C$) and sufficient oxygen supply most cultivations are performed within 1 day using a fresh inoculum of 1% of the total volume. When oxygen supply continues after early stationary phase, the amount of biomass does not increase and eventually decreases. Sometimes the transition to stationary phase is accompanied by a rapid increase in specific urease activity (SUA) in the suspension. However, most of this increased activity is present in the supernatant (measured as the activity of the supernatant/filtrate after centrifugation or filtering through a 2μm filter). Apparently, the bacteria react on the depletion of nutrients by releasing their enzymes.
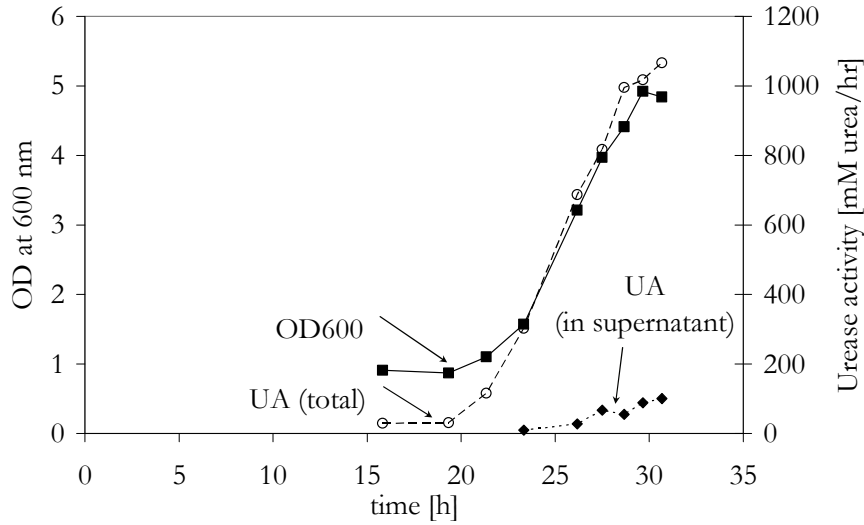
Figure 2 Typical growth curve of a cultivation of Sporosarcina pasteurii at 30ºC. After about 20 hours of cultivation the exponential growth of the bacteria results in an increase in both optical density (OD at 600 nm (■)) and urease activity (UA total) (○) of the suspension. After about 30 hours the optical density reaches a maximum of about 5, while the urease activity continues to increase slightly to a maximum of 1 M urea h⁻¹. A large part of this latter increase in activity appears in the supernatant (UA in supernatant; ♦ after centrifugation of the suspension), indicating the enzymes are loosely attached to or detached from the bacterial cells. After 33 hours the suspension is harvested and stored in the fridge at 4ºC.

Eventually, when bacteria start to lyse, the specific urease activity drops as well. After growth, the broth can be stored for several weeks in the fridge at 4ºC before being used, with only slight decrease in cell-bound urease activity. Longer storage or storage at higher temperatures results in faster decay of cells and urease enzymes.

2.1.2 The effect of environmental conditions on urease activity

Apart from the amount and type of bacteria and their specific urease activity after growth and storage, the hydrolysis rate in the reacting environment still depends on many factors, like: the concentration of substrates and products; the presence of other compounds (solid, liquid or dissolved); and other conditions, such as pH and temperature, which might inhibit or enhance the reaction rate (Stocks-Fischer et al. 1999; Bang et al. 2001; Bachmeier et al. 2002).

Effect of urea
When urea is almost depleted, the hydrolysis rate decreases, according to Michaelis-Menten kinetics.

$$\frac{r_h}{r_{h0}} = \frac{C_{urea}}{K_{m,urea} + C_{urea}} \tag{2}$$

In which the ratio between the actual hydrolysis rate r_h and the maximum hydrolysis rate r_{h0}, is a function of the urea concentration C_{urea} and the half saturation constant $K_{m,urea}$, i.e. the concentration at which the rate is reduced by 50%. Reported values for $K_{m,urea}$ vary between 26 mM for cell free extract at pH 7.7 (Stocks-Fischer et al. 1999) to 200 mM for a cell suspension (Whiffin 2004). Figure 3 shows normalized measurements of urease

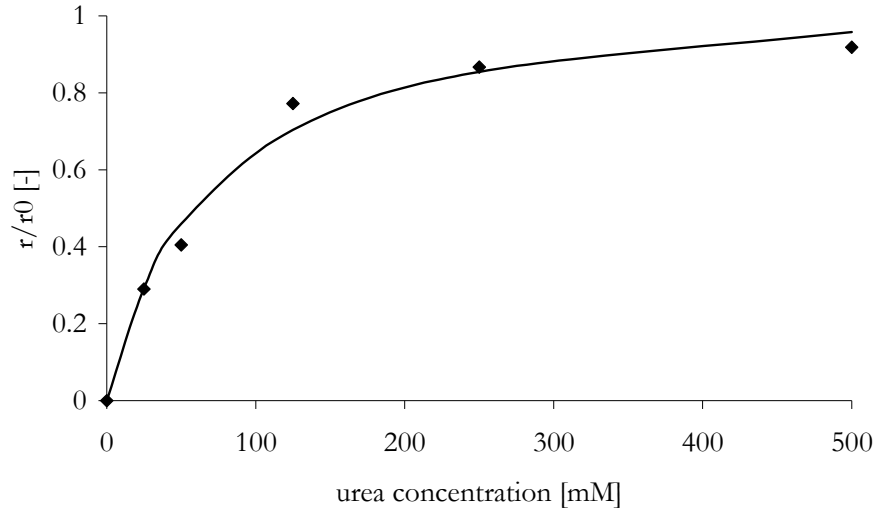activities at different initial urea concentrations and similar amounts of suspended cells of *Sporosarcina pasteurii.*

Figure 3 Measured effect of urea concentration on the urease activity of suspended cells of Sporosarcina pasteurii. (Km ≈ 55 mM)

Effect of pH

The urease activity is also affected by the pH. Using cell free extract Stocks Fisher et al (1999) found an optimum rate at pH 8.5. Within a certain pH range, below and above this optimum pH the urease activity decreased, forming a bell shaped inhibition curve, which can be described using the following expression (Batstone 2002):

$$\frac{r_h}{r_{h0}} = \frac{1 + 2 \cdot 10^{0.5(pH_{LL} - pH_{UL})}}{1 + 10^{(pH - pH_{UL})} + 10^{(pH - pH_{LL})}}$$

(3)

in which r_{h0} is the hydrolysis rate at pH optimum and pH_{LL} and pH_{UL} are the values at which the hydrolysis rate is reduced by 50%.
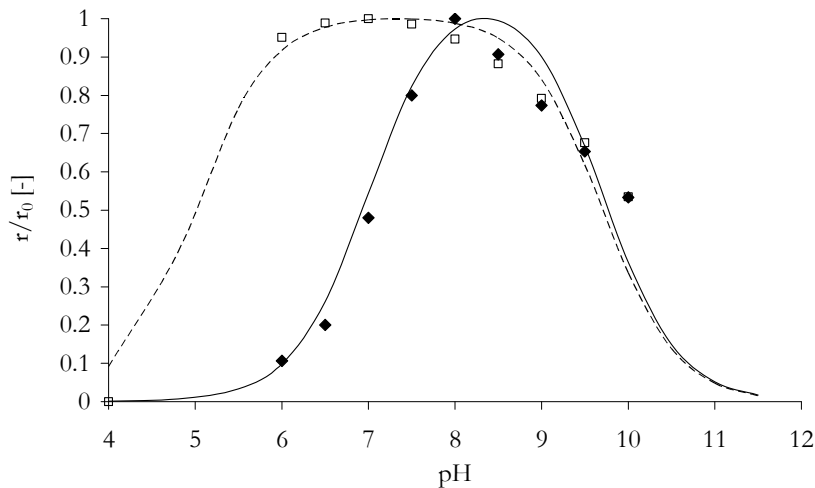

Figure 4 Effect of pH on urease activity measured on cell free extract (•; Stocks-Fischer et al. 1999) and whole supended cells (□; Whiffin 2004) of Sporosarcina pasteurii. Note that these are normalized activities. The absolute specific urease activity in mol-urea L-1 h-1 gDW-1 is significantly higher for cell free extract.

Stocks- Fisher et al. (1999) found a narrow pH range with pH_{LL} at 7 and pH_{UL} at 9.7 (solid line in figure 4). Using whole cells in suspension Whiffin (2004) found a pH optimum at 7, with pH_{LL} at 5 and pH_{UL} at 9.7 (dashed line in figure 4). The results show clearly that the urease activity of the cell free extract is more vulnerable for changes in pH, especially on the acidic side. For the whole cells in suspension (Whiffin, 2004) the effect of pH on urease activity seems negligible between 6 and 8.5. Apparently, the cells protect the enzymes from acidity.

Effect of calcium (or other salts)

The presence of calcium ions also affects the urease activity. Whiffin (2004) observed a little effect at low calcium chloride concentrations, up to 50 mM, but at higher concentrations the activity decreases with increasing calcium concentration up to 1 or 2 M, where urea hydrolysis is almost completely inhibited depending on the calcium source being either calcium chloride or calcium nitrate. This inhibitory effect of calcium chloride can be approximated using the following expression:

$$\frac{r_h}{r_{h0}} = e^{-C_{Ca}/K_{iCa}} \qquad (4)$$

Where the coefficient, $K_{i,Ca}$, can be fitted to experimental data and is the concentration at which the urease activity is reduced to 37% of its original value. For the data presented in figure 5 $K_{i,Ca}$ is 0.6 mol/L.
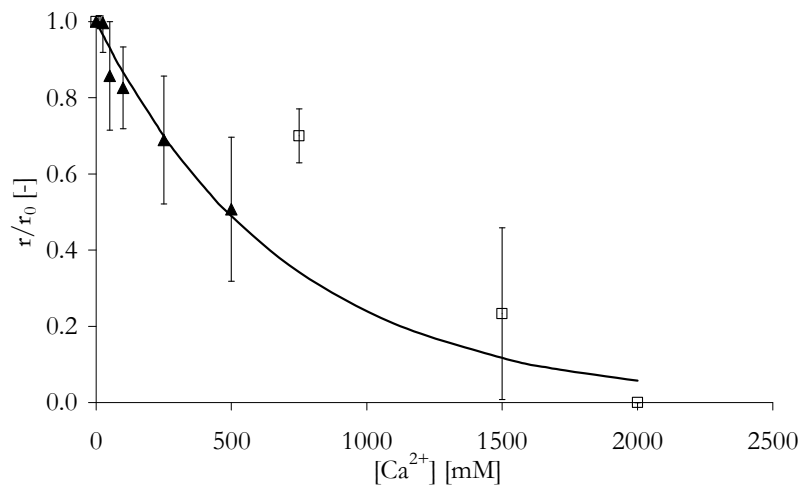

Figure 5 Effect of calcium concentration on urease activity using calcium chloride (▲, this study), and using calcium nitrate (□, Whiffin (2004)). The effect of calcium is approximated with a trendline fitted to the data of calcium chloride in this study (solid line) using equation (4) with constant, Ki,Ca = 0.6 mol/L

Sodium chloride showed similar inhibitory effect as calcium chloride, but to a lesser extent at similar chloride concentrations (results not shown). Ammonium chloride on the other hand did not seem to affect the urease activity at all up to concentrations of 3 M (Whiffin 2004). Differences in the apparent inhibition are probably related to differences in valence and size of the ions. Similarly, divalent calcium caused bacteria to flocculate, while monovalent sodium did not (chapter 4). It is not clear whether the effect of calcium on urease activity is reversible. (e.g. as the calcium concentration decreases during the process the hydrolysis rate might increase again).

Temperature has a significant effect on the hydrolysis rate. Between 5 and 35°C a rise of 10°C causes an increase of the urease activity by a factor (Q_{10}) of 3.4 (figure 6). Below 5 °C, no urease activity was measured. The effect of temperature within this range can be described using:

$$\frac{r_b}{r_{b0}} = \exp\left(\left(T - T_0 \right) \frac{\ln Q_{10}}{10} \right)$$
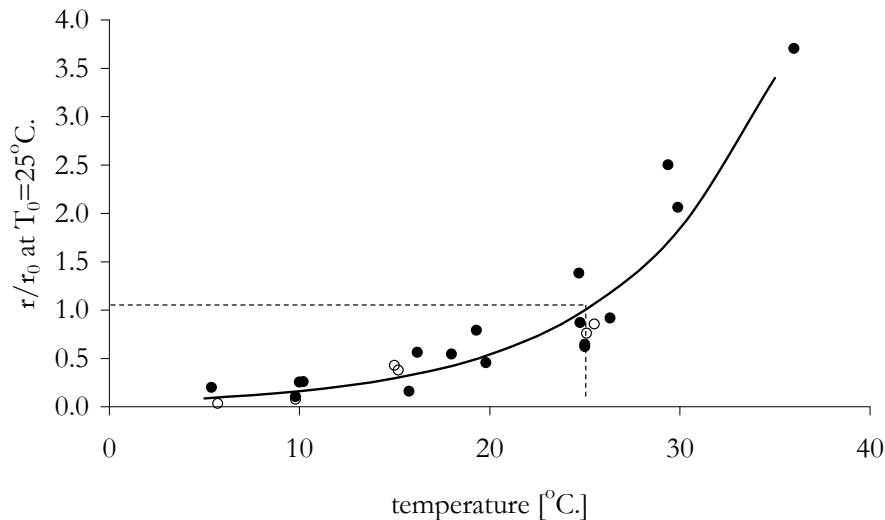(5)

Figure 6 The effect of temperature on urease activity was measured in experiments where a constant amount of bacteria was supplied with 0.5 M urea (●) and 0.5M urea and CaCl2 (○) and the temperature was varied.

Whiffin (2004) observed a linear increase between 25 and 60°C reaching an optimum at 70°C. Above 70°C the urease activity quickly decreases (probably due to enzyme deactivation).

2.1.3 Decay of urease activity in time

The conditions affecting the hydrolysis rate can vary in time during the hydrolysis reaction. In general, the urease activity decays in time, due to cell lysis (and subsequent wash-out of urease from the sand or faster denaturation of the loose enzyme) or due to encapsulation in the calcium carbonate crystals.

Cell lysis occurs during the cementation process as the aerobic bacteria get without nutrients and oxygen. The effect of cell lysis on urease activity can be described, assuming e.g. exponential decay:

$$\frac{r_b}{r_{b0}} = \exp\left[-\frac{t}{t_d} \right]$$
(6)

Where t_d is the exponential time constant, at which the urease activity has reduced by a factor e to about 63% of its original value. At temperatures around 10°C, which prevail in the Dutch subsurface, cell lysis is rather slow (in the order of weeks). High salt concentrations or presence of toxic compounds and high temperatures accelerate cell

lysis and loss of hydrolyzing capacity. Even if bacteria can survive these harsh environmental conditions without nutrients, they tend to excrete their enzymes which degrade more easily outside then inside the cells.

During the precipitation of calcium carbonate bacteria are being encapsulated in the crystals, causing further decay of the urease activity. This can be described similarly as cell lysis assuming exponential decay.

$$\frac{r_b}{r_{b0}} = \exp\left[-\frac{S_{CaCO_3}}{S_d}\right] \tag{7}$$

Where S_d is the characteristic decay concentration of precipitated $CaCO_3$ at which the urease activity has reduced by a factor e to about 63% of its original value.

2.1.4 Conditions effecting the in-situ urease activity during MICP in sand

The apparent urease activity when used for biocementation is affected by many factors:

$$r_b = \frac{dC_{urea}}{dt} = f\left(C_{bacteria}, SUA, C_{urea}, pH, C_{Ca^{2+}}, T, t, S_{CaCO_3}, ...\right) \tag{8}$$

After the bacteria are injected in the subsurface, the distribution of bacteria in the pores is affected by the factors which determine the flow and transport of bacteria through porous media. When flushed through the soil a fraction of the bacteria is adsorbed to the solid surface or get strained in the narrow pores. When after placement of the bacteria the solution of urea and calcium chloride is supplied, a part of the adsorbed bacteria detach and flush further and are eventually washed out of the treatment area. Adsorption, straining and detachment are affected by many factors, including: fluid properties like water chemistry and flow regime (Torkzaban et al. 2008), cell wall characteristics like hydrophobicity, charge and appendages (van Loosdrecht et al. 1987; Gilbert et al. 1991) and solid properties, like grain size distribution, surface texture and mineralogy (Scholl et al. 1990; Foppen & Schijven 2005; Foppen & Schijven 2006). When cells release their enzymes, the excreted urease is more easily flushed away than the whole cells. Larsen et al (2008) investigated how the attachment and stability of urease enzymes from jack bean was affected by the addition of organic stabilizers and found that is was comparable with the stability of the enzyme in grinded jack bean meal. While Ciurli et al (1996) and Marzadori et al (1998) showed enhanced adsorption of urease enzymes to roots of plants and minerals.

Another effect on the urease activity during biocementation in soils is the reduction of pore space due to precipitation. By filling up the pores the crystals directly reduce the porosity, but can also block pores for liquid flow, creating stagnant areas within the pore network. When a constant flow rate is applied this reduction in "mobile" porosity causes an increase in the average linear flow velocity, and a reduction of the residence time of the substrates within the soil volume. Consequently, the urease activity per soil volume decreases as well.

Experiments performed by Booster et al. (2008) showed that the cumulative effect of enzyme excretion, cell decay, wash out, encapsulation and porosity reduction caused a decay in urease activity by a factor 3 in about 80 hours of continuous flushing with 1M

urea and calcium chloride at 20°C. After 170 hours the remaining urease activity was close to zero while 400 g-$CaCO_3$ L^{-1}-soil was precipitated.

Although transport conditions do significantly affect the spatial and temporal distribution of urease activity in the subsurface, these effects are not further included in this study.

2.2 Speciation and acid-base equilibria

Once urea is hydrolyzed and ammonium and bicarbonate are released by the cells into the solution, these products react into a wide range of dissolved species, including ammonia (NH_3), ammonium (NH_4^+), carbonate (CO_3^{2-}), bicarbonate (HCO_3^-), carbonic acid (H_2CO_3 or dissolved carbon dioxide CO_2), hydroxide (OH^-), and protons (H^+). When calcium ions are present in solution several of the anions can form dissolved complexes with calcium, including calcium hydroxide ($CaOH^+$), calcium bicarbonate ($CaHCO_3^+$) and calcium carbonate ($CaCO_3$) (Parkhurst 1995). The speciation of these compounds is governed by acid-base equilibria which depend on pH, temperature and salinity.

When a general speciation reaction is described as:
$$A + B \rightleftharpoons C + D \tag{9}$$
the equilibrium constant of this reaction is defined as:
$$K_a = \frac{a_C a_D}{a_A a_B} \tag{10}$$
in which K_a is the equilibrium constant, a_A, a_B, a_C and a_D are the molar activities in for reagents A and B and products C and D. The activity is defined as:
$$a_i = \gamma_i C_i \tag{11}$$
In which γ_i is the activity coefficient and C_i the concentration in [mol L^{-1}] for ion i. For infinitely diluted systems, the ion activity coefficients can be assumed 1 and concentration is equal to the activity. For solutions with higher concentrations, the activity can differ significantly from the concentration. Using Davies extended version of the Debye-Hückel equation the activity coefficients can be calculated, according to:
$$\log \gamma_i = -0.5 z_i^2 \left(\frac{\sqrt{IS}}{1 + \sqrt{IS}} - 0.3IS \right) \tag{12}$$
In which γ_i is related to ion valency, z, and the ionic strength of the solution, *IS*, which is calculated using:
$$IS = 0.5 \sum_i C_i z_i^2 \tag{13}$$
The rate of the speciation reactions is assumed linearly related to the deviation from equilibrium and can be described using:
$$r_i = k_i \left(C_C \gamma_C C_D \gamma_D - C_A \gamma_A C_B \gamma_B \cdot 10^{pK} \right) \tag{14}$$
Most speciation reactions are fast and can be considered instantaneous, taking an infinitely high value for rate constant k_i. Hydrolysis of CO_2 (2 and 3) is a relatively slow process with a rate constant at an order of 100 s^{-1} (Ebrahimi et al. 2003). Table 1 gives an overview of the acid-base equilibria with corresponding rates and constants, which are taken into account in this study.

Table 1 Molar stoichiometry and reaction rates for acid-base equilibria included in this model, with corresponding pK_a-values (negative logarithms) of the equilibrium constants at $T = 25^0C$ and $p = 1$ bar (Parkhurst 1995).

Reaction name	Reaction equation	Reaction rate	Constants
1.Water dissociation	$H_2O \rightleftarrows OH^- + H^+$	Equilibrium: $K_{a1} = a_{H^+} a_{OH^-}$	$pK_{a1} = 14.00$
2.Bicarbonate dissociation	$HCO_3^- \rightleftarrows CO_3^{2-} + H^+$	$r_{a2} = k_{a2}\left(a_{CO_3^{2-}} a_{H^+} - a_{HCO_3^-} 10^{pK_{a2}}\right)$	$pK_{a2} = 10.33$ $k_{a2} = 10^{12}$ h^{-1}
3.Carbonic acid dissociation (acid)	$CO_2 + H_2O \rightleftarrows HCO_3^- + H^+$	$r_{a3} = k_{a3}\left(a_{H^+} a_{HCO_3^-} - a_{CO_2} 10^{pK_{a3}}\right)$	$pK_{a3} = 6.35$ $k_{a3} = 3\times10^5$ L h^{-1} mol^{-1}
4.Carbonic acid dissociation (basic)	$CO_2 + OH^- \rightleftarrows HCO_3^-$	$r_{a4} = k_{a4}\left(a_{CO_2} a_{OH^-} - a_{HCO_3^-} 10^{pK_{a4}}\right)$	$pK_{a4} = -7.64$ $k_{a4} = 3\times10^5$ L h^{-1} mol^{-1}
5.Ammonium dissociation	$NH_4^+ \rightleftarrows NH_3 + H^+$	$r_{a5} = k_{a5}\left(a_{NH_3} a_{H^+} - a_{NH_4^+} 10^{pK_{a5}}\right)$	$pK_{a5} = 9.25$ $k_{a5} = 10^{12}$ L h^{-1} mol^{-1}
6.Calcium hydroxide complexation	$Ca^{2+} + H_2O \rightleftarrows CaOH^+ + H^+$	$r_{a6} = k_{a6}\left(a_{CaOH^+} a_{H^+} - a_{Ca^{2+}} 10^{pK_{a6}}\right)$	$pK_{a6} = 12.78$ $k_{a6} = 10^{12}$ L h^{-1} mol^{-1}
7.Calcium bicarbonate complexation	$Ca^{2+} + CO_3^{2-} + H^+ \rightleftarrows CaHCO_3^+$	$r_{a7} = k_{a7}\left(a_{CaHCO_3^+} - a_{Ca^{2+}} a_{CO_3^{2-}} a_{H^+} 10^{pK_{a7}}\right)$	$pK_{a7} = -3.22$ $k_{a7} = 10^{12}$ h^{-1}
8.Calcium carbonate complexation	$Ca^{2+} + CO_3^{2-} \rightleftarrows CaCO_3$	$r_{a8} = k_{a8}\left(a_{CaCO_3} - a_{Ca^{2+}} a_{CO_3^{2-}} 10^{pK_{a8}}\right)$	$pK_{a8} = -11.44$ $k_{a8} = 10^{12}$ h^{-1}

2.3 Precipitation of calcium carbonate

Although the precipitation of calcium carbonate is widely studied for its relevance in biomineralization, geosciences and industry (scaling) and for its use as a model system, still quantitative models to predict the amount of crystals, crystal type and the crystal size and surface area are scarce as these properties vary in time and space and are influenced by many factors, especially in a complex system such as a soil. Precipitation consists of several phases, nucleation, crystal growth and secondary changes in the crystal lattice. These processes occur sequentially with some overlap (Söhnel 1992). Each process has a different rate, depending on the precipitation conditions. Secondly, calcium carbonate is polymorph meaning that different mineral types can form. Under ambient temperatures and pressures, calcite is the most common and stable mineral (Stumm 1996).

2.3.1 Solubility product

When urea hydrolyzing bacteria produce sufficient carbonate in presence of calcium the solution becomes oversaturated: i.e. the ionic activity product exceeds the solubility product. In an oversaturated solution calcium carbonate can precipitate:

$$Ca^{2+} + CO_3^{2-} \rightarrow CaCO_3(s) \qquad (15)$$

At thermodynamic equilibrium, the ionic activity of the ions in solution (*IAP*) is equal to the solubility product K_{sp}:

$$K_{sp} = IAP = \gamma_{Ca^{2+}} \gamma_{CO_3^{2-}} C_{Ca^{2+}} C_{CO_3^{2-}} \qquad (16)$$

The solubility product depends on the mineral type and the temperature (Plummer & Busenberg 1982; Gal et al. 1996). E.g. at $25^{\circ}C$ K_{sp} of calcite is 10-8.33 mol2 L-2. Figure 7 shows the solubility product as a function of temperature for different mineral types of $CaCO_3$. The most stable form in the temperature range 0-80$^{\circ}C$ is calcite.
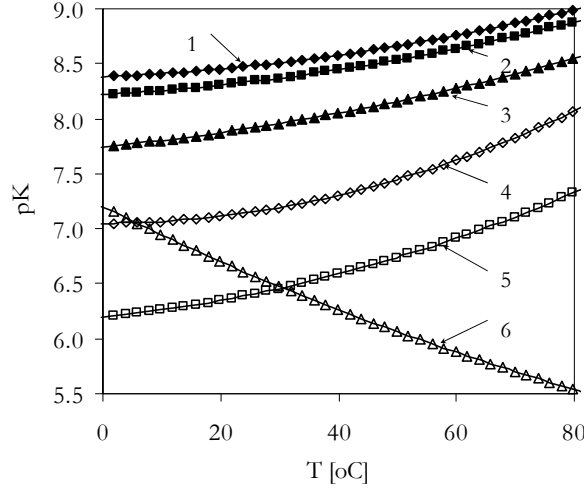

Figure 7 Solubility product as a function of temperature for different polymorphs and hydrates of CaCO₃: 1) calcite (♦), 2) aragonite (■), 3) vaterite (▲), 4) calcium carbonate monohydrate (◊), 5) amorphous calcium carbonate (□) and 6) ikaite or calcium carbonate hexahydrate (△) (Plummer & Busenberg 1982; Gal et al. 1996). Note that pK ($-log$ (K_{sp})) is shown on the y-axis.

2.3.2 Bulk precipitation

The precipitation rate, r_p, of calcium carbonate is often described using (Nancollas & Reddy 1971; Reddy & Nancollas 1971; Söhnel 1992) an equation of the form:

$$r_p = \frac{dS_{CaCO_3}}{dt} = k_p \left(S - 1 \right)^n \tag{17}$$

In which k_p is the bulk kinetic constant in [kmol m^{-3} h^{-1}], n is the kinetic order and S is the supersaturation, which is defined as:

$$S = \frac{c}{c_{eq}} = \sqrt{\frac{IAP}{K_{sp}}} \tag{18}$$

Sometimes alternative definitions for supersaturation, like saturation index $SI = $ log(IAP)$-$ log(K_{sp}) are used in equation (17). The bulk kinetic constant, k_p, is a function of the growth mechanism, mineral type, crystal surface area and number of crystals:

$$k_p = \frac{k_g A_{c,total}}{V_m} = \frac{k_g \left\langle A_c \right\rangle (t) N(t)}{V_m} \tag{19}$$

in which k_g is the crystal growth rate constant in [m h-1], $<A_c>$ is the average crystal surface area [m^2], N is the number of crystals in [m^{-3}] and V_m is the molar volume of the crystallizing solid in [m^3 mol^{-1}], which is the ratio between molar mass (M_c) and solid density (ϱ_c). For calcite M_c = 100 kg kmol^{-1}, ϱ_c = 2710 kg m^{-3} and consequently V_m = 0.0369 m^3 kmol^{-1}. Both $<A_c>$ and N can vary in time.

The bulk kinetic constant lumps several precipitation processes: i.e. nucleation, growth and secondary changes in the crystal lattice. Assuming a constant bulk kinetic constant for precipitation is therefore in principle incorrect, especially when few crystals (or crystal surface area) are present, e.g. shortly after nucleation. Still the rate equation (17) is often used. A bulk kinetic constant can be considered when the crystal surface is constant, which is for example the case in scaling studies (Udert et al. 2003) or when MICP is applied in carbonate sand, in which the sand grain surface could act as a crystallizing substrate. Assuming precipitation takes place at the sand grain surface, the bulk kinetic constant can be calculated from grain size and porosity (table 2).

Table 2 Grain surface area, $A_{c,total}$ as a function of grain size and porosity and calculated bulk kinetic constant k_p using equation (19) and assuming V_m at 0.0369 m^3 $kmol^1$ and k_g at 10-11 m s^{-1}.

Grain size [mm]	Porosity	$A_{c,total}$ [m² m⁻³]	k_p [kmol m⁻³ h⁻¹]
100	0.3	21000	0.020
100	0.4	18000	0.018
200	0.4	9000	0.0088

For fine sands k_p is estimated in the range of 0.1 and 0.001 kmol m⁻³ h⁻¹. With a high bulk kinetic constant the supersaturation remains close to 1 and the precipitation reaction can be considered at thermodynamic equilibrium.

As a result of nucleation and crystal growth, supersaturation drops which reduces the nucleation and crystal growth rate. However, when urea hydrolysis and calcium carbonate precipitation are combined, the reduction of supersaturation by precipitation is compensated by the continuous production of carbonate by urea hydrolysis. Consequently, the solution remains oversaturated for a longer period of time.

2.3.3 Nucleation

Nucleation, i.e. the birth of new crystals, occurs when the solution becomes sufficiently oversaturated that clusters of molecules coagulate and get a critical size, which enables them to resist the tendency to redissolve and start growing as a solid. When nuclei appear in a pure liquid phase this is called (primary) homogeneous nucleation. The theoretical rate of homogeneous nucleation for a spherical cluster of molecules is described using an Arrhenius equation, in which ΔG_{crit} is the activation energy, which needs to be exceeded before nuclei can start to grow (Mullin 2001):

$$J = \frac{dN}{dt} = A \exp\left[-\frac{\Delta G_{crit}}{kT}\right] = A \exp\left[-\frac{16\pi\gamma^3 v^2}{kT 3(kT(\ln S))^2}\right] \qquad (20)$$

Where J is the nucleation rate in [m⁻³ s⁻¹], A is the pre-exponential constant [m⁻³ s⁻¹], γ is the interfacial tension in [J m⁻²], v is the number of ions per mole of solute (in case of $CaCO_3$, $v = 2$), k is Boltzman constant (1.3805 x 10⁻²³ J K⁻¹) and T is temperature in [K]. Figure 8 shows the theoretical nucleation rate for homogeneous nucleation of calcium carbonate (calcite) crystals for different literature values of γ and T.
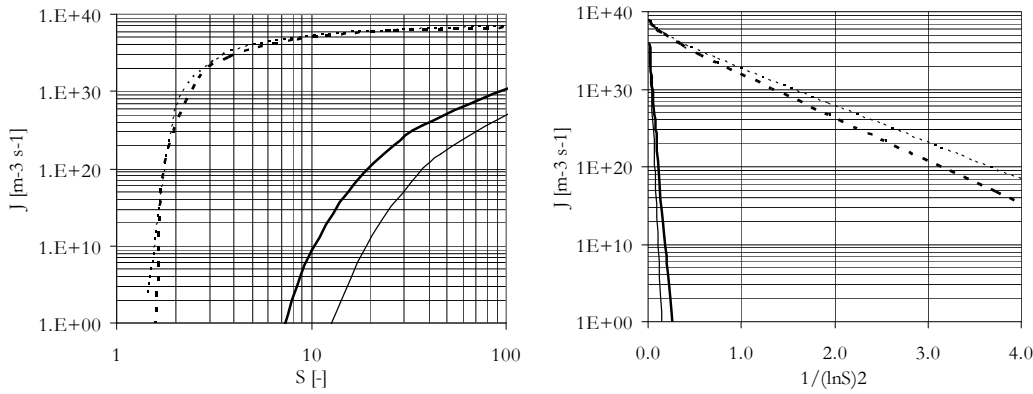
Figure 8 The theoretical nucleation rate for homogeneous nucleation of calcite crystals in S-J-plot (left) and 1/(lnS)2-J-plot (right) for γ = 0.098 J m-2 (solid lines) for CaCO3 in a pure solution (Sohnel & Mullin 1982) and for γ = 0.029 J m-2 (dashed lines) in presence of polymeric substrate (Dalas et al. 1988). Thick lines are for T = 283 K and thin lines for T = 298 K.

Assuming constant temperature, equation (20) can be rearranged to:

$$\frac{dN}{dt} = 10^{\left(40 - \frac{k_N}{(\ln S)^2}\right)} \tag{21}$$

Where k_N can be determined from temperature and surface tension. For the curves presented in figure 8, k_N varies between 8 for low surface tension, ($γ = 0.029$ J m^{-2}; $T = 298$ K) and 300 for spontaneous nucleation in homogeneous solution in absence of nucleation sites ($γ = 0.098$ J m^{-2}; $T = 283$ K). The wide range of theoretical nucleation rates presented in figure 8 illustrates the difficulty for predicting the rate of precipitation in case of spontaneous nucleation. On top of that once seed crystals are present or other surfaces, which can act as a crystal nucleus, like bacteria or other minerals, new crystals can appear through secondary or heterogeneous nucleation. The activation energy for nucleation is reduced by the presence of seed crystals or other nucleation sites. Consequently, nucleation takes place at lower supersaturation or is skipped completely (Tai & Chen 1995; Mitchell & Ferris 2006; Lioliou et al. 2007). Not all particles can act as a nucleus. E.g. LioLiou et al. (2007) distinguish between calcite and quartz, the latter being hardly active as nucleation site. Also the role of bacteria as nucleation sites is being doubted (Mitchell & Ferris 2006).

2.3.4 Crystal growth

Once stable nuclei are formed they start growing. Different CaCO$_3$ mineral types can be formed, each having a different crystal lattice and solubility product and resulting from a different growth mechanism (mononuclear, polynuclear, spiral growth) as a function of supersaturation, temperature and the solution chemistry (see figure 8) (Plummer & Busenberg 1982; Gal et al. 1996; Teng et al. 2000). At high supersaturation precipitation of metastable phases (amorphous CaCO$_3$, CaCO$_3$.H$_2$O and vaterite) is kinetically favored over the more stable mineral calcite, which is also directly formed at lower supersaturation levels (Kralj et al. 1990; 1994; 1997). In presence of magnesium aragonite is formed instead of the more stable calcite (Berner 1975). At low temperatures, ikaite (CaCO$_3$.6H$_2$O) can be a stable mineral phase (Gal et al. 1996). The crystal growth rate for each of these mineral phases or growth mechanism is directly related to the

supersaturation in the solution. For large crystals the supersaturation at the surface of the crystal can be lower than in the liquid.

Assuming crystals grow spherically and the reaction order is 2 (Sohnel & Mullin 1982), the growth rate is described by:

$$r_g = \frac{dR}{dt} = k_g \left(S - 1 \right)^2 \tag{22}$$

In which R is the crystal radius, S is the supersaturation for the specific mineral phase and k_g is the growth rate constant. k_g is derived empirically and depends on the growth mechanism, mineral type and temperature. E.g according to Kralj et al (1997) k_g for calcite is 1.2×10^{-11} m s^{-1} at 20°C. Figure 9 shows rate constant for vaterite and calcite after Kralj et al. (1990; 1994; 1997). For amorphous $CaCO_3$ and $CaCO_3.H_2O$ no rate constants for crystal growth could be found in literature, but they must be higher than the rate constant of vaterite.
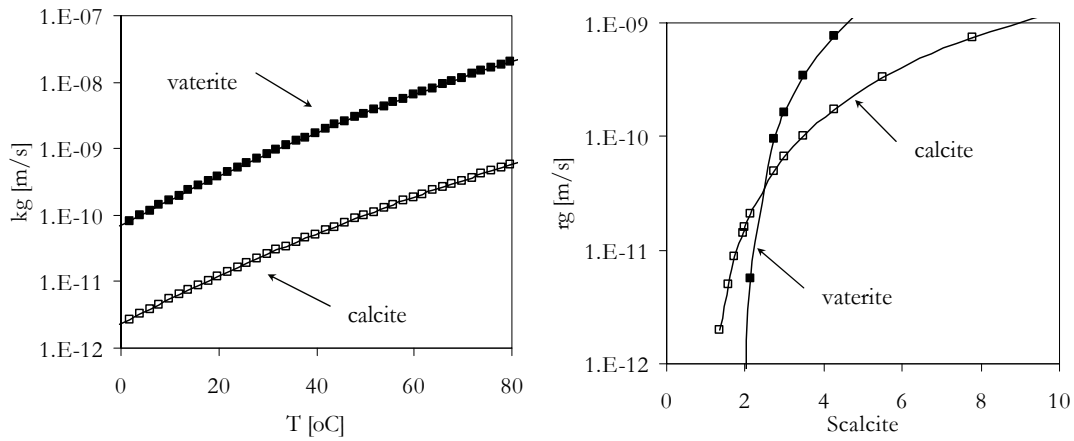

Figure 9 Rate constants, k_g, (left) and resulting crystal growth rate (right) for crystal growth of vaterite (■) and calcite (□) at 25°C according to equation (23) and using 8.48 and 7.91 as pK_{sp} for calcite and vaterite after Kralj et al (1990; 1994; 1997). Above $S_{calcite}$ of 2.3 vaterite growth is kinetically favoured over calcite.

Using the crystal growth rate according to equation (22) with the rate constant according to figure 9, the development of the crystal radius in time can be calculated. Crystal surface area is calculated using:

$$A_c = 4\pi R^2 \tag{23}$$

Combining equations (17) and (19) and calculating for each time step the number of crystals and the average crystal surface area, the overall precipitation rate in mol m-3 s-1 can be calculated using:

$$r_p = \frac{k_g \langle A_c \rangle (t) N(t)}{V_m} \left(S - 1 \right)^2 \tag{24}$$

When crystals become large the crystal growth can become limited by diffusion. Still the growth rate is calculated using equation (22), but the ionic activity product at the surface of the crystal is lower than in the bulk liquid. In this study diffusion limitations are not included.

2.3.5 Secondary changes in the crystal lattice

Once crystals are formed they can be subject to changes in the crystal lattice. When the crystal remains in contact with the solution it will dissolve when the ionic activity product in the solution drops below the solubility product. In this way, a crystal undergoes several transitions: metastable mineral phases like amorphous calcium carbonate and vaterite, which are formed at high supersaturation, will eventually dissolve and reprecipitate as the more stable calcite or aragonite. The kinetics of the transformation of vaterite to calcite, i.e. the precipitation and the dissolution of vaterite and recrystallization into calcite is well described by Kralj et al (1990; 1994; 1997). These secondary changes are not yet implemented in these numerical simulations.

3 Materials and methods

To study the factors which affect the kinetics of combined urea hydrolysis and calcium carbonate precipitation, several theoretical models are developed with increasing complexity. The results of the theoretical evaluation are compared to several experiments which were performed in continuously stirred batch reactors.

3.1 Theoretical models

To describe the process of urea hydrolysis and calcium carbonate precipitation kinetic models were developed and implemented in the AQUASIM 2.1 software (Reichert 1998). The level of detail and complexity in these models was stepwise increased:

1. assuming a single reaction
2. including acid-base equilibria and assuming thermodynamic equilibrium
3. including precipitation kinetics:
   a) assuming a constant crystallizing surface using bulk kinetics: $A_c = A_{c0}$.
   b) assuming constant number of crystals, including crystal growth: $N = N_0$, $A_c = f(t)$
   c) including nucleation and crystal growth kinetics: $N = f(t)$, $A_c = f(t)$

The different models are compared assuming the hydrolysis rate can be described by Michaelis-Menten kinetics with r_0 of 40 mM urea h^{-1} and with K_m of 10 mM and initial concentrations, C_0 of 0.5 M urea and 0.5 M CaCl$_2$. Using the different models, the effect of varying initial process conditions - i.e. the initial reagent concentration and hydrolysis rate – on the process kinetics was evaluated.

3.1.1 Single reaction approach (M1)

In the first and most simple model we assume that hydrolysis of urea produces ammonium and carbonate and all the produced carbonate immediately precipitates with calcium to form solid calcium carbonate. The process can be described using a single reaction:

$$CO(NH_2)_2 + 2\,H_2O + Ca^{2+} \xrightarrow{\;urease\;} 2\,NH_4^+ + CaCO_3(s) \qquad (25)$$
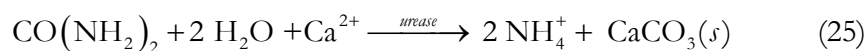
Charge balance is satisfied as the calcium ion is replaced by two ammonium ions. The model has only three state variables: C_{urea}, C_{NH4+}, and S_{CaCO3}. Using equimolar solutions of calcium chloride and urea C_{Ca} is equal to C_{urea} and C_{Cl} is constant. The fact that consumption of water increases the solute concentration is neglected, although it can

become significant at high solute concentrations. When urea and calcium levels are in the molar range an increase in solute concentration up to 4% occurs due to water consumption.

For simplicity it is assumed that the reaction rate is just a function of the initial rate, r_0 (i.e. the amount of added bacteria and their specific urease activity) and the urea concentration:

$$r = r_0 \frac{C_{urea}}{K_m + C_{urea}} \tag{26}$$

3.1.2 Acid-base equilibria at thermodynamic equilibrium (M2)

A first improvement of the model includes implementation of acid-base equilibria and precipitation reactions according to Parkhurst (1995), which enables the calculation of *pH*. The model involves eleven state variables: C_{urea}, C_{Ca2+}, C_{NH4+}, C_{NH3}, C_{CO2}, C_{HCO3-}, C_{CO32-}, C_{CaCO3}, C_{CaOH+}, $C_{CaHCO3+}$ and C_{H+}.

Urea is hydrolyzed according to reaction (1), $CaCO_3$ precipitates according to (15) and all other compounds form according to acid-base equilibria in table 1. The rates of these reactions are calculated using (26) and (14), in which equilibrium constants $pK_{a,i}$ and rate constants k_i are according to table 1. The precipitation rate is calculated using equation (17). Using *n* is 2 and rate constant k_p is set at 10^{12} mol m^{-3} s^{-1}.

The concentration of protons C_{H+} is calculated using the charge balance similar to (Wolf et al. 2007):

$$C_{H^+} + C_{NH_4^+} + 2C_{Ca^{2+}} + C_{CaOH^+} + C_{CaHCO_3^+} - C_{HCO_3^-} - 2C_{CO_3^{2-}} - C_{OH^-} = 0 \tag{27}$$

Where the sum of ions (excluding C_{H+} and C_{OH-}) is defined as:

$$C_{NH_4^+} + 2C_{Ca^{2+}} + C_{CaOH^+} + C_{CaHCO_3^+} - C_{HCO_3^-} - 2C_{CO_3^{2-}} = \sum_i \left(C_{i,ion} \right) \tag{28}$$

And C_{OH-} is considered in equilibrium with C_{H+} according to:

$$C_{OH^-} = \frac{K_{a,H_2O}}{C_{H^+}} \tag{29}$$

Substituting equation (28) and (29) in (27) and re-arranging yields equation (30) for the calculation of C_{H+}, where *pH* (31) can be determined from.

$$C_{H^+} = 0.5 \left(\sqrt{\left(\sum_i \left(C_{i,ion} \right) \right)^2 + 4K_{a,H_2O}} - \sum_i \left(C_{i,ion} \right) \right) \tag{30}$$

$$pH = -\log\left(C_{H^+} \right) \tag{31}$$

The charge balance is solved using:

$$r_c = k_c \left(C_{H^+} - 0.5 \left(\sqrt{\left(\sum_i \left(C_{i,ion} \right) \right)^2 + 4K_{a,H_2O}} - \sum_i \left(C_{i,ion} \right) \right) \right) \tag{32}$$

Where k_c is set at 10^{12}.

3.1.3 Precipitation kinetics (M3)

Next step is including precipitation kinetics in the model. When the precipitation rate is limited, i.e. the hydrolysis rate is faster than the precipitation rate, the solution will get supersaturated. Due to an increasing supersaturation, the precipitation rate increases until hydrolysis rate and precipitation rate are in equilibrium. For continuous hydrolysis of urea at a high rate extended periods of supersaturation are expected. High supersaturation levels are accompanied by metastable mineral types, e.g. vaterite instead of calcite will form (Figure 9). Calculating supersaturation is therefore essential to predict the mineral type. Three types of precipitation kinetics are distinguished:

a. Assuming constant surface area is relevant for cases where the surface can act as a substrate for crystal growth, (simulating e.g. scaling of pipelines or precipitation in carbonate sands). In this case a similar approach is used as for the previous model M2, but now the bulk precipitation rate constant k_p is varied at 0.1, 0.01 and 0.001 mol m^{-3} s^{-1}.

b. Assuming a constant number of crystals and increasing surface area by crystal growth is relevant for seeded experiments, where crystal growth is not restrained by physical boundaries. In this case the number of crystals, N_0, is set at 10^{15} m^{-3} and the initial radius, R_0, is assumed at 10 nm. Speciation equations are similar to the previous model M3a, but the crystal growth is calculated using equation (22). From crystal radius, R, the crystal surface area, A_s, is calculated using equation (23), which is then used with, N, to calculate S_{CaCO3} using equation (24). Growth rate constant k_g is assumed constant at 10^{-11} m s^{-1}, i.e. the rate constant for calcite growth.

c. Assuming spontaneous nucleation followed by crystal growth, is relevant for cases where nucleation sites limited or absent, e.g. in unseeded aqueous solution or in the (large) pores of quartz sand. The model is similar to the previous model M3b, but the number of nuclei is calculated using equation (21). Nucleation rate constant k_N is varied at respectively 8, 100 and 300 and k_g are is assumed constant at 10^{-11} m s^{-1} (crystal growth rate for calcite). The initial number of crystals, $N_0 = 0$ and the initial crystal radius (nucleus) R_0 is set at 10 nm. Crystals can only grow when $N > 0$. Once growing crystals are present nucleation and crystal growth can occur simultaneously (dN/dt and $dR/dt > 0$). New crystals appear with the same radius as the existing crystals (thereby overestimating the average crystal size).

3.1.4 Multiple mineral phases and secondary changes in the crystal lattice

The model could be further improved if growth (and dissolution) of different mineral phases would be included. Experiments (Chapter 3) have shown that when hydrolysis rates above 18 mM urea h^{-1} are applied, vaterite is the dominant mineral phase formed. Kinetic constants for vaterite growth and calcite growth are shown in figure 9 after Kralj et al. (1990; 1994; 1997). For the other mineral phases no kinetic constant were found in literature. In this study it is assumed that calcite is the only precipitating mineral. The growth (and dissolution) of other mineral phases is not included.

3.1.5 Process variables

Using the models presented in paragraph 3.1.3. including precipitation kinetics, the effect of urea hydrolysis rate (at 10, 40, 80 and 300 mM urea h^{-1}) and reagent concentration (at

250, 500 and 1000 mM urea and calcium chloride) on supersaturation, pH and the number and size of crystals is calculated with for M3.1 k_p at 0.001 mol m^{-3} s^{-1}, for M3.2 N at 10^{15} m^{-3} and k_g of 10^{-11} m s^{-1} and for M3.3 k_N of 300 and k_g of 10^{-11} m s^{-1}.

3.2 Experimental

3.2.1 Cultivation of bacteria

Sporosarcina pasteurii DSM 33 (DSMZ, FRG) were cultivated under axenic aerobic batch conditions in a medium containing 20 g L^{-1} yeast extract, 10 g L^{-1} NH$_4$Cl and 10 μM NiCl$_2$. Before the cultivation medium was sterilized at 121°C and pH of the medium was adjusted to 8.5 by slowly adding 4M NaOH. The organisms were grown for 24 hours at 35°C in which late exponential/early stationary phase was reached (i.e. all readily available nutrients were consumed from the medium). The bacteria were stored suspended in their growth medium in the fridge at 4°C prior to use.

3.2.2 Batch experiments

Experiments have been performed in a continuously stirred batch reactor (beaker glass) at constant temperature, containing 200 mL of demineralized water in which equimolar amounts of urea and CaCl$_2$ were dissolved and different amounts of bacterial suspension were added. Electrical conductivity, κ, and pH were measured continuously using electrodes SP10B and SK10B and desktop meter C864 (Consort, Belgium), using automatic temperature correction (ATC) to 25°C. The measured conductivity is normalized using:

$$\kappa = \frac{\kappa - \kappa_{min}}{\kappa_{max} - \kappa_{min}} \qquad (33)$$

3.2.3 Electrical conductivity measurement

As the electrical conductivity for the reagent solution containing urea and CaCl$_2$ is much lower than for the product solution containing mainly NH$_4$Cl, the electrical conductivity can be used as a measure for the conversion percentage. Figure 9 shows the electrical conductivity of the main components CaCl$_2$ and NH$_4$Cl after (Lyde 2009), in which the CaCl$_2$ concentration is divided by two considering the molar stoichiometry of the combined hydrolysis and precipitation reactions. For different mixtures of CaCl$_2$ and NH$_4$Cl solution a linear trend is assumed between minimum and maximum conductivity.
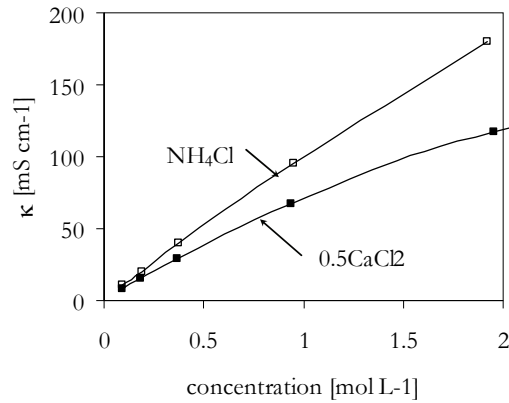
Figure 9 Electrical conductivity as a function of concentration for solutions of ammonium chloride (□) and calcium chloride (■) after (Lyde 2009).

According to Eaton et al (1995) the theoretical conductivity of a solution with multiple ions at infinite dilution, κ^o, can be calculated from the equivalent ionic conductances, λ_i°, using:

$$\kappa^o = \sum_i |z_i| \lambda_i^o C_i \tag{34}$$

where the absolute value of the charge, z_i, of the i-th ion is multiplied with concentration C_i and equivalent ionic conductances of i-th cation or anion, λ_i°, at infinite dilution at 25°C. Equivalent ionic conductances for the main component are presented in table 3. Ionic conductance values for calcium complex ions were not found in literature and were neglected in this study.

Table 3 Ionic equivalent conductance (Vanýcek 2009)

Ion	λ°
	10^{-4} m^2 S mol^{-1}
½ Ca^{2+}	59.47
NH$_4^+$	73.5
Cl$^-$	76.31
OH$^-$	198
H$^+$	349.65
HCO$_3^-$	44.5
½ CO$_3^{2-}$	69.3

Both Eaton et al (1995) and Vanycek (2009) present methods to calculate the conductivity for higher solute concentrations. However, these methods were only valid for solute concentration up to 0.25 M and did not fit to our experimental measurements. Therefore, the theoretical conductivity for the main compounds, calcium, ammonium and chloride was calculated using the empirical data presented in figure 9. The additional conductivity of the other ions in the solution was calculated using the equivalent ionic conductance at infinite dilution in equation (34) in which for the calcium complex ions 50x10-4 m2 S mol-1 was assumed for the ionic equivalent conductance. The cumulated theoretical conductivity was normalized using equation (33).

4 Results

4.1 Theoretical model

To study the kinetics of combined hydrolysis of urea and precipitation of calcium carbonate a theoretical model was developed in which the level of detail and complexity was stepwise increased: M1) a model based on a single irreversible reaction; M2) a model including acid-base equilibria and assuming thermodynamic equilibrium; M3) a model including precipitation kinetics. The models are used to investigate the effect of variable process conditions.

4.1.1 Simplified single reaction approach (M1)

Figure 10 shows the results of model M1 at an initial hydrolysis rate, r_0, of 40 mM urea h-1, K_m of 10 mM and initial urea concentration, C_0 of 0.5 M (and similar for CaCl$_2$). Within 15 hours all urea is consumed resulting in 1M ammonium and 0.5 M CaCO$_3$. The hydrolysis rate is more or less constant until urea gets depleted.
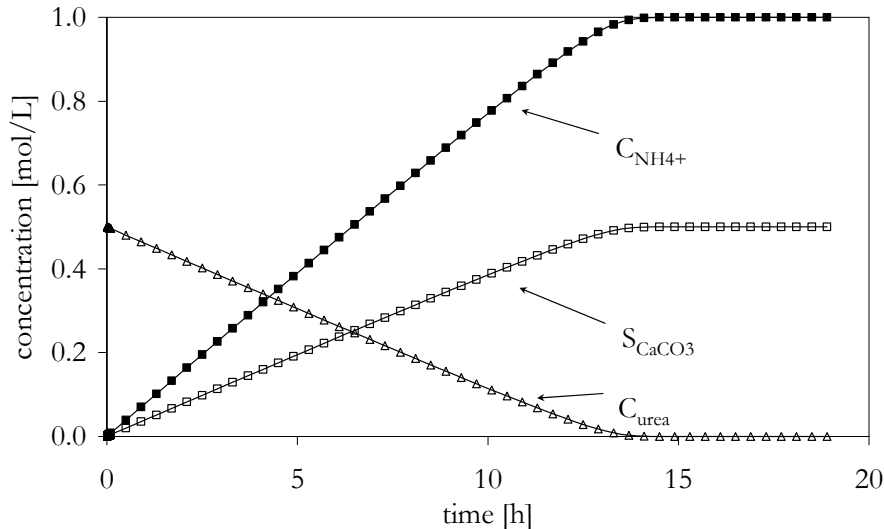

Figure 10 Concentrations of urea, C_{urea} (Δ), ammonium, C_{NH4+} (■) and precipitated calcium carbonate, S_{CaCO3} (□) in time calculated using a simplified single reaction model (M1).

4.1.2 Acid-base equilibria at thermodynamic equilibrium (M2)

Figure 11 shows that the concentrations of the main compounds C_{urea}, C_{Ca2+}, C_{NH4+} and S_{CaCO3} calculated using a model including acid-base equilibria (M2) do not differ from the concentrations calculated by a simplified single reaction model (M1; Figure 10). Concentrations of all other species seem negligible (less than 1% of the main compounds). However, including them in the model enables the calculation of pH. Figure 12 shows the speciation of all dissolved calcium and inorganic carbon species at a logarithmic scale still assuming thermodynamic equilibrium. In the initial solution containing only urea and CaCl$_2$ a part of the calcium reacts with water to form the calcium hydroxide (C_{CaOH+}) complex, resulting in a slightly acidic pH at 6.56. As soon as a little urea is hydrolyzed, pH rises reaching a maximum of 7.91. At that point the produced carbonate exceeds the solubility product and calcium carbonate starts to

precipitate. After that, the pH drops quickly below 7 reaching a minimum of 6.62. The slightly acidic pH is mainly a result of the equilibrium between free calcium and the calcium bicarbonate complex ($C_{CaHCO3+}$), which is the most abundant compound of dissolved inorganic carbon during the first half of the process when calcium concentration is still high. While calcium is becoming depleted by precipitation, the total amount of CO_3^{2-} and hence dissolved inorganic carbon (TDC) increases. About halfway the pH starts to increase again and more unbound bicarbonate (C_{HCO3-}) is present in solution. After 15 hours a steady state is reached at which 3.3 mM calcium remains in equilibrium with 3.1 mM bicarbonate (250 µM carbonic acid and 6.2 µM carbonate) at a pH of 7.24. From the 1M ammonium about 3.6 mM is present as ammonia.

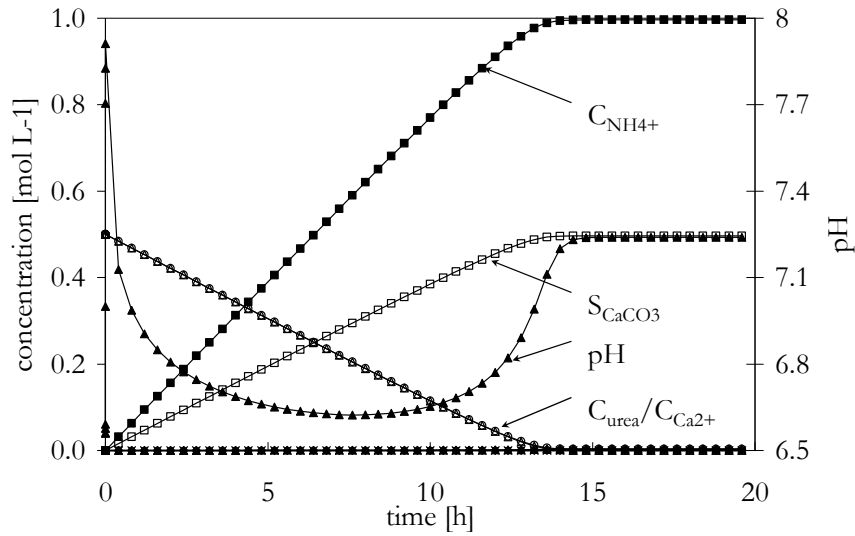*Figure 11 Concentrations of the main dissolved species, C_{urea} (⊿), C_{Ca2+} (○), C_{NH4+} (■) and precipitated calcium carbonate, S_{CaCO3} (□) and pH (▲) calculated using a numerical model including acid-base equilibria and assuming thermodynamic equilibrium.*
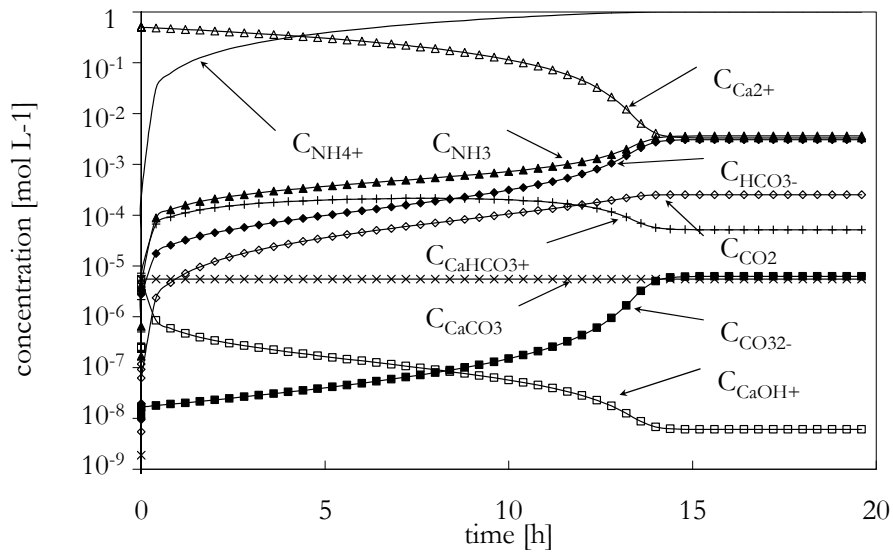

Figure 12 Calculated concentration of all dissolved acid-base equilibrium species assuming thermodynamic equilibrium and plotted on logarithmic scale: C_{NH4+} (-), C_{NH3} (▲), C_{Ca2+} (⊿), C_{CO2} (◊), C_{HCO3-} (♦), C_{CO32-} (■), C_{CaCO3} (✗), C_{CaOH+} (□), and $C_{CaHCO3+}$ (+).

4.1.3 Precipitation kinetics (M3)

Including precipitation kinetics in the model (M3) allows calculating supersaturation. Still for the scenarios at high supersaturation calculated with model M3, the concentration profiles of the main compounds C_{urea}, C_{Ca2+}, C_{NH4+} and S_{CaCO3}, did not show significant deviation (about 1%) from the more simple models M1 and M2.

Constant surface area (M3a)

Considering precipitation takes place as crystal growth from a surface (e.g. scaling of membranes, tubes and pipes or in a packed carbonate sand) the precipitation rate is described using equation (17). For fine sands (grain diameter 100-200μm) the surface area is about 30000 m^2 m^{-3}. Assuming the full grain surface is available for crystal growth, the kinetic constant kinetic constant kp can be determined and varies between 0.1 and 0.001 M h^{-1}. Figure 13 shows the supersaturation and pH as a function of k_p.
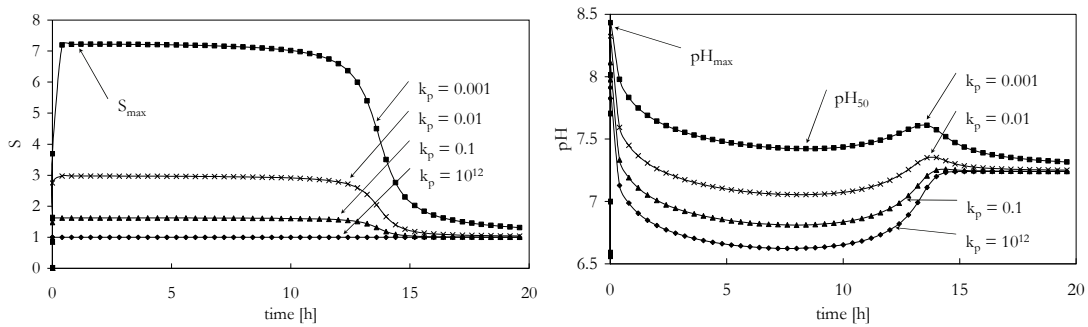

Figure 13 Supersaturation (left) and pH (right) using a model with precipitation kinetics assuming a constant surface area and varying precipitation rate constant k_p: 10^{12}, 0.1, 0.01 and 0.001 kmol m^{-3} h^{-1}.

For k_p at 10^{12} kmol m^{-3} h^{-1} the supersaturation remains 1, indicating precipitation takes place at thermodynamic equilibrium. For lower k_p, supersaturation rises quickly up to a level (S_{max}) where it remains constant until urea starts to deplete. The maximum supersaturation level increases with decreasing k_p up to 7.2 at k_p is 0.001 kmol m^{-3} h^{-1}. The pH profiles show a similar pattern as in figure 11 where equilibrium is assumed (M2). Both the peak level (pH_{max}), which is reached within the first minutes before precipitation starts, and the level at 50% of the conversion (pH_{50}) increase with decreasing k_p: from 7.9 to 8.4 for pH_{max} and from 6.8 to 7.4 for pH_{50} when k_p decreases from 10^{12} to 0.001 kmol m^{-3} h^{-1}. Once C_{urea} and C_{Ca2+} are depleting both *pH* and *S* decrease to thermodynamic equilibrium values.

Constant number of crystals (M3b)

Assuming a constant number of crystals, which grow in time, shows a different pattern for supersaturation (Figure 14). Initially, when the crystals are still small, a peak supersaturation is reached (S_{max}), as the precipitation rate is still significantly limited due to little available crystal surface area. As the crystals become bigger supersaturation decreases first fast, then more gradual nearly reaching a flat level at 50% conversion (S_{50}). A smaller number of crystals gives higher values for S_{max} and S_{50} and results eventually in larger crystals. When urea has been depleted, *S* reduces further to thermodynamic equilibrium. pH shows a similar pattern as in figure 13, where pH_{max} is independent of *N* at about 8.7 and pH_{50} increases with decreasing number of crystals from 6.8 to 7.1. For

decreasing number of crystals the peak supersaturation, pH_{max}, is reached at a later time(about 7 minutes for N of 10^{13} m^{-3}). As a result the pH is flattened out over a similar time period.
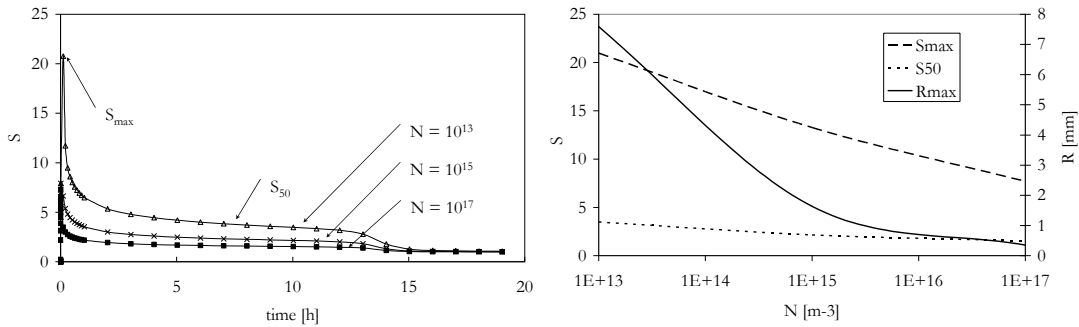

Figure 14 Supersaturation in time for different amounts of nuclei (left) using a model with precipitation kinetics assuming a constant number of crystals. S_{max} and S_{50} are plotted together with final crystal radius as a function of number of nuclei (right).

Nucleation and growth kinetics (M3c)

Including the kinetics of nucleation and crystal growth both the number and the size of the crystals are calculated. Supersaturation and pH show similar patterns as in Figure 14. Figure 15 shows the values for supersaturation (S_{max}, S_{50}), acidity (pH_{max}, pH_{50}), crystal radius (R_{max}) and number of crystals (N_{max}) as a function of nucleation rate constant k_N using a crystal growth rate constant k_g of 10^{-11} m s^{-1}.
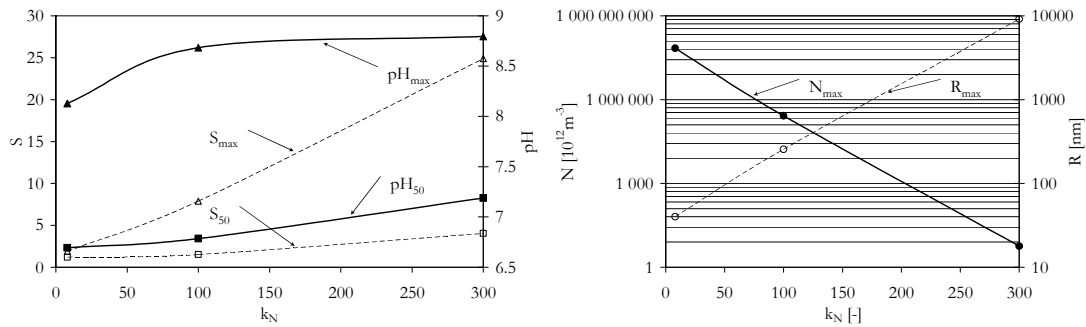

Figure 15 Calculated supersaturation (S_{max}, S_{50}), acidity (pH_{max}, pH_{50}), crystal radius (R_{max}) and number of crystals (N_{max}) as a function of nucleation rate constant k_N using a crystal growth rate constant k_g of 10^{-11} m s^{-1}.

If compounds are present in the solution, which lower the activation energy for nucleation ($k_N = 8$) a large number of crystals (10^{20} m^{-3}) is formed. The crystal size is very small (20 nm). Supersaturation and pH profiles are close to thermodynamic equilibrium. When no nucleation sites are present and a high activation energy has to be exceeded for spontaneous homogeneous nucleation to occur ($k_N = 300$), the number of crystals is relatively low (10^{12} m^{-3}), but the crystals grow up to 9 μm in size. Initially supersaturation rises quickly reaching a maximum of 25 within 8 minutes, after which it decreases to a level of 4 halfway the conversion. The peak pH level increases up to about 8.7 with increasing activation energy, but above k_N is 100 the maximum pH does not increase further but is flattened out over a longer period similar as the time to reach supersaturation.

4.1.4   Process variables

Industrial applications of MICP by urea hydrolysis require high concentrations and high hydrolysis rates to minimize the number of treatments and treatment time. Using the theoretical models the effect of concentration and hydrolysis rate on the amount of precipitate, supersaturation, pH and the number and size of crystals were evaluated.

Higher hydrolysis rates lead to faster precipitation at higher supersaturation and higher pH. Supersaturation reached maxima between 18 and 29 at a hydrolysis rate of 300 mM urea h^{-1}, compared to 7 to 22 for an hydrolysis rate of 40 mM urea h^{-1}. The actual vale depended on the assumed type of precipitation kinetics: when assuming a constant surface area, S_{max} remained constant similar to figure 13 but at a level of 18; When assuming a variable surface area S_{max} showed a peak similar to figure 14, going back to a level S_{50} of about 5 compared to 3 at a hydrolysis rate of 40 mM urea h^{-1}. When assuming spontaneous nucleation from solution, higher hydrolysis rates also resulted in a larger number of relatively smaller crystals.

The initial (equimolar) concentration urea and calcium chloride did not seem to influence the supersaturation nor the pH. Profiles for pH reached lower minimum values around 50% conversion (P_{50}) for higher initial concentrations as low as 6.5 for 1M urea and calcium chloride. When non-equimolar solutions are used, the pH profiles do look different. If the initial calcium concentration is zero or smaller than the urea concentrations, the pH will rise to about 9.3 after the calcium is depleted, at which ammonium, ammonia, bicarbonate and carbonate are in equilibrium. When the initial urea concentration is smaller than the calcium concentration the pH remains around 7.

4.2   Experimental

Experiments were performed in a continuously stirred vessel at constant temperature. Different concentrations of bacteria were added to a solution containing 0.5 M urea and calcium chloride. Continuous measurements of pH and electrical conductivity were several times interrupted when the precipitating $CaCO_3$ accumulated in the electrodes possibly affecting the measurements. At several times the electrodes were cleaned by dissolving the $CaCO_3$ in 1 M HCl and rinsing the electrode afterwards with demineralized water before putting them back in the suspension. Figure 16 shows the measured conductivity and pH during two experiments of which one had an average urease activity of 80 mM urea h^{-1} (fast) and the other 40 mM urea h^{-1} (slow).

In both experiments the electrical conductivity increases in time as expected. However, the increase was not linear, which was expected assuming a constant hydrolysis rate and considering calcium, ammonium and chloride were the main ions contributing to the electrical conductivity (Figure 9). Even for the models in which relatively high supersaturation was obtained, the ions, other than ammonium, calcium and chloride, did not exceed 1% of the main compounds. Consequently, the contribution of these minor ions to the conductivity is considered negligible. Both conductivity profiles show initially a fast increase, which slowed down after about 3 hours. In the slow experiment, the increase in conductivity accelerated again slightly after about 8 hours. The maximum conductivity was reached after about 6 hours for the fast experiment and 13 hours for the slow one, indicating all urea had been depleted.

The pH in both experiments started below 7 (due to complexation of calcium ions with water, according to reaction 6 in table 1). In the fast experiment the pH rose quickly upon the addition of the bacteria, reaching a maximum of about 7.4 within 6 minutes, after which crystals started to appear in the suspension and pH decreased again reaching a minimum of 7 within 1 hour. Then pH rose again relatively quick reaching a value of about 7.2 after 3 hours where it slighty increased further until the end of the hydrolysis reaction. The slow experiment showed a similar trend, but with slightly higher pH values.
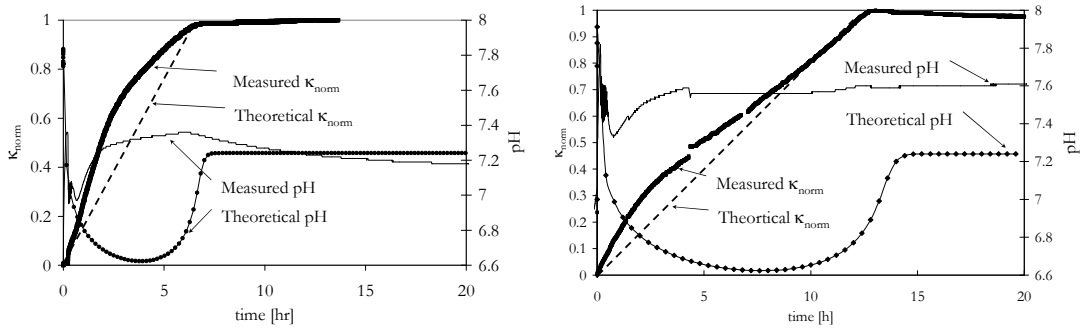

Figure 16 Measured and calculated pH and normalized electrical conductivity of two precipitation experiments in stirred vessels using 0.5 M urea and 0.5 M CaCl₂ at 20°C with different amounts of added bacteria, resulting in average urease activities of about 80 (left) and 40 (right) mM urea h⁻¹. For the calculations thermodynamic equilibrium was assumed.

In the first hour of the experiment (Figure 17), the pH in the fast experiment stayed constant for another 6 minutes and then dropped suddenly to 7.2 after which it showed oscillating behavior which dampened out during the first 30 minutes. A similar oscillating effect was seen in the slow experiment.
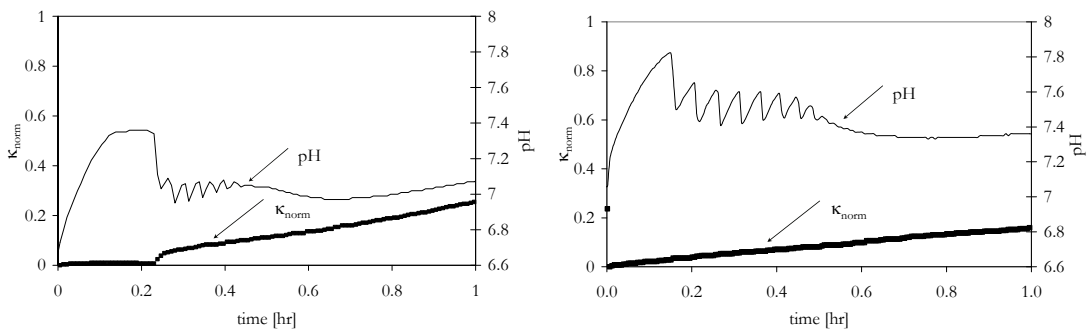

Figure 17 Detail of figure 15 showing the first two hours of batch precipitation experiments using 0.5 M urea and 0.5 M CaCl₂ at 20°C with different amounts of suspension containing the highly ureolytic bacteria.

5 Discussion

The trends of the experimental results and the theoretical models are in rough agreement. Measured and calculated electrical conductivity both increased during the induced conversion from calcium chloride to ammonium chloride until all urea and CaCl₂ are depleted. Also the measured and calculated pH show similar trends. Before any the solution is supersaturated, pH increases, followed by a rapid decrease once precipitation commences. Later pH increases again when calcium is depleting reaching a more or less stable value once all substrates are depleted.

An interesting observation in this study was that the major part of the precipitation takes place around neutral pH. Contrary to other suggestions in literature (Hammes & Verstraete 2002; Hammes 2003; Ferris et al. 2004; Mitchell & Ferris 2006) it appears that increase in pH is not a requirement for microbial induced carbonate precipitation, but a result of the speciation in acid-base equilibria and the (dis-) equilibrium between the acid-consuming urea hydrolysis and acid-producing $CaCO_3$ precipitation. During precipitation the pH dropped below neutral as a result of the high concentrations used in this study, yet precipitation occurred. Another interesting finding was the oscillating behavior of the pH in the experiments during the first hour of nucleation and growth, which seems to illustrate nicely the small disequilibrium between the hydrolysis and precipitation reaction rates. Once the hydrolysis reaction has produced sufficient carbonate that the activation energy for nucleation is exceeded, nuclei appear rapidly in the solution. Due to nucleation pH drops below the critical supersaturation preventing more new nuclei to appear. The nuclei start growing, but when the consumption of carbonate (and calcium) by crystal growth is slower than the carbonate production by urea hydrolysis, supersaturation will increase again until the critical supersaturation is exceeded and a new nucleation period occurs (at a lower supersaturation this time due to the presence of other crystals lowering the activation energy). This cycle will repeat itself until carbonate consumption by crystal growth (and nucleation) will keep up with the carbonate production rate. It has been shown that the induction period before the first crystals appear can take more than 15 minutes and the nucleation period another 15 minutes. Before the crystals have a reasonable size of several μm will take even longer.

When the different models are compared with each other, it shows that the simplified model based on a single reaction predicts the concentration of the main compounds with similar accuracy as the more complex models which take acid-base equilibria and precipitation kinetics into account. The simplified model would therefore be preferable for designing treatment procedures. However, the more complex models provide more information about relevant quantities such as the pH, supersaturation and the number and size of crystals. The development of number and size of crystals is important for the application as ground improvement method when predicting the distribution of $CaCO_3$ in the sand, which is a result of transport of reagents and bacteria and crystals through the porous medium. The supersaturation is an important factor determining the mineral properties, such as the occurrence of metastable precursors, like amorphous $CaCO_3$ or vaterite.

The choice of precipitation kinetics depends on applied process and encountered environmental conditions. E.g. in case of soil stabilization in carbonate sands a constant surface can be assumed as the grains act as a substrate for crystallization, while in the pores between the grains and in quartz sand spontaneous nucleation can takes place in the absence of nuclei.

Quantitative prediction to a level at which the pH and conductivity are simulated accurately for the combined hydrolysis and precipitation at high rate and high concentration seems still too complex. The kinetics of hydrolysis and precipitation are still not fully incorporated in the model or well controlled in the experiment. On the other hand, calculating the pH properly requires an accuracy of at least 10^{-7} M, which is

extremely accurate compared to the concentrations of the main dissolved compounds. Most other studies determining the speciation of calcium and carbon species in solution and the kinetic constants of $CaCO_3$ precipitation by measuring the pH used concentrations in the mM range (Nancollas & Reddy 1971; Reddy & Nancollas 1971; Sohnel & Mullin 1982; Kralj et al. 1990; Kralj et al. 1994; Kralj et al. 1997; Ferris et al. 2004). The deviation of the measured electrical conductivity from the expected values (Figure 15) could be the result of:

- Overestimated precipitation rate. If the precipitation rate is slower (lower k_p or k_g or higher k_N), e.g. due to diffusion limitation towards the crystal surface or physical constraints, the solution has a higher supersaturation, which could cause a temporary higher value in electrical conductivity. On the other hand the kinetic models show that higher supersaturation corresponds with higher pH, causing part of the ammonium to dissociate to ammonia, which would reduce the electrical conductivity. By performing seeded experiments at least the calculated profiles assuming thermodynamic equilibrium could be checked.

- A wrong assumption of linearity of electrical conductivity and underestimated interaction for mixed ions at high concentration.

- A variable hydrolysis rate. Several processes are identified (paragraph 2.1) which can affect the hydrolysis in time, e.g. encapsulation of cells or cell lysis could cause a decay in activity, which might explain the decreasing slope in the conductivity plot (Figure 16).

The deviation of the measured pH from the expected values (Figure 15) could be the result of:

- Gas stripping. The theoretical models show that both dissolved carbon dioxide and ammonia are present in the mM range. Considering experiments were performed in vessels open to the atmosphere these dissolved gas concentrations are well oversaturated compared to the partial pressure of these gasses in the atmosphere (0.038% for CO_2 and negligible for NH_3). Consequently, both ammonia and carbon dioxide can strip to the atmosphere. Although the amount of gas stripping is limited and probably not observed in the electrical conductivity, it could affect the pH significantly, where stripping of CO_2 increases the pH and NH_3 decreases pH. Considering the relatively low pH (7 to 7.4) and low total dissolved carbon concentration it is likely that the increase in the measured pH after about 50 minutes in both curves of figure 15 is caused by stripping of CO_2. The decrease in pH after 7 hours in the left curve is probably due to stripping of NH_3. To fit the pH curves of the model to the experiments, either the gas equilibria should be taken into account in the model or the experiments should be performed in a closed vessel with defined atmosphere on top of it.

- Precipitation of metastable mineral phases and the transition of these minerals to more stable (slower growing) phases. E.g. Kralj et al. (1997) observed the transition of the more soluble vaterite to calcite by a decrease in pH. Transition from other metastable phases will cause another response in pH. Currently new evidence is found for the existence of pre-nucleation clusters during the initial stages of crystallization (Gebauer et al. 2008; Pouget et al. 2009). The kinetics of all these precipitation and dissolution processes effect the speciation of dissolved compounds and should be taken into account to properly predict the pH and speciation.

Although the initial measurements were qualitatively in confirmation with the model(s), experimental validation is still required. Apart from testing under a wider range of conditions (e.g. varying hydrolysis rate, concentrations, temperature and in presence of various solids or in sand columns), additional variables could be measured, like ammonium and calcium concentration (using analytical methods or ion selective electrodes), particle size and mineral type during different stages in the process.

6 Conclusions

When urea is hydrolyzed at high rate (>1 M-urea day^{-1}) in a highly concentrated solution with calcium chloride (>0.25 M) the solubility product of $CaCO_3$ is exceeded within a short period (less than 30 minutes), due to the increase in pH and production of inorganic carbon. The supersaturation remains high for a long period in which the carbonate consumption rate by precipitation is in balance with the carbonate production rate by urea hydrolysis, resulting in prolonged periods of nucleation and crystal growth and extended growth of metastable mineral phases. The pH, being a result of the speciation, quickly rises until the first nuclei appear. Then pH drops (sometimes showing oscillating behaviour) to about neutral and stays there until all substrates are depleted.

The conversion of the main substrates (urea and calcium) to the main products (ammonium and calcium carbonate) can be reasonably measured with electrical conductivity. Using a simplified model based on a single reaction, the concentrations of the main compounds can be reasonably predicted as long as the urea hydrolysis rate is known. When more detailed information needs to be predicted, like the supersaturation, pH, and the number, size and type of crystals, more complex models are required including the kinetics of precipitation. In general higher hydrolysis rates lead to high supersaturation and pH and relatively many small crystals. Higher concentrations lead to a lower equilibrium pH. Accurate prediction of pH, conductivity and crystal properties is not yet possible with these models.

References

Bachmeier, K.L., Williams, A.E., Warmington, J.R. & Bang, S.S. 2002. "Urease activity in microbiologically-induced calcite precipitation." *Journal of Biotechnology* 93(2): 171-181.

Bang, S.S., Galinat, J.K. & Ramakrishnan, V. 2001. "Calcite precipitation induced by polyurethane-immobilized Bacillus pasteurii." *Enzyme and Microbial Technology* 28(4-5): 404.

Benini, S., Rypniewski, W.R., Wilson, K.S., Miletti, S., Ciurli, S. & Mangani, S. 1999. "A new proposal for urease mechanism based on the crystal structures of the native and inhibited enzyme from Bacillus pasteurii: why urea hydrolysis costs two nickels." *Structure* 7(2): 205-216.

Berner, R.A. 1975. "The role of magnesium in the crystal growth of calcite and aragonite from sea water." *Geochimica et Cosmochimica Acta* 39(4): 489-494, IN3, 495-504.

Booster, J.L., van Meurs, G.A.M., Pruiksma, J.P., van Paassen, L.A., Harkes, M. & Whiffin, V.S. 2008. 1D-modelling of microbially induced calcite precipitation for

geotechnical applications. International conference on BioGeoCivil Engineering. Delft.

Ciurli, S., Marzadori, C., Benini, S., Deiana, S. & Gessa, C. 1996. "Urease from the soil bacterium Bacillus pasteurii: Immobilization on Ca-polygalacturonate." *Soil Biology and Biochemistry* 28(6): 811-817.

Dalas, E., Kallitsis, J. & Koutsoukos, P.G. 1988. "The crystallization of calcium carbonate on polymeric substrates." *Journal of Crystal Growth* 89(2-3): 287-294.

DeJong, J.T., Fritzges, M.B. & Nusslein, K. 2006. "Microbially Induced Cementation to Control Sand Response to Undrained Shear." *Journal of Geotechnical and Geoenvironmental Engineering* 132(11): 1381-1392.

Ebrahimi, S., Picioreanu, C., Kleerebezem, R., Heijnen, J.J. & van Loosdrecht, M.C.M. 2003. "Rate-based modelling of SO_2 absorption into aqueous $NaHCO_3/Na_2CO_3$ solutions accompanied by the desorption of CO_2." *Chemical Engineering Science* 58(16): 3589.

Ferris, F.G., Phoenix, V., Fujita, Y. & Smith, R.W. 2004. "Kinetics of calcite precipitation induced by ureolytic bacteria at 10 to 20[deg]C in artificial groundwater." *Geochimica et Cosmochimica Acta* 68(8): 1701-1710.

Foppen, J.W.A. & Schijven, J.F. 2005. "Transport of E-coli in columns of geochemically heterogeneous sediment." *Water Research* 39(13): 3082-3088.

Foppen, J.W.A. & Schijven, J.F. 2006. "Evaluation of data from the literature on the transport and survival of Escherichia coli and thermotolerant coliforms in aquifers under saturated conditions." *Water Research* 40(3): 401-426.

Gal, J.-Y., Bollinger, J.-C., Tolosa, H. & Gache, N. 1996. "Calcium carbonate solubility: a reappraisal of scale formation and inhibition." *Talanta* 43(9): 1497-1509.

Gebauer, D., Völkel, A. & Cölfen, H. 2008. "Stable Prenucleation Calcium Carbonate Clusters." *Science* 322: 1819-1822.

Gilbert, P., Evans, D.J., Evans, E., Duguid, I.G. & Brown, M.R.W. 1991. "Surface characteristics and adhesion of Escherichia coli and Staphylococcus epidermidis." *Journal of Applied Bacteriology* 71(1): 72-77.

Hammes, F., Boon, N., de Villiers, J., Verstraete, W. & Siciliano, S.D. 2003. "Strain-Specific Ureolytic Microbial Calcium Carbonate Precipitation." *Appl. Environ. Microbiol.* 69(8): 4901-4909.

Hammes, F. & Verstraete, W. 2002. "Key roles of pH and calcium metabolism in microbial carbonate precipitation." *Reviews in Environmental Science and Biotechnology* 1(1): 3.

Hammes, F.A. 2003. Ureolytic microbial calcium carbonate precipitation No pp , Given.

Kralj, D., Brecevic, L. & Kontrec, J. 1997. "Vaterite growth and dissolution in aqueous solution III. Kinetics of transformation." *Journal of Crystal Growth* 177(3-4): 248-257.

Kralj, D., Brecevic, L. & Nielsen, A.E. 1990. "Vaterite growth and dissolution in aqueous solution I. Kinetics of crystal growth." *Journal of Crystal Growth* 104(4): 793-800.

Kralj, D., Brecevic, L. & Nielsen, A.E. 1994. "Vaterite growth and dissolution in aqueous solution II. Kinetics of dissolution." *Journal of Crystal Growth* 143(3-4): 269-276.

Larsen, J., Poulsen, M., Lundgaard, T. & Agerbæk, M. 2008. "Plugging of fractures in chalk reservoirs by enzyme-induced calcium carbonate precipitation." *SPE Production & Operations* 23(4): 478-483.

Lioliou, M.G., Paraskeva, C.A., Koutsoukos, P.G. & Payatakes, A.C. 2007. "Heterogeneous nucleation and growth of calcium carbonate on calcite and quartz." *Journal of Colloid and Interface Science* 308(2): 421-428.

Lyde, D.R. 2009. Electrical conductivity of aqueous solutions. *CRC Handbook of chemistry and physics*. Lyde DR.

Marzadori, C., Miletti, S., Gessa, C. & Ciurli, S. 1998. "Immobilization of jack bean urease on hydroxyapatite: urease immobilization in alkaline soils." *Soil Biology and Biochemistry* 30(12): 1485-1490.

Mitchell, A. & Ferris, F. 2006. "The Influence of Bacillus pasteurii on the Nucleation and Growth of Calcium Carbonate." *Geomicrobiology Journal* 23(3 - 4): 213.

Mullin, J.W. 2001. *Crystallization*, Oxford : Butterworth-Heinemann, 2001

Nancollas, G.H. & Reddy, M.M. 1971. "The crystallization of calcium carbonate. II. Calcite growth mechanism." *Journal of Colloid and Interface Science* 37(4): 824.

Parkhurst, D.L. 1995. "User's guide to PHREEQC--A computer program for speciation, reaction-path, advective-transport, and inverse geochemical calculations: U.S. Geological Survey Water-Resources Investigations." *Report 95-4227*: 143 p. .

Plummer, L.N. & Busenberg, E. 1982. "The solubilities of calcite, aragonite and vaterite in CO2-H2O solutions between 0 and 90[degree sign]C, and an evaluation of the aqueous model for the system CaCO3-CO2-H2O." *Geochimica et Cosmochimica Acta* 46(6): 1011.

Pouget, E.M., Bomans, P.H.H., Goos, J.A.C.M., Frederik, P.M., de With, G. & Sommerdijk, N.A.J.M. 2009. "The Initial Stages of Template-Controlled CaCO3 Formation Revealed by Cryo-TEM." *Science* 323(5920): 1455-1458.

Reddy, M.M. & Nancollas, G.H. 1971. "The crystallization of calcium carbonate : I. Isotopic exchange and kinetics." *Journal of Colloid and Interface Science* 36(2): 166.

Reichert, P. 1998. "AQUASIM 2.0 User Manual - Computer program for the identification and simulation of aquatic systems."

Scholl, M.A., Mills, A.L., Herman, J.S. & Hornberger, G.M. 1990. "The influence of mineralogy and solution chemistry on the attachment of bacteria to representative aquifer materials." *Journal of Contaminant Hydrology* 6(4): 321-336.

Söhnel, O., Garside, J. 1992. *Precipitation: Basic principles and Industrial Applications*. Oxford, Butterworth-Heinemann Ltd.

Sohnel, O. & Mullin, J.W. 1982. "Precipitation of calcium carbonate." *Journal of Crystal Growth* 60(2): 239.

Stocks-Fischer, S., Galinat, J.K. & Bang, S.S. 1999. "Microbiological precipitation of $CaCO_3$." *Soil Biology and Biochemistry* 31(11): 1563-1571.

Tai, C.I. & Chen, P.-C. 1995. "Nucleation, agglomeration and crystal morphology of calcium carbonate." *AIChE Journal* 41(1): 68-77.

Teng, H.H., Dove, P.M. & De Yoreo, J.J. 2000. "Kinetics of calcite growth: surface processes and relationships to macroscopic rate laws." *Geochimica et Cosmochimica Acta* 64(13): 2255-2266.

Torkzaban, S., Tazehkand, S.S., Walker, S.L. & Bradford, S.A. 2008. "Transport and fate of bacteria in porous media: Coupled effects of chemical conditions and pore space geometry." *Water Resources Research* 44(4): 12.

Udert, K.M., Larsen, T.A., Biebow, M. & Gujer, W. 2003. "Urea hydrolysis and precipitation dynamics in a urine-collecting system." *Water Research* 37(11): 2571.

van Loosdrecht, M.C., Lyklema, J., Norde, W., Schraa, G. & Zehnder, A.J. 1987. "The role of bacterial cell wall hydrophobicity in adhesion." *Applied and Environmental Microbiology* 53(8): 1893-1897.

Vanýcek, P. 2009. Ionic Conductivity and diffusion at infinite dilution. *CRC Handbook of chemistry and physics*. Lide DR, Taylor & Francis Group: 76-78.

Whiffin, V.S. 2004. *Microbial CaCO3 Precipitation for the production of Biocement*. Science and Engineering, School of Biological Sciences & Biotechnology Perth, Western Australia, Murdoch University. Ph.D thesis 154.

Whiffin, V.S., van Paassen, L.A. & Harkes, M.P. 2007. "Microbial Carbonate Precipitation as a Soil Improvement Technique." *Geomicrobiology Journal* 24(5): 417-423.

Wolf, G., Picioreanu, C. & Van Loosdrecht, M.C.M. 2007. "Kinetic Modeling of Phototrophic Biofilms: The PHOBIA Model." *Biotechnology and Bioengineering* 97(5): 1064-1079.

Supplementary material

Table 4 Maximum yields and specific activity for different media compositions in a shake flask cultivations of Sporosarcina pasteurii.

| Medium	Amount of bacteria $[OD_{600nm}]$	Maximum specific urease activity $[mS\ cm^{-1}\ min^{-1}\ OD^{-1}]$
Yeast extract 20 g L^{-1}, urea 10 g L^{-1}, $NiCl_2.6H_2O$ $4.5 \cdot 10^{-3}$ g L^{-1}	0.81	0.024
Tryptone 10 g L^{-1}, Yeast extract 5 g L^{-1}, NaCl 10 g L^{-1}, Urea 20 g L^{-1}, pH adjusted to 7 (NaOH / HCl) before autoclaving	0.70	0.019
Yeast extract 20 g L^{-1}; $(NH_4)_2SO_4$ 10 g L^{-1}; Tris.HCl 130 mM (pH 9); Individual ingredients were autoclaved separately and mixed afterwards	1.40	0.42
Yeast Extract 7 g L^{-1}; Urea 20 g L^{-1}; Tryptone 5 g L^{-1}; Meat peptone 5 g L^{-1}	0.74	0.20
Marmite (Unilever) 54 g L^{-1}; Urea 10 g L^{-1}; $NiCl_2.6H_2O$ $4.5 \cdot 10^{-3}$ g L^{-1}	0.80	0.086
Yeast extract 20 g L^{-1}; Urea 10 g L^{-1};	1.93	0.22
Yeast extract 20 g L^{-1}; $(NH_4)_2SO_4$ 10 g L^{-1}	3.52	0.36
Yeast extract 20 g L^{-1}; NH_4Cl 10 g L^{-1}	3.82	0.38
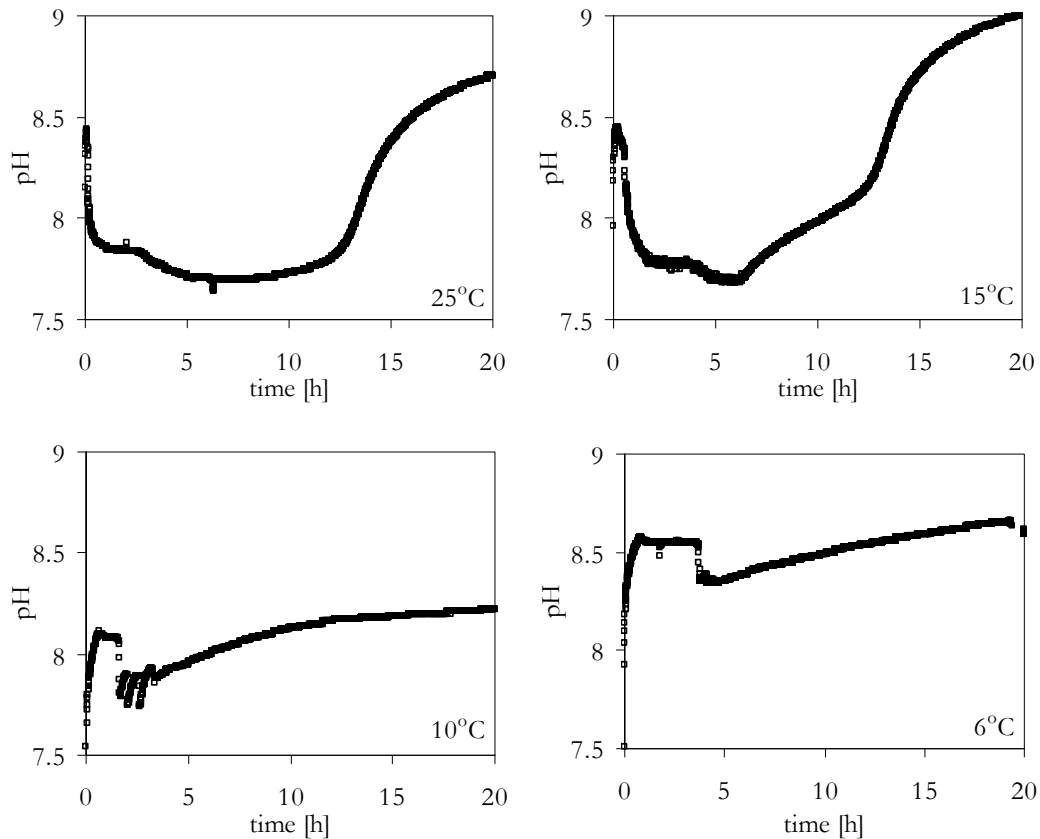
Figure 18 Measured pH profiles during the initial 20 hours of stirred batch precipitation experiments at different temperatures using 1 M urea and 1 M CaCl$_2$ with similar amounts of added bacteria. At 25°C the pH curve shows reasonable correspondence with the calculated pH profiles (figures 11 and 13). Still some differences were observed: The decrease in pH after reaching the peak supersaturation is much faster in the experiment compared to the model. pH drops to a level of 7.8 where it remains constant for about 2 hours and then drops again to about 7.7. Similar profiles are observed for the transition of vaterite to calcite Kralj et al. (1997). When substrates are depleting after 15 hours pH starts to rise above 8.5. The pH curve at 15°C show a similar unexplainable increase after 6 hours, which is observed in figure 15, but here the pH rises to about 9. At 10°C the pH remains stable for about 1 hour. After an initial drop pH oscillates for another 2 hours and then immediately rises. For 6°C the stable pH is maintained for 5 hours, before it drops by 0.2 and starts to rise as well.

3

## Crystal characteristics of calcium carbonate induced by microbial hydrolysis of urea

Abstract

Calcium carbonate ($CaCO_3$) is a polymorph meaning that several mineral types exist with similar molecular composition. The crystal properties (size, shape, mineral type) can vary depending on the precipitation conditions. In this study we investigated the characteristics of calcium carbonate crystals formed by microbially catalyzed hydrolysis of urea in a highly concentrated solution with calcium chloride, based on experimental observation. By varying the precipitation conditions in stirred and unstirred suspension and flushed sand columns we determined which factors affected the crystal characteristics. The $CaCO_3$ mineral type depended mainly on the urea hydrolysis rate: At high hydrolysis rate, spherical vaterite crystals were formed, whereas at low hydrolysis rate rhomboidal calcite crystals were dominant. Crystal properties were also influenced by transport limitations and sand grain properties. Apart from hydrolysing urea the bacterial cells were not found to significantly affect the crystal characteristics, e.g. by acting as a nucleation site. The experimental results are in line with conventional precipitation theory and observations in literature. The occurrence of vaterite and its effect on the mechanical behaviour of cemented ground are considered limited when applying microbially induced carbonate precipitation for ground improvement applications.

1 Introduction

Microbially induced carbonate precipitation (MICP) is gaining increased attention for its application in improving the physical properties of porous solid materials. Typical examples are: surface restoration of monuments and buildings (Castanier et al. 2000), clogging of pores and cracks in rocks (Nemati and Voordouw 2003), or the reinforcement of sand (DeJong et al. 2006; Whiffin et al. 2007). In most of these studies the MICP process involves microbial hydrolysis of urea. When bacteria with ureolytic activity are mixed or injected into a porous material and supplied with a solution of urea, the urea is hydrolysed to ammonium and carbonate:

$$CO\left(NH_2\right)_2 + 2\,H_2O \xrightarrow{\;urease\;} 2\,NH_4^+ + CO_3^{2-} \tag{1}$$
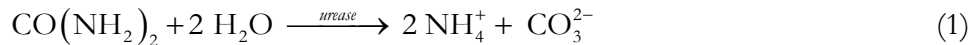
In the presence of dissolved calcium ions, the microbially produced carbonate precipitates and solid calcium carbonate crystals are formed:

$$Ca^{2+} + CO_3^{2-} \rightarrow CaCO_3\left(s\right) \tag{2}$$
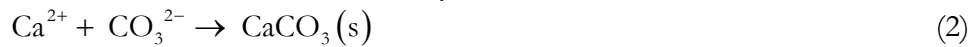
These crystals partially fill the pore space and thereby decrease the porosity and permeability of the sand. They also form a coating on the grains or bridges between them, resulting in an improvement in strength and stiffness of the material.

Control of the MICP process and prediction of the resulting material properties (such as, porosity, strength, stiffness and permeability) are essential for its use in improving the engineering properties of porous solid materials. Empirical correlations have been found between the amount of precipitated calcium carbonate and soil engineering parameters, like porosity, strength, stiffness and permeability (Ismail et al. 2002a; Ismail et al. 2002b; Whiffin et al. 2007). However, such correlations are in general relatively weak, as the engineering parameters of cemented sediments depend on many factors. Using a $CaCO_3$ cementation method called "Calcite In situ Precipitation System (CIPS)", in which two fluids were mixed, rapidly injected in a sand column and left to precipitate for several hours, it was shown that the resulting strength of two cemented sand columns having the same amount of $CaCO_3$ depended on the concentration of the cementing solution and the rate at which $CaCO_3$ precipitated (Ismail et al. 2002a). For each concentration a precipitation rate existed at which the resulting compressive strength was optimal. The authors also showed that the resulting strength was very different in siliceous sand compared to calcareous sand. An explanation for the observed differences in strength was not provided.

Microscopic observations from experiments using MICP by urea hydrolysis or CIPS (Ismail et al. 2002a; Mitchell and Ferris 2006; Warren et al. 2001) and natural $CaCO_3$ occurrences in the subsurface (Morse and Mackenzie 1990) showed that calcium carbonate minerals can vary significantly in mineral type, shape, size and texture. The different properties and spatial distribution of the calcium carbonate crystals might give an explanation for the observed differences in resulting engineering properties at similar amount of $CaCO_3$.

The aims of this study were two-fold. First, to get an overview of the observed crystal characteristics of calcium carbonate precipitated by microbial hydrolysis of urea in

ground reinforcement applications. Second, to provide insight in the conditions that control the observed crystal characteristics, using controlled batch experiments and precipitation theory. Further, the implications of the crystal properties on the resulting engineering properties and treatment protocol for ground reinforcement are also discussed.

2   Materials and methods

2.1   MICP experiments in sand environments

To test the feasibility of microbially induced carbonate precipitation (MICP) as ground reinforcement method, many experiments have been performed in which sand was flushed with bacterial suspension. Samples of $CaCO_3$ crystals presented in this paper are taken from sand columns (length 20 cm, diameter 4.5 cm) containing three sand types provided by (Kucharski et al. 1996): A white siliceous sand (Silica F), a grey calcareous sand (Calcareous M) and a yellow siliceous sand (Silica M). About 18 cm of sand was packed between two porous filters and a layer of 1 cm gravel. The columns were flushed with one pore volume (150 mL) of bacterial suspension with an activity of 130 mM urea h^{-1} at a flow rate of 300 mL h^{-1}. Afterwards the columns were left overnight in order to let the bacteria settle from the suspension and adhere to the sand grains. Next morning, a 150 mL solution of 0.5 M $CaCl_2$ was injected with a flow rate of 300 mL h^{-1}. The presence of Ca^{2+}-ions causes bacteria to flocculate and improves settlement and attachment of the bacteria to the sand grains (Whiffin et al. 2007). The first 150 mL effluent, still containing some washed out bacteria, was collected and re-injected after the 0.5 M $CaCl_2$ pulse at the same flow rate. After recycling the bacterial suspension, the effluent liquid showed very little turbidity indicating that no or very little bacteria were flushing out. Finally, the columns were flushed with 1 litre of solution containing 0.5 M urea and 0.5 M $CaCl_2$, which was recycled through the column for 24 hours, at a flow rate 100 mL h^{-1}. Afterwards the columns were rinsed with water and dried. After drying the samples were prepared for XRD and SEM analysis to analyse the crystal properties. Samples for SEM analysis were taken from the different sand types at various distances from the inlet. Samples of precipitate for XRD analysis were scraped from the inlet and outlet filters.

2.2   Unstirred batch experiments in a liquid suspension

To determine the effect of urea hydrolysis rate on crystal properties batch experiments were performed using unstirred liquid suspensions. A thin glass slide was placed tilted in a 30 mL plastic jar. The jar was filled successively with solutions of $CaCl_2$ and urea, water and a bacterial suspension up to a total volume of 20 mL and in such a way that each suspension contained 1M $CaCl_2$, 1M urea and had an initial hydrolysis rate ranging from approximately 9 to 180 mM urea h^{-1}. The suspensions were left reacting for 20 hours at room temperature, after which the liquid was removed. The crystals, attached to the glass slides and the side of the plastic jar, were rinsed with water and chemically dried by flushing with ethanol and acetone, then observed with an optical microscope. After microscopic observation the precipitate was collected for powder XRD analysis.

2.3   Stirred batch experiments in a liquid suspension

To determine the effect of transport conditions experiments were performed using stirred liquid suspensions. A glass bottle was filled successively with solutions of $CaCl_2$ and urea, water and bacterial suspension up to a total volume of 200 mL and in such a way that the final suspensions contained a concentration of 1 M $CaCl_2$ and 1 M urea and variable amounts of bacterial suspension, resulting in initial hydrolysis rates ranging from 30 to 60 mM urea h^{-1}. At regular time intervals after the addition of the bacteria samples of the suspension were taken (including the bacteria and crystals) to collect the solid precipitates. The precipitates were filtered from the suspension, rinsed and dried at 55ºC. and used for powder XRD and SEM analysis.

2.4   Microscope slide experiments

To visually observe crystal development in time, experiments were performed on a microscope slide. A drop (50 µL) of solution, containing dissolved urea and $CaCl_2$ was placed on a microscope slide together with a similar drop of suspension containing bacteria, resulting in initial concentrations of 1M urea and 1M $CaCl_2$ and an initial urease activity of approximately 170 mM urea h^{-1}. A cover slip was placed on top of the drop and the edges of the cover slip were sealed using nail polish. The slide was then placed under an optical microscope to follow the growth of crystals in time. After 1 week of incubation at room temperature the slides were analyzed using scanning electron microscopy (SEM) to study the resulting crystal morphologies in more detail.

2.5   Cultivation of bacteria

For each experiment, a bacterial suspension was used containing the urease positive microorganism *Sporosarcina pasteurii* (DSMZ 33), which was isolated from soil. Cultivation of the organism was conducted under aerobic batch conditions at 30ºC. in a heat sterilized (121ºC.) medium containing 20 g L^{-1} yeast extract, 10 g L^{-1} NH_4Cl and 10 µM $NiCl_2$. After sterilization pH was adjusted to 8.5 before inoculation. The organism was grown to early stationary phase (i.e., no increase in optical density and urease activity indicating all readily available nutrients were consumed from the medium), and stored at 4°C for maximum two weeks prior to use. Before each experiment, the urease activity of the bacterial suspension was measured. Tests were performed at different initial bacterial activities. When not measured during the experiment, the mentioned bacterial activity in this paper is always the activity measured in the suspension, just after the bacteria were added to the solution containing the reagents.

2.6   Analyses

X-ray diffraction (XRD). Powder XRD was performed using Cu-Kα radiation, with 2θ between 10 and 90 degrees. The XRD results were compared with typical diffraction spectra for calcite and vaterite (e.g. as in (Ismail et al. 2002a)). From the XRD results the relative abundances of the different calcium carbonate minerals were quantified by comparing the ratios of the integral area of the major characteristic peaks with measured ratios in a sample of known composition.

Microscopic analysis was performed using several optical microscopes with variable magnification (25x to 400x) and built-on digital cameras. SEM analysis was performed using a Philips XL30 ESEM Tungsten filament electron microscope.

Urease activity was determined either prior to an experiment using a conductivity method (Whiffin, 2004) or during an experiment by determining the ammonium concentration according to a modified Nessler method (Whiffin et al. 2007) and divide this concentration by stoichiometric ratio and the reaction time.

3 Results

3.1 Sand experiments
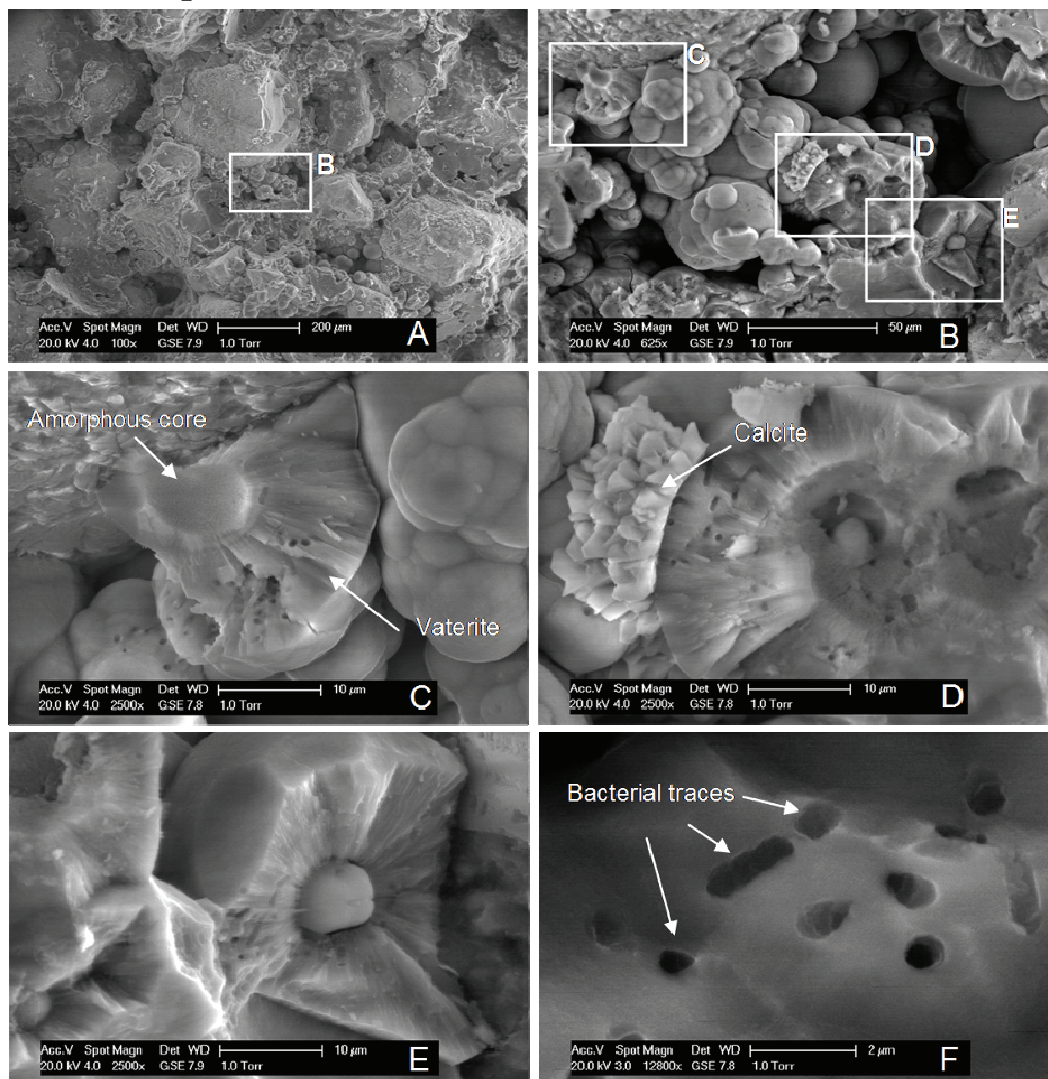
Figure 1: SEM images of a sample of siliceous sand containing calcium carbonate crystals formed by microbially induced hydrolysis of urea collected at 1 cm from the inlet of a sand column: (A) A 100x magnification shows that sand grains are hard to distinguish as they are fully covered with calcium carbonate precipitate; (B) A 625 x magnification shows that agglomerated spherical crystals, up to 50 μm in size, form bridges between the sand grains; (C and E) At a 2500x magnification some dissected spheres show typical layering: a non crystalline core, surrounded by a more crystalline layer up to 20 μm thick (likely vaterite); (D) In some cases the core is absent and the second layer is covered with agglomerated rhomboids (likely calcite); (F) At the highest magnification (12800x) bacterial imprints leaving holes in the crystalline structure are clearly visible.

SEM images of a sample of cemented white siliceous sand collected at 2 cm from the inlet of the sand column showed that the pores between the siliceous sand grains were heavily filled with spherical crystals (figure 1A). The spheres had sizes up to 50 μm and formed bridging networks between the sand grains (figure 1B).

Some spheres were cracked and their dissections showed they consisted of several layers: a core of less crystalline texture, 5 to 10 μm in diameter (figure 1C-E), surrounded by a layer of more crystalline material, optically reminding of vaterite, with variable thickness 2-20 μm depending on the crystal size. Within this layer holes were present, which are likely places where bacteria were trapped in the growing crystal lattice. The SEM method - beaming electrons on an uncoated sample - burns away organic material, leaving a black imprint in the crystal surface (figure 1F). In some cracked spheres the core was absent, possibly dissolved, and sometimes the second layer was covered by a third layer consisting of agglomerated rhomboids (figure 1D).

SEM images of a sample of calcareous sand collected at 10 cm from the inlet (figure 2) showed a different picture. The calcareous sand grains were fully covered by a thin layer (figure 2 A,B) of small precipitated rhomboidal crystals. At the contacts between the grains the rhomboids overlapped (figure 2C). Imprints of bacteria, like in figure 1, were not observed on this sample. SEM images of a sample of yellow siliceous sand collected at 15 cm from the inlet showed a thin layer of small rhomboidal crystals, similar to figure 2.
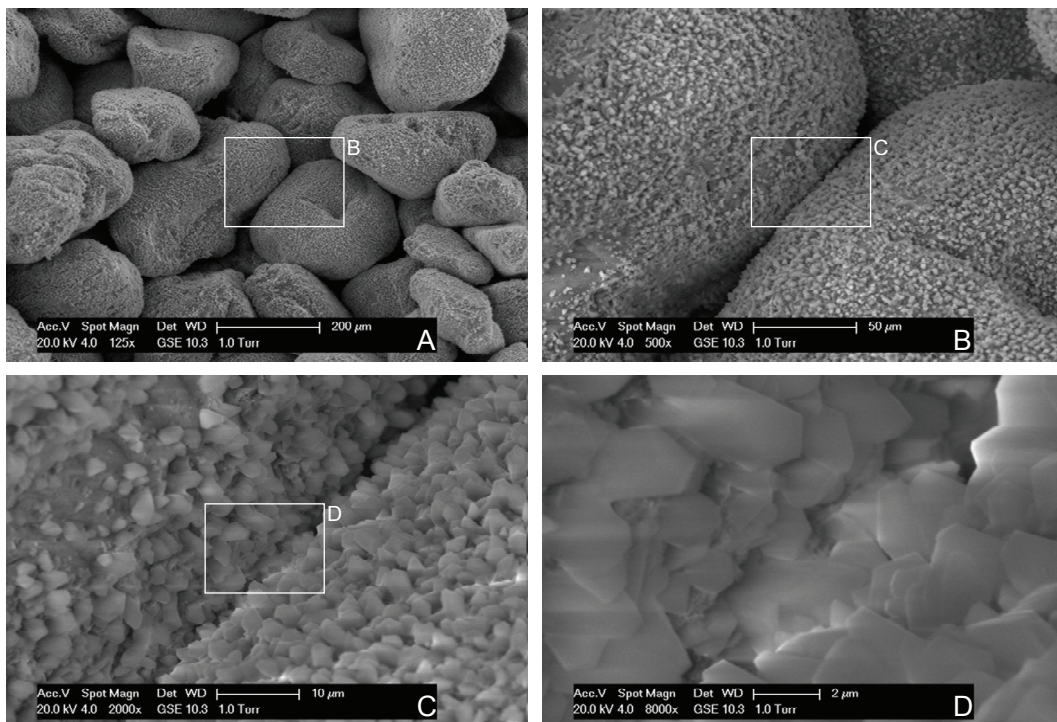

Figure 2: SEM images of a sample of calcareous sand containing calcium carbonate crystals formed by microbially induced hydrolysis of urea collected at 10 cm from the inlet of a sand column: (A-B) Sand grains are fully covered with a thin layer of calcite crystals, 2-5 μm in size; (C). At the grain contacts the calcite crystals overlap.

XRD analysis of the precipitate scraped from the inlet filter showed a mineral composition of about 70% vaterite and 30% calcite, while the precipitate collected from the outlet filter was identified as pure calcite.

3.2 Unstirred batch experiments in a liquid suspension

Microscopic analysis of the precipitates formed on the glass slides immersed in the unstirred cementation solution after 20 hours of incubation showed a clear relationship between bacterial urease activity and crystal characteristics (figure 3). Firstly, the higher the bacterial activity the more crystals were formed. Secondly, the crystal morphology changed as a function of bacterial activity. For activities higher than 40 mM urea h^{-1} mainly spherical crystals were observed, while below 4 mM urea h^{-1} rhomboidal crystals with clearly visible crystal faces were dominating the precipitate.
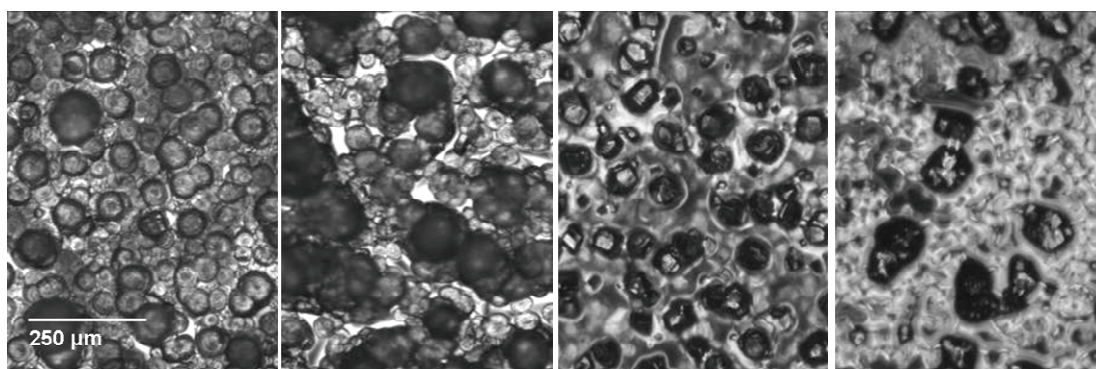

Figure 3: Microscopic images of precipitate formed on submerged glass slides in an unstirred liquid suspension containing urea hydrolyzing bacteria, 1M urea and 1M CaCl₂. The initial urease activities varied: from left to right 44, 22, 4.4, and 2.2 mM urea h^{-1}. Samples were taken after 20 hours incubation at room temperature. With decreasing hydrolysis rate the number of crystals decreases, and the most frequent shape changes from spherical to rhomboidal.

The change in crystal morphology appeared gradually when the activity was between 4 and 20 mM urea h^{-1}. XRD analyses of the precipitates (figure 4 and 5), showed that when the hydrolysis rate increased from 9 to 36 mM urea h^{-1}, the relative abundance of vaterite increased from 5 to 90%, while the amount of calcite decreased. At higher activities (90 and 180 mM urea h^{-1}), the amount of calcite slightly increased, while vaterite remained highly abundant. Microscopic observations of crystal type and shape correlate well with those obtained by XRD. Apparently the spherical crystals, which were preferably formed at urea hydrolysis rates higher than 30 mM h^{-1}, were vaterite. The rhombiodal crystals, which were preferably formed at bacterial activities lower than 10 mM urea h^{-1}, were calcite.

3.3 Stirred batch experiments in a liquid suspension

SEM images of precipitate samples taken from a stirred liquid suspension containing urea hydrolysing bacteria with an initial hydrolysis rate of 60 mM urea h^{-1}, 1 M urea and 1M CaCl₂ after 4 hours of incubation showed all crystals were spherical (Figure 6). The spheres had a maximum size of 30 μm. On most of the spheres black imprints of bacteria were seen on the crystal surface. Some spheres were cracked, which is probably a result of the SEM sample preparation and also suggests that some spheres were hollow.
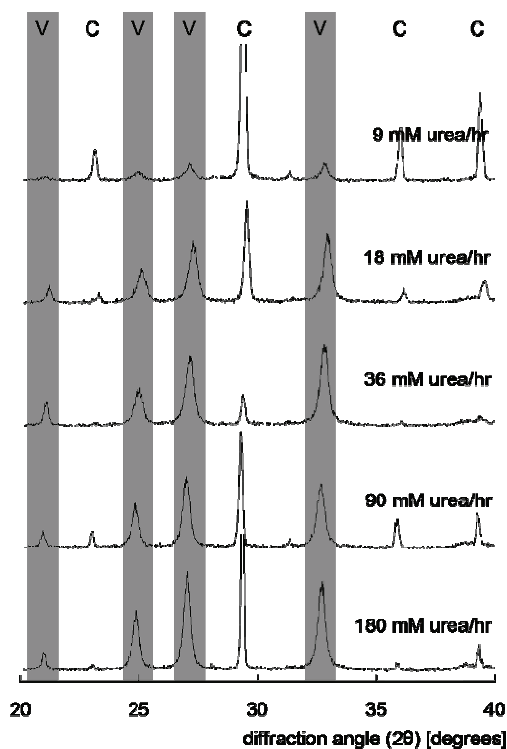
Figure 4: Diffractograms of precipitates formed in an unstirred liquid suspension containing urea hydrolyzing bacteria, 1M urea and 1M CaCl2. The initial urease activities varied from 9 to 180 mM urea h^{-1}. Samples were taken after 20 hours incubation at room temperature. The peaks marked with 'C' at 23, 29.6, 36 and 39.4 degrees are characteristic for calcite and those marked with 'V' at 21, 24.8, 27 and 32.8 degrees are characteristic for vaterite. At a hydrolysis rate of 9 mM urea h^{-1} almost no vaterite is observed, while at 36 mM urea h^{-1} the precipitate is almost entirely vaterite. At higher hydrolysis rates the amount of vaterite is still high but the amount of calcite increases.
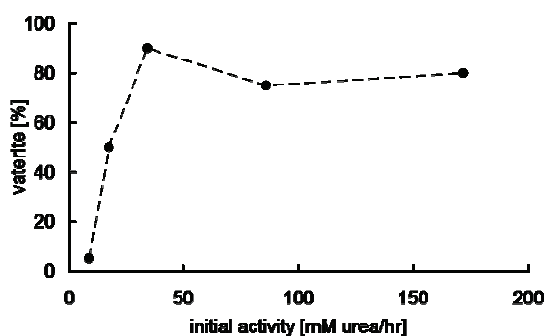

Figure 5: Quantitative interpretation of the X-ray diffractograms in Figure 4 showing the relative abundance of vaterite as a function of bacterial activity.

XRD analyses of samples taken at several times from a stirred liquid suspension with an initial urease activity of 33 mM urea h^{-1} and 1M urea/CaCl$_2$ showed that the only mineral formed after 1 and 8 hours of incubation was vaterite (Figure 7). XRD analysis of the precipitate taken some 20 days after the stirring was stopped, showed that the vaterite, which was left to settle in the liquid, was not transformed into calcite, but remained the main solid phase (Figure 7).
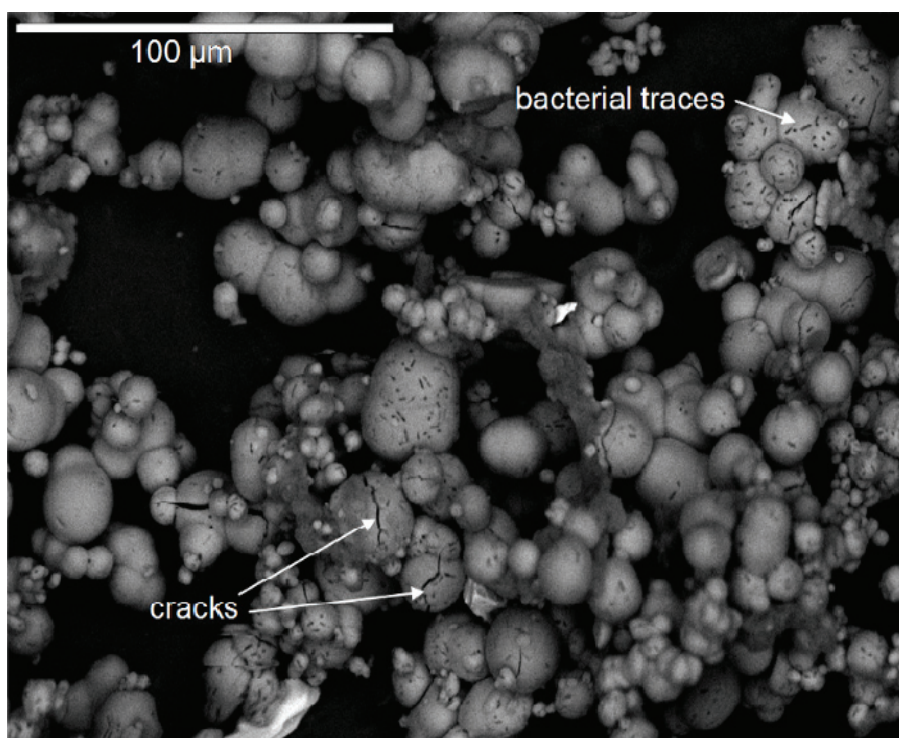
Figure 6: SEM image of precipitate formed in a stirred liquid suspension containing urea hydrolysing bacteria with an initial hydrolysis rate of 60 mM urea h^{-1}, 1 M solution of urea and CaCl$_2$ The sample was obtained after 4 hours of incubation. The crystals grew up to 30μm in size, were spherical in shape and clustered together. Most crystals have black imprints of bacteria and some are cracked.

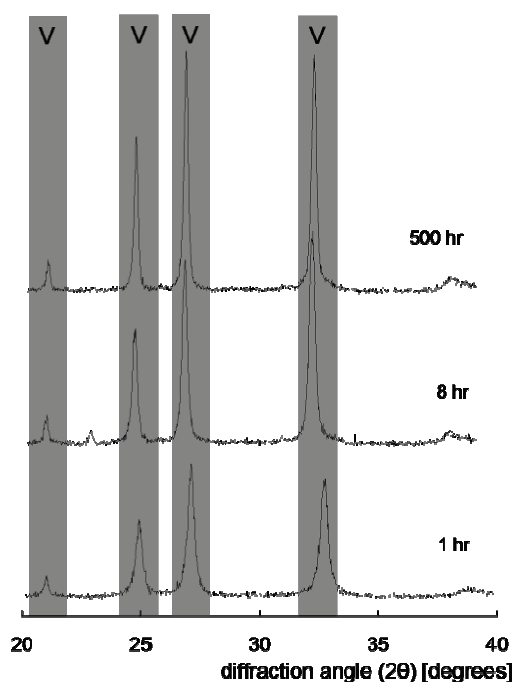*Figure 7: Diffractograms of precipitate formed in a continuously stirred batch experiment at an initial rate of 33 mM urea h^{-1} in a 1M solution of urea and CaCl$_2$. Samples taken during the stirring phase after 1 and 8 hours show only the presence of vaterite. After 48 hours the stirring is stopped and the precipitate is left to settle in the liquid. The sample taken after 500 hours still shows only vaterite.*

3.4 Microscope slide experiments

Some minutes after bacteria were added to the urea/CaCl$_2$ solution (activity of 170 mM urea h^{-1}) spherical crystals appeared randomly distributed over the slide, some within or attached to bacterial flocs, others away from the bacteria. Most of the crystals were spherical in shape (figure 8). Some had the shape of dumbbells (figure 9). At the core of these dumbbells black rods were distinguished indicating the bacteria had acted as nuclei. After 2 hours no more new crystals appeared on the slide, indicating the end of the nucleation phase. The existing crystals continued to grow. After 20 hours the spheres had grown up to a maximum size of approximately 50 µm. The slides were then left to rest for one week.
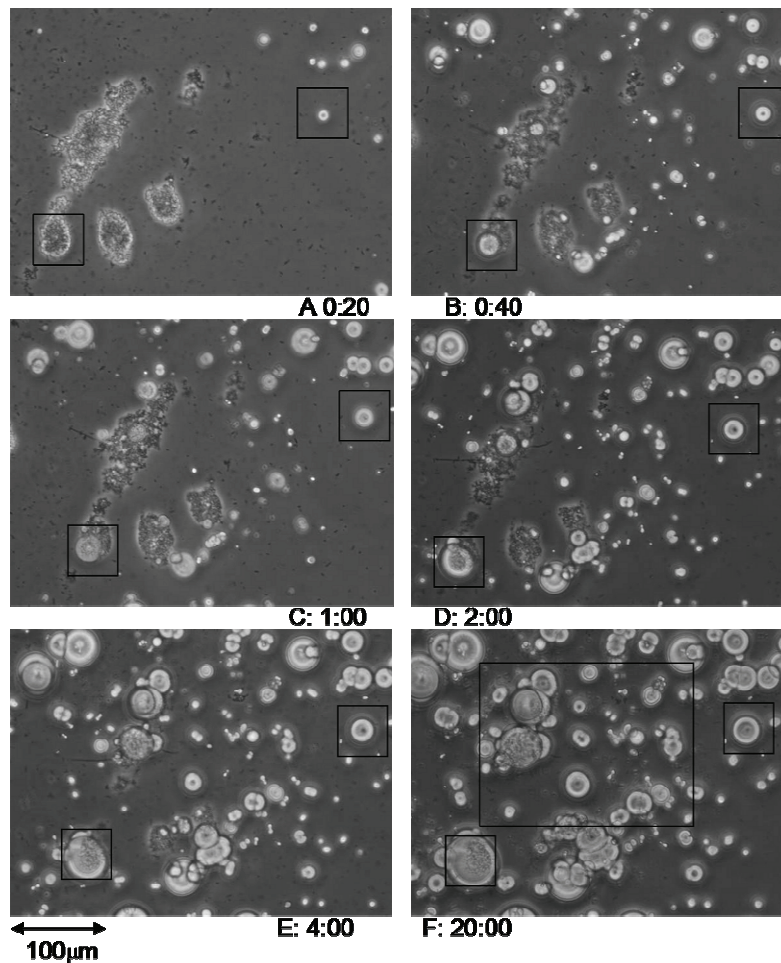

Figure 8: The growth of crystals is followed during a continuous observation of a batch precipitation on a microscope slide, using 125 mM Urea/CaCl2 solution and an bacterial activity of 170 mM urea h^{-1}. At different times from the start of the experiment a photo is taken: 20, 40 minutes and 1, 2, 4 and 20 hours. Most crystals initiate within 1 hour. Afterwards, most of the crystals grow spherically. The squares in the pictures are drawn around single crystals to follow their growth in time. The rectangle in figure 8F shows the area of Figure 9A.

SEM images of slides incubated for 1 week showed typically two shapes of mineral precipitates, spherulites and rhomboids (figure 10). The spherulites had a typical size of 20 - 40 µm, a smooth outer surface and formed agglomerations with smooth contacts.

Some of the spheres were hollow, probably showing signs of dissolution, with sometimes agglomerated crystalline material inside. Other spheres did not show a smooth outer surface but were covered by rhombiodal crystals. The rhomboids also appeared as agglomerations of 20 - 40 µm, either attached to a spherulite or away from it. The individual rhomboids had a size of 2 to 6 µm.
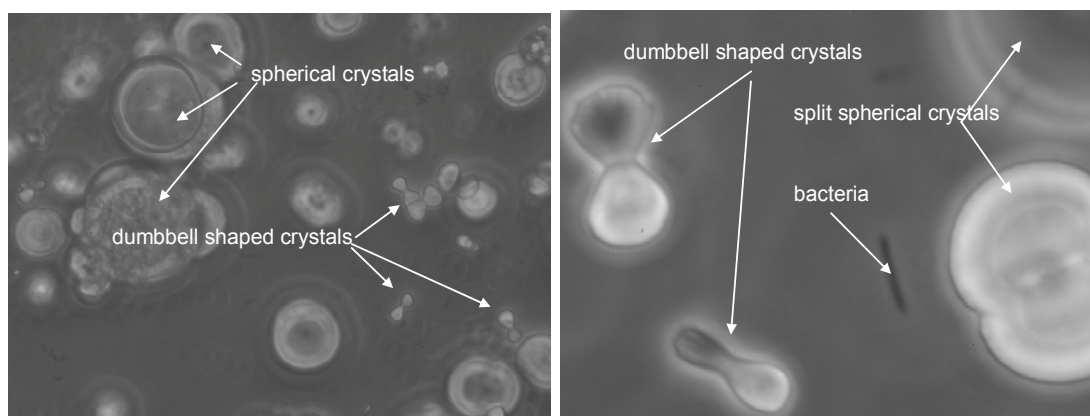

Figure 9: Detail of figure 8F showing that next to the spherical "vaterite" crystals some 'dumbbell shaped' crystals have formed. Zooming in on these dumbbells (Figure 9B) showed that some crystals contained a black rod as core, likely to be a bacterial cell, which acted as nucleation site. Some of the spherical crystals seem to be composed of 2 or 3 sections, perhaps as a result of bacteria acting as a crystal nucleus.
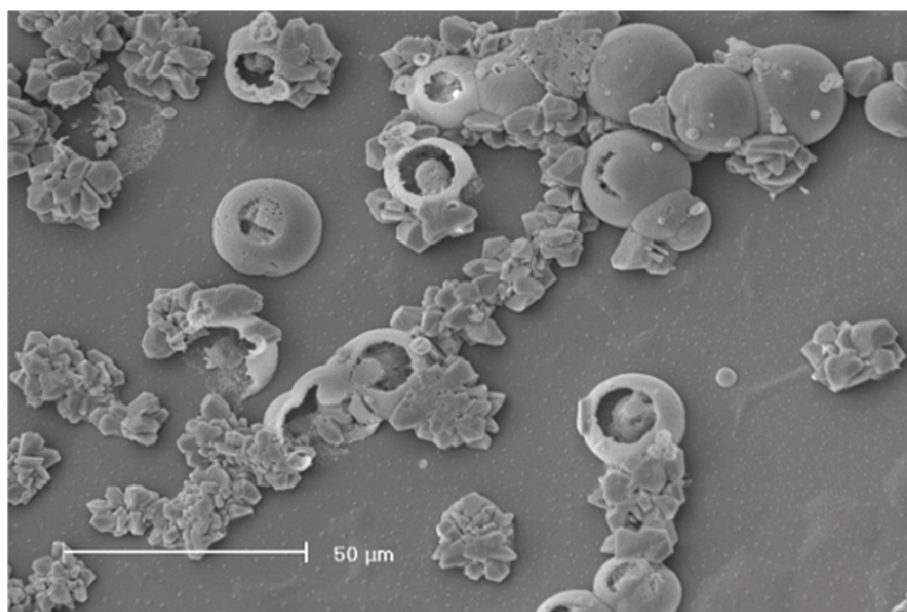

Figure 10: SEM image of calcium carbonate crystals on a microscope slide incubated for 1 week at room temperature in a suspension initially containing bacteria with a urease activity of 170 mM urea h^{-1}, 1 M urea and 1MCaCl₂. The image shows a mixture of spherical crystals and agglomerated rhombiodal crystals. The spherical crystals are sometimes hollow with crystalline material inside.

4 Discussion

The variety in crystal properties as observed in the different experimental environments is in agreement with general precipitation theory e.g. (Söhnel 1992). According to this theory, different $CaCO_3$ mineral types can be formed, each having a different crystal

lattice and solubility product and resulting from a different growth mechanism (mononuclear, polynuclear, spiral growth) as a function of supersaturation, temperature and the solution chemistry (Plummer & Busenberg 1982; Gal et al. 1996; Teng et al. 2000). At high supersaturation precipitation of metastable phases (amorphous $CaCO_3$, $CaCO_3.H_2O$ and vaterite) is kinetically favored over the more stable mineral calcite, which is also directly formed at lower supersaturation levels (Kralj et al. 1990; 1994; 1997). In presence of magnesium aragonit e is formed instead of the more stable calcite (Berner 1975). At low temperatures, Ikaite ($CaCO_3.6H_2O$) can be a stable mineral phase (Gal et al. 1996). The crystal growth rate for each of these mineral phases is directly related to the supersaturation in the solution. For large crystals the supersaturation at the surface of the crystal can be lower than in the liquid due to diffusion limitation. Assuming crystals grow spherically (Sohnel & Mullin 1982), the crystal growth rate is described by:

$$r_g = \frac{dR}{dt} = k_g \left(S - 1 \right)^2$$

(3)

In which R is the crystal radius, k_g is the growth rate constant which is derived empirically and depends on the growth mechanism, mineral type and temperature. S is the supersaturation for the specific mineral phase, which is defined as:

$$S = \frac{c}{c_{eq}} = \sqrt{\frac{IAP}{K_{sp}}}$$

(4)

In which IAP is the ionic activity product of calcium and carbonate in solution and K_{sp} is the solubility of the specific mineral phase. As vaterite has a higher solubility product than calcite, but also a higher rate constant, precipitation of vaterite is kinetically favoured over the more stable calcite at high supersaturation levels. E.g. figure 11 shows that at 25°C the growth and at a supersaturation (for calcite) above 2.3 vaterite growth is preferred over calcite growth.
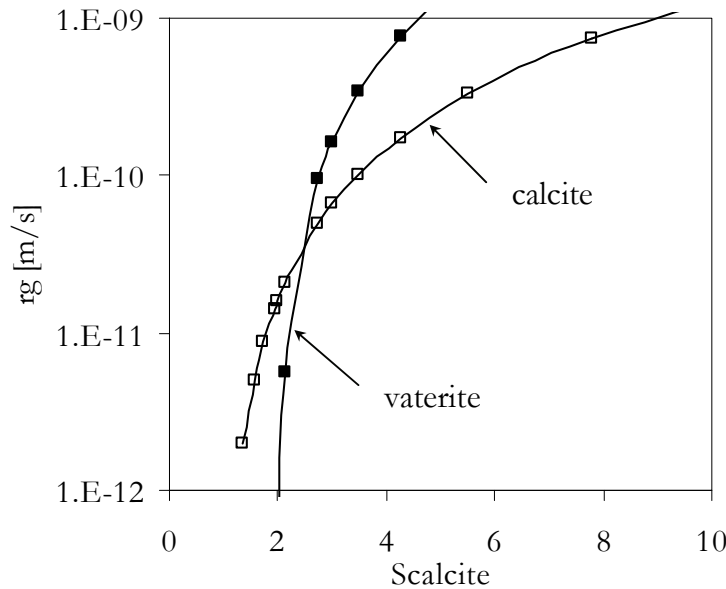

Figure 11 Theoretical crystal growth rate for vaterite (■) and calcite (□) at 25°C) after Kralj et al (1990; 1994; 1997) using pK_{sp} at 8.48 and 7.91 and k_g at $1.8 \cdot 10^{-11}$ and $5.6 \cdot 10^{-10}$ for calcite respectively vaterite. Above $S_{calcite}$ of 2.3 vaterite growth is kinetically favored over calcite.

Based on the experimental results, the factors of the MICP process, which influence crystal nucleation, growth, dissolution and recrystallization are discussed, in particular: urea hydrolysis rate, transport regime, presence of bacteria and presence of sand particles.

4.1 Effect of urea hydrolysis rate

Hydrolysis of urea results in a continuous production of carbonate, as long as urea is available. The continuous production of carbonate results in a prolonged period of supersaturation. A high hydrolysis rate corresponds to a high supersaturation, which remains high for a longer period of time. Consequently, prolonged growth of metastable precursors, like vaterite, is very likely as observed in the controlled batch experiments with hydrolysis rates greater than around 20 mM urea h^{-1} (Figure 5). The dissolution of metastable phases and recrystallization into the more stable calcite is prevented as long as carbonate is produced at a sufficient rate. When supersaturation drops, e.g. when urea gets depleted causing the hydrolysis rate to decrease, calcite growth becomes kinetically favoured over vaterite. This could be the reason for the increase in relative abundance of calcite in the batch experiments at higher hydrolysis rates. At 90 and 180 mM urea h^{-1}, 1M urea is consumed within 10 or respectively 5 hours (Figure 4 and 5). A drop in hydrolysis rate might also explain the occurrence of calcite crystals forming a crust on top of the vaterite as seen in figure 1. Further decrease of the ionic activity product below the solubility product of the amorphous calcium carbonate or vaterite, causes these metastable phases to dissolve and recrystallize as calcite, which is also seen in figure 10.

Another explanation for the increase in relative abundance of calcite at high hydrolysis rates (Figure 4 and Figure 5) could be a prolonged nucleation. A longer nucleation phase results in relatively more and smaller crystals and hence a higher total crystal surface area. When a lot of crystallizing surface is available, supersaturation drops more quickly and dissolution and recrystallization are accelerated.

Most studies on MICP by urea hydrolysis and also by other metabolic pathways showed calcite as the predominant mineral phase (Bachmeier et al. 2002; Ferris et al. 2004; Mitchell and Ferris, 2006; Stocks-Fischer, 1999). The maximum hydrolysis rate in these reported experiments varying between 0.15 and 10 mM urea h^{-1}, compared to the 9 to 180 mM urea h^{-1} in this study, which explains the absence of vaterite in these experiments. Warren et al. (2001) showed also vaterite formation at high urea hydrolysis rates and Xyla et al. (1991) ascribe the formation of vaterite to conditions of sustained supersaturation. Castanier et al. showed that amorphous and other metastable phases formed at eutrophic conditions, while calcite is formed at oligotrophic conditions (Castanier et al. 2000), which is in correspondence with our results considering eutrophic conditions are characterized by high conversion rates.

4.2 Effect of transport regime

Crystal growth requires the supply of ions towards the crystal surface. The transport conditions of solutes and bacteria can affect the supply of precipitating ions towards the crystal surface and hence affect the crystal properties (Söhnel, 1992). The layered structure of the spherical crystals observed in figure 1C-E can be a result of diffusion

limited ion supply. At high hydrolysis rates, carbonate is produced at such a rate as that the ions cannot form a proper crystalline framework. This results in amorphous calcium carbonate as the first mineral phase to precipitate, forming the core of the crystals. When the crystal becomes larger more ions need to be incorporated in a single crystal layer and the supply of calcium or carbonate ions towards the crystal surface can become limited by diffusion. Consequently, supersaturation at the crystal surface becomes lower than in the bulk solution. At a lower supersaturation the more stable vaterite is kinetically favoured, forming the second layer. After a while a further drop of the supersaturation due to diffusion limitation could even have caused the third phase of calcite to form (figure 1D).

On a bigger scale the intensity of stirring affects the transport of ions. Vigorous stirring increases the transport of ions to/from the crystals, thus attenuating the diffusion limitations inherent in non-stirred batch systems. The occurrence of 10-20% of calcite at high urea hydrolysis rates in the unstirred batch experiments (Figure 4 and Figure 5) can be caused by limited transport of ions due to the lack of stirring, as in the stirred experiment at a similar hydrolysis rate 100% vaterite was formed (Figure 7). A second effect of stirring is that it prevents settlement of the crystals. When the liquid is unstirred and crystals reach a size of approximately 5 μm, they tend to settle, carrying the attached or entrapped bacteria with them. As a result of settlement, the crystals and bacteria get concentrated at the bottom of the vessel. In these new concentrated conditions, the rate of hydrolysis and precipitation are easily limited by diffusion. Another effect of low stirring conditions might be that bacteria get more easily trapped within the growing crystals causing the hydrolysis rate to decrease. Finally, the stirring conditions affect the secondary transformations of crystals. The prolonged stability of metastable phases after stirring was stopped (Figure 7) can also be explained by settlement and limited ion transport. The vaterite crystals formed in a stirred suspension were allowed to settle, which decreased the crystal surface area available for dissolution and recrystallization. Similarly, prolonged stability might occur when the metastable crystal phase is covered by a more stable phase (figure 1D).

In a sand environment the urease activity can vary in space and time. The local urease activity at pore scale depends on the amount of bacteria attached to the sand grains or flocculated and trapped in narrow pore throats. Adsorption and filtration of bacteria are directly related to flow velocity (Foppen and Schijven, 2006). Higher flow velocities cause more shear at the grain surface and consequently less bacteria to remain attached or strained by the sand grains. A heterogeneous flow field at pore scale or preferential flow paths at a larger scale during the different injections can result in a heterogeneous spatial distribution of bacteria or reagents. A heterogeneous distribution of bacteria or limited supply of reagents results in a wide variety in hydrolysis rates and consequent crystal properties. Due to the variety in flow directions and velocities at different scales the exact crystal properties will be unpredictable. However, when the ammonium concentrations at the in- and outlet, the average flow velocity and direction and hydraulic residence time in the sand are determined the average conversion rate can be calculated and the likelihood of sustained metastable precursor formation predicted.

4.3 Effect of bacteria

Apart from hydrolysing urea, the bacteria used in MICP might also affect crystal nucleation. Their effect has been largely are ascribed to the organic macromolecules that make up the cell membrane. These molecules can act as nucleation site (Braissant et al. 2003), inhibit or stimulate formation of a specific mineral phase or are able to stabilize a metastable phase after it is formed (Giralt et al. 2001; Xyla et al. 1992). However, several studies showed that the effect of Sporosarcina pasteurii on nucleation and growth of calcium carbonate crystals (Bachmeier et al. 2002; Mitchell and Ferris, 2006) is limited. The difference in morphology between crystals formed in bacterial suspension and in solution free of bacteria was minimal and also nucleation was not affected by the presence of bacteria. Their findings correspond with our observations in figure 8 and figure 9. Some single bacteria do act as a crystal nucleus resulting in the rod or dumbbell shaped crystals. (similar to (Warren et al. 2001)). The presence of bacteria was also noticed by the black rod shaped marks they left on the crystals when they were encapsulated like in figure 1F and similar to Mitchell and Ferris (2006).

4.4 Effect of ground material properties

The properties of the sand grains can also influence the precipitation conditions and consequent crystal properties when MICP by urea hydrolysis is applied in a sand environment. The grain size distribution and mineral type influence the attachment of bacteria and hence the local hydrolysis rate. (Foppen and Schijven, 2005; Foppen and Schijven, 2006). The mineralogy of the sand also affects the calcium carbonate precipitation process itself. Lioliou et al. (Lioliou et al. 2007) showed that when calcite seeds were added to a metastable supersturated solution $CaCO_3$ started to precipitate immediately on the surface of the seeds at a rate directly proportional to the squared supersaturation, implying a surface integration growth process. When adding silica seeds to a similar solution no precipitation occurred. Nucleation in presence of silica seeds occurred at a much higher supersaturation and only slightly quicker than in spontaneous homogeneous nucleation experiments. The new $CaCO_3$ crystals appeared in the bulk liquid or only loosely attached to the silica seeds. Similarly in our experiments using white siliceous sand or glass slides (figure 1 and figure 10) a relatively small number of large crystals is observed randomly distributed over the surface of the sand grains and on the glass slides. Conversely, many small (calcite) crystals are observed in carbonate sand and coral or shell fragments (figure 2), forming thin layers that cover the whole grain surface. The observation of sheets of many small calcite crystals in the yellow siliceous sand might indicate that the surface of these sand grains is covered by a compound (e.g. iron oxide), which can act as a nucleus for calcium carbonate precipitation.

4.5 Implications for the application of MICP as ground reinforcement method

For practical applications of MICP as ground reinforcement method, high concentrations and high hydrolysis rates are preferred to limit the amount of time and flushed volume required to reach a desired level of cementation. Based on a high hydrolysis rate the occurrence of vaterite can be expected. On the other hand within the ground there will

be sufficient surface available for crystal growth, especially after the soil is calcareous or has been treated with MICP once before, in which case calcite growth will be more likely.

Another question is, which mineral is favourite for ground reinforcement. Based on solubility product and density, calcite is both physically and chemically more stable than vaterite or amorphous $CaCO_3$. Vaterite spheres are easily cracked, especially when they are hollow, as shown in figure 1 and figure 6. Possible dissolution and recrystallization of vaterite might cause the mechanical properties to change after treatment. Therefore it seems that precipitation of calcite is preferred for a permanent stable cementation.

The mechanical behaviour of cemented sand, however, will not only depend on mineral type, but also on the distribution of precipitate at pore scale – preferably at the grain contact points – and at large scale throughout the sand body. As the number, size and type of crystals are influenced by the hydrolysis rate, transport regime and sand grain properties so is the crystal distribution. Ismail et al. (2002a) mentioned that the rate at which calcium carbonate precipitates is crucial for the strength obtained. On CIPS' treated siliceous sand samples they observed an optimum rate at which strength was maximized. This might be explained by the effects of crystal properties and distribution. Comparing calculated CIPS' precipitation rates with the MICP rates in this study, it is likely that vaterite is formed in all their experiments. At rates below the optimum vaterite crystals are expected to be limited in number, relatively large in size and poorly distributed throughout the pores. At rates above the optimum the precipitation might be so fast that most crystals are filtered near the inlet and hence poorly distributed throughout the core. At the optimum rate the combined effects of sustained nucleation and fast crystal growth may have lead to many small crystals, optimally distributed at both pore and core scale. Applying a second treatment on already treated quartz sand, results in different crystallizating conditions, as the crystals precipitated in the first treatment will act as a nucleation site during the second treatment.

Assuming that reaction rate, transport conditions and the essential sand properties are known or measured, an estimate of the distributed in situ urease activity might be made and consequently the resulting crystal characteristics, including mineral type, size and number and spatial distribution might be predicted for a given treatment protocol. Also the treatment variables, e.g. flow rate, injection duration, the amount and properties of the urease containing bacteria, concentrations of dissolved urea and calcium salts and the type and number of treatments (single batch, multiple batch or continuous flow), might theoretically be optimized in order to get the preferred crystal properties.

However, in practice a single correlation between the mineral properties and the bulk mechanical properties of cemented soil with similar amounts of cement will remain impossible to make. Factors not related to the cementation process influence the strength of the cemented material, for example the moisture content (Hawkins and McConnell, 1992), and properties of the sand grains such as the mineral type, texture, shape, angularity, size distribution, and packing density (Bell and Lindsay, 1999; Carter and Bentley, 1991). In addition, there is a large variation in strength values depending on the sampling and testing method used to determine these values: sample shape (cube or

cylinder), size, height:diameter ratio, failure mode (compression, extension, direct shear), type of test (UCS, point load strength, Brazilian Tensile strength), sample orientation relative to lamination (Hawkins, 1998). To make a proper comparison between two mineral types all the other factors should be kept constant. In practice this condition is hardly ever achieved. Consequently reported relations between amount and type of cementation and mechanical properties show a large variability (Airey, 1993; Allman and Poulos, 1988; DeJong et al. 2006; Ismail et al. 2002b), making a direct relation between mineral type and strength even more difficult.

5 Conclusions

This study shows that the mineral type of calcium carbonate crystals formed by microbially catalyzed hydrolysis of urea depends strongly on the hydrolysis rate. At high hydrolysis rates vaterite is kinetically favoured over calcite growth, while at low hydrolysis rates calcite is predominant. It is shown that, once formed, vaterite or other metastable precursors can remain stable when covered by more stable calcite, resulting in composite mineral structures. In a sand environment the transport regime and the properties of sand grains affect the in situ urease activity and precipitation conditions and hence the resulting crystal properties to a significant extend. For the application of MICP as ground reinforcement method the occurrence of vaterite and its effect on the mechanical behaviour of cemented ground are limited.

References

Airey DW. 1993. Triaxial Testing of Naturally Cemented Carbonate Soil. *Journal of Geotechnical Engineering* 119:1379-1398.

Allman MA, Poulos HG. 1988. Stress-strain behaviour of an artificially cemented calcareous soil. In: *Proceedings of the international conference on calcareous sediments*, Perth, Australia. Rotterdam: A.A.Balkema. 2: P 51-58.

Bachmeier KL, Williams AE, Warmington JR, Bang, SS. 2002. Urease activity in microbiologically-induced calcite precipitation. *Journal of Biotechnology* 93:171-181.

Bell FG, Lindsay P. 1999. The petrographic and geomechanical properties of some sandstones from the Newspaper Member of the Natal Group near Durban, South Africa. *Engineering Geology* 53:57-81.

Braissant O, Cailleau G, Dupraz C, Verrecchia, EP. 2003. Bacterially induced mineralization of calcium carbonate in terrestrial environments: the role of exopolysaccharides and amino acids. *Journal of sedimentary research* 73:485-490.

Carter M, Bentley SP. 1991. *Correlations of soil properties*. London: Pentech Press Limited 130 p.

Castanier S, Le Metayer-Levrel G, Orial G, Loubiere JF, Perthuisot, JP. 2000. Bacterial carbonatogenesis and applications to preservation and restoration of historic property. In: Ciferri O, Tiano P, Mastromei G, editors. *Of microbes and art: the role of microbial communities in the degradation and protection of cultural heritage*. Amsterdam: Kluwer Academic-Plenum. P 246–262.

DeJong JT, Fritzges MB, Nusslein K. 2006. Microbially Induced Cementation to Control Sand Response to Undrained Shear. *Journal of Geotechnical and Geoenvironmental Engineering* 132:1381-1392.

Ferris FG, Phoenix V, Fujita Y, Smith RW. 2004. Kinetics of calcite precipitation induced by ureolytic bacteria at 10 to 20°C in artificial groundwater. *Geochimica et Cosmochimica Acta* 68:1701-1710.

Foppen JWA, Schijven JF. 2005. Transport of E-coli in columns of geochemically heterogeneous sediment. *Water Research* 39:3082-3088.

Foppen, JWA, Schijven JF. 2006. Evaluation of data from the literature on the transport and survival of Escherichia coli and thermotolerant coliforms in aquifers under saturated conditions. *Water Research* 40:401-426.

Giralt S, Julia R, Klerkx J. 2001. Microbial Biscuits of Vaterite in Lake Issyk-Kul (Republic of Kyrgyzstan). *Journal of sedimentary research* 71:430-435.

Hawkins AB. 1998. Aspects of rock strength. *Bulletin of Engineering Geology and the Environment* 57:17-30.

Hawkins AB, McConnell BJ. 1992. Sensitivity of sandstone strength and deformability to changes in moisture content. *Quarterly Journal of Engineering Geology & Hydrogeology* 25(2):115-130

Ismail MA, Joer HA, Randolph MF, Meritt A. 2002a. Cementation of porous materials using calcite. *Géotechnique* 52(5):313-324.

Ismail MA, Joer HA, Sim WH, Randolph, MF. 2002b. Effect of Cement Type on Shear Behavior of Cemented Calcareous Soil. *Journal of Geotechnical and Geoenvironmental Engineering* 128(6):520-529.

Kralj D, Brecevic L, Kontrec J. 1997. Vaterite growth and dissolution in aqueous solution III. Kinetics of transformation. *Journal of Crystal Growth* 177: 248-257.

Kralj D, Brecevic L, Nielsen AE. 1990. Vaterite growth and dissolution in aqueous solution I. Kinetics of crystal growth. *Journal of Crystal Growth* 104: 793-800.

Kralj D, Brecevic L, Nielsen, AE. 1994. Vaterite growth and dissolution in aqueous solution II. Kinetics of dissolution. *Journal of Crystal Growth* 143: 269-276.

Kucharski, ES, Price, GP, Li, H, Joer, HA. 1996. Laboratory Evaluation of CIPS Cemented Calcareous and Silica Sands. In: *Proceedings of the seventh Australia New Zealand conference on geomechanics*, Adelaide, Australia. P 102-107

Lioliou, MG, Paraskeva, CA, Koutsoukos, PG, Payatakes, AC. 2007. Heterogeneous nucleation and growth of calcium carbonate on calcite and quartz. *Journal of Colloid and Interface Science.* 308: 421-428.

Loste, E, Meldrum, FC. 2001. Control of calcium carbonate morphology by transformation of an amorphous precursor in a constrained volume. *Chemical Communications* 901-902.

Mitchell A, Ferris F. 2006. The influence of Bacillus pasteurii on the nucleation and growth of calcium carbonate. *Geomicrobiology Journal* 23: 213-226.

Morse JW, Mackenzie FT. 1990. *Geochemistry of Sedimentary Carbonates.* Amsterdam: Elsevier. 705p.

Nemati M, Voordouw G. 2003. Modification of porous media permeability, using calcium carbonate produced enzymatically in situ. *Enzyme and Microbial Technology* 33:635-642.

Söhnel O, Garside J. 1992. *Precipitation: Basic principles and Industrial Applications.* Oxford: Butterworth-Heinemann Ltd. 391p.

Stocks-Fischer S, Galinat JK, Bang SS. 1999. Microbiological precipitation of CaCO3. *Soil Biology and Biochemistry* 31:1563-1571.

Warren, LA, Maurice PA, Parmar N, Ferris FG. 2001. Microbially mediated calcium carbonate precipitation: Implications for interpreting calcite precipitation and for solid-phase capture of inorganic contaminants. *Geomicrobiology Journal* 18: 93-115.

Whiffin, VS. 2004. Microbial CaCO3 Precipitation for the production of Biocement. Ph.D thesis, Murdoch University, Perth, Australia. 154 p.

Whiffin, VS, van Paassen, LA, Harkes, MP. 2007. Microbial Carbonate Precipitation as a Soil Improvement Technique. *Geomicrobiology Journal* 24: 417-423.

Xyla, AG, Mikroyannidis J, Koutsoukos PG. 1992. The inhibition of calcium carbonate precipitation in aqueous media by organophosphorus compounds. *Journal of Colloid and Interface Science* 153: 537-551.
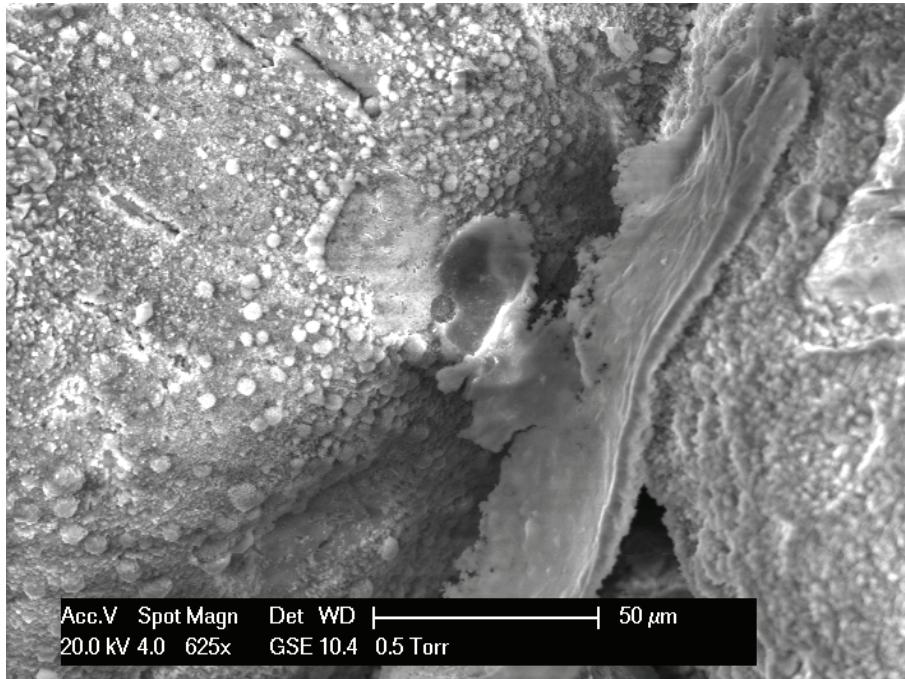
Supplementary material

Figure 12 SEM image of sand grains in a column treated using the CIPS protocol (Kucharski et al, 1996): a solution containing all ingredients for continuous CaCO₃ precipitation is injected within 10 minutes into a sand column, after which the solution is left to react for 24 hours. The rate of CaCO3 precipitation in the CIPS method is in general relatively high. Crystals are well distributed and form sheets. XRD analysis showed the crystals are mainly calcite.
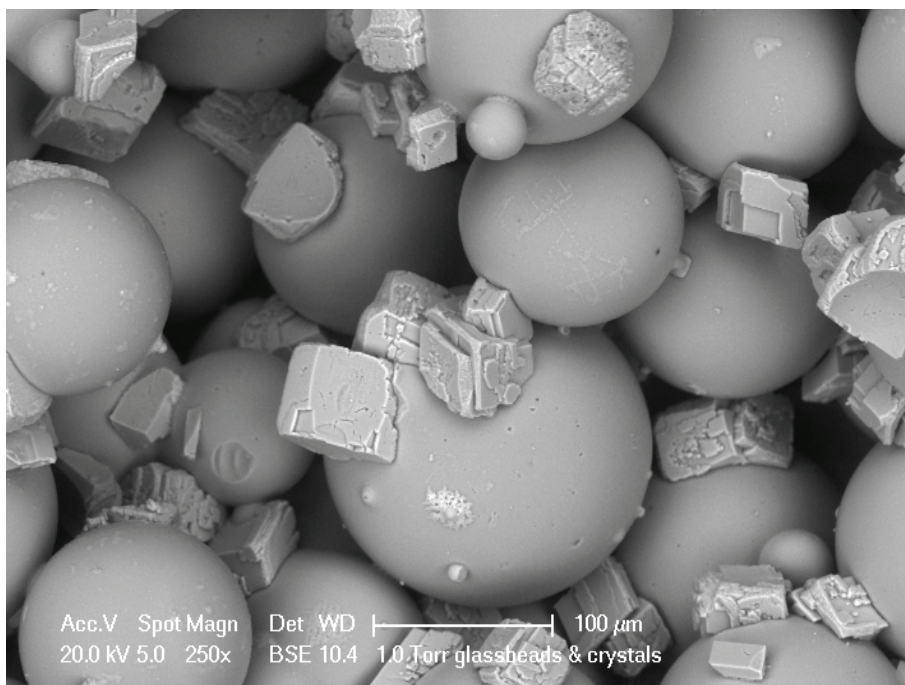
Figure 13 SEM image of CaCO₃ crystals on glass beads. Crystals are formed by MICP with urea hydrolysis. After injection of bacteria a 1M CaCl₂/urea solution was percolated through the glass beads by gravity induced flow. After 2 days of flushing a limited number of relatively large rhombiodal calcite crystals was formed on the surface of the glass beads. The urease activity and flow rate are not measured but estimated to be very low.
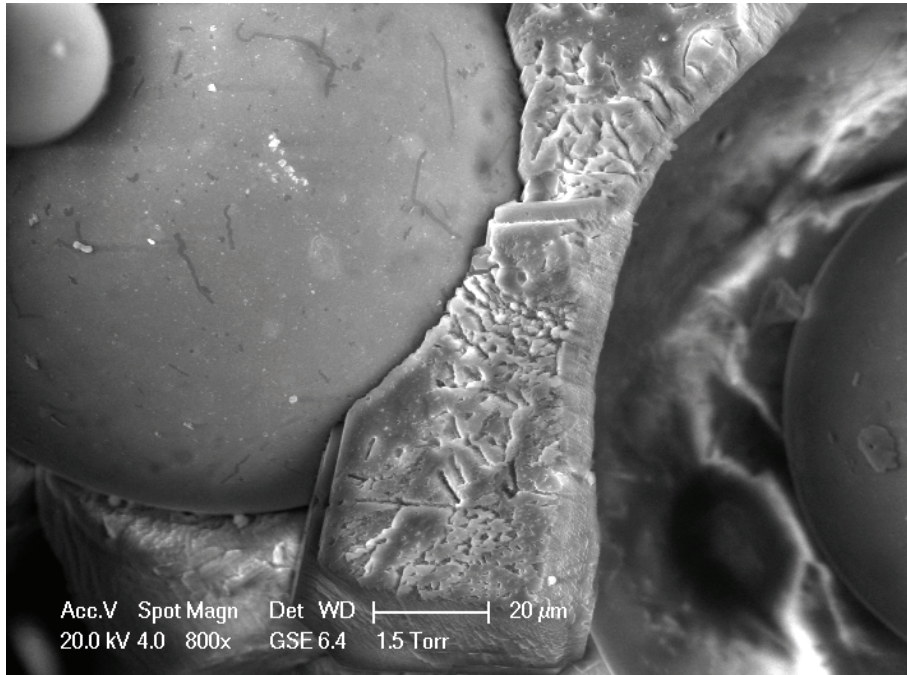
Figure 14 Detail of sample in figure 13: The calcite crystals are perfectly shaped around the glass beads, The crystal and grain surfaces are very smooth and cohesion between the surfaces in relatively low. When shear stress is applied on this type of material, the strength improvement is mainly caused by an increase in dilatancy.
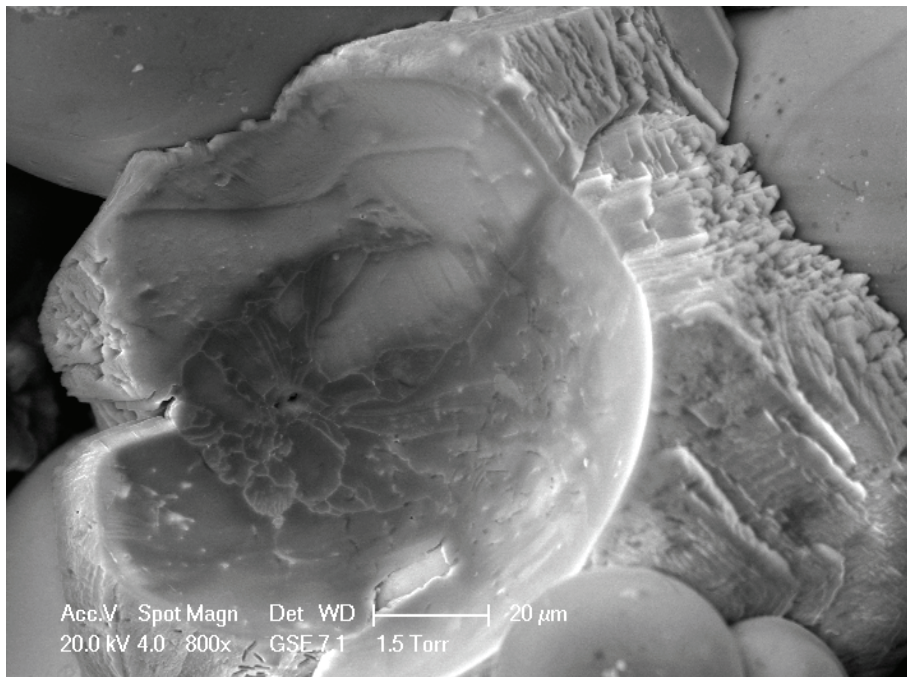

Figure 15 Detail of sample in figure 13: Looking at the surface of the calcite crystal, which made contact with a glass bead shows that the single rhombiodal calcite crystal contained a core of smaller agglomerated calcite crystals, like in the agglomerated structure observed in of which the crystal faces merged while growing outward.
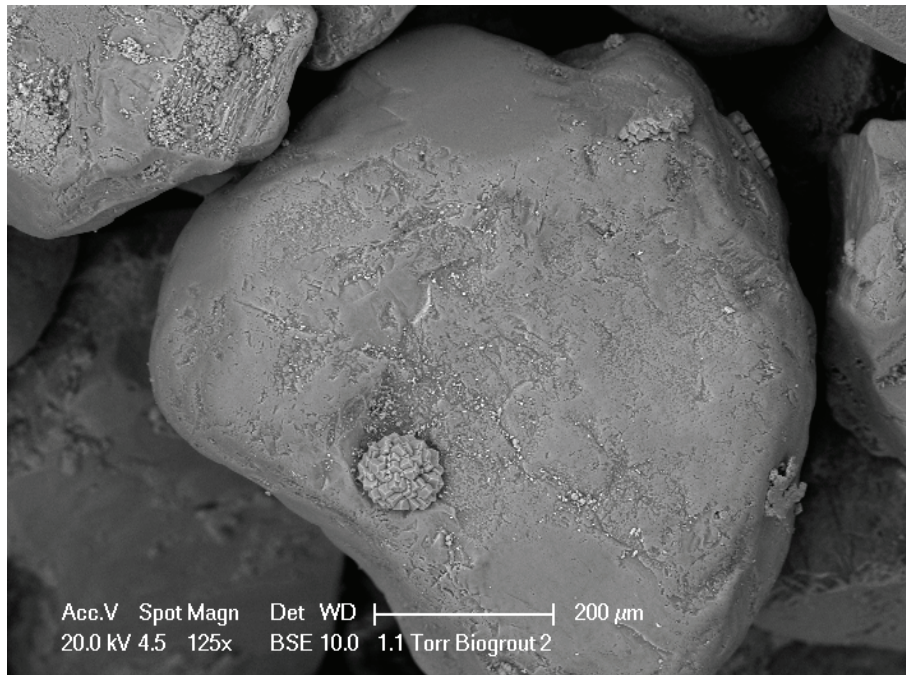
Figure 16 SEM image of a CaCO₃ crystal on sand. The sample was taken from a 2D flow experiment at a location where little CaCO₃ was observed. The crystal is an agglomeration of calcite crystals and is formed in a depression of the sand grain. The rest of the sand grain surface is clear of any crystals.
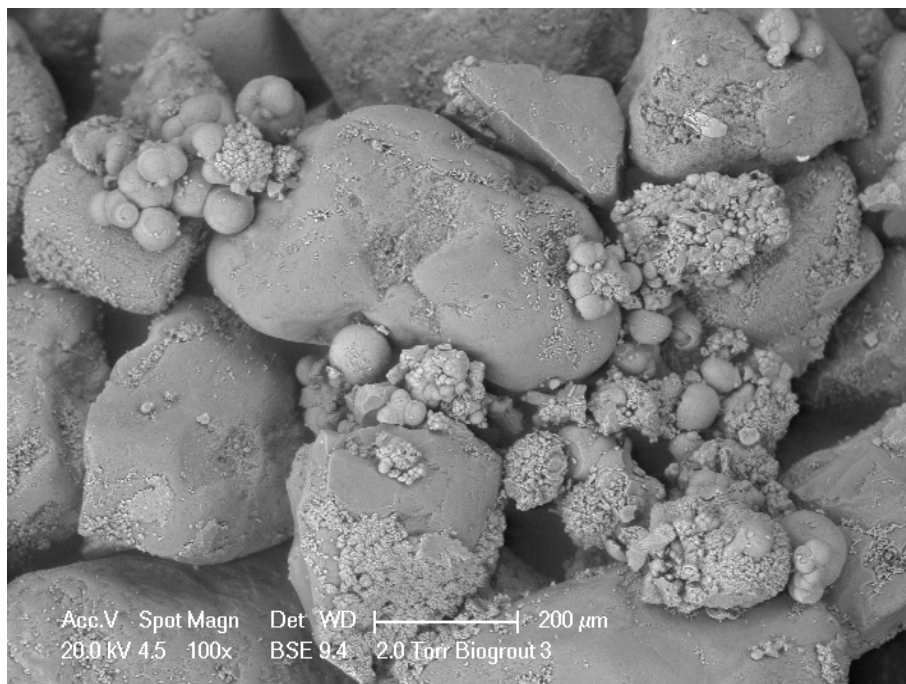

Figure 17 SEM image of CaCO₃ crystals on sand. The sample was taken from a 2D flow experiment at a location where a lot of CaCO₃ was formed. Various crystal shapes, sizes and distributions were observed: vaterite spheres up to 50μm, some covered with agglomerated calcite crystals. At other places part of the sand grains are covered with a sheet of agglomerated calcite crystals. The crystal are mainly located close to grain contacts. The major part of the sand grain surface is clear of any crystals. Dispersed over the grain surface 1μm rod shaped crystals are observed, which are likely calcified bacteria.
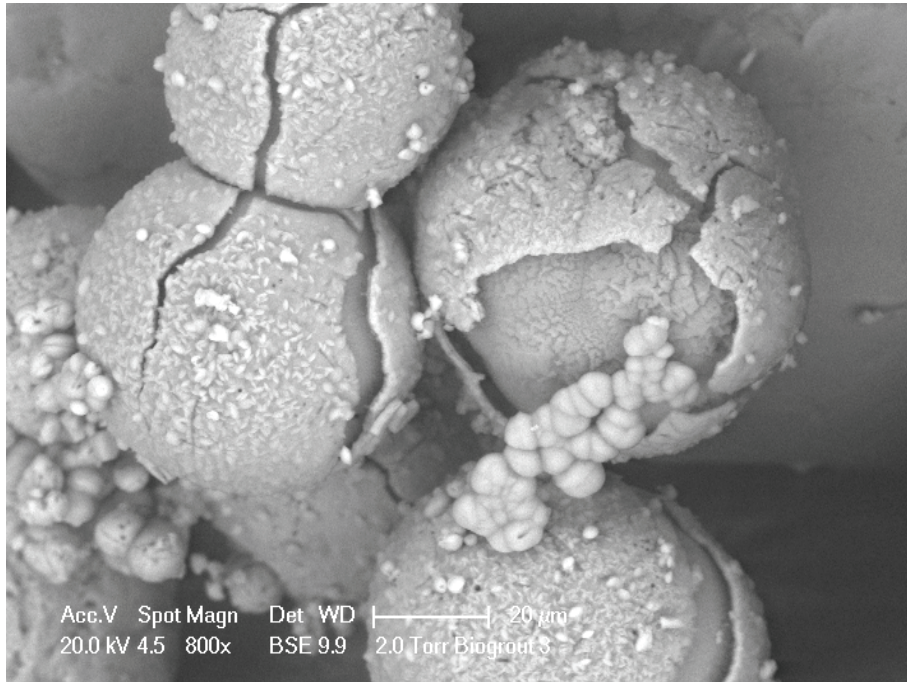
Figure 18 SEM image of CaCO₃ crystals on sand. A detail from the sample of Figure 17. The vaterite spheres easily crack and show a shell like outer surface. On the outer surface of the cracked shells 1μm rod shaped crystals are observed, which are either calcified bacteria or small calcite crystals.

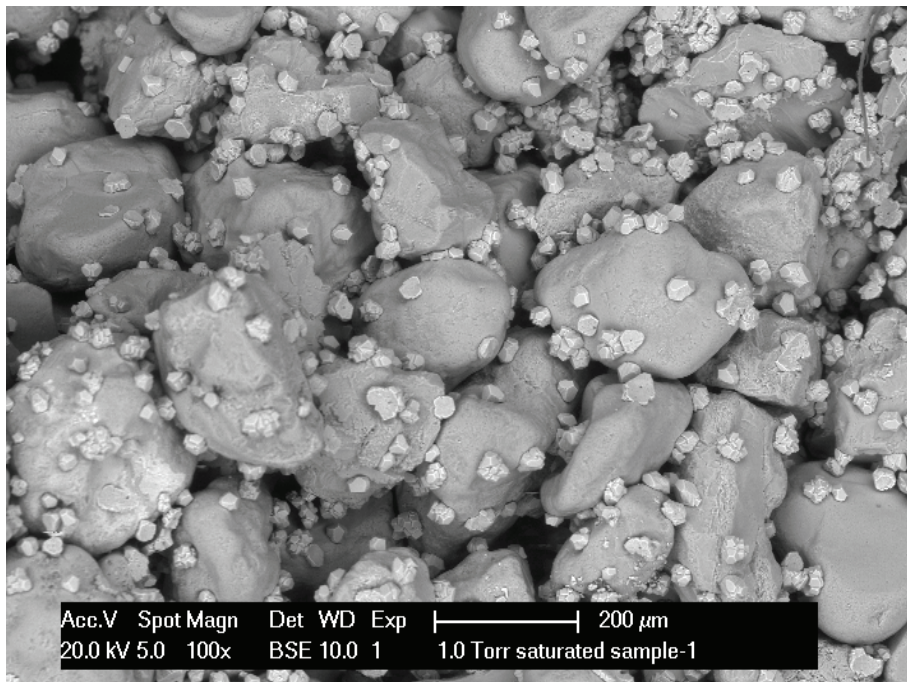*Figure 19 SEM image of CaCO₃ crystals on sand, of a sand column treated with a procedure as described in chapter 4 and 5.*

4

Fixation and distribution of bacterial activity in sand to induce carbonate precipitation

Abstract

The mechanical properties of soil (cohesion, friction, stiffness and permeability) are important parameters for engineering constructions and ecosystems in sedimentary environments. Biogrout is an *in situ* soil strengthening technique involving microbial induced carbonate precipitation (MICP). This process involves hydrolysis of urea by bacteria containing the enzyme urease in the presence of dissolved calcium ions, resulting in calcium carbonate precipitation. In order to control the Biogrout process for engineering applications, it is necessary to improve understanding of the relevant phenomena and develop efficiencies to enable up-scaling of the technology to suit commercial applications. Control of a homogeneous distribution of bacterial activity in a sand bed is considered crucial in order to prevent clogging during injection and provide homogeneous reinforcement results. This paper describes a methodology to distribute and fix bacteria (with their enzyme activity) relatively homogeneously in a sand bed, before supplying cementation reagents. The methodology is based on a two-phase injection procedure: Firstly, a bacterial suspension is injected into the sand body, immediately followed by a fixation fluid (i.e. a solution with high salt content). It is proposed that bacteria are retarded by adsorption and filtration processes and are permanently adsorbed to the sand grains when overtaken by the fixation fluid. The presented experimental approach for optimizing bacterial fixation in porous media can be used as a tool to design the treatment protocol for engineering applications in practice.

1   Introduction

The mechanical properties of soil (cohesion, friction, stiffness, permeability) are important when engineering constructions in sedimentary environments. Traditionally, soil properties are specific for each location depending on current and historical sedimentary conditions and on human interventions. When soils are unfavourable for desired use measures can be taken. For example, the stability of slopes can be improved using anchors, bolts and fences, but also vegetation can have a positive effect on slope stability (Fan and Su 2008; Normaniza et al. 2008). Erosion and deposition of soils along coasts and river banks can be controlled by continuous dredging and nourishment, by introducing constructions like dikes, jetties, groins and breakwaters, by making use of reefs (Frihy et al. 2004) and vegetation or by integrated approaches (Jones and Hanna 2004).

Recently, techniques are being developed, which aim at changing soil properties on demand by stimulating natural (bio-)chemical processes *in situ* (Whiffin et al. 2005; Van Meurs et al. 2006; Ivanov and Chu 2008). One of these technologies is Biogrout: an *in situ* soil strengthening technique, involving microbial induced carbonate precipitation.

Microbial induced carbonate precipitation (MICP) has been the subject of research for several industrial applications. Several researchers have shown that MICP can be used to improve the mechanical properties of porous materials (Le Metayer-Levrel et al. 1999; Nemati and Voordouw 2003; DeJong et al. 2006; Whiffin et al. 2007). In most of these studies, calcium carbonate precipitation was induced by hydrolysis of urea in a solution with calcium chloride. Purified urease enzymes or whole bacterial cells, containing the enzyme in high concentrations, were used to catalyse the hydrolysis of urea and produce ammonium and carbonate ions.
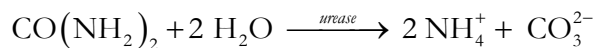
$$CO\left(NH_2\right)_2 + 2\,H_2O \xrightarrow{\;urease\;} 2\,NH_4^+ + CO_3^{2-}$$

In the presence of dissolved calcium ions, the produced carbonate ions will precipitate and form calcium carbonate crystals.

$$Ca^{2+} + CO_3^{2-} \rightarrow CaCO_3\left(s\right)$$
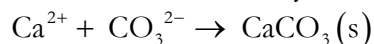
When these crystals form coatings on or bridges between the existing sand grains they prevent movement of the grains and hence improve the strength and stiffness properties of the material.

In order to induce MICP in the soil subsurface, reagents and catalysts need to be injected and transported to the location where strengthening is required. Treatment over large distances is preferred for economical reasons (to limit the number of required injection wells) and enable ground improvement without disturbing the serviceability of any urban infrastructure present in the vicinity. Mixing bacteria and reagents prior to injection results in immediate flocculation of bacteria and crystal growth. Whilst this method can be applied for treatment of surfaces, very coarse grained materials and mixed in place applications (Le Metayer-Levrel et al. 1999), this would cause rapid clogging of the injection well and surrounding pore space for many (fine) sands. In order to prevent crystal accumulation around the injection point and encourage a more homogeneous

distribution of $CaCO_3$ over large distance, a two-phase injection for bacterial retainment has been suggested (Whiffin et al. 2007).

Microbial transport in saturated porous media is well studied (Murphy and Ginn 2000; Foppen and Schijven 2006). Many physical, chemical and biological factors, which influence the transport of bacteria have been investigated, including: fluid properties like chemistry and flow regime (Torkzaban et al. 2008), cell wall characteristics like hydrophobicity, charge and appendages (Van Loosdrecht et al. 1987; Gilbert et al. 1991) and solid properties, like grain size distribution, surface texture and mineralogy (Scholl et al. 1990; Foppen and Schijven 2005).

The fixation methodology, suggested by Whiffin et al. (2007), is based on the effect of ionic strength on microbial transport. Many authors have shown that adsorption of bacteria increases with an increasing salinity of the bacterial suspension (Sharma et al. 1985; Van Loosdrecht et al. 1989; Scholl et al. 1990; Torkzaban et al. 2008). By flushing low salinity solutions after the bacterial suspension, a large part of the adsorbed bacteria can be remobilised from the solid surface into the liquid phase. A decrease in electrolyte concentration or ion valence causes the repulsive energy between two equally charged particles (bacteria-bacteria or bacteria-sand grain) to increase and loosely adsorbed bacteria to resuspend. For homogeneous immobilisation of bacteria the opposite is suggested: first the bacterial suspension is injected, directly followed by a fixation fluid, i.e. a solution with high salinity. When the bacteria are retarded by adsorption and filtration processes, the fixation fluid (with high salinity) will overtake the weakly adsorbed cells and strongly fix them to the soil particles by reducing the electrostatic repulsion, resulting in homogeneously distributed bacteria (i.e. enzyme activity) along the sand column. This is considered essential for obtaining a homogeneous $CaCO_3$ distribution and hence strength of the grouted column.

Using one pore volume of bacterial suspension, followed by one pore volume of a 50mM $CaCl_2$ solution before injection the cementation solution Whiffin et al. (2007) showed that it was possible to precipitate $CaCO_3$ at a distance of 5 m from the injection point. However, $CaCO_3$ cement content and consequent reinforcement were not homogeneously distributed over the sand column. Also the process was inefficient as much of the bacterial activity was lost from the column and the injection of two full pore volumes prior to cementation is not practical for field applications. In order to improve this efficiency and optimise MICP for engineering applications we have conducted a set of biogrouting experiments with laboratory sand columns. Based on the results we discuss the factors that influence bacterial distribution and fixation for MICP in porous media, and the implications for practical applications.

2 Materials and Methods

2.1 Column parameters

The columns were made of PVC tubing (internal diameter 6.6 cm, length 18 cm) and packed in the following order: First a layer of approximately 1 cm filter gravel was placed, with a layer of scouring pad (Scotch Brite) on top of it, followed by 16 cm of Itterbeck

sand (Grain size characteristics: d_{10} = 110 µm ; d_{50} = 165 µm; d_{90} = 275 µm). The sand was packed by tamping to a dry density of approx 1.7 g cm^{-3} (porosity around 33%). Packing was performed under water to avoid the inclusion of air pockets. On top of the sand the column was filled up to the top with another layer of approximately 1 cm of filter gravel followed by another scouring pad.(Figure 1). The column was closed and positioned vertically. A peristaltic pump (Ismatec, ip-12, Glattbrug, CH) was connected to an injection point at the top of the column to regulate the flow rate, inducing flow from top to bottom.
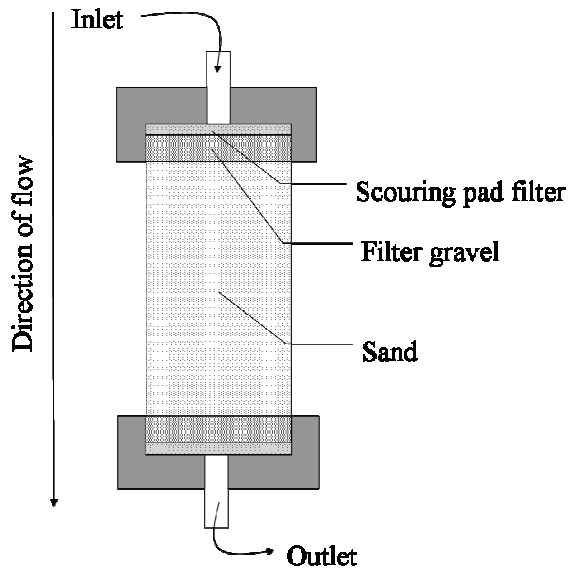

Figure 1: Schematic of column filter setup

Before any experiments were conducted, tap water was flushed through the column to calibrate the flow regulation of the pump. All experiments were performed at ambient temperature of 20°C. ± 2.

2.2   Treatments

To evaluate the effect of the bacterial fixation procedure on the MICP process results various sand column experiments were performed in which the fixation protocol was varied. First, the procedure, derived from Whiffin et al. (2007) was applied in column I:

A bacterial suspension was grown to late exponential phase to a final optical density of 2.88 (OD600) and urease activity of 3.1 mS min^{-1}. Prior to injection, the bacterial suspension was diluted by a factor 10 with saline solution (9 g L^{-1} NaCl) to provide lower initial urease activity. Saline solution was used for diluting the suspension in order to prevent osmotic shock of the bacterial cells, which could result in urease enzymes being released from the cells into solution. 270 mL (approximately 1.5 pore volume) of diluted bacterial suspension was injected into the sand core and then immediately followed by 270 mL of fixation fluid. The fixation fluid contained 50 mM $CaCl_2$. Immediately after the fixation fluid was fully injected, a third fluid - the cementation fluid, containing 1 M equimolar $CaCl_2$ and urea was flushed through. After the first batch of cementation fluid was fully loaded into the column, the flow was stopped for 2 hours. After two hours of reaction time a second batch of cementation fluid was flushed through the column. The

fluid in the column was then allowed to react for 24 hours. The next day, the column was flushed with a third batch of cementation fluid. During all flushes the flow rate was kept constant at approximately 220 mL per hour (one pore volume per hour; Darcy velocity of $1.8 \cdot 10^{-5}$ m s^{-1}; Re $<<$ 1). Samples were taken periodically from the effluent to analyze optical density, urease activity and ammonium concentration.

In column II, the bacterial suspension was not diluted prior to injection. Instead a smaller volume, 30 mL, of undiluted bacterial suspension was injected, followed by similar treatment as column I. In column III-V the fixation fluid composition was varied. Instead of 50 mM CaCl$_2$, deionised water, fresh surface water ($<$ 0.5g L^{-1} total dissolved solids) from a local waterway and saline solution (9 g L^{-1} or 155mM NaCl) was used. In column VI, the fixation fluid step was omitted and the first batch of cementation fluid was flushed immediately after the bacterial suspension. In column VII, the flow rate was kept constant at a higher level of 660 ml (3 pore volumes) per hour. A summary of the column treatments is given in Table 1.

Table 1: Overview of the column injections for determining the effect of the fixation procedure on the MICP process.

Column	Fixation fluid	Injected bacteria [mL] (OD/activity)[1]	Flow rate [mL h^{-1}]	OD[2] % retained	Activity % retained
I	50 mM CaCl$_2$	270 (0.29/0.51)	220	14	17
II	50 mM CaCl$_2$	30 (3.78/2.15)	220	99	100
III	Demineralised water	30 (4.04/2.20)	220	0	0
IV	Fresh surface water	30 (3.44/1.64)	220	36	74
V	9 g/L NaCl	30 (3.51/2.06)	220	92	93
VI	Cementation solution	30 (3.92/2.06)	220	100	100
VII	50 mM CaCl$_2$	30 (3.00/0.96)	660	79	72

[1]: *Values between parentheses are the optical density at 600 nm and the enzyme activity in mS cm^{-1}min^{-1} of the bacterial suspension immediately before injection (1 mS cm^{-1}min^{-1} ≈ 660 mM urea h^{-1})*
[2]: *Fine particles or calcium carbonate crystals were sometimes shown to interfere with optical density measurements, resulting in higher values for wash-out and lower values for retention of bacteria.*

The optical density and urease activity in the effluent were normalized and are represented as a percentage of the initial values before injection. By integration of the normalized curves, the loss of OD and activity by flush out and the remaining average in situ bacterial concentration and urease activity could be determined. The distribution of the *in situ* urease activity after 3 hours and 24 hours of incubation could be estimated from the ammonium measurements.

2.3   Bacterial suspension

The urease positive microorganism used was *Sporosarcina pasteurii* DSM33 (DSMZ, FRG). Organisms were cultivated under aerobic batch conditions in a medium containing 20 g L^{-1} yeast extract, 10 g L^{-1} NH$_4$Cl and 10 μM NiCl$_2$, at a pH of 8.5. The organism was grown to late exponential or early stationary phase before harvest (i.e. all readily available nutrients were consumed from the medium), and stored at 4°C prior to use. The optical

density and urease activity of the bacterial suspension were determined immediately before use in the experiments. When harvested, optical density (OD_{600}) varied between 2.9 and 4.0 and urease activity varied between 1.0 and 2.2 mS min^{-1} (or 1 and 2 M urea h^{-1} under standard conditions, as described under urease activity) The specific activity, which is determined as the ratio between urease activity and OD_{600}, varied between 0.32 and 1.0 mS min^{-1} OD^{-1}.

2.4 Monitoring methods

2.4.1 Optical density (OD$_{600}$)

During the course of the experiments the optical density was used as an indication of biomass concentration. Optical density was measured using a spectrophotometer at a wavelength of 600 nm. Samples were diluted to a value between 0.2 and 0.8 (where the relationship between absorbance and particle concentration was linear). The measured values were multiplied by the dilution factor to obtain the undiluted value.

2.4.2 Urease activity

Urease activity was measured immediately after sampling. In the absence of calcium ions, urease activity was determined by a conductivity method. The urease reaction involves the hydrolysis of non-ionic substrate urea to ionic products thus generating a proportionate increase in conductivity under standard conditions. 1 mL of bacterial suspension was added to 9 mL of 1.11 M urea (reaction concentration 1 M urea) and the relative conductivity change in mS min^{-1} was recorded over 5 minutes at 20°C. The urease activity was then calculated taking the dilution into account to provide the undiluted value. In the measured range of activities 1 mS min^{-1} correlated with a hydrolysis activity of 11mM urea min^{-1}.

2.4.3 Ammonium concentration

For ammonium measurements samples were centrifuged and the supernatant transferred to a clean tube, which was frozen at -18°C awaiting analysis. Ammonium concentration was determined by a modified Nessler method. The sample was diluted with deionised water to be in the range of 0 - 0.5 mM NH_4^+, using a volumetric flask. 2 ml of sample was added to a cuvette and mixed with 100 µl of Nessler reagent, then allowed to react for exactly 1 min. The sample was then read in a spectrophotometer at 425 nm. Absorbance readings were calibrated with several NH_4Cl standards measured under the same conditions.

3 Results

The effect of several methods on distribution and fixation of bacterial activity in porous media was evaluated with several sand column experiments. Table 1 provides a summary of the results.

First, the original bacterial fixation protocol, modified from Whiffin et al. (2007), was trialled (column I). Dilution of the bacteria with saline solution resulted in an increase in specific activity from 1.0 to 1.8 (more activity per biomass). After centrifuging the diluted

suspension it was observed that a large part of the activity remained in supernatant, while for the undiluted suspension activity remained bound to the bacteria. Apparently, diluting the bacterial suspension had caused a release of urease enzymes from the cells into solution, although it was done with saline solution. The observed increase in specific activity was therefore likely caused by the release of the enzymes in the bulk liquid. Cellular bound enzymes could have a lower apparent activity due to diffusional resistance for the substrates over the cell wall of the bacteria.

While flushing 270 ml (approximately 1.5 pore volume) of diluted bacterial suspension, immediately followed by 270 ml of 50 mM $CaCl_2$ solution, measurements of both optical density and apparent urease activity in the effluent of the sand columns showed that a large proportion of the injected bacteria was flushed out (Figure 2). Integration of the normalized breakthrough curves showed a significant loss of bacteria: about 85% of the injected bacterial activity ended up in the effluent. The activity loss is partly attributed to the dilution effect - assuming that enzymes are released from the cells and that enzymes in solution are less retarded than suspended bacteria - and partly to the low salinity of the bacterial suspension reducing bacterial attachment.
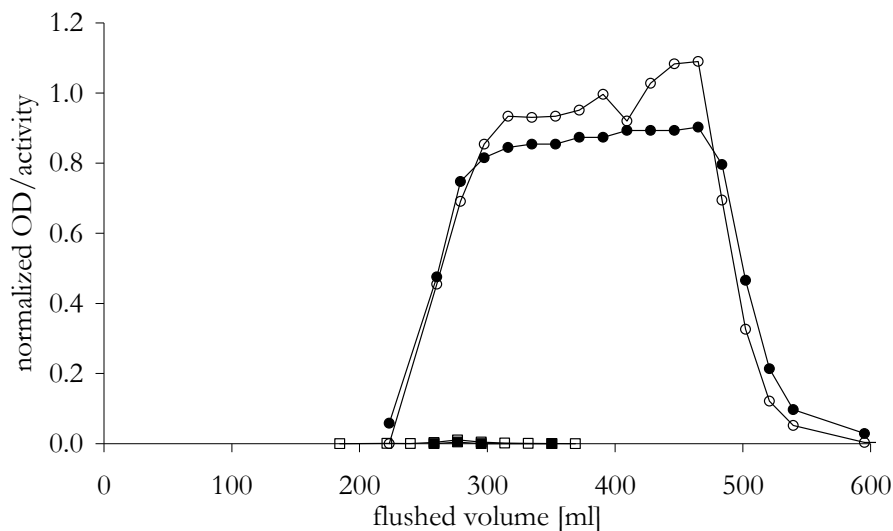

Figure 2: Effluent measurements for two columns flushed with equal amounts of bacteria in different volumes followed by a flush of 50 mM $CaCl_2$: column I, 270 mL diluted bacterial suspension (OD (●), activity (○)) and column II, 30 mL undiluted suspension (OD (■), activity (□)). One pore volume is approximately 200 mL

In the second experiment, approximately the same amount of bacterial biomass was injected, but now within 30 mL of undiluted bacterial suspension (column II), followed by 270 mL of 50 mM $CaCl_2$ (similar to column I) in order to lower the total flushed volume and improve bacterial retention. Effluent measurements indicated that almost all of the bacteria were retained in the column (Figure 2). The higher retention of bacteria in the second experiment could be explained by the higher salinity and significantly higher bacterial concentration of the undiluted suspension, which increase both the adsorption and the filtration of the bacteria (Scholl et al. 1990; Ritvo et al. 2003; Torkzaban et al. 2008). Additionally, the smaller volume of the injected bacterial suspension may improve

retention by providing a smaller volume for the fixation fluid to overtake before reaching the outlet.

To evaluate the effect of the fixation fluid composition, three sand columns were treated similarly as column II, but with different composition of the fixation fluid (Figure 3). When demineralised water was used (column III) nearly all of the cells were washed out. Use of fresh surface water might be an option in practice (< 0.5 g L^{-1} TDS). In this case about 73% of the bacteria were retained in the column (column IV). When a saline solution (9 g L^{-1} NaCl) was used, 93% of the introduced bacteria were retained (column V).
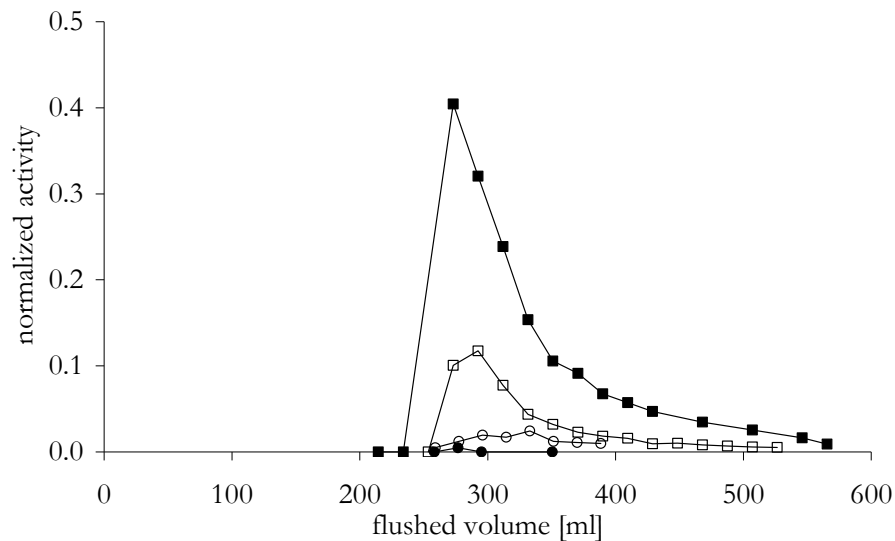

Figure 3: Effluent measurements for four columns with different compositions of the fixation fluid, flushed behind a bacterial suspension: column II (●), with 50mM CaCl$_2$; column III (■), with deionised water; column IV (□), with surface water and column V (○), with 9 g L^{-1} NaCl.

When, instead of the fixation fluid, a cementation fluid (comprising 1M urea and 1M CaCl$_2$) was injected immediately after the bacterial suspension (column VI), no activity or bacteria were observed in the effluent, similar to the observations in column II.

To evaluate the effect of flow rate on bacterial retention a column was treated using the same procedure as column II, but with 3 times higher flow rate, 660 mL h^{-1} (column VII). The effluent measurements (Figure 4) showed that the higher flow rate resulted in more wash-out of cells and activity: only 72% of bacterial activity was retained.

To study the distribution of urease activity over the column length, a pulse of 270 mL of cementation solution containing 1M urea and 1M CaCl$_2$ was injected after the fixation fluid. After the first batch of cementation fluid was injected, the flow was stopped for two hours before the next batch of cementation fluid was injected. Measurements of ammonium concentration in the effluent during the injection of the second batch of cementation fluid, were used to get an impression of the distribution of urease activity along the column (Figure 5).
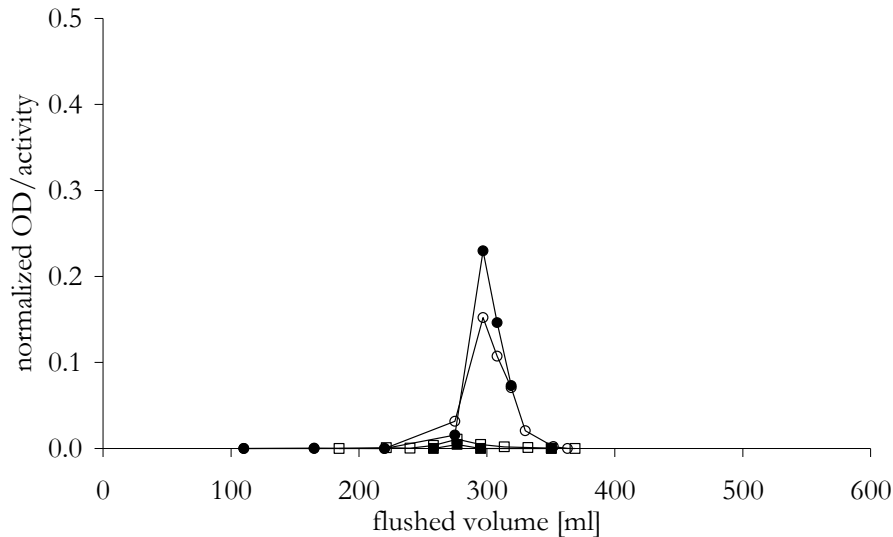
Figure 4: Effluent measurements for two columns with different flow velocity: column II, at a flow rate of 240 mL h^{-1} (OD (■), activity (□)) and column VII, at a flow rate of 660 mL h^{-1} (OD (●), activity (○)).

Assuming plug flow with little dispersion through the column, the fluid that came out at about 20 mL represented the first part of the first batch of cementation fluid, which was injected immediately after the fixation procedure and had reacted mostly near the outlet of the column. The fluid that came out at 200 mL represented the last part of the first batch cementation fluid, which had reacted mostly near the inlet of the column. After 200 mL (about one pore volume) the reacted cementation fluid of the first batch was diluted by the fresh cementation fluid of the second batch. An estimate of the local urease activity could be made, by dividing the measured ammonium concentration by the residence time of 3 hours and the stoichiometric ammonium-urea ratio of 2.
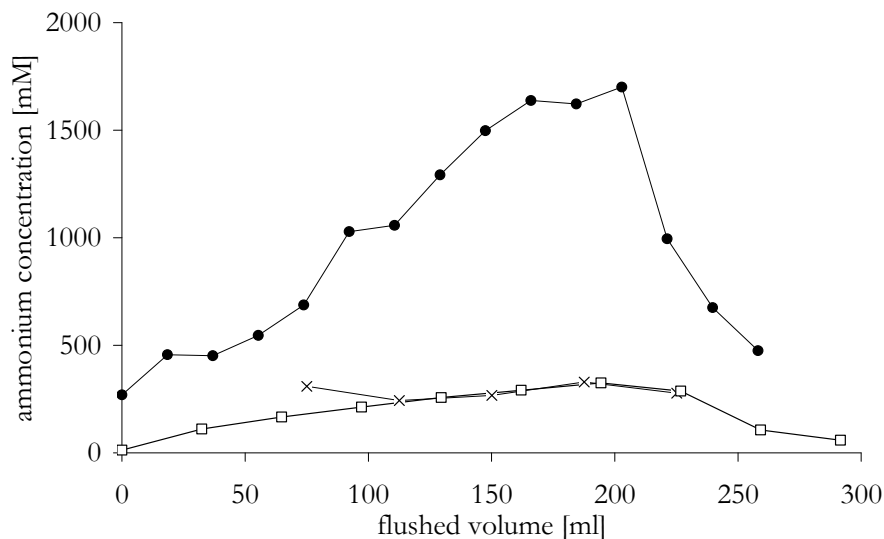

Figure 5: Ammonium concentration measurements in the effluent, which was flushed out after three hours of incubation, were used to determine the (heterogeneous) distribution of urease activity along the column for several of the fixation procedures: column I (✗), II (●) and VII (□).

The ammonium profiles (Figure 5) corresponded with the measurements of optical density and activity. Columns I and VII, where significant bacterial wash-out was observed, showed much lower ammonium concentrations than column II, where no bacteria were observed in the effluent. For column I, flushed with 270 mL of diluted bacterial suspension, followed by fixation and cementation fluid, the ammonium concentration and corresponding urease activity were approximately 300 mM and 50 mM-urea h^{-1}. For column II, flushed with 30 ml of undiluted bacterial suspension, followed by fixation and cementation fluid, the average ammonium concentration and activity were much higher: approximately 1200 mM and 200 mM urea h^{-1}. However, the ammonium concentration increased linearly with flushed volume from 500 mM (84 mM urea h^{-1}) representing the concentration (activity) near the outlet, up to a maximum 1800 mM (300 mM urea h^{-1}) when about 160 mL was flushed out. Near the inlet activity might have been higher, but the concentration of ammonium remained fairly constant as substrates were likely depleted. Flushing at a 3-fold higher flow rate of 660 mL h^{-1} (column VII) resulted in an average ammonium concentration of approximately 200 mM (32 mM urea h^{-1}), which increased slightly from 150 mM (25mM urea h^{-1}) at the outlet to 300 mM (50 mM urea h^{-1}) at the inlet, indicating a more even distribution of bacteria than observed in column II.
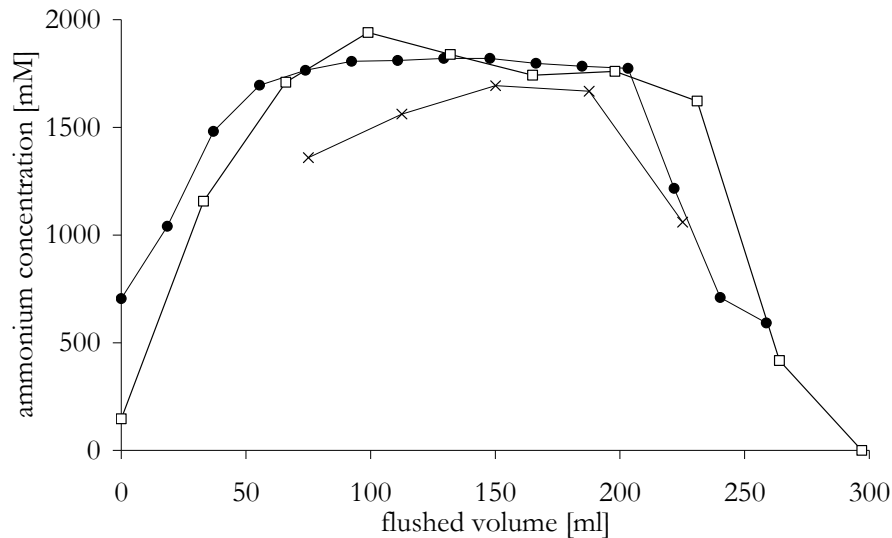

Figure 6: Ammonium measurements in effluent, which was flushed out after 24 hours of incubation, showed close to complete conversion over the entire column for all fixation procedures (see Table 1): column I: (×), II (●)and VII (□).

Measurements of the ammonium concentration in the effluent, during the injection of a third cementation batch after 24 hours (Figure 6) indicated that all columns had nearly reached full conversion of the injected urea. This suggests that although the bacteria might not be homogeneously distributed over the column, homogeneous cementation may still be reached as long as bacteria are present over the entire column and the batch time is long enough compared to the average urease activity and the time required to inject the cementation reagents.

4 Discussion

In order to use Biogrout for engineering applications it is important to precipitate calcium carbonate homogeneously throughout the entire treated sand body, preferably over large injection distance, within short time and using as little flushed volume as possible. To achieve homogeneous strength it is considered essential to control the transport and adhesion of bacteria, or better their urease activity, which defines the precipitation rate and hence the distribution of $CaCO_3$ crystals both spatially and temporally.

Although many phenomena affecting bacterial transport and adhesion, are well described in literature (Murphy and Ginn 2000; Foppen and Schijven 2006), including solution chemistry, flow regime (Torkzaban et al. 2008), cell wall characteristics (Van Loosdrecht et al. 1987; Gilbert et al. 1991), grain size distribution and mineralogy (Scholl et al. 1990; Foppen and Schijven 2005), most of these studies do not aim at both optimizing the amount of adsorbed bacterial activity and homogeneity of its distribution over the sand volume. They are generally aimed at bacterial transport through aquifers. Therefore, bacterial and solute concentrations, reaction and flow rates used in this study are at the high range of most of these other studies.

The experimental observations shown in this paper were consistent with described phenomena in literature. It has been well established that an increase in solution ionic strength promotes bacterial adsorption or filtration (Scholl et al. 1990; Foppen and Schijven 2005; 2006; Torkzaban et al. 2008)). During the injection of bacteria the salinity of the bacterial suspension affects the retention of bacteria. Bacterial suspension can be diluted using various solutions. Dilution of the bacterial suspension with a solution of low salinity can be advantageous in cases where a limited bacterial adsorption is desirable. The low ionic strength would promote bacterial transport over large distances and improve the homogeneity of the distribution of bacteria throughout a large sand body. On the other hand, a lower salinity of the bacterial suspension may lead to significantly less adsorbed bacteria in the sand column, similar to the findings of Torkzaban et al. (2008). Diluting the bacterial suspension with high salinity solutions would result in the opposite: increased adsorption and less homogeneous distribution of bacteria. A disadvantage of dilution is the risk that bacteria endure an osmotic shock and may lose part of their cell bound extracellular enzymes. Free enzymes will filter to a lesser extent and are less protected against denaturation than enzymes which are bound to the cell wall or inside bacterial cells, resulting in a lower and faster decaying activity in the sand (Hoffman and Deccho 1999). Another disadvantage of dilution is the increase in total flushed volume of bacterial suspension required to reach a desired level of in situ activity. The volume of injected fluids may become too large for the fixation fluid to overtake, resulting in more bacteria being washed out and less efficient use of the bacteria. Larger flushed volume and lower *in situ* activity could increase the required treatment time for the same cementation effect.

The effect of the fixation fluid, following the bacterial suspension, on the retention of the bacterial cells is also consistent with other observations in literature. Solutions with high

salinity, like 50 mM $CaCl_2$ (ionic strength 150 mM), 9 g L^{-1} NaCl (ionic strength 155 mM) and reagent solution (ionic strength 1500 mM), promote cell adsorption, while solutions with low salinity, like fresh surface water or demineralised water remobilise the retained bacterial cells, resulting in nearly complete wash out and limited respectively no *in situ* activity remaining. In practice, both effects of the fixation fluid - fixation or remobilization - can be desired. In sand bodies, where bacterial cells attach too quickly and consequently accumulate close to the injection point, a low salinity flush can be used to remobilise (part of) the bacterial cells and enhance homogeneity of the bacterial distribution.

A non-uniform distribution of bacterial cells in the sand body can be compensated for by a batch wise injection of the cementation fluid as observed in figure 6. In this case the injection speed should be high compared to the conversion rate by the urease in the sand column, while the reaction time in between the batches of cementation fluid should be long enough to let all reagents be converted even at the places with minimal urease activity.

The retention of bacterial cells may vary for different types of sand with varying grain size distribution and mineral composition (Scholl et al. 1990; Foppen and Schijven 2006). In practical field applications, a suitable bacterial placement procedure design will be required for the sand encountered on site. Very coarse grained materials may still require mixing bacteria and reagents in advance as sequential flushing will lead to limited adsorbed bacterial activity and consequent long treatment times. By performing several sand column tests prior to field application, and using simple measurements such as optical density, urease activity and ammonium concentration, a custom-made placement protocol can be designed and a prediction of the expected distribution of bacteria and cement on site can be provided.

The interpretation of the presented experimental results is limited as no information is provided on the actual distribution of flow, biomass and biological activity at pore-scale. Local accumulation of injected bacteria or crystals leads to a decrease in permeability and could result in preferential flow paths, which in turn effect the distribution of biomass, bacterial activity and an increase the dispersion of solutes (Thullner et al. 2002). Measurements of pressure drop over the column could be used to identify this effect of bioclogging. Destructive sampling and analysis of the sand during the different stages of treatment could give a more detailed picture of the distribution of bacteria at pore scale in both axial and lateral direction. Recently non-destructive methods like X-ray computerised tomography are being developed to analyse the distribution of biomass or crystals in a porous materials (Louis et al. 2007).

Measurement of effluent composition as performed still provides insight in the distribution of bacterial activity along the column axis, assuming plug flow with little dispersion. This is a valid assumption considering the breakthrough curves of diluted bacteria in figure 2 and ammonium in figure 6. The value of the presented experimental approach is that it can be used for quick screening of different fixation procedures.

5 Conclusions

A procedure has been developed to enhance fixation and distribution of bacterial cells and their enzyme activity in sand in order to improve the potential of microbially induced carbonate precipitation as ground reinforcement technique in fine grained sand. The procedure comprises a multistep injection in which first a bacterial suspension is introduced, potentially followed by a fixation fluid before the cementation fluid is introduced. The composition of the bacterial suspension and fixation fluid can be varied to either stimulate adsorption and flocculation with high salinity or stimulate transport and remobilization of reversibly adsorbed bacterial cells to improve bacterial distribution with low salinity.

References

DeJong, J.T., M.B. Fritzges, and K. Nusslein 2006. Microbially Induced Cementation to Control Sand Response to Undrained Shear. *Journal of Geotechnical and Geoenvironmental Engineering*, 132(11): p. 1381.

Fan C-C and C-F Su. 2008. Role of roots in the shear strength of root-reinforced soils with high moisture content. *Ecological Engineering* 33(2):157-166.

Foppen, J.W.A. and J.F. Schijven, 2005. Transport of E-coli in columns of geochemically heterogeneous sediment. *Water Research*, 39: 3082-3088.

Foppen, J.W.A. and J.F. Schijven, 2006. Evaluation of data from the literature on the transport and survival of Escherichia coli and thermotolerant coliforms in aquifers under saturated conditions. *Water Research*, 40: 401-426.

Frihy O.E., M.A. El Ganaini, W.R. El Sayed and M.M.Iskander. 2004. The role of fringing coral reef in beach protection of Hurghada, Gulf of Suez, Red Sea of Egypt. *Ecological Engineering* 22(1):17-25.

Gilbert, P., D.J. Evans, E. Evans, I.G. Duguid and M.R.W. Brown, 1991. Surface characteristics and adhesion of Escherichia coli and Staphylococcus epidermidis. *Journal of Applied Bacteriology*, 71: 72-77.

Hoffman, M. and A.W. Deccho, 1999. Extracellular enzymes within microbial biofilms and the role of the extracellular polymer matrix. In: J. Wingender, T.R. Neu and H.-C. Flemming (Eds), *Microbial Extracellular Polymeric Substances: Characterization, Structure, and Function*, Springer, pp. 217-227.

Ivanov V. and J., Chu. 2008. Applications of microorganisms to geotechnical engineering for bioclogging and biocementation of soil in situ. *Reviews in Environmental Science and Biotechnology* 7(2):139-153.

Jones K and E. Hanna. 2004. Design and implementation of an ecological engineering approach to coastal restoration at Loyola Beach, Kleberg County, Texas. *Ecological Engineering* 22(4-5):249-261.

Le Metayer-Levrel, G., S. Castanier, G. Orial, J.F. Loubiere and J.P. Perthuisot, 1999. Applications of bacterial carbonatogenesis to the protection and regeneration of limestones in buildings and historic patrimony. *Sedimentary Geology*, 126: 25-34.

Louis, L., P. Baud and T.F. Wong, 2007. Characterization of pore-space heterogeneity in sandstone by X-ray computed tomography. *Geological Society, London, Special Publications* 284: 127-146.

Murphy, E.M. and T.R. Ginn, 2000. Modeling microbial processes in porous media. *Hydrogeology Journal*, 8: 142-158.

Nemati, M. and G. Voordouw, 2003. Modification of porous media permeability, using calcium carbonate produced enzymatically in situ. *Enzyme and Microbial Technology*, 33: 635.

Normaniza O, Faisal HA, Barakbah SS. 2008. Engineering properties of Leucaena leucocephala for prevention of slope failure. *Ecological Engineering* 32(3):215-221.

Ritvo, G., O. Dassa and M. Kochba, 2003. Salinity and pH effect on the colloidal properties of suspended particles in super intensive aquaculture systems. *Aquaculture*, 218: 379-386.

Scholl, M.A., A.L. Mills, J.S. Herman and G.M. Hornberger, 1990. The influence of mineralogy and solution chemistry on the attachment of bacteria to representative aquifer materials. *Journal of Contaminant Hydrology*, 6: 321-336.

Sharma, M.M., Y.I. Chang and T.F. Yen, 1985. Reversible and irreversible surface charge modification of bacteria for facilitating transport through porous media. *Colloids and Surfaces*, 16: 193-206.

Torkzaban, S., S.S. Tazehkand, S.L. Walker and S.A. Bradford, 2008. Transport and fate of bacteria in porous media: Coupled effects of chemical conditions and pore space geometry. *Water Resources Research*, 44: 1-12.

Thullner, M., J. Zeyer and W. Kinzelbach, 2002. Influence of microbial growth on hydraulic properties of pore networks. *Transport in Porous Media*, 49: 99-122.

Van Loosdrecht, M.C.M., J. Lyklema, W. Norde, G. Schraa and A.J.B. Zehnder, 1987. The role of bacterial cell wall hydrophobicity in adhesion. *Applied and Environmental Microbiology*, 53(8): p. 1893-1897.

Van Loosdrecht, M.C.M., J. Lyklema, W. Norde and A.J.B. Zehnder, 1989. Bacterial Adhesion - a Physicochemical Approach. *Microbial Ecology*, 17: 1-15.

Van Meurs G.A., W.H. Van der Zon, J.W.M. Lambert, C.C.D.Van Ree, V.S. Whiffin and W.O. Molendijk. 2006. The challenge to adapt soil properties. In: Thomas HR, editor; *Proceedings of the 5th International Congress on Environmental Geotechnics: Opportunities, Challenges and Responsibilities for Environmental Geotechnics*; Cardiff, Wales. Thomas Telford Ltd. p 1658.

Whiffin V.S., J.W.M Lambert and C.C.D. Van Ree. 2005. Biogrout and Biosealing — Pore-Space Engineering with Bacteria. *Geostrata - Geo Institute for ASCE* 5(5):13-16,36.

Whiffin, V.S., L.A. Van Paassen and M.P. Harkes, 2007. Microbial Carbonate Precipitation as a Soil Improvement Technique. *Geomicrobiology Journal*, 24(5): p. 417-423.

5

# Strength at a distance:
a 5 m column experiment

Abstract

In order to evaluate MCP as a soil strengthening process, a five meter sand column was treated with bacteria and reagents under conditions that were realistic for field applications. The injection and reaction parameters were monitored during the process and both bacteria and process reagents could be injected over the full column length at low pressures (hydraulic gradient < 1; a flow rate of approximately 7 m day^{-1}) without resulting in clogging of the material. After treatment, the column was subjected to mechanical testing, which indicated a significant improvement of strength and stiffness over several meters. Calcium carbonate was precipitated over the entire 5 m treatment length. Improvement of the load bearing capacity of the soil without making the soil impermeable to fluids was shown with microbial carbonate precipitation, and this is a unique property compared to alternative soil treatment methods that are currently available for use in the subsurface.

1 Introduction

Microbial carbonate precipitation (MCP) has experienced an increased level of interest in recent years, for applications such as restoration of calcareous stone materials (Tiano et al. 1995; Castanier et al. 2000; Stocks-Fisher et al. 1999; Rodriguez-Navarro et al. 2003), bioremediation (Ferris 2003; Fujita et al. 2000; Warren et al. 2001), wastewater treatment (Hammes et al. 2003), strengthening of concrete (Ramachandran et al. 2001) and selective plugging for enhanced oil recovery (Ferris & Setehmeir 1992; Gollapudi et al. 1995; Nemati & Voordouw 2005). From a geotechnical perspective, the potential of MCP has been identified as a means of adapting soil properties to suit desired land-uses. Controlled precipitation of minerals in the pore space in such a way as to change macro-soil properties or so-called "pore-space engineering", is a new innovative approach in soil geotechnics with significant scope for development.

MCP can occur via a variety of processes whereby microbial activities result in the generation of carbonate in a calcium-rich environment (Castanier et al. 1999). The resulting $CaCO_3$ precipitation is governed by four key parameters: (i) calcium concentration, (ii) carbonate concentration, (iii) pH and (iv) the availability of nucleation sites (Hammes & Verstraete 2002). Many biological reactions can result in the production of carbonate or carbonate species. Because of its simplicity and the lack of an excess proton production, the most commonly studied system of applied MCP to date is urea hydrolysis via the enzyme urease, in a calcium rich environment.
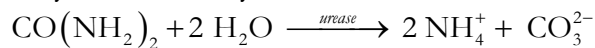
$$CO(NH_2)_2 + 2\,H_2O \xrightarrow{\;urease\;} 2\,NH_4^+ + CO_3^{2-}$$

In the presence of dissolved calcium ions, the produced carbonate ions will precipitate and form calcium carbonate crystals.

$$Ca^{2+} + CO_3^{2-} \rightarrow CaCO_3(s)$$
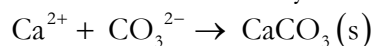
Other studies have concluded that an improvement in material strength is possible by inducing MCP, but usually the treatment has limited injection depth (in the order of centimeters) and it is often associated with a major reduction in permeability. In most cases bacteria and reagents are mixed with the granular material, sprayed on a surface or injected together under high velocity or pressure. Injection of bacteria and reagents together at low flow rates can result in full clogging of the system near the injection point (Stocks-Fischer et al. 1999). For the purposes of soil improvement, the reduction of permeability is an undesired characteristic. Lowering permeability in the treated area will promote redirection of natural groundwater flow paths. This can result in an increase in pore pressure in the soil which increases the risk of soil failure. The retention of soil permeability offers an additional advantage in that it also allows the additional application of further strengthening treatments and thus control over the amount of strengthening that is finally achieved.

The MCP investigations to date have focused on microbial carbonate precipitation for applications other than soil improvement, thus the important parameters for this specific application are yet to be evaluated (e.g. significant penetration depth (in the order of

meters) at low hydraulic gradients, retention of permeability, and the correlation of mechanical parameters with calcium carbonate content). The objective of this paper is to make a first correlation of these parameters and evaluate the feasibility of MCP for use as a soil improvement technique.

2   Materials and Methods

2.1   Column parameters and sampling

The five meter long PVC tube (internal diameter 66 mm) was positioned vertically and packed with 125-250 μm Itterbeck sand (Grain size characteristics: d_{10} = 110 μm (10% of the grains have a diameter of this size or lower); d_{50} = 165 μm; d_{90} = 275 μm) to a dry density of 1.65 g cm^{-3} (porosity of 37.8%). The column was positioned vertically with downward flow direction to avoid any settling of the packing material and generation of preferential flow paths that may occur if the column was positioned horizontally. Each end of the column was fitted with filter material consisting of three layers of scouring pad (Scotch Brite) at the outside and approximately 8 cm of filter gravel on the inside, next to the sand (Figure 1). Packing of the sand column was conducted under water to the required density to avoid the inclusion of air pockets.

Five water pressure transducers were fitted to monitor water pressure inside the column at 0, 0.5, 1, 2 and 3 m from the top of the column. In addition to these, the column was fitted with 10 pore fluid sampling ports (0.25, 0.5 and thereafter at 0.5 m intervals till 4.5 m). Fluid reservoirs containing the injected fluids (water, bacteria, CaCl$_2$, urea etc). were connected at the top of the column. A pump was installed at the bottom of the column to regulate the outflow rate and hydraulic head between free gravity flow of 1 L h^{-1} at a hydraulic head of 5 m when the pump was fully open and zero when the pump was fully closed.
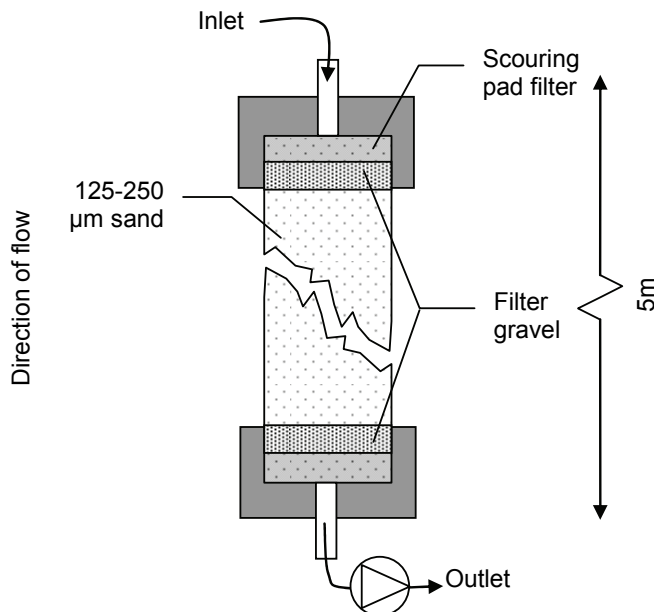

Figure 1: Schematic of column filter setup

Before any experiments were conducted, tap water was flushed through the column to test the pressure transducers and check the flow regulation of the pump at a constant flow rate of about 0.50 L h^{-1}. A hydraulic gradient of about 0.4 m m^{-1} was measured, yielding an initial hydraulic conductivity of 1 x 10^{-4} m s^{-1}. All subsequent experiments were performed at a constant injection flow rate of approximately 0.35 L h^{-1} and ambient temperature of 18°C ± 2.

During the course of the experiment, samples were taken from the sampling ports positioned along the column length and with an in-line feed from the effluent stream to an automated fraction collector. Immediately after collection the samples were centrifuged and the supernatant transferred to a clean tube, which was frozen at -18°C awaiting analysis. Samples were tested for urease activity, ammonium and calcium concentrations as required.

2.2   Microorganism

The urease positive microorganism used was *Sporosarcina pasteurii* DSM 33(DSMZ, FRG). Cultivation of the organism was conducted under aerobic batch conditions in a medium containing 20 g L^{-1} yeast extract and 10 g L^{-1} NH$_4$Cl, at a pH of 9. The organism was grown to early stationary phase before harvest (i.e. all readily available nutrients were consumed from the medium), and stored at 4°C for 48 hours prior to use.

2.3   Monitoring methods

2.3.1   Urease activity

In the absence of calcium ions, urease activity was determined by a conductivity method. The urease reaction involves the hydrolysis of non-ionic substrate urea to ionic products thus generating a proportionate increase in conductivity under standard conditions. 1 mL of bacterial suspension was added to 9 mL of 1.11 M urea (reaction concentration 1 M urea) and the relative conductivity change was recorded over 5 minutes at 20°C ± 2. The urease activity was then calculated taking the dilution into account.

This method was not suitable for determining urease activity in the presence of calcium ions (due to precipitation of calcium carbonate particles and the dampening effect of the counter ion on the solution conductivity), thus in these cases urease activity was determined from the ammonium production rate (see below). Both methods for determining urease activity were independently calibrated and correlated with each other.

2.3.2   Ammonium concentration

Ammonium concentration was determined by a modified Nessler method (Greenburg *et al.* 1992). The sample was diluted with deionised water to be in the range of 0-0.5 mM, using a volumetric flask. 2 mL of sample was added to a cuvette and mixed with 100 µl of Nessler reagent (Merck, Germany), and allowed to react for exactly 1 min. The sample was then read in a spectrophotometer at 425 nm. Absorbance readings were calibrated with several NH$_4$Cl standards measured under the same conditions.

2.3.3   Calcium concentration

Calcium concentration was determined with a commercial cuvette test for water hardness (LCK 327 – Hach Lange, Germany). Samples were diluted with deionised water to be within the concentration range of 5-100 mg-Ca^{2+} L^{-1}.

2.3.4   Calcium carbonate content

The calcium carbonate content of the cemented samples was measured with a U-tube manometer, under standard conditions (298 K, 1 atm). A 1-4 g sample was weighed into a glass vial, 2 mL of 2 M HCl was added in a separate compartment and the vial was sealed. The initial gas volume in the manometer was recorded, and then the two compartments were allowed to mix, resulting in acid dissolution of the sample and evolution of a proportionate amount of carbon dioxide gas. Samples were blanked against untreated sand and the method was calibrated with analytical grade $CaCO_3$.

2.3.5   Water pressure

The water pressure was measured using water pressure transducers (Model PDCR 10F – Druck Ltd, UK) that were numbered 1 to 5 (top to bottom) and were placed at 0, 0.5, 1, 2 and 3 m along the length of the column.

2.3.6   Flushed volume

The flushed volume (excluding the effluent and port samples) was collected in a container. The weight of the container was continuously monitored using a weight sensor (Model U2A - S/N 51759, maximal range 0-40 kg – HBM, Germany). The overall column flow rate was calculated from the total flushed volume (liquid in container plus effluent and port samples) versus time.

2.3.7   Strength, Stiffness, Porosity and Permeability

After dismantling of the column, the column was cut into 25 cm sections and compressive strength (q) and stiffness (E_{50}, Young's modulus at 50% of the peak stress) of the sections were determined by single-stage confined drained triaxial tests with a confining pressure of 50 kPa (conform to Dutch standard NEN-5117). Porosity was determined from the wet and dry densities of the samples after strength testing. Hydraulic conductivity (K) (which is directly related to permeability) was measured by a constant head test (conform to Dutch standard NEN-5123). The hydraulic conductivity and porosity of the cemented samples were compared with a sample of untreated material, which was prepared separately at similar dry density in a triaxial cell.

3   Results

3.1   Placement of bacteria prior to cementation

In order to immobilize bacteria in the column for use in subsequent cementation, a two-phase injection was conducted. First bacteria were injected to fill the column volume. When bacteria were detected in the outlet by visually observing an increase in turbidity and measuring the urease activity of the outflow fluid, one pore volume of 50 mM

calcium chloride solution (6.1 L) was injected to immobilize the bacteria in a moving reaction front in the column (European patent pending; EU05077869.5). A summary of column injections is given in Table 1.

Table 1: Summary of column injections - OD_{600} is the injected biomass concentration (measured by optical density at 600 nm); Act is the urease activity.

Phase	Description	Duration (h)	Flow rate (L h^{-1})	Volume (L)	Details
Rinse	water flush	30.7	0.35	10.75	Tap water
Placement	Bacterial injection	18.1	0.35	6.34	OD_{600}: 1.583
					Act: 0.23 mS min^{-1}
	CaCl$_2$ injection	17.1	0.35	5.99	0.05 M CaCl$_2$,
Cementation	Reaction fluid injection	24.9	0.35	8.72	1.1 M urea and CaCl$_2$
	No flow – reaction	102	0	0	-
Rinse	water flush	23.7	0.35	8.30	Tap water

3.2   Injection of urea and calcium for cementation

Immediately after the bacterial placement step, 8.7 L (1.43 pore volume) of 1.1 (equi-) molar urea and calcium chloride solution was injected to initiate cementation (Table 1). Under the constant flow conditions during injection, the movement of the front of reaction fluid (1.1 M urea/calcium) could be followed in the column until it reached the end of the column after about 18 hours (see supplementary material, figure 9). The first appearance of ammonium at each of the sampling ports along the column length was measured and matched with the residence time that the fluid had been present in the column (Figure 2).
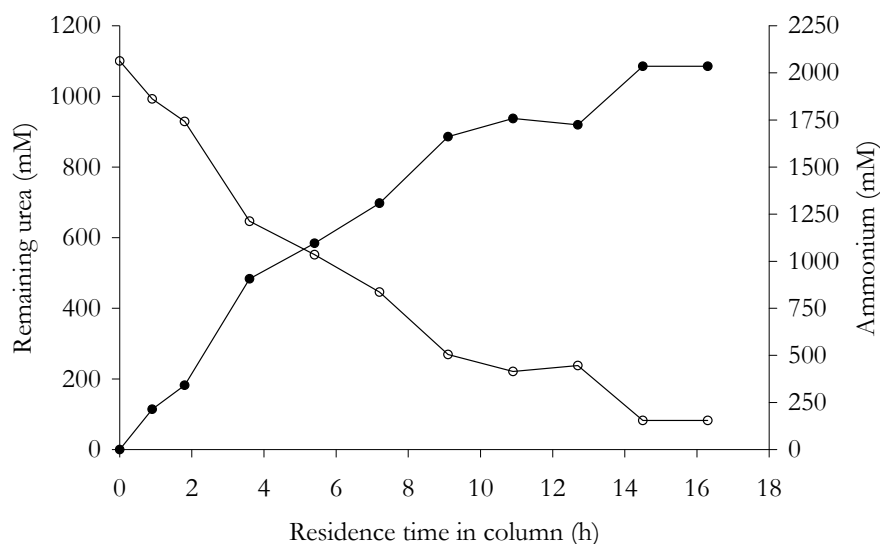

Figure 2: Movement of reaction front (estimate of front 250 mL of fluid) in column during the injection phase (0-17 hours). Ammonium concentration (●) and calculated available urea concentration (○) from the known molar ratio (2 NH$_4^+$: 1 urea).

The linear slope of the ammonium versus retention time line suggested that the ammonium was continuously being produced during injection and that the production

rate was relatively constant throughout the column (Figure 2). According to the ammonium production at the reaction front, 75-80% of injected urea was used in the top of the column (up to 2.85m) leaving only 20-25% for bottom section of column and thus only the possibility of significantly lower $CaCO_3$ precipitation in this section relative to the top of the column.

In an attempt to extend the injection distance, the injection of urea and calcium chloride solution was continued beyond one pore volume. During this time the ammonium concentration in the column effluent decreased, indicating that less urea was hydrolyzed during the time in the column. No bacteria were observed in the effluent. These observations suggested that the urease activity in the column had decreased over time.

In order to allow some cementation at the end of the column, the injection was continued at the same flow rate until less than 1.5 M ammonia was measured in the effluent, which indicated that at least 0.25 M unreacted urea had reached the end of the column. The total amount of calcium/urea injected was equivalent to 1.43 times the pore volume of the column (8.7 L).

The ammonium production rates were directly calculable: during the flow phase as the accumulation of ammonia between two sampling points and during the stationary phase as the accumulation in time at each particular sampling point of the column. The average ammonium production rate during stationary phase (27-53 h) was approximately a third of the rate observed at the reaction front during the injection phase (0-24 h) (180 mM NH_4^+ h^{-1}) during the injection phase versus 60 mM NH_4^+ h^{-1} in stationary phase (Figure 3).
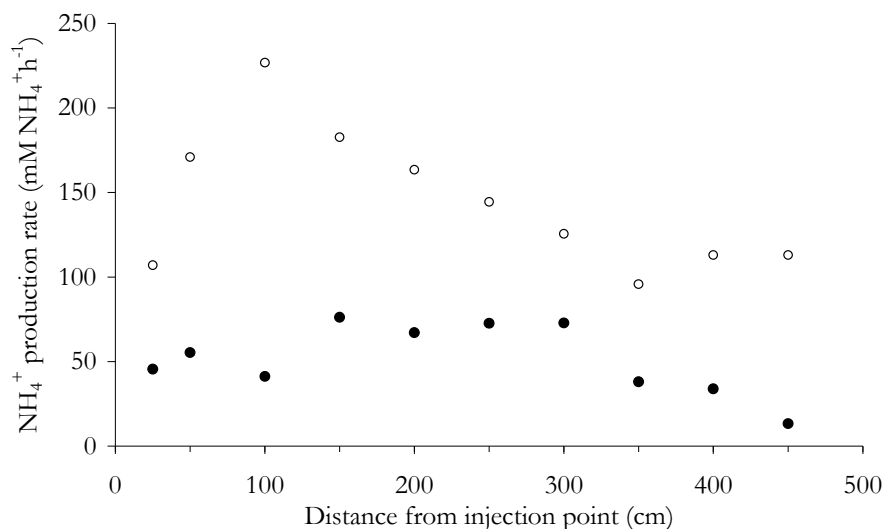

Figure 3: Ammonium production rates at each port along the column length at the first appearance of the urea/calcium (○) (during continuous flow) and at beginning of the stationary phase (●) (these rates were calculated between 27-53 hours, during which the R^2-values were greater than 0.93).

Calcium concentrations were measured in the pore fluid of the column at the end of the injection phase (24 h) and over several intervals until 124 hours. After 124 hours no

soluble calcium was detected in the pore fluid and the precipitation reaction was complete (Figure 4).
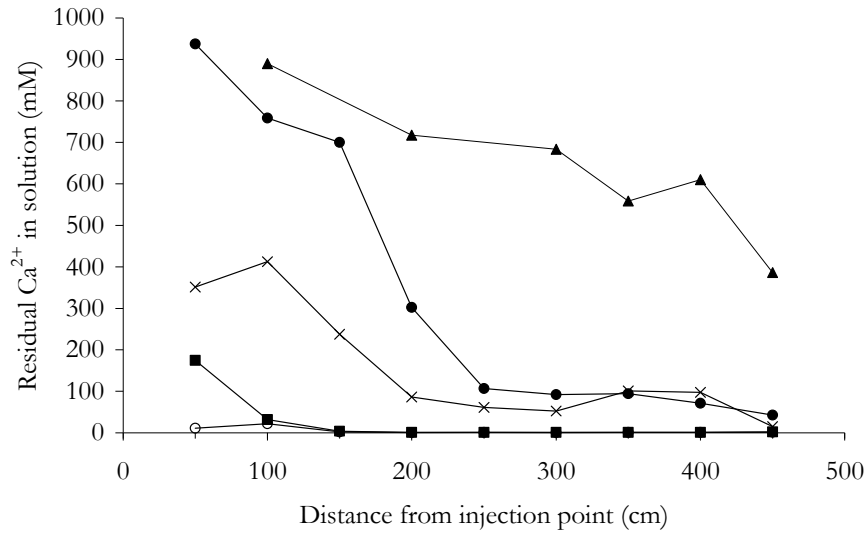

Figure 4: Calcium concentration in the pore fluid (i.e. not yet precipitated) after 24 h (▲) (at the end of the injection phase), 32.5 h (●), 53 h (x), 96 h (■) and 124 h (○). Injected calcium concentration was 1.1 M.

3.3   CaCO$_3$ profile along the column

After cementation was complete, the column was flushed with excess water, the filter material was removed and the remaining sand column was cut with a saw into 25 cm sections for evaluation of the mechanical properties. An average calcium carbonate content value was determined from at least three samples for each column section (Figure 5).
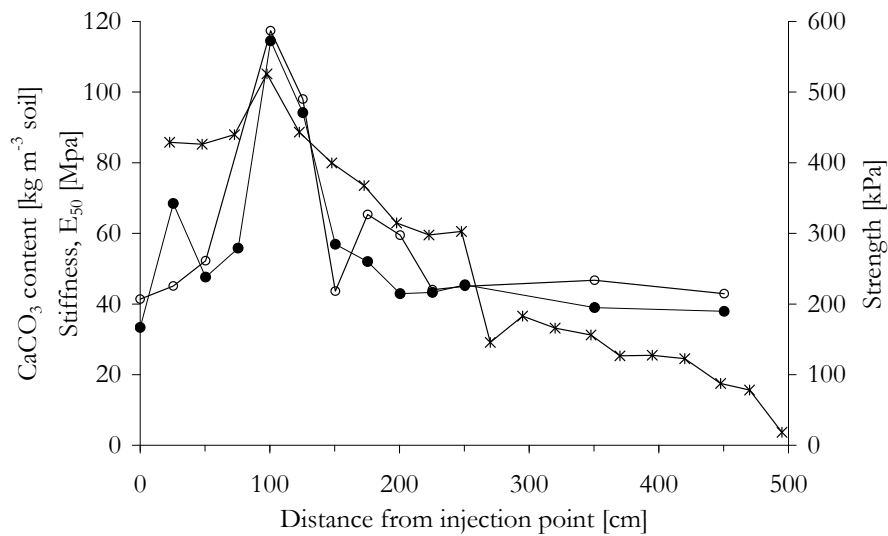
Figure 5:   Calcium carbonate content (*), stiffness, E$_{50}$ (○) and compressive strength (●) profiles along the column length.   The column was injected with 8.715 L of 1.1 M urea/calcium which can react to produce an average overall column value of 59.2 kg CaCO$_3$ m^{-3}.

3.4 Effect of cementation on porosity

Porosity was determined from the difference between wet and dry densities during strength testing assuming full saturation with water. The porosity was compared with the porosity of an untreated sand column prepared at similar initial density in the triaxial cell. The presence of calcium carbonate had a clear effect on porosity of the material and a reasonably linear relationship between the two parameters was observed. At the maximum calcium carbonate content (105 kg m^{-3} CaCO$_3$) the column porosity was decreased to 90% of the untreated material (Figure 6).
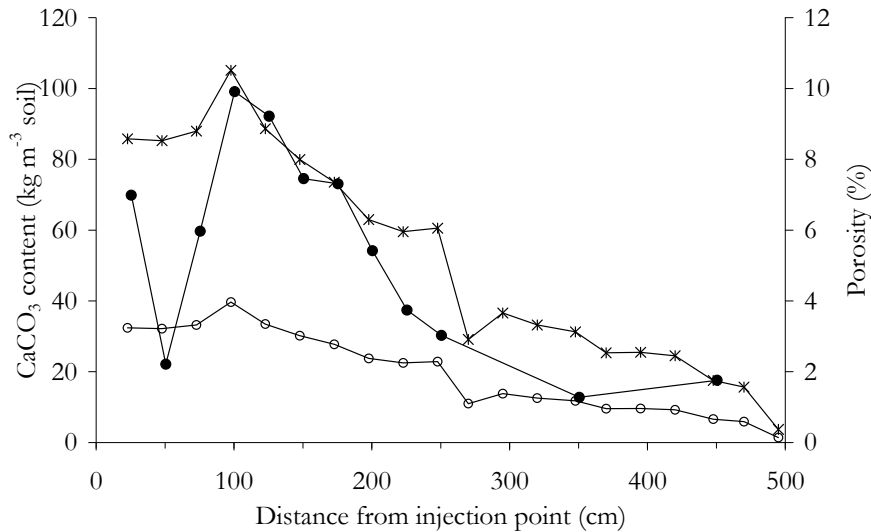
Figure 6: Profiles over the length of the column for the calcium carbonate content (*) and relative decrease in porosity. Porosity is determined by the differences between wet and dry density of treated samples compared to an untreated sample at similar initial density (●) and based on the calcium carbonate content (○).

Alternatively the porosity can be determined from dry density alone assuming a particle density of 2650 kg m^{-3} for the solid fraction (Chapter 7). The decrease in porosity after treatment can be calculated from the average CaCO$_3$ content and using a density of calcite (2710 kg m^{-3}) and assuming that the decrease in porosity is equal the increase in solid fraction by precipitation of calcium carbonate. This alternative method gives a slightly different picture for the porosity and for the decrease of porosity after treatment. Where a maximum porosity reduction is reported of 10% according to the alternative method the amount of precipitated CaCO$_3$ can only account for 4% porosity reduction. The difference between the two methods might be due to variations in the porosity before treatment. By subtracting the calcium carbonate content from the dry mass after treatment the initial dry density can be calculated (as in chapter 7). According to this procedure, the initial dry density of the sand packed column varied between 1487 and 1600 kg m^{-3}. A structural difference exists between the average dry density during packing (1650 kg m^{-3}) and the average calculated initial dry density of the tested samples after extraction from the column (1542 kg m^{-3}), which might be explained by differences in the volumetric measurements or disturbance during sample extraction. The variation in dry density might be causing the lack of correlation between CaCO$_3$ content and porosity in

figure 6. Observing that the strength correlates better to dry density than to $CaCO_3$ content supports the use of the latter method, which is also discussed in chapter 7.

3.5   Effect of cementation on strength, stiffness and permeability

The strength and stiffness was determined along the length of the column (figure 5). In order to determine the effect of calcium carbonate precipitation on the mechanical properties of the treated material, the strength, stiffness and permeability results were correlated with the calcium carbonate content of each of the tested samples (figure 7 and 8).   Low calcium carbonate concentrations (below 60 kg m^{-3}) did not significantly improve the strength of the samples. At higher calcium carbonate contents there was a significant improvement in strength relative to untreated sand.   The highest strength in the column was 570 kPa, which was measured at the same location as the maximum amount of $CaCO_3$, at approximately 1 m from the injection point (figure 5).   An apparent minimum calcium carbonate content of 60 kg m^{-3} was required for a measurable strength improvement in the material under the testing conditions (figure 7).
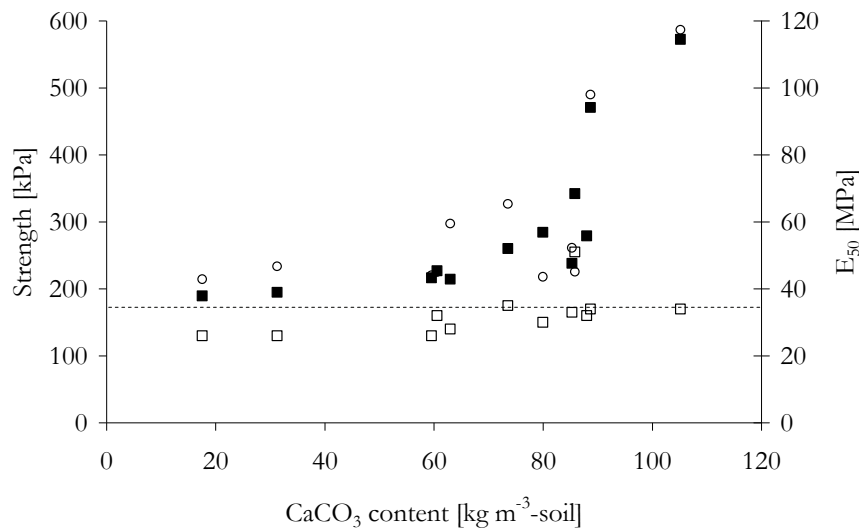

Figure 7:   Confined compressive strength (■), stiffness, E_{50} (○; Young's modulus at 50% of the peak stress) and residual strength of material after failure (□) versus calcium carbonate content.   Confining pressure was 50 kPa.   Under the same consolidation conditions, untreated sand of the same density gave a strength value of 167 kPa (dashed line) and a residual strength of 130 kPa.

The stiffness showed a similar trend as strength, where E_{50} is about 200 times the peak stress. Residual strength was also determined after failure and the residual strength values were comparable with unconsolidated sand, irrespective of the amount of calcium carbonate present (Figure 7).   This indicated that once the bonds were broken, the increase in strength of the material was almost completely lost.   The low residual strength attribute of the material highlights the importance of careful sample handling prior to evaluation.

Pressure measurements showed that the hydraulic conductivity over the top 50 cm of the column already significantly decreased during the injection of bacteria from 1 x 10^{-4} m s^{-1} to 3 x 10^{-5} m s^{-1} (supplementary material, figure 10). After the column was rinsed the pressure measurements showed that in the top 50 cm the permeability was reduced by

80% to 2 x 10^{-5} m s^{-1}, between 0.5 and 2 m by 40% to 6 x 10^{-5} m s^{-1} and between 2 and 3 m by 20% to 8 x 10^{-5} m s^{-1}.

After the column was dismantled, permeability was directly measured on each section prior to triaxial testing. Permeability was slightly reduced over the entire column after treatment but the effect was constant and did not appear to be related to calcium carbonate content (Figure 8).
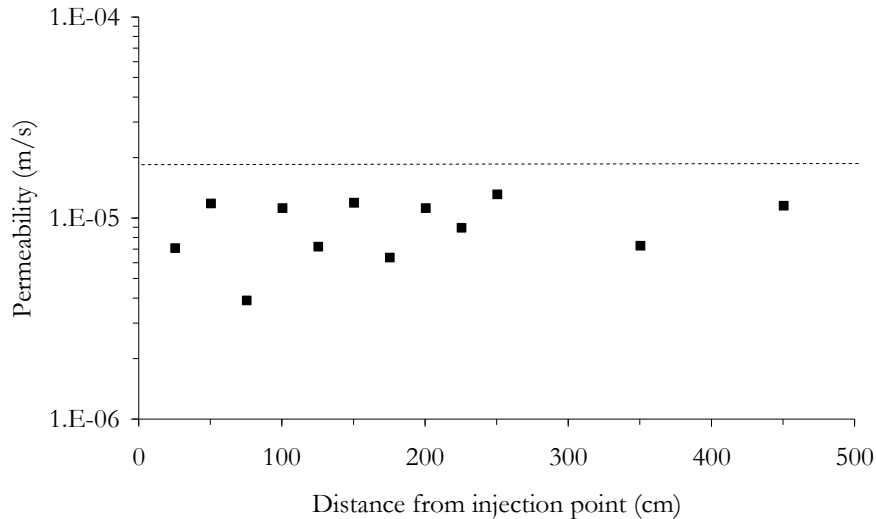

Figure 8: Permeability over the core length determined after treatment during the triaxial test. Permeability was determined by constant head test. Initial material permeability before treatment is indicated by a dashed line (1.92 x 10^{-5} m s^{-1}).

4 Discussion

Precipitated calcium carbonate was detected over the entire length of the column (Figure 5), indicating that bacteria and reactants were present at all locations. However, the profile of calcium carbonate was not homogeneous over the column length. A gradient was evident with relatively high amounts of calcium carbonate at the injection end (top) that decreased over the length (Figure 5).

Under the low flow conditions that are suitable for field applications (i.e. in order to avoid soil fracturing), it is clear that the cementation process had already begun during the injection phase. This was evident by production of ammonium during injection (Figure 2) and lower concentrations of calcium in the pore fluid at the end of the column compared to the beginning (Figure 4). Because of the high conversion and slow flow rates, the top of the column closest to the injection port was exposed to significantly more reactants than the bottom and the profile of calcium carbonate reflected this (Figure 5). In order to produce a more homogeneous result, the balance between supply and conversion needs be shifted. For example faster flow rates will move the cementation reactants further into the column allowing less time for reaction along the path, and similarly lower conversion rates will leave more reactants in the fluid, also resulting in further infiltration distances.

The capability of bacteria to degrade urea appeared to decrease during the reaction time (Figure 3, 4). During the injection phase (0-24.5 h) the average ammonium production rate was 180 mM NH_4^+ h^{-1} compared to 60 mM NH_4^+ h^{-1} during the stationary phase (24-48 h). Possible reasons for this reduction in activity could be related to:

- *A reduction of the pore volume*, caused by precipitation of calcium carbonate in the pore spaces, resulting in an increase in flow velocity and a consequent decrease in residence and thus reaction time.
- *Increase in the amount of CaCO₃ solids precipitated* – resulting in a diffusion barrier around the microorganisms and limiting access to substrate or removal of by-products.
- *Decrease in urea concentration* – this is not a very likely possibility according to the Michaelis Menten kinetics (K_m = 18.5 mM; V_{max} = 200 mS min^{-1} OD_{600}^{-1})
- *Degeneration of bacterial viability in cementation conditions* – this could be related to conditions or possibly the formation of a diffusion barrier around the cell surface.

4.1   Effect of cementation on engineering parameters

Lower concentrations of calcium carbonate (below 60 kg m^{-3} or 3.5% w/w) had no significant effect on strength or stiffness properties relative to untreated sand (Figure 7). At calcium carbonate contents above this value, a clear improvement was evident that was proportional to the amount of precipitate present. After the initial strength measurement, the residual strength after failure was also determined and in all samples this value approximated the strength of untreated sand (Figure 7). This indicated that any strength improvement given by the treatment was lost after failure and thus the material was more characteristic of rock than soil. In future experiments it would be useful to extend the upper range of calcium carbonate precipitated, to give a broader understanding of the relationship between strength/stiffness and calcium carbonate content.

The apparent minimum calcium carbonate content for strength may also partly be attributable to other characteristics of the process (e.g. sand type, solute concentrations, initial density, etc.) or perhaps sample handling after treatment. For example, the solute concentrations rate of hydrolysis are known to play a role in speed and hence type of crystals that are formed (chapter 3). Given the changes in concentration over the course of the reaction, it is possible that qualitative factors (i.e. factors other than simple quantity) may also contribute to lower strength crystals. In addition, lower strengths are more difficult to preserve with sample handling (e.g. sawing of the column into sections, removal and handling during testing). It is possible that lower strengths are compromised during these procedures.

Two essential parameters for understanding fluid movement in soils are porosity and permeability (or hydraulic conductivity). Porosity is the proportion of non-solid (void) volume relative to the total volume of the material. The precipitation of calcium carbonate in the pore spaces reduces the void volume. Consequently, a decrease in porosity was expected proportional to the amount of calcium carbonate present at a given location (Figure 6). At the highest calcium carbonate content, the porosity changed from 38% to 33% when calculated from the amount precipitated calcium carbonate. When calculated from the difference between wet and dry density, assuming a constant initial density in the column and comparing it to an untreated sample at similar density

the porosity at maximum carbonate content decreased from 41% before treatment to 31% after treatment. Difference between the two methods might be explained by variations in the initial density before treatment (see chapter 7) and differences in the volumetric measurements or disturbance during sample extraction.

Permeability indicates how easy fluids flow through porous media or how the voids in the soil are interconnected. Porosity and permeability are often related. If the porosity is high and the pores are well connected, (such as uncemented granular materials) permeability will be high. If the porosity is low or the pores are badly connected the permeability will be low. The permeability was slightly reduced after treatment over the entire column, irrespective of calcium carbonate content (Figure 8). The average permeability over the column after treatment was $9x10^{-6}$ m s^{-1} compared to the original material permeability of $2x10^{-5}$ m s^{-1} (when measured in the triaxial cell). The lack of correlation between $CaCO_3$ content and permeability might be due to several factors:

1. A large part of the reduction in permeability (especially in the top part) might be caused by strained bacteria (Supplementary material, Figure 10).
2. Secondly, in the top part of the column the $CaCO_3$ content was not homogeneously distributed. Where strength depends more on average values for $CaCO_3$ content, the permeability is more affected by heterogeneities. A small zone with low permeability can affect the measured permeability over a whole column section, while compressive strength remains hardly influenced.
3. Another aspect is that the obtained amount of $CaCO_3$ is relatively little. In this range it is even hard to establish a correlation between strength and $CaCO_3$ content.
4. There might also be some trapped air entrapped in the column either during packing or due to the degradation of biomass or during the handling between demobilizing the column and setting it up in the triaxial cell.

The lack of correlation between $CaCO_3$ content and permeability suggested either that the reduction of permeability was more affected by the nature and packing of the original material and the treatment (the flowing of fluids though the material) than by the cementation process itself or that the method of evaluation was not sensitive enough to detect the small changes caused by the process. Finally there was also a large difference between the permeability which is measured over the whole 5 m column ($1 x 10^{-4}$ m s^{-1}; Supplementary material Figure 10) and the permeability measured over different sections in the triaxial cell. This difference is considered due to wall effects along the sides of the PVC column.

5 Conclusions

The following conclusions can be drawn from this work:

- Bacteria were placed in the column over the entire 5 m length to a reasonable degree of homogeneity at a low injection rate and with no associated clogging.
- The maximum attainable injection distance did not appear to be limited to 5 meters and it may be possible to extend this distance further.
- The bacterial activity is not a constant but declines over the injection time.
- A significant strength increase was demonstrated after the treatment. The strength improvement was higher at the top compared to the bottom of the column, however

this is largely related to the supply of cementation reactants versus the bacterial activity in the column.

- An apparent minimum calcium carbonate content was required for a measurable increase in strength (60 kg m^{-3}). This could be linked to over saturation concentrations of the crystal pre-cursors (calcium and carbonate) and/or possible handling limitations of low strength samples.

- The flow conditions in this experiment were limited to 1-D by the column walls. In a real application flow will have 3-D properties and fluid density and transport times will play a more significant role.

- A continuous cementation process is more realistic of field conditions and may be necessary in a 3-D fluid flow situation. Control under these conditions will be essential for real applications.

This work presents a new application for MCP as a ground improvement technique. Precipitation of calcium carbonate by microbial methods made a significant improvement in soil strength without a major reduction in permeability. For ground improvement requirements, it is desirable to achieve this result at low injection pressures, which are acquired with relatively low flow rates (<10 m day^{-1}). This study was conducted under such conditions and successful soil strengthening was achieved. In addition a clear critical aspect of this process has been identified. Balancing the rate of urea hydrolysis in the column with the delivery of reactants via the flow rate is essential to precipitate calcium carbonate at locations where strengthening is desired. When these two parameters are out of balance, a non-homogeneous result will be attained with higher strengths near the injection point. This work demonstrated that microbial carbonate precipitation can be applied for large-scale soil improvement work and further development of the technique for this application area is warranted.

References

Castanier S, Le Metayer-Levrel G, Perthuisot JP. 1999. Ca-carbonates precipitation and limestone genesis - the microbiogeologist point of view. *Sedimentary Geology* 126:9-23

Castanier S, Le Metayer-Levrel G, Perthuisot JP. 2000. Bacterial carbonatogenesis and applications to preservation and restoration of historic property. In: Ciferri O, Tiano P, Mastromei G, editors. *Of microbes and art: the role of microbial communities in the degradation and protection of cultural heritage*. Kluwer Academic-Plenum, Amsterdam. P 246-262.

Ferris FG, Setehmeir LG. 1992. Bacteriogenic mineral plugging. United States patent 664769.

Ferris FG, Phoenix V, Fujita Y, Smith RW. 2003. Kinetics of calcite precipitation induced by ureolytic bacteria at 10°C to 20°C in artificial groundwater. *Geochemica et Cosmochimica Acta* 67:1701-1722.

Fujita Y, Ferris FG, Lawson RD, Colwell FS, Smith RW. 2000. Calcium carbonate precipitation by ureolytic subsurface bacteria. *Geomicrobiology Journal* 17:305-318.

Greenburg AE, Clesceri LS, Eaton AD. 1992. *Standard methods for the examination of water and wastewater*, 18th edn. American Public Health Association, Washington.

Gollapudi UK, Knutson CL, Bang SS, Islam MR. 1995. A new method for controlling leaching through permeable channels. *Chemosphere* 30:695-705.

Hammes F, Verstraete W. 2002. Key roles of pH and calcium metabolism in microbial carbonate precipitation. *Reviews in Environmental Science & Biotechnology* 1:3-7.

Hammes F, Seka A, De Knijf S, Verstraete W. 2003. A novel approach to calcium removal from calcium-rich industrial wastewater. *Water Research* 37:699-704

Nemati M, Voordouw G. 2005. Permeability profile modification using bacterially formed calcium carbonate: comparison with enzymic option. Process Biochemistry 40:925-933.

Ramachandran SK, Ramakrishnan V, Bang SS. 2001. Remediation of concrete using micro-organisms. *ACI Materials Journal* 1:3-9.

Rodriguez-Navarro C, Rodriguez-Gallego M, Chekroun KB, Gonzalez-Munoz MT. 2003. Conservation of ornamental stone by *Myxococcus xanthus* induced carbonate biomineralisation. *Applied and Environmental Microbiology* 69:2182-2193.

Stocks-Fischer S, Galinat JK, Bang SS. 1999. Microbiological precipitation of $CaCO_3$. *Soil Biology and Biochemistry* 31:1563-1571.

Tiano P. 1995. Stone reinforcement by calcite crystal precipitation induced by organic matrix macromolecules. *Studies in Conservation* 40:171-176

Warren LA, Maurice PA, Parmar N, Ferris FG. 2001. Microbially mediated calcium carbonate precipitation: Implications for interpreting calcite precipitation and for solid-phase capture of inorganic contaminants. *Geomicrobiology Journal* 18:93-115.

Supplementary material
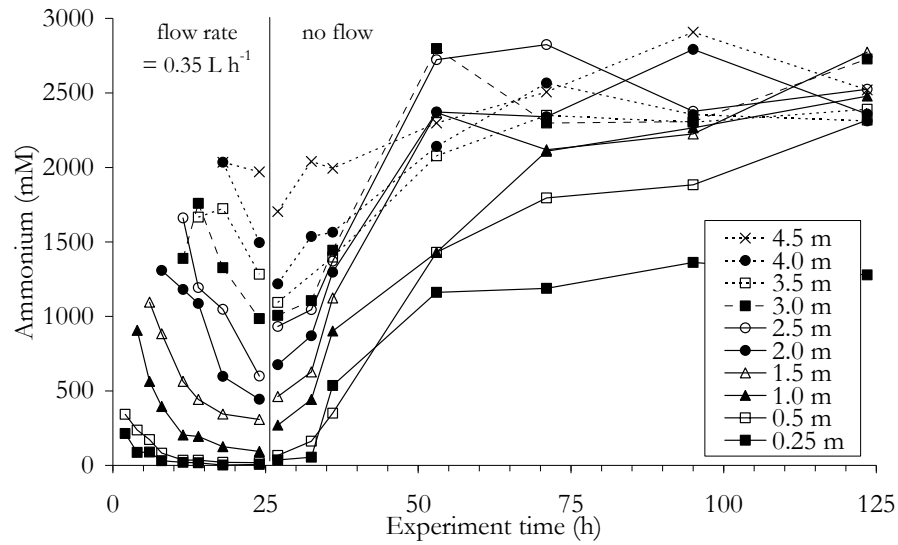
Figure 9 Measured ammonium concentrations in time (t=0 is the start of the cementation solution)
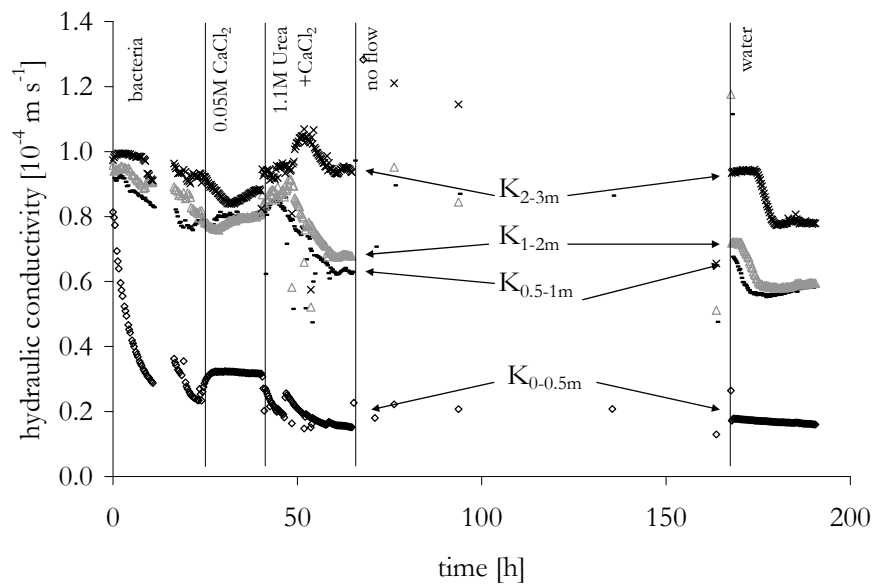
Figure 10 Hydraulic conductivity from pressure measurements along the column calculated using Darcy's law, while neglecting the changes in viscosity and density (At t=0 is the injection of bacteria is initiated).

6

Scale up of Biogrout: experiments at $1m^3$ and $100m^3$ scale

Abstract

Biogrout is a ground improvement method based on microbiologically induced precipitation of calcium carbonate by urea hydrolysis. So far, the feasibility of Biogrout has been studied in the laboratory using (one-dimensional) sand column experiments. The next challenge was to scale up the new technology and establish strengthening over larger soil volumes. In practice, grouting is often not a one-dimensional process. Fluids are injected in the subsurface through wells. Around these wells liquids move either spherically in case of a single point injection or radially in case of a linear well. In this study the feasibility of the Biogrout process is demonstrated in a stepwise scale-up approach using similar conditions and techniques to field scale applications. First, two experiments in sand filled boxes of one cubic meter are presented, which simulate a spherical injection from a single point. The gained experience from these experiments enabled a large scale experiment (100 m³) in which sand was treated over a distance of 5 m using screens of injection and extraction wells. Both scale up experiments showed significant strength increase, but also distinct spatial heterogeneity. Possible causes of this heterogeneity are discussed.

1 Introduction

The potential of biological techniques for ground reinforcement -biogrouting- is being investigated (DeJong et al. 2006; Whiffin et al. 2007; Ivanov & Chu 2008). Most studies on biogrouting, use micro-organisms containing the enzyme urease and in particular the bacterium *Sporosarcina pasteurii* DSM 33 (DSMZ, FRG), renamed from *Bacillus pasteurii* (DeJong et al. 2006; Whiffin et al. 2007). These micro-organisms are cultivated aerobically in the laboratory, introduced in the soil and supplied with a solution of urea and calcium chloride. The microbial urease catalyzes the hydrolysis of urea into ammonium and carbonate. In the presence of dissolved calcium ions, the produced carbonate ions will precipitate and form calcium carbonate crystals. The remaining ammonium chloride solution is removed by physical extraction and rinsing with water. Once precipitated, the calcium carbonate will only dissolve very slowly (at a geological time scale), either by continuously flushing with buffered acidic groundwater or as a result of acidifying processes in the pores (e.g. nitrification, degradation of biomass). When sufficient calcium carbonate is precipitated, durable soil stabilization can be achieved.

Using an injection procedure in which bacteria and reagents were injected sequentially (Harkes et al. 2009) in order to prevent clogging near the inlet, the feasibility of Biogrout has been demonstrated in 20 cm sand column experiments, which were cemented to a controllable strength varying from loosely cemented sand to moderately strong rock with unconfined compressive strengths of 0.2 – 20 MPa (Harkes et al. 2008). The corresponding amount of precipitated calcium carbonate varied from 30 to 600 kg m^{-3} and a clear correlation was established between $CaCO_3$ content and unconfined compressive strength (Harkes et al. 2008). Subsequently Whiffin et al. (2007) showed that cementation could be induced over a long distance from an injection well, by performing a 5 m column experiment.

In practice, conventional ground reinforcement methods are not one-dimensional processes. Cement and chemical grouts are mostly injected in the ground by wells, either radially when injected through a linear tube well or spherically when injected from a single point. To evaluate the potential of Biogrout for field applications, experiments were performed in controlled 3D environments, using conditions and injection techniques resembling those envisioned in practice.

2 Scale up experiments

2.1 1 m³ experiments

To mimic a spherical injection from a single point, two experiments were performed in a multibox container set-up (0.9x1.1x1 m³), having drainage filters on the sides. The drainage filters were covered with geotextile preventing sand transport. The box was filled with sand, which was packed by dropping the filled box a few times using a forklift to a homogeneous density. Two types of sand were used. In the first container a sand

from river Meuse was used, which was uniform, medium grained (d_{50}: 0.367 mm; d_{60}/d_{10}: 1.6; (BSI 1999)) and mainly siliceous (93%). In the second, a sand from a quarry in Itterbeck, Germany (Smals IKW, SZI 0032, also referred to as Itterbeck fine) was used. This sand was uniform, fine to medium grained (d_{50}: 0.166 mm; d_{60}/d_{10}: 1.64; (BSI 1999)) and mainly siliceous (97%) and similar as the sand used to previously reported column experiments (Whiffin et al. 2007). 100 L bacterial suspension was aerobically cultivated using a sterilized nutrient medium containing yeast extract (20 g L^{-1}), ammonium chloride (10 g L^{-1}) and a trace amount of nickel chloride (10μM to promote the assimilation of urease enzymes). Reagent solutions were prepared containing 0.5 M urea and calcium chloride (industrial grade). Fluids were injected sequentially with constant flow rate (50 L h^{-1}) at the centre of the box and drained along the sides, maintaining a constant flow rate and a constant water level at the sides.

The first test, using sand from Meuse river, showed that the majority of bacteria flushed out and the remaining urease activity decreased exponentially in time. After 50 days, in which 3.5 m³ of reagent solution was flushed through in 8 batches, about 200 mol $CaCO_3$ (20 kg m^{-3}) had been precipitated inside the sand with 12% of the reagents being converted. Excavation of the sand body showed that hardly any $CaCO_3$ was retained in the sand, apart from some areas along the sides mostly in the corners and at the bottom. The conversion was probably restricted to those areas where bacteria were not flushed out. The bacteria were either retained due to relatively low flow velocity or trapped in the geotextile.

In the second experiment with Itterbeck fine sand the injection pressure rose gradually during treatment to a maximum of 1 bar. Several times a pressure drop was observed during flushing, indicating the likely occurrence of fracturing events. After three of such events, sand transporting wells appeared at the sand surface, indicating preferential flow paths upwards, diverging from the ideal spherical injection. After these events, flow was stopped and a clay/cement plug installed (or enlarged) to prevent further leakage. The urease activity dropped gradually in time. During day 20 (after 2500 L was flushed through) the ammonium concentration in the effluent, which was produced in 48 hours, reached only 0.4 M, indicating that the average urease activity had dropped below 5 mM urea h^{-1} (less than 25% of the observed activity during the first flushes). At day 25 (after 2650 L was flushed through) 50 L of additional bacterial suspension was injected increasing the maximum ammonium production rate up to 0.7 M day^{-1}, or 15 mM urea h^{-1}, which dropped only slightly during the further duration of the experiment. After 40 days, in which 4000 L of reagent solution was flushed through in 16 batches, about 1000 mol $CaCO_3$ (100 kg m^{-3}) was formed inside the sand box with 50% of the injected urea being hydrolysed. Manual cone penetration tests indicated cone resistances higher than 5 MPa at shallow depth. Removing the loose sand with a water hose from the top revealed a strongly cemented surface. At one side ridges with high $CaCO_3$ content were observed in a regular pattern parallel to the induced flow direction, which is assumed to be perpendicular to the drainage filters (Figure 2).

Figure 2 The surface of the cemented sand body of the second cubic meter test. Ridges with high CaCO₃ content are visible in a regular patterns on the left.

Figure 3 The spherically shaped cemented sand body.

Opening the box showed that the cemented sand body had a spherical shape, which could be expected from a single point injection (Figure 3). Further excavation indicated that the areas close to the injection point and along the principal flow axes (horizontally towards the drained sides and vertically upwards as result of the leakage events) contained less CaCO$_3$, which was attributed to a lower retention of bacteria or crystals in those areas due to a higher velocity and lower hydraulic residence time. In the lower half towards the bottom corners of the sand body the highest amount of CaCO$_3$ was found

(up to 250 kg m⁻³ or 17% of dry weight, Figure 4). The unconfined compressive strength (BSI 1999) varied between 0 (loose sand which could not be tested) and 9 MPa, reasonably correlating with the $CaCO_3$ content.
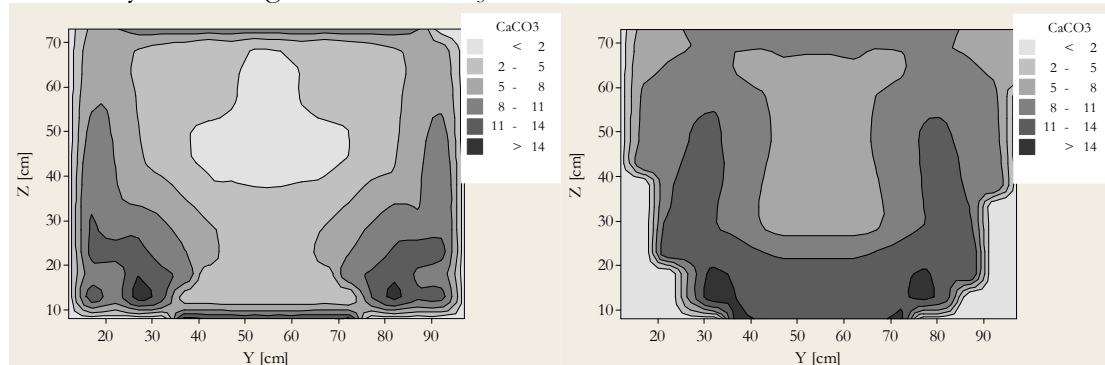
Figure 4 CaCO₃ measurements on samples taken from a quarter of the second cubic meter enabled the construction of cross-sections through the cemented sand body. Both cross-sections are parallel to the side showing in figure 3: on the left close to mid cross-section (at x = 39 cm) and on the right close to the side (at x = 14 cm) (Contours are mirrored over the mid cross-section (y = 55 cm). Gray scales indicate CaCO₃ content from <2 (light) to >14 (dark) in % of dry weight.

2.2 100m³ experiment

The last scale up step before commercial application was an experiment at large scale (100 m³, Figure 5). A concrete box (8 x 5.6 x 2.5 m) set-up was filled (under wet conditions) with sand (Itterbeck fine) with an average dry density of 1560 kg m⁻³. A bioreactor was build on site, in which bacteria were cultivated in 5 m³ nutrient broth under non-sterile conditions, but using an axenically cultivated 100 L inoculum.

Figure 5 set-up for large scale Biogrout experiment (100m³). Three injection wells (left) and three extraction wells (right) were used to flush liquids through the sand body.

Fluids were injected sequentially in batches through three injection wells and transported over a distance of 5 m along the length of the sand box towards three extraction wells. Total flow rate was approximately 1 m^3 h^{-1} with a hydraulic gradient of about 0.3 m m^{-1}.

Geophysical measurements (shear wave transmission from top to bottom) indicated a significant increase in average stiffness (almost tenfold, see chapter 8) around the injection points, after 1 day of flushing. Manual cone penetration tests showed that after several days of flushing the cone resistance around the phreatic surface became higher than 5 MPa.

Within 12 days 100 m^3 of reagent solution containing 1M urea and calcium chloride was flushed through in 10 batches. Measurement of ammonium concentration in the effluent indicated that at least 80% of the urea was hydrolyzed. After treatment the sand was rinsed with water and excavated. The cemented sand body, about 40 m^3 became clearly visible and was limited by the induced hydrological flow field. Flow lines could be distinguished, especially close to the extraction wells (Figure 6).

Cementation along the flow lines was reasonably homogeneous, while perpendicular to the flow lines $CaCO_3$ content varied significantly. Excavation of a vertical cross-section along the centre flow line (Figure 7) showed that below the cemented phreatic surface lenses were formed with $CaCO_3$ content varying from 0.8 to 24 % of the dry weight.
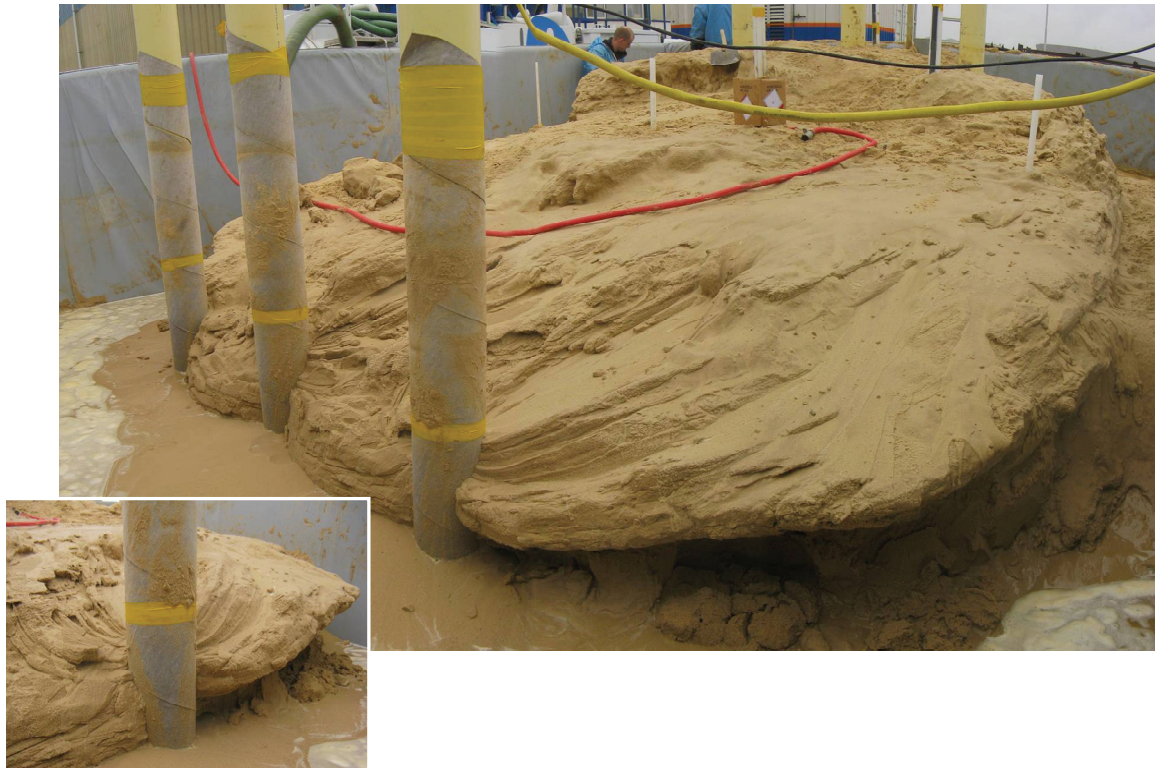

Figure 6 The exposed cemented sand body of the 100m3 sxcale experiment. Close to the extraction point the cemented patterns are clearly related to the flow paths through the sand body.
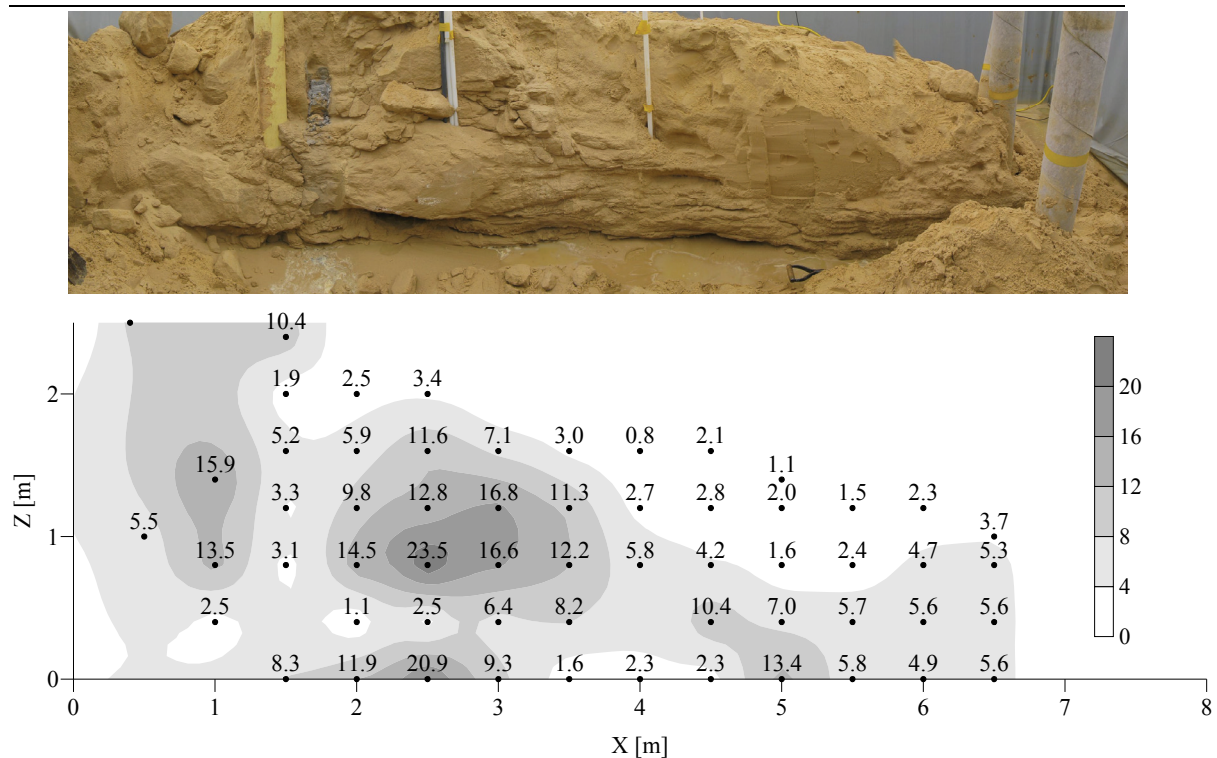
Figure 7 Cross-section along the longitudinal centre line through the centre injection and extraction well of the large scale Biogrout experiment showing CaCO₃ content in [% of total dry weight]. The injection well is located at 1.5 m and the extraction well at 6.5 m.

Lenses had a thickness in the order of centimetres and extended horizontally at a scale of meters. Several cemented blocks were sampled, from which cores were drilled to test geotechnical parameters. Unconfined compressive strength varied considerably from 0 to 12 MPa and showed reasonable correlation with dry density and CaCO₃ content (see chapter 7).

3 Discussion on the heterogeneity of resulting properties

The scale up experiments showed significant cementation at large distance from the injection points, proving the technical feasibility of Biogrout for ground reinforcement. However, the CaCO₃ content and consequent geotechnical parameters were not as homogeneously distributed as desired, both on a macro as well as on a micro-scale. Although initial conditions, like layers in the sand packing, could explain part of the observed variability, it is assumed that a large part of the observed heterogeneity is process induced. Several mechanisms, which might explain the observed heterogeneities, are discussed below:

Firstly, the amount of precipitated CaCO₃ at a specific location depends on the amount available urea catalyzing bacteria. The distribution of bacteria and bacterial activity, both in time and space, is hard to assess. During injection of bacteria, the distribution of

bacteria varied over the distance and between different flow paths. The attachment of bacteria depends on many factors, including grain size distribution, mineralogy, properties of the pore fluid and of the bacteria themselves (Scholl et al. 1990; Torkzaban et al. 2008). After placement, the attached bacteria could have lysed (and excreting their enzymes), flushed out, or become encapsulated in the crystals, all resulting in a decrease in activity in time. Difference in bacterial attachment is one of the possible explanations for the difference in $CaCO_3$ content and strength results between the two 1 m³ experiments and the distribution of these properties within each experiment.

Secondly, the $CaCO_3$ content depends on the amount of supplied reagents and the way of supplying it. During the injection of urea and calcium chloride, the reagents are converted, while being transported within the soil. Consequently, close to the injection points more $CaCO_3$ will form than towards the extraction points as the downstream areas have received less reagents, which is observed in both the 5 m column and the large scale test. Decay of bacterial activity by encapsulation or flush out of enzymes or bacteria might lessen this effect.
Process induced preferential flow paths can explain part of the heterogeneity. Limited overburden pressure in the cubic meter and large scale tests, caused close to inlet preferential flow upward towards the surface, resulting in an increased $CaCO_3$ content along the phreatic surface.

The variation in $CaCO_3$ content in the first meter of the 5 m column experiment (Whiffin et al 2007), at the top surface of the 2nd cubic meter test and close to the extraction wells in the large scale test, could be a result of locally clogged areas (by bacteria or crystals). These clogs will cause the development of preferential flow paths with a faster flow velocity around the clog and stagnant zones in the areas downstream of the clog where supply of bacteria and nutrients can become limited. Normally, such flow diversions converge shortly after a clogged zone, but in this case precipitation along the preferential flow paths might hinder reconvergence. The difference in $CaCO_3$ content revealing the flow lines close to the extraction wells in the large scale test, might also be explained alternatively: as the rate of crystal growth is directly related to the available crystalline surface, large crystals tend to consume more $CaCO_3$. Hence, an initial difference in number and size of crystals between two flow paths will increase in time, due the directly related difference in crystallization rate.

The lack of $CaCO_3$ close to the injection points in all three scale up experiments, could be the result of a higher flow velocity, causing more bacterial flush out and hence lower activity and less $CaCO_3$. This was shown especially in the cubic meter test with sand from Meuse river, where the bacterial attachment was lower due to the coarser grain size (Foppen & Schijven 2006). Another possible explanation for the lack of $CaCO_3$ around the injection points, considers the kinetics of $CaCO_3$ precipitation and transport of crystals. Initially the crystals are still small or not even present if the solution is not yet sufficiently oversaturated that nucleation has taken place, which is likely in quartz sand (Söhnel 1992; Lioliou et al. 2007), that they are still easily transported through the pores.

Once flow velocity drops or crystals become bigger, they are more easily trapped in the narrow pores.

The high amount of $CaCO_3$ in the lower half 2nd cubic meter test might be a result of buoyancy-driven flow induced by the density differences between the injected fluids. The fluid density of the reagent solution containing 0.5 M urea and $CaCl_2$ being 1046 kg m^{-3}, while of the solution containing the product 1 M NH_4Cl being 1013 kg m^{-3}. At such a density difference buoyancy driven flow can be expected, especially if the distance between injection distance increases or the flow rate decreases (Post & Prommer 2007). Viscosity and density vary during different phases in the process. Initial in situ pore fluid, bacterial suspension, fixation solution, reagent solution, product solution and rinsing fluid all have different viscosity and density. Apart from buoyancy driven flow these differences can lead to instabilities and fingering patterns (Rosen et al. 2001), especially at the interface between two liquids.

Understanding and control of this (process induced) heterogeneity is considered essential for practical applications. Not only does it affect the mechanical behaviour of the treated sand body, but also it might affect the extraction of resulting ammonium chloride. On the other hand, traditional ground reinforcement methods, like jet-grouting or deep mixing methods, are often characterized by a comparable level of heterogeneity. E.g. Bruce (2000) reports that for deep-mixing methods UCS strengths of excavated samples vary between 0.2 and 5 MPa. Another aspect is that for many applications the heterogeneity might be less important. For example the amount of eroded sand in river beds, the stiffness under a railway track or the stability of slopes are more often a function of rock/soil mass characteristics instead of local material characteristics, making the homogeneity of the cemented sand probably less important. Some numerical simulations are described, which take (random) heterogeneity into account (Hicks & Samy 2002). The relation between heterogeneity and flow direction might also prove beneficiary, as it supposes that the direction of heterogeneity is controllable by changing the injection and extraction well positions. Instead of horizontal layers, vertical walls might be constructed if flow is induced from top to bottom.

4 Conclusions

Scale up experiments have shown the technical feasibility of Biogrout as ground improvement method under conditions and techniques as used in practice, both as single point injection or over a horizontal distance using screens of injection and extraction wells. Engineering parameters correlate well with $CaCO_3$ content or dry density. Control of the in situ distribution of bacterial activity and reagents and the resulting distribution of $CaCO_3$ and related engineering properties in the subsurface are the greatest challenge for further optimization, especially if Biogrout is applied in an open system. Further research should demonstrate which of the suggested mechanisms are responsible for the observed heterogeneity in deposition of carbonate and consequent geotechnical parameters. Further optimization of the process performance (improving efficient use of bacteria and reagents and reducing heterogeneity) is required for commercial application.

References

BSI 1999. BS 5930:1999 *Code of practice for site investigations*, London, British Standard Institution.

Bruce, D.A. 2000. *An introduction to the deep soil mixing methods as used in geotechnical applications*, FHWA-RD-99-138, Fedral Highway Administration, U.S. Department of Transportation, McLean, VA, 143p

Castanier, S., Le Metayer-Levrel, G. & Perthuisot, J.-P. 1999. "Ca-carbonates precipitation and limestone genesis -- the microbiogeologist point of view." *Sedimentary Geology* 126: 9-23.

DeJong, J.T., Fritzges, M.B. & Nusslein, K. 2006. "Microbially Induced Cementation to Control Sand Response to Undrained Shear." *Journal of Geotechnical and Geoenvironmental Engineering* 132(11): 1381-1392.

Fan, C.-C. & Su, C.-F. 2008. "Role of roots in the shear strength of root-reinforced soils with high moisture content." *Ecological Engineering* 33(2): 157-166.

Foppen, J.W.A. and J.F. Schijven, 2006. Evaluation of data from the literature on the transport and survival of Escherichia coli and thermotolerant coliforms in aquifers under saturated conditions. *Water Research*, 40: 401-426.

Harkes, M.P., Booster, J.L., Van Paassen, L.A., Van Loosdrecht, M.C.M. & Whiffin, V.S. 2008. Microbial induced carbonate precipitation as ground improvement method – bacterial fixation and empirical correlation $CaCO_3$ vs strength. *International conference on BioGeoCivil Engineering*, June 23-25, Delft, The Netherlands.

Harkes, M.P., van Paassen, L.A., Booster, J.L., Whiffin, V.S. & van Loosdrecht, M.C.M. 2009. "Fixation and distribution of bacterial activity in sand to induce carbonate precipitation for ground reinforcement." *Ecological Engineering*, online (doi 10.1016/j.ecoleng.2009.01.004).

Hicks, M.A. & Samy, K. 2002. "Influence of heterogeneity on undrained clay slope stability." Quarterly Journal of Engineering Geology and Hydrogeology 35(1): 41-49.

Ivanov, V. & Chu, J. 2008. "Applications of microorganisms to geotechnical engineering for bioclogging and biocementation of soil in situ." *Reviews in Environmental Science and Biotechnology* 7(2): 139-153.

Karol, R.H. 2003. Chemical grouting and soil stabilization. New York, Dekker.

Lioliou, M.G., Paraskeva, C.A., Koutsoukos, P.G. & Payatakes, A.C. 2007. "Heterogeneous nucleation and growth of calcium carbonate on calcite and quartz." *Journal of Colloid and Interface Science* 308(2): 421-428.

Mitchell, J.K. & Santamarina, J.C. 2005. "Biological Considerations in Geotechnical Engineering." *Journal of Geotechnical and Geoenvironmental Engineering* 131(10): 1222-1233.

Post, V.E.A. & Prommer, H. 2007. "Multicomponent reactive transport simulation of the Elder problem: Effects of chemical reactions on salt plume development." *Water Resources Research*. 43: 1-13.

Rosen, M., Freytes, V.M., D'Onofrio, A., Allain, C.A. & Hulin, J.P. 2001. "Density difference driven instabilities in porous media." *Granular Matter* 3(1): 63-67.

Scholl, M.A., Mills, A.L., Herman, J.S. & Hornberger, G.M. 1990. "The influence of mineralogy and solution chemistry on the attachment of bacteria to representative aquifer materials." *Journal of Contaminant Hydrology* 6(4): 321-336.

Söhnel, O., Garside, J. 1992. *Precipitation: Basic principles and Industrial Applications*. Oxford, Butterworth-Heinemann Ltd.

Torkzaban, S., Tazehkand, S.S., Walker, S.L. & Bradford, S.A. 2008. "Transport and fate of bacteria in porous media: Coupled effects of chemical conditions and pore space geometry." *Water Resources Research* 44(4): 12.

Van Paassen, L.A., Whiffin, V.S. & Harkes, M.P. 2007. *Immobilization of bacteria to a geological material.* Netherlands. Patent assignee Stichting GeoDelft. EP1798284-A1; WO2007069884-A1.

Whiffin, V.S., van Paassen, L.A. & Harkes, M.P. 2007. "Microbial Carbonate Precipitation as a Soil Improvement Technique." *Geomicrobiology Journal* 24(5): 417-423.

Widdows, J. & Brinsley, M. 2002. "Impact of biotic and abiotic processes on sediment dynamics and the consequences to the structure and functioning of the intertidal zone." *Journal of Sea Research* 48(2): 143-156.

7

Strength and deformation of biologically cemented sandstone

Abstract

A new method for ground improvement is being developed: Biogrout, a method based on microbial-induced carbonate precipitation. The feasibility of this method was tested in a field scale experiment: within 12 days 40 m^3 of sand was biologically cemented stretching over a length of 5 m between three injection and three extraction points. In this paper we present the mechanical characteristics of the biologically cemented sand, based on strength tests on the cores collected from the field scale experiment. The results are compared with other natural and artificially cemented sandstones. Correlations could be established between $CaCO_3$ content, dry density and strength at several confining stresses. From the strength tests the parameters describing the failure criterion - cohesion and friction angle- could be derived, which enable engineering design.

1 Introduction

In many regions in the world the mechanical properties of soils do not satisfy human demand. Currently a new method for ground improvement is being developed: Biogrout, a method based on microbial induced carbonate precipitation by urea hydrolysis (Whiffin et al. 2007; DeJong et al. 2009). Bacteria, which are able to catalyze the hydrolysis of urea, are introduced in the soil and supplied with a solution of urea and calcium chloride. Hydrolysis of urea produces ammonium and carbonate.
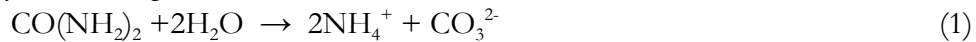
$$CO(NH_2)_2 + 2H_2O \ \rightarrow \ 2NH_4^+ + CO_3^{2-} \tag{1}$$

The produced carbonate precipitates with calcium as calcium carbonate crystals.

$$Ca^{2+} + CO_3^{2-} \rightarrow CaCO_3 \ (s) \tag{2}$$

The solution containing remaining ammonium chloride is removed. The calcium carbonate crystals enhance the material strength by forming bridges between the grains or coatings on the grain surfaces at the contact points (Figure 1). The reduction in porosity and permeability are limited.
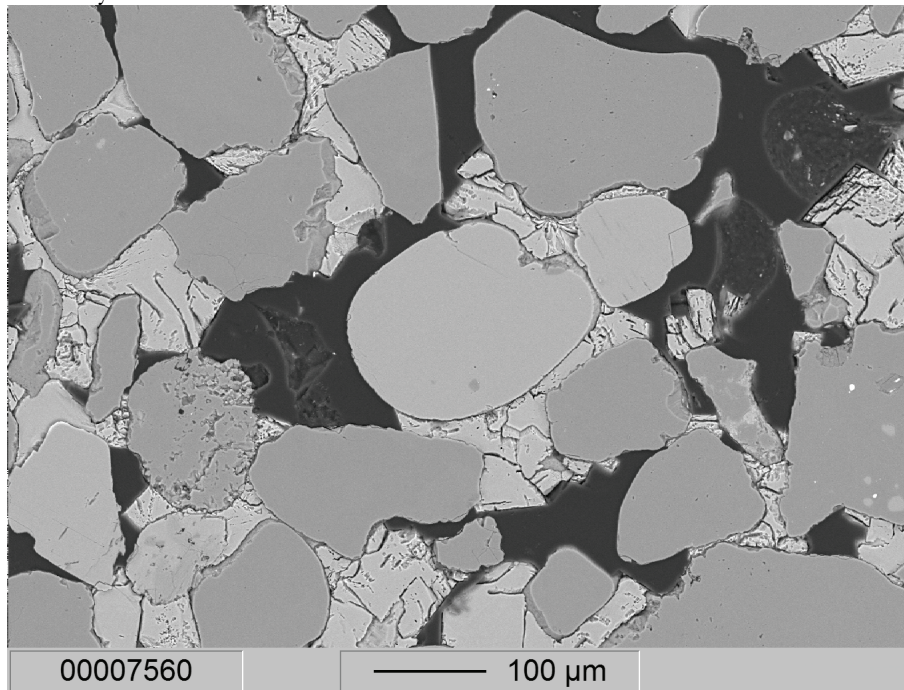
Figure 1 Electron microprobe image of a thin section of biogrouted sandstone. Calcium carbonate (calcite) crystals (light gray) have precipitated between the sand grains (dark gray) induced by microbially catalyzed hydrolysis of urea. The sandstone remains porous (black).

In this paper we present the mechanical characteristics of the biologically cemented sand and compare this to other natural and artificially cemented sandstones. Correlations were established between $CaCO_3$ content, dry density and strength. Strength tests were performed at several confining pressures to define failure criteria and derive the parameters required for engineering design.

2 Materials and methods

To determine the strength and deformation behaviour of biologically cemented sand, samples were obtained from a field scale experiment (Van Paassen et al. 2009).

2.1 Field scale experiment

A concrete container (8.0mx5.6mx2.5m) was filled (under wet conditions) with sand (Itterbeck, Smals IKW) with an average dry density of 1560 kg m^{-3}. A suspension containing the ureolytic bacteria, *Sporosarcina pasteurii* DSM33 (DSMZ, FRG) and solutions containing reagents urea and calcium chloride were injected sequentially in batches through three injection wells and pumped towards three extraction wells at a distance of 5 m from the injection wells. Total flow rate was approximately 1 m^3 h^{-1} with a hydraulic gradient of about 0.3 m m^{-1}. After treatment the sand body was excavated and five large block samples (0.1-0.5 m^3) were collected and prepared for coring and laboratory analysis.

2.2 Treatment of the cores

Sixty-four cores were drilled from the five block samples and prepared (diameter ± 50 mm; height ± 106 mm) for unconfined compressive strength (UCS) and triaxial compression tests. Seventeen cores were drilled and prepared (diameter ± 50 mm; height ± 18 mm) for brazilian tensile strength (BTS) tests. Cores were drilled in perpendicular directions to identify potential anisotropic behavior. All cores were preserved in tap water before testing. Samples were tested 2-12 weeks after excavation.

2.3 Strength and stiffness

2.3.1 Unconfined Compressive Strength test

UCS tests were performed on 45 cores according to ASTM D2938-95, -D3148-96 and -D4543-85 standards. Lateral strain was measured at mid-height of the cores, using a radial strain extensometer. Axial strain was measured with two axial strain transducers over the length of the core. Volumetric strain was calculated from the measured axial strain assuming radial strain was constant over the full height of the core:

$$\varepsilon_{vol} = \varepsilon_{ax} + 2\varepsilon_{rad} \ . \tag{3}$$

2.3.2 Triaxial Compression test

Triaxial tests were performed on nineteen cores according to BS 1377: Part 8. Seven cores were tested at confining stress of 100 kPa, of which four under drained and three under undrained conditions. Twelve cores were tested at confining stress of 500 kPa of which seven under drained and five under undrained conditions.

First, the samples were completely saturated. Then, consolidation was applied and after consolidation the compression test was started up.

During drained tests axial force and axial and volumetric displacements were measured, while pore pressure and confining pressure were kept constant. From the axial and volumetric strain, the radial strain was calculated assuming radial strain was constant over the full height of the core using equation 3.

During undrained tests axial force, axial displacement and pore pressure were measured, while volumetric displacement and confining pressure were kept constant.

2.3.3 Brazilian Tensile Strength test

Brazilian or Splitting Tensile Strength tests were performed on seventeen cores according to ASTM D3967-95a.

2.4 Dry density

After testing, the cores including broken fragments and loose grains were placed in the oven for at least 24 hours at 105°C. The oven-dried cores were weighed. With the diameter and length measurements that were done before strength testing, the dry density could be calculated. From measured dry density and $CaCO_3$ content, the initial dry density was calculated according to:

$$\rho_{ini} = \rho_{dry} - f_{CaCO_3}.$$
(4)

In which f_{CaCO_3} is the $CaCO_3$ content in kg m^{-3}.

2.5 CaCO$_3$ content

The calcium carbonate content was measured with a U-tube manometer, under standard conditions (25°C, 1 bar). A 1-4 g representative sample of the dried broken cores was weighed into a glass vial, 2 ml of 2 mol L^{-1} HCl was added in a separate compartment and the vial was sealed. The initial gas volume in the manometer was recorded, and then the two compartments were allowed to mix, resulting in acid dissolution of the sample and generation of a proportionate amount of carbon dioxide gas. Samples were blanked against untreated sand and the method was calibrated with analytical grade $CaCO_3$.

3 Results and discussion

3.1 Heterogeneity of the cemented mass

Excavation of the field scale experiment showed that about 40 m^3 of sand was cemented stretching over the full length (5 m) between injection and extraction points (Figure 2). The contours of the cemented sand body were limited by the induced flow field. Within the cemented sand body $CaCO_3$ was not uniformly distributed. Lenses were formed with $CaCO_3$ content varying from 0.8 to 27 % of total dry weight.

Although the observed heterogeneity indicated that control of the BioGrout process requires further optimization to improve the homogeneity of the distribution of $CaCO_3$ and related engineering properties, the high variability enabled to determine the mechanical behavior of biologically cemented sand over a wide range of calcium carbonate contents or (initial) dry densities and establish correlations between $CaCO_3$ content, dry density and strength. The collected block samples also showed significant variability. Within each block, zones were observed in which grain size, pore size, porosity or density and $CaCO_3$ content significantly varied. The locations of the cores were carefully selected for homogeneity. The selected cores covered a wide range of

characteristics. Table 1 gives an overview of test results on the biologically cemented cores and the ranges of measured properties.

Figure 2 The cemented sand body in the first field scale experiment on BioGrout: a ground improvement method based on microbial induced carbonate precipitation by urea hydrolysis.

Table 1 Overview of test results and ranges of measured properties on cores of biologically cemented sand.

Test	Range	Nr of tests
$CaCO_3$ content (% of dry weight)	12-27	81
$CaCO_3$ content (kg m^{-3})	160-530	
Dry density (kg m^{-3})	1640-2140	81
Porosity*	0.19-0.35	
Initial dry density (kg m^{-3})*	1420-1630	
Initial porosity*	0.39-0.46	
UCS / Q_u (MPa)	0.7-12	45
E_{50} (MPa)	110-430	
E_{50}/UCS	150-840	
E_{ur} (MPa)	1300-13000	
$Q_{100 kPa}$ (MPa)	2.2-7.5	7
E_{50} (MPa)	640-2210	
Q_{500kPa} (MPa)	3.8-13	12
E_{50} (MPa)	730-1530	
BTS (MPa)	0.11-0.62	17

* calculated from $CaCO_3$ content and dry density

3.2   Correlations between UCS, CaCO$_3$ content and dry density

A correlation was established between UCS and $CaCO_3$ content (Figure 3) similar to previous studies (Ismail et al. 2002). The correlation showed high variance ($R^2 = 0.77$), which caused several inconsistent results. For example, although core *a* had a higher amount of $CaCO_3$ than core *b*, it had a lower strength, or while core *c* and *d* had similar $CaCO_3$ content, they differed significantly in strength.
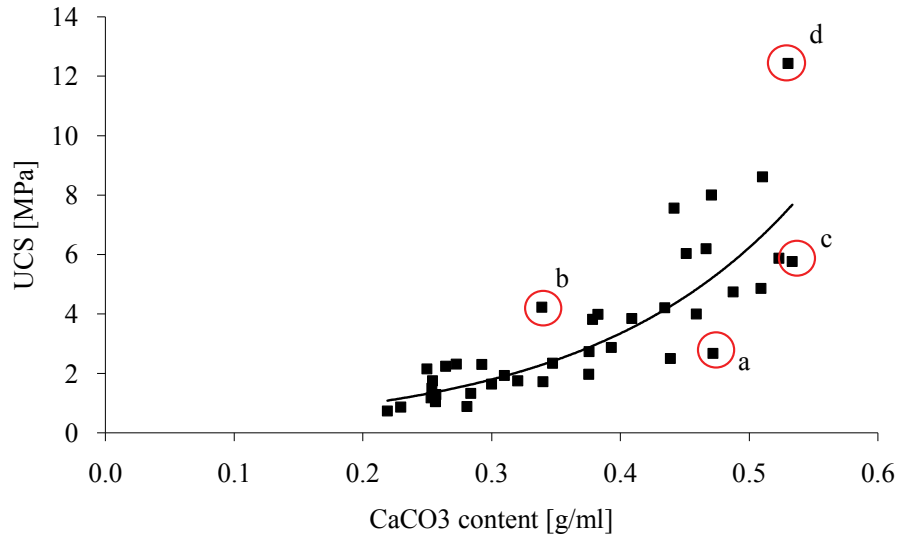
Figure 3 Correlations between CaCO₃ content and UCS. Points a, b, c and d correspond to the same cores as in figure 4.

Plotting UCS against dry density showed a much better correlation (Figure 4) than with $CaCO_3$ content. Higher strengths for cores *b* and *d* compared to cores *a* and *c* were a result of higher initial densities. Apparently, at the $CaCO_3$ contents used in this study (12-27%) the final dry density is a more important indicator for strength than the $CaCO_3$ content. A more densely packed sand therefore needs less cementation than a less dense sand to achieve the same strength.

However, still the correlation between UCS and dry density shows significant variance ($R^2 = 0.84$), which might be caused by other factors, such as sample disturbances before testing or heterogeneity within the tested cores. Several times failure did not occur in the whole core, but was restricted to the (weakest) bottom or top part. This resulted in an underestimation of the strength based on average dry density or $CaCO_3$ content.
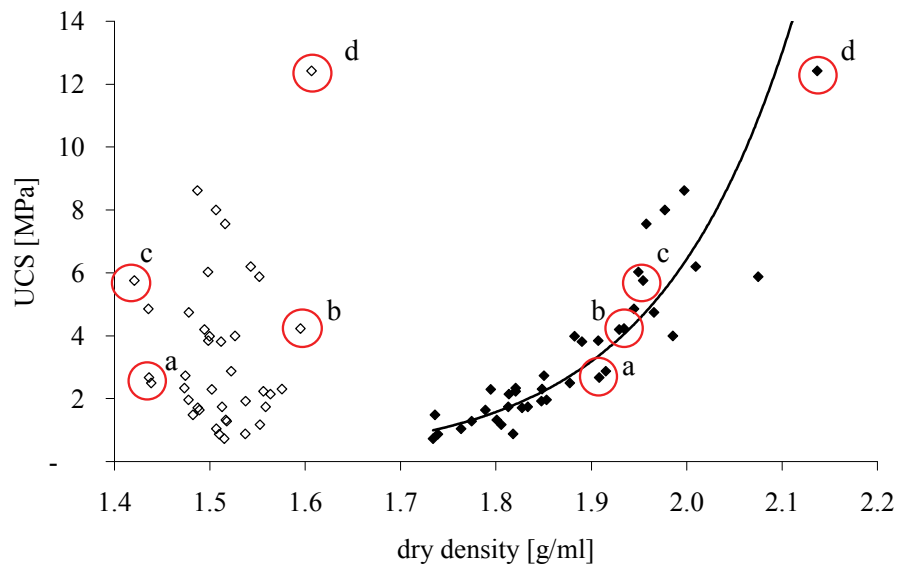
Figure 4: The UCS plotted against dry density before (◊) and after Biogrout treatment (♦). The initial dry density is calculated from CaCO₃ content and final dry density. Points a, b, c and d correspond to the same cores as in figure 3.

123

The effect of height diameter ratio or moisture content as reported in other studies (Hawkins & McConnell 1992; Hawkins 1998; Shakoor & Barefield 2009) were assumed insignificant as all samples were tested under wet conditions and at comparable height-diameter ratio.

The influence of anisotropy as reported by Cuss et al. (2003) appeared insignificant, as the cores were drilled in different directions through the blocks and no clear deviation from the trends in figure 3 and 4 was observed.

3.3 Deformation behaviour

The biologically cemented sand showed typically stiff and brittle deformation behaviour during compression tests, similar to previous studies on naturally and artificially cemented sands at low confining pressures (Clough et al. 1981; Dyke & Dobereiner 1991; Abdulla & Kiousis 1997; Ismail et al. 2002; Cuss et al. 2003; DeJong et al. 2006). For all compression tests peak strength was obtained within less than 10‰ axial strain. A difference with the experiments by Dyke and Dobereiner (1991) and Cuss et al (2003) performed on naturally cemented sands is the relatively low radial strain. Especially for the UCS tests the radial strain was negligible during the first 2-4‰ axial strain, resulting in Poisson's ratios close to zero. Figure 5 shows the response on axial loading for three cores with comparable $CaCO_3$ content (13-14%) and dry density (1790-1800 kg m^{-3}).

The relatively low strength and low Poisson's ratio compared to natural sandstones might be a result of the difference in diagenesis. As many natural sandstones have been subject to high stresses, while being buried for buried for very long time, the origin of cementation is often attributed to pressure solution or biogeochemically induced dissolution and reprecipitation combined with groundwater transport (Lynch & Land 1996; Goldstein & Rossi 2002).
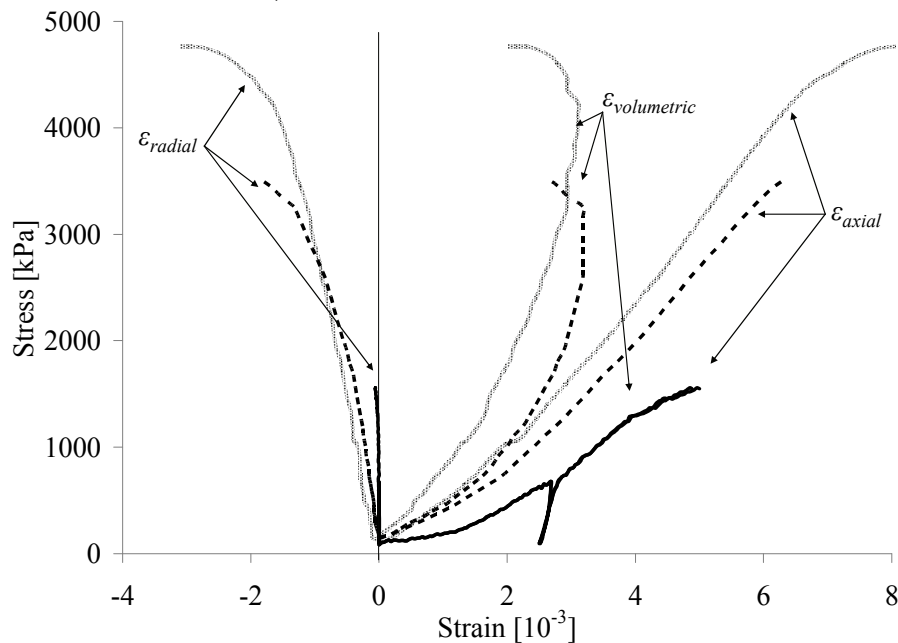

Figure 5: Deformation behavior of three representative cores with comparable dry densities of about 1800 kg/m³ tested at confining pressures of 0 kPa (solid), 100 kPa (dashed) and 500 kPa (gray). The axial, lateral and volumetric strain are set out against the stress. The elastic loop in the UCS test is at approximately 50% of the UCS.

Secondly, most sandstones contain quartzitic cement or cement from other mineral composition instead of calcium carbonate. The high pressures often also result in abrasion and enlargement of the grain contact area. When these sandstones are unloaded by geological uplift or by sampling, a stiffer, more elastic axial response and higher Poisson's ratio is expected than for the biologically cemented sands, which are cemented under nearly unconfined conditions close to the surface.

In many cases during the UCS tests no clear failure planes could be distinguished after failure. Several times tensile cracks appeared vertically from top to bottom. For the confined tests, failure planes were observed at a steep angle through the core.

At failure, the broken cores entirely lost cohesion at grain scale within a narrow zone around the failure plane, or throughout the whole core in case failure planes were absent. The loss of cohesion became even more apparent after drying the cores in the oven. It was also observed on other weak sandstones (Cuss et al. 2003).

3.4 Strength at different confining pressures

Similar to the UCS tests the peak strengths (maximum deviatoric stress) of triaxial and tensile tests were also plotted against dry density, showing reasonable correlation between 1700 and 1900 kg m^{-3}. (Figure 6) The peak strength for drained and undrained triaxial tests fitted both to the same correlations. Apparently, the relatively high stiffness of the sand caused little volumetric strain and consequent small increase in pore pressure compared to the peak strength. As a result, differences in peak strength between drained and undrained tests were small.

The equations shown on the figure:

$$q_{500kPa} = 1\cdot10^{-4}\exp(6\rho_{dry})$$
$$q_{100kPa} = 7\cdot10^{-5}\exp(6\rho_{dry})$$
$$UCS = 4\cdot10^{-5}\exp(6\rho_{dry})$$
$$BTS = 5\cdot10^{-6}\exp(6\rho_{dry})$$
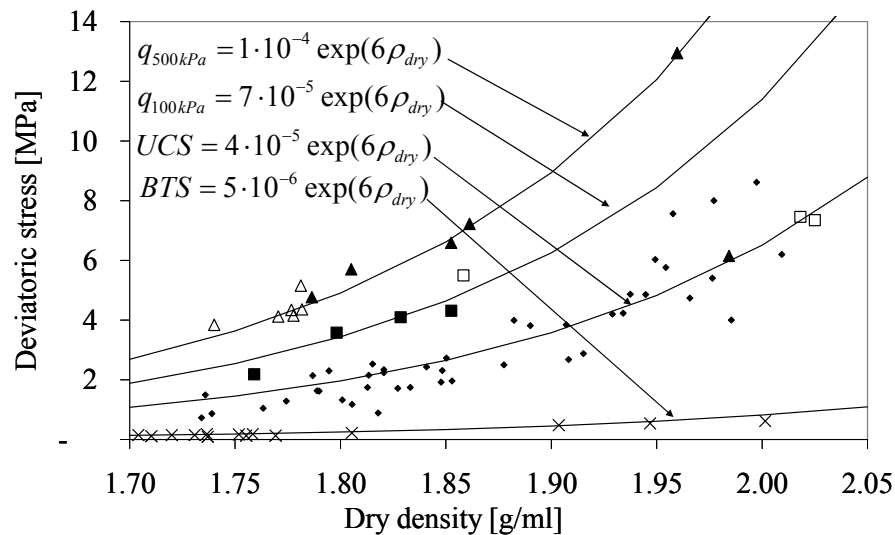
Figure 6 Peak strength (maximum deviatoric stress) for UCS (•), triaxial at 100 kPa (■/□) and 500 kPa (▲/⊿) confining pressure and BTS (✕) tests plotted as a function of dry density. Triaxial tests were performed under drained (■/▲) and undrained conditions (□/⊿).

3.5 Derivation of engineering parameters

Using the correlations presented in figure 6, the principal stresses at failure were calculated for dry densities of 1700, 1800 and 1900 kg m^{-3} (Figure 7). To capture the curvature of the failure envelops, a Hoek-Brown failure criterion was fitted for each

density (Hoek et al. 2002). The Hoek and Brown parameters were calculated using the computer program Roclab (RocScienceInc 2006) with a least squares fit (numerically determined using Levenberg–Marquardt algorithm), assuming intact rock properties (with a geological strength index (GSI) of 100).
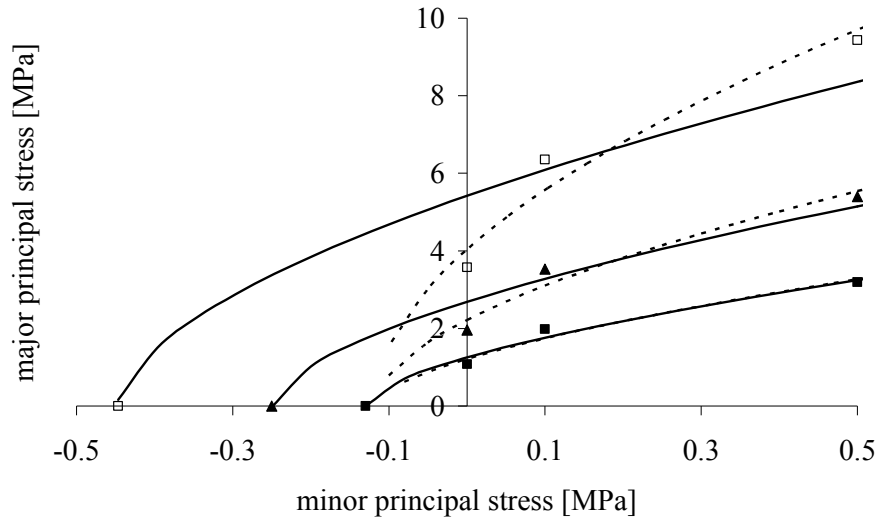

Figure 7 Peak strengths (major principal stress) were calculated using correlations in figure 6 at different confining pressures (minor principal stress: BTS, 0 (UCS), 100 and 500 kPa) for different dry densities of 1700 (■), 1800 (▲) and 1900 kg m³ (□). Hoek-Brown failure criteria were numerically fitted on these principal stresses including BTS (solid lines) and excluding BTS (dashed lines).

According to Hoek et al. (2002), the Hoek-Brown criteria (and the Mohr-Coulomb failure criteria) based on normal and shear stresses can be calculated from the Hoek-Brown criteria based on principal stresses. These relations between normal and shear stress are presented (including Mohr circles) for a dry density of 1800 kg m^{-3} in figure 8.
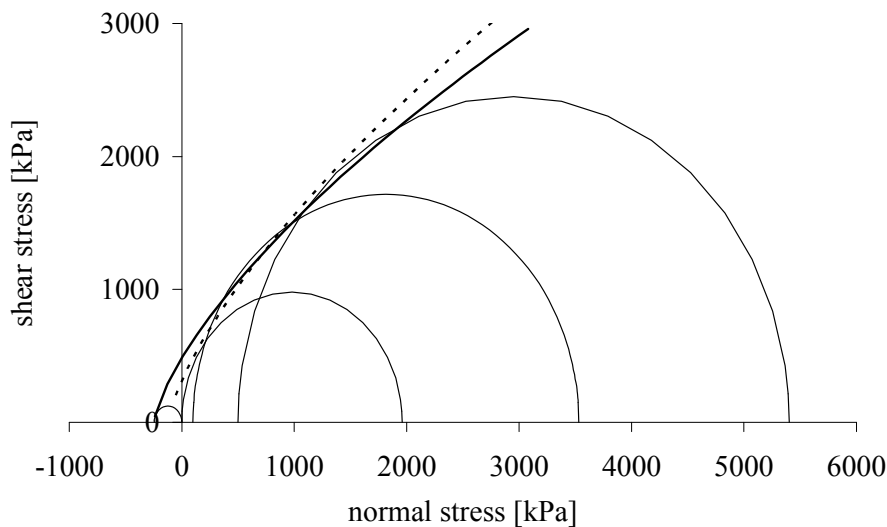
Figure 8 Numerically derived Hoek-Brown failure criteria for a dry density of 1800 kg m³ including BTS (solid line) and excluding BTS (dashed line) fit to the Mohr circles for different confining stresses.

The Hoek-Brown failure criteria for different dry densities of biologically cemented sand were derived using two approaches: with and without taking the empirically calculated BTS into account. Including BTS in the fitting procedure led to the impression that

calculating UCS from the empirical correlations in figure 6 leads to underestimation, especially at high values for dry density. Excluding BTS in the fitting procedure resulted in a better fit to the empirically calculated compressive results. It must be noted that in these calculations the major principal strength for the BTS test is assumed to be zero. This is in contrast with Goodman (1989) who mentions that the major principal stress for the BTS test is actually 3 times the inverse of the tensile strength value. However, increasing the major principle stress for BTS in figure 7 would lead to an even higher difference between numerically fitted and empirically calculated values for the UCS. On the other hand the obtained values for UCS might be underestimations of the real compressive strength. The often observed vertical orientation of the failure planes indicates that the cores might have been subject to tensile lateral stress. Consequently, the minor principal strength for UCS in figure 7 and 8 would be negative, resulting in a better fit including BTS. Alternatively, Goodman mentions also that tensile strength determined with the BTS test can be up to ten times higher than from a direct tensile test owing to the weakening effect of fissures in the latter. Assuming the BTS tests overestimate the actual tensile strength the dashed lines in figures 7 and 8 would be more appropriate.

Table 2 Summary of parameters describing the failure criteria of biologically cemented sand at low confining stresses (< 500 kPa) for different dry densities.

Dry density (kg m^{-3})	1700		1800		1900	
Including BTS	Yes	No	Yes	No	Yes	No
Hoek-Brown fit						
UCS, sigc$_i$ (MPa)	1.3	1.2	2.7	2.2	5.4	4.0
Material constant, m$_i$	10	10	11	19	12	34
Mohr-Coulomb fit						
Cohesion, c (MPa)	0.28	0.27	0.51	0.39	0.92	0.54
Friction angle, φ (^{o})	39	40	45	50	50	58

An overview of the derived parameters describing the different failure criteria using both approaches is presented in table 2. For increasing dry density from 1700 to 1900 kg m^{-3} (or CaCO$_3$ content from 200 to 400 kg m^{-3} assuming an initial dry density of 1500 kg m^{-3}) the cohesion increases from 280 to 920 kPa and the friction angle from 39 to 50° when including BTS in the failure criterion (or when BTS is excluded from 270 to 540 kPa and from 40 to 58°). Both approaches indicate a significant increase in strength compared to the untreated sand. Triaxial compression tests on uncemented sand with a dry density between 1400 and 1670 kg m^{-3} showed no cohesion and a friction angle between 32 and 39°. Similarly, stiffness increased with increasing CaCO$_3$ content (or increasing dry density), which is discussed in chapter 8.

The actual choice of strength parameters for designing the demands for a treatment procedure depends on many factors including the application, the stress and strain ranges, the failure mode, the required safety factor, etc. Other important aspects to take into account are the initial ground heterogeneity, the heterogeneous distribution of CaCO$_3$ and consequent geotechnical parameters. Either the treatment procedure should be optimized to minimize heterogeneity or suitable methods should be applied to determine the in situ heterogeneity and take it into account in stability analysis such as proposed by Hicks & Samy (2002) or properly convert the "intact" rock or soil material

properties into parameters which describe the mechanical behaviour of rock or soil mass as described by Hoek et al. (2002).

4 Conclusions

It has been shown that biologically induced carbonate precipitation can significantly improve mechanical properties of sand. The strength and deformation behaviour of biologically cemented sand were determined at different levels of $CaCO_3$ and dry density and different confining stresses on cores collected from a field scale experiment. Using these test results, failure criteria (angle of internal friction and cohesion) were determined, which can be used for assessing the stability of (biologically) cemented ground construction or designing a treatment procedure based on the required stability.

References

Abdulla, A.A. & Kiousis, P.D. 1997. "Behavior of cemented sands - I. Testing." *International Journal for Numerical and Analytical Methods in Geomechanics* 21(8): 533-547.

Clough, G.W., Shafii Rad, N., Bachus, R.C. & Sitar, N. 1981. "Cemented Sands Under Static Loading." *Journal of the Geotechnical Engineering Division, Proceedings of the American Society of Civil Engineers* 107(6): 799-817.

Cuss, R.J., Rutter, E.H. & Holloway, R.F. 2003. "The application of critical state soil mechanics to the mechanical behaviour of porous sandstones." *International Journal of Rock Mechanics and Mining Sciences* 40(6): 847-862.

DeJong, J.T., Fritzges, M.B. & Nusslein, K. 2006. "Microbially Induced Cementation to Control Sand Response to Undrained Shear." *Journal of Geotechnical and Geoenvironmental Engineering* 132(11): 1381-1392.

DeJong, J.T., Mortensen, B.M., Martinez, B.C. & Nelson, D.C. 2009. "Bio-mediated soil improvement." *Ecological Engineering In Press, Corrected Proof.*

Dyke, C.G. & Dobereiner, L. 1991. "Evaluating the strength and deformability of sandstones." *Quarterly Journal of Engineering Geology and Hydrogeology* 24(1): 123-134.

Goldstein, R.H. & Rossi, C. 2002. "Recrystallization in Quartz Overgrowths." *Journal of sedimentary research* 72(3): 432-440.

Goodman, R.E. 1989. *Introduction to rock mechanics.* New York, John Wiley & Sons.

Hawkins, A.B. 1998. "Aspects of rock strength." *Bulletin of Engineering Geology and the Environment* 57(1): 17-30.

Hawkins, A.B. & McConnell, B.J. 1992. "Sensitivity of sandstone strength and deformability to changes in moisture content." *Quarterly Journal of Engineering Geology and Hydrogeology* 25(2): 115-130.

Hicks, M.A. & Samy, K. 2002. "Influence of heterogeneity on undrained clay slope stability." *Quarterly Journal of Engineering Geology and Hydrogeology* 35(1): 41-49.

Hoek, E., Carranza-Torres, C.T. & Corkum, B. 2002. Hoek-Brown failure criterion – 2002 edition. *Proceedings of the North American Rock Mechanics Society meeting, Toronto.*

Ismail, M.A., Joer, H.A., Sim, W.H. & Randolph, M.F. 2002. "Effect of Cement Type on Shear Behavior of Cemented Calcareous Soil." *Journal of Geotechnical and Geoenvironmental Engineering* 128(6): 520-529.

Lynch, F.L. & Land, L.S. 1996. "Diagenesis of calcite cement in Frio Formation sandstones and its relationship to formation water chemistry." *Journal of sedimentary research* 66(3): 439-446.

RocScienceInc 2006. *Roclab - Rock mass strength analysis using the Hoek-Brown failure criterion.* Toronto www.rocscience.com.

Shakoor, A. & Barefield, E.H. 2009. "Relationship between Unconfined Compressive Strength and Degree of Saturation for Selected Sandstones." *Environmental and Engineering Geoscience* 15(1): 29-40.

Van Paassen, L.A., Harkes, M.P., Van Zwieten, G.A., Van der Zon, W.H., Van der Star, W.R.L. & Van Loosdrecht, M.C.M. 2009. "Scale up of BioGrout: a biological ground reinforcement method". *17th International Conference on Soil Mechanics & Geotechnical Engineering, 5-9 October, Alexandria, Egypt*, in press.

Whiffin, V.S., van Paassen, L.A. & Harkes, M.P. 2007. "Microbial Carbonate Precipitation as a Soil Improvement Technique." Geomicrobiology Journal 24(5): 417-423.

8

Biological ground improvement for stabilization of railroad tracks

Abstract

Railroad tracks on soft soils require continuous maintenance to counteract unacceptable deformations. Biogrout is a ground improvement method based on microbial induced precipitation of calcium carbonate, which could be used to minimize maintenance of these tracks without disturbing its functionality by increasing the stiffness of the embankment in situ. In this paper the feasibility of Biogrout as stabilizing method for sand embankments is presented based on the results of a demonstration scale experiment. In situ geophysical measurements indicated that the stiffness significantly increased within one day of treatment. The geophysical measurements at the end of the experiment correlated well with laboratory experiments on excavated samples. Based on the results of these experiments the potential of Biogrout to improve the stability of railroad embankments on soft soils is evaluated theoretically using a case study in The Netherlands.

1 Introduction

In the western part of the Netherlands, many (old) railroads are constructed on embankments consisting of a layer of ballast or bitumen on top of sand, which are placed on the preexisting soft clay and peat layers. Due to the high compressibility of the soft soils these tracks need continuous maintenance to counteract unacceptable deformations of the tracks. With the current wish for faster trains, railroad maintenance faces another problem. The passage of a train induces waves in the railroad track and underlying soils. Three types of waves are induced: compressional, shear and Rayleigh (surface) waves. The transmission velocity of these waves depends on the stiffness of the embankment and underlying soils. Peat, organic clays and soft marine clays may have a low shear wave velocity, and thus a Rayleigh wave velocity as low as 40-50 m/s (144 – 180 km/h). When the train speed approaches the Rayleigh wave velocity, the resonance leads to amplification of loads and increased maintenance or risk of failure. This Rayleigh velocity is defined as the critical velocity. When this critical velocity is reached at high-speed lines, but sometimes even at traditional tracks, problems can easily occur. Demands for safe railway lines, rapid construction methods and cost-effective solutions are increasing. Railway companies in France, Germany, Switzerland, The Netherlands and Great Britain observed a substantial increase in the vertical movement of the track as the train speed approaches the Rayleigh wave speed in the ground (Madshus and Kaynia, 2000). With rising groundwater level - which is expected due to a wetter climate and a reduced drainage capacity when tracks are widened - effective stresses underneath the track will reduce, increasing the risk of failure even further.

To minimize maintenance and increase the critical velocity along new tracks, minimum thicknesses of sand embankments are prescribed in design regulations. At even higher velocities, like for the high speed railway link from Amsterdam to Antwerp, the railway tracks have been founded on piles for a major part of the track. This is an effective but very expensive method. For other (already existing) tracks soil improvement has been implemented at places to increase the strength and stiffness of the embankment underneath the tracks, by mixing the sand with cement (Kaynia et al. 2000). For existing tracks, traditional soil improvement methods such as deep mixing, cement or chemical grouting (Karol 2003) are often not suitable, as the zone of influence of these methods is limited to the proximity of the mixing equipment due to the high viscosity or short hardening time of the injected grouts. Moreover, chemical or cement grouting techniques are costly and have significant impact on the environment and require heavy machinery which disturbs the nearby infrastructure or facilities. These techniques also significantly reduce the permeability of the strengthened soil, which hinder groundwater flow and drainage. The combination of these aspects makes large-scale treatment with traditional methods unfeasible. More sustainable techniques for track reinforcement should use less sand or constructive elements like piles and should be less invasive.

In order to tackle these disadvantages, alternative ground improvement methods are being developed using micro-organisms which are able to increase strength and stiffness

by inducing the precipitation of calcium carbonate (DeJong et al. 2006; Whiffin et al. 2007; Ivanov & Chu 2008; DeJong et al. 2009). Most studies on 'biogrouting' use micro-organisms containing the enzyme urease and in particular the bacterium *Sporosarcina pasteurii* DSM 33 (DSMZ, FRG), renamed from Bacillus pasteurii) (DeJong et al. 2006; Whiffin et al. 2007). These micro-organisms are cultivated aerobically in the laboratory. The suspension containing the bacteria is introduced in the soil and supplied with a solution of urea and calcium chloride. The microbial urease catalyzes the hydrolysis of urea into ammonium and carbonate.

$$CO(NH_2)_2 + 2H_2O \rightarrow 2NH_4^+ + CO_3^{2-} \tag{1}$$
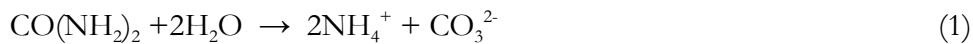
The produced carbonate ions precipitate in the presence of calcium ions as calcium carbonate crystals, which form cementing bridges between the existing sand grains.

$$Ca^{2+} + CO_3^{2-} \rightarrow CaCO_3 \, (s) \tag{2}$$

The remaining ammonium chloride solution is removed by physical extraction and rinsing with water. Once precipitated, the calcium carbonate will only dissolve very slowly (at a geological time scale), either when continuously flushed by buffered acidic groundwater or as a result of acidifying processes in the pores (e.g. oxidation of ammonium). When sufficient calcium carbonate is precipitated, durable soil stabilization is achieved (Whiffin et al. 2007; Van Paassen et al. 2009). Currently, also other Biogrout processes are being investigated, based on the oxidation of dissolved calcium fatty acids and reduction of calcium nitrate. This process results also in precipitation of calcium carbonate, while the micro-organisms can use the energy are stimulated, which are already existing in the ground.

To test the feasibility of biogrouting for ground improvement, sand column experiments were performed by mixing bacteria with urea and calcium chloride and injecting the suspension simultaneously. However, as mixing bacteria and reagents results in flocculation of the bacteria and immediate precipitation, the sand columns containing medium grained sand clogged close to the inlet and significant cementation was established only over a few centimeters. The injection procedure was adjusted by injecting bacteria and reagents sequentially, with an optional pulse in between to stimulate a homogeneous distribution of adsorbed bacteria to the sand grains and prevent clogging near the inlet (Van Paassen et al. 2007; Harkes et al. 2008). Using this bacterial placement procedure, sand column experiments were performed in which 20 cm of packed sand was homogeneously cemented to a desired strength varying from loosely cemented sand to moderately strong rock with unconfined compressive strengths of 0.2 – 20 MPa (Harkes et al. 2008). In this case, the amount of precipitated calcium carbonate varied from 30 to 600 kg m^{-3} and a clear correlation was established between CaCO$_3$ content and unconfined compressive strength. Using a sand column 5 m in length Whiffin et al. (2007) proved that cementation could be induced over a long distance from the injection point, while bacteria and reagents could be injected at low pressures (hydraulic gradient < 1 m m^{-1}; a flow rate of approximately 7 m day^{-1}) and without resulting in clogging of the pores. Confined compressive strength tests indicated a significant improvement of strength and stiffness over several meters. The maximum treatment distance did not appear to be limited to 5 meters and it seemed to be possible to extend this distance further.

A demonstration scale Biogrout experiment was performed in order to scale up the process and check the feasibility of this technique for commercial applications (Van Paassen et al. 2009). In this paper we present the results of this large-scale experiment in context of the potential use of Biogrout for the stabilization of existing railroad embankments. In particular, the effect of Biogrout treatment on the effect of the critical train velocity is addressed by using a candidate location in The Netherlands, as a case study.

2 Materials and methods

A large-scale (100m^3) experiment was performed to test the feasibility of Biogrout as ground improvement method. The location of this test was an industrial complex in Papendrecht, The Netherlands (Van Paassen et al. 2009).

2.1 Test set-up and preparation

A concrete container (8.0 m x 5.6 m x 2.5 m) was filled with a thin layer of sand (25 cm), in which 48 seismic sensors (geophones) were planted. These geophones were distributed on 3 arrays aligned along the length of the container. The geophones and the sides of the container were covered with geotextile sheets. The container was then filled (under water) with 2.25 m of sand up to an average dry density of 1560 kg m^{-3}. The sand came from a quarry in Itterbeck, Germany (Smals IKW, SZI 0032, also referred to as Itterbeck fine). This sand was uniform, fine to medium grained (d$_{50}$: 0.166 mm; d$_{60}$/d$_{10}$: 1.64; (BSI 1999)) and mainly siliceous (97%).) Three injection wells (PVC Ø300mm, 5mm thick with 100 μm slots) were installed with 1 m distance between each other and about 1.5 m from the sides. At a distance of 5 m along the length direction of the chamber (x-direction) three extraction wells were placed opposite to the injection wells The extraction wells of similar type as the injection wells were covered by geotextile to prevent sand erosion and extraction from around the extraction well (Figure 1).
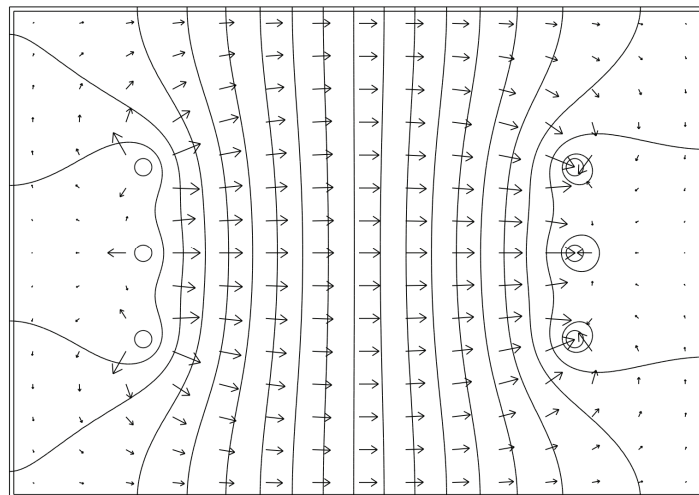
Figure 1 Applied flow field (top view) in the experimental set-up (a concrete chamber (8m x 5.6m x 2.5m) with three injection wells at the left and three extraction wells at the right). Arrows indicate flow velocity and direction, which is perpendicular to the equipotential lines. Cross-sections (seismic and geotechnical) presented in the figures 3, 7 and 9 are along the line through the centre injection and extraction well.

2.2   Applied treatment procedure

Highly ureolytic bacteria (*Sporosarcina pasteurii*, DSM 33 (DSMZ, FRG) were cultivated aerobically from frozen stock suspension up to 5 m^3 in a reactor build on site. Calcifying solutions containing $CaCl_2$ and urea were prepared using industrial grade brines mixed with tap water to the desired concentration. Fluids were injected sequentially through the three injection wells and pumped towards the extraction wells. Total flow rate was approximately 1 m^3 h^{-1} divided equally over the three wells. The hydraulic gradient was about 0.3 m m^{-1}. After placing the bacteria, the reagent solution containing $CaCl_2$ and urea was injected in 10 batches over a period of 12 days.

2.3   Geotechnical laboratory measurements

After treatment, the cemented sand body was examined first by removing the loose sand on top of it. Then, several cemented blocks were excavated. On these blocks cores were drilled, which were then used for unconfined compressive strength (UCS) tests (BSI 1999) and for the determination of dry density (BSI 1999) and calcium carbonate content (Whiffin et al. 2007). UCS tests were performed under wet conditions.

2.4   In situ seismic measurements

In order to monitor the biogrouting process stepwise, time-lapse shear-wave seismic measurements were conducted. Targets of seismic monitoring were the temporal and lateral (as a function of distance from the injection well) variations of the in-situ stiffness of the sand at different stages of the biogrouting process.

An electromagnetic horizontal vibratory source (Ghose et al. 1996; Ghose and Goudswaard. 2004) was used for generation of high-frequency seismic shear waves for monitoring the stiffness variations. With this small, high-frequency shear-wave source, which is especially suitable for shallow applications, the frequencies put into the ground can be controlled, which is not possible with a traditional impulsive seismic source (like a sledge hammer). This allows us to achieve a relatively high resolution in the shallow subsurface. Additionally, because this source is well monitored in its amplitude and phase response, the source wavelet including the ground coupling effect can be removed from the observed wavefield, leaving only the propagation effects (Ghose, 2003). This improves the reliability further. In total 72 geophones were planted under and above the sand to measure the wavefield. Because we generated SH waves (shear waves with polarization in the horizontal plane and orthogonal to the installed seismic lines), horizontal single-component geophones were used; this helped reducing the boundary effects on the seismic wavefield. The shear wave source was located on the top surface of the sand body at various locations right above the 3 seismic lines below, and the generated shear wave was recorded by the geophones arrays. From the arrival times of the transmitted shear wave through the sand, the velocity was estimated.

Because we used the arrival time in a fixed array in stead of one single geophone, the velocity estimates are quite stable and independent of time picking uncertainties. The geophone arrays remained untouched for the entire time of the experiment. One major strength of this in-situ time-lapse (repeat) seismic measurements was that it gives the

stiffness of the sand at several intermediate stages of biogrouting, in contrast with the geotechnical measurements on sand samples which provided sand properties only at the beginning and at the very end of the entire experiment and none in between.

3   Results and discussion

3.1   Cementation process

After 12 days in which 100m^3 of reagent solution was flushed through, the sand was rinsed with water and then excavated. The cemented sand body, about 40 m^3 in volume, became clearly visible. Its shape was limited by the induced hydrological flow field: above the phreatic surface obviously no cementation had taken place and below this level the cemented sand body was restricted to volume within the flow lines with significant discharge.

Figure 2 Cemented sand body observed from the corner behind the extraction points. The cementation patterns are clearly related to the flow field (Figure 1) through the sand body.

Flow lines could be distinguished in the cemented sand body, especially close to the extraction wells. Apparently, the cementation along these flow lines was reasonably homogeneous, while perpendicular to these flow lines the $CaCO_3$ content varied significantly. After excavating the cemented body along a vertical cross-section through the middle injection and extraction wells, analysis of samples collected from this cross-section showed that $CaCO_3$ content varied from 0.8 to 24 % of the total dry weight (Figure 3). Lenses were observed varying in thickness from several centimetres up to decimetres and extending horizontally for several meters from the injection well. Around the injection points the $CaCO_3$ content was lower (which was also seen on smaller scale tests as well and could be explained by high flow velocities and disturbances close to injection (Van Paassen et al. 2009)).
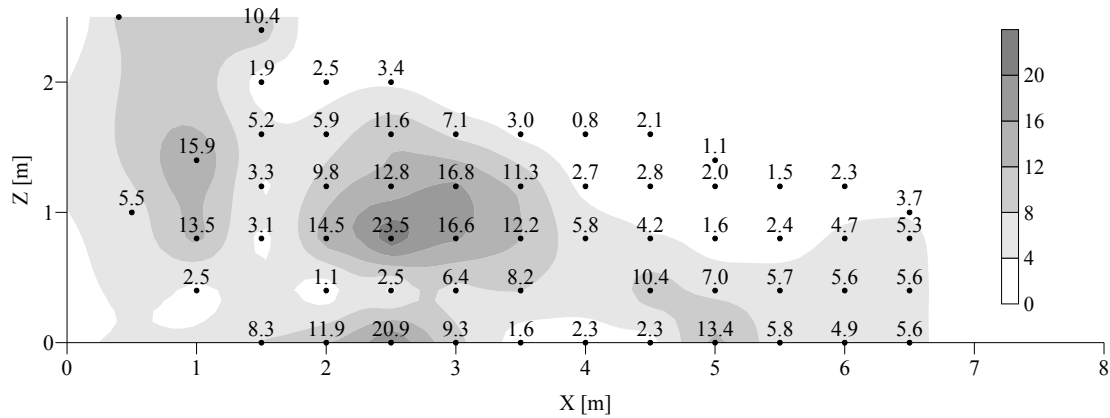
Figure 3 Cross-section along the middle line of the Biogrout demonstration scale experiment showing the measured CaCO₃ content in [% of dry weight]. This line is identical with the middle seismic line (Figure 9) and also marked in Figure 1. The middle injection and extraction wells are located respectively at x = 150 cm and x = 650 cm. The white area in the upper and right part of the figure was easily removed while the cemented body was excavated. The CaCO₃ content in this part was neglected.

3.2 Geotechnical measurements

Unconfined compressive strength (UCS) tests on the cored samples excavated from the cemented sand body after the biogrouting experiment showed peak strength varying considerably from 0.7 to 12.4 MPa. The $CaCO_3$ content of the samples tested for UCS varied between 12.6% and 27.3% of final dry weight. From the stress-strain curves of the UCS tests (Figure 4) the Young's moduli were determined for the primary loading curves at 50 % of the peak stress (E_{50}) and for the unloading-reloading curves (E_{ur}), which varied respectively between 100 and 8500 MPa and between 1300 and 13500 MPa. At low strains the unconfined compression tests showed very little radial strain compared to the axial strain resulting in a Poisson's ratio close to zero (Figure 5). Only when the strain response reached maximum stiffness (E_{50}) radial strain started to increase probably because of opening of cracks. This material behaviour is not common for natural soils and rocks and requires future investigation.
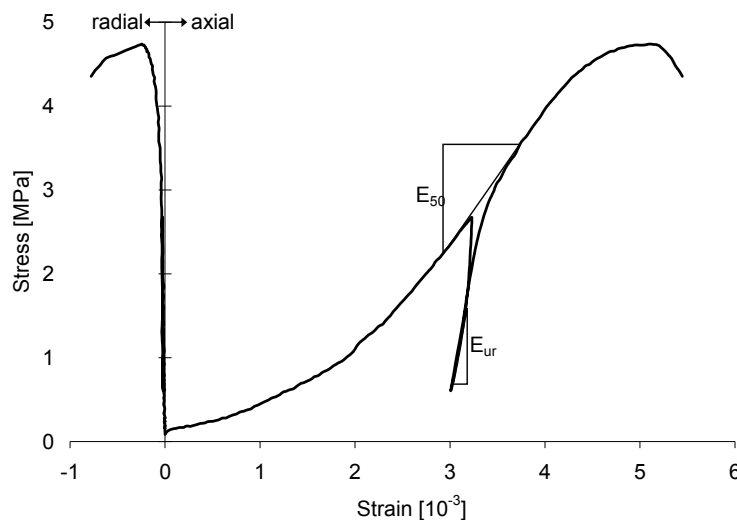
Figure 4 Typical stress-strain curve of an unconfined compressive strength test. The tangent and elastic Young's modulus E_{50} and E_{ur} are respectively derived from the slope of the primary stress-strain curve and the unloading reloading curve.
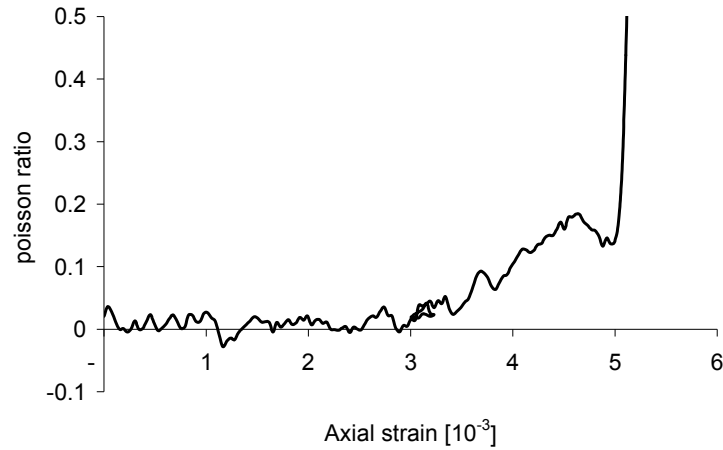
Figure 5 Poisson's ratio as a function of axial strain derived from the ratio between the slopes of the measured axial and radial stress-strain curves shown in Figure 4.

From a large collection of UCS tests correlations were established between the $CaCO_3$ content and the values for UCS (chapter 7) and Young's moduli (E_{50} and E_{ur}) (Figure 6).
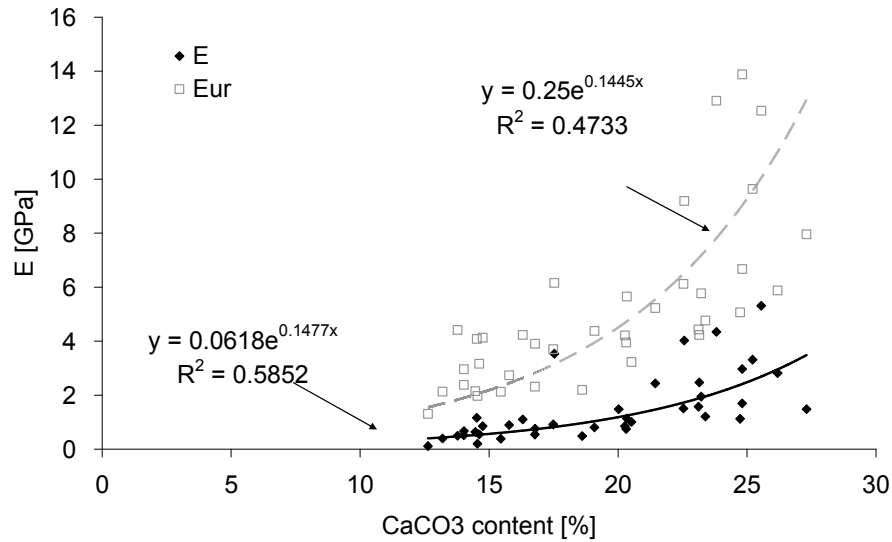
Figure 6 Empirical correlation between Young's moduli E_{50} (□) and E_{ur} (■) and $CaCO_3$ content

$$E_{ur} = 0.25 \exp\left(0.1445\left[CaCO_3\%\right]\right) \qquad (3)$$

The correlations of UCS, E_{50} and E_{ur} with $CaCO_3$ content established from the samples from this experiment showed high variance compared to similar correlations from homogeneously packed sand columns (Harkes et al. 2008). Part of this variance was caused by differences in initial dry density, which varied between 1420 and 1610 [kg.m^{-3}] (Van Paassen et al. 2009). Dry density after treatment showed better correlation with UCS and stiffness, but as values for dry density along the cross-section were not available equation 3 was used to determine the elastic stiffness E_{ur} for each $CaCO_3$ measurement along the cross-section in Figure 3.

According to the theory of elasticity, the shear modulus at low strains (G_0) can be calculated from the Young's modulus E_{ur} and Poisson's ratio v:

$$G_0 = \frac{E_{ur}}{2(1+v)} . \tag{4}$$

From the correlation between $CaCO_3$ content and elastic Young's modulus E_{ur} and using a Poisson's ratio of 0 (see Figure 3 and arguments presented above), G_0 was calculated for the CaCO3 contents measured along the cross-section shown in Figure 3, which is illustrated in Figure 7.
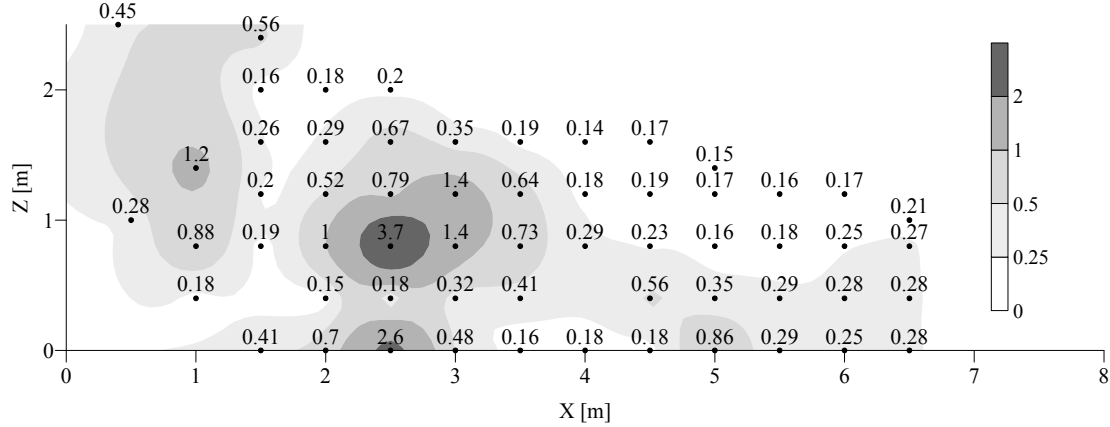
Figure 7 The shear modulus (G_0) in [GPa] along the cross section calculated from the measured Young's modulus E_{ur} and $CaCO_3$ content shown in Figure 3and Figure 6.

3.3   In-situ seismic measurements

Seismic shear waves generated by the vibrator source located on top of the sand container and then transmitted through the sand body were received by the underlying geophone arrays. Because the vibrator sends a long sweep signal representing a wide frequency range, the recorded data first need to be compressed in order to distinguish the phase arrivals. In this case, we compressed the raw vibrograms using the ground force estimated from the measured source motion (Ghose, 2002) The seismograms for the first two days of measurements (before the start of biogrouting treatment and just after the first day of biogrouting) are shown in Figure 8 for the middle line of geophones located below the sand. The location of the source is vertically above geophone no. 6 (indicated by the small arrow on the top margin in Figure 8).

In this paper, we illustrate the results of seismic monitoring along the middle array of 15 geophones, the results are similar in the other two geophone arrays (not shown here). Note the sharp change in the arrival time of shear waves and the curvature of the first arrivals (the moveout) in the geophone array: the dramatic increase of V_S indicates significant change of the average stiffness of the sand after the first day of flushing with the biogrouting reagents. Similar data were recorded for 4 other progressive stages of biogrouting. Note also in Figure 8 that while before the Biogrout treatment a clearly symmetrical moveout curve for the transmitted shear-wave first arrivals can be seen on the seismic array, after one day of treatment the moveout becomes asymmetrical with earlier arrivals close to the injection well. Apparently, the increase of sand stiffness is higher close to the injection well and decreases as one goes further towards the extraction, which is expected as on the first day only 9 m^3 of reagent solution (about half the pore volume of the cemented sand body) was injected. As a result most of the $CaCO_3$

had reacted in the area up to 2 m from the injection wells, where the increase in stiffness was visible on the seismic data.
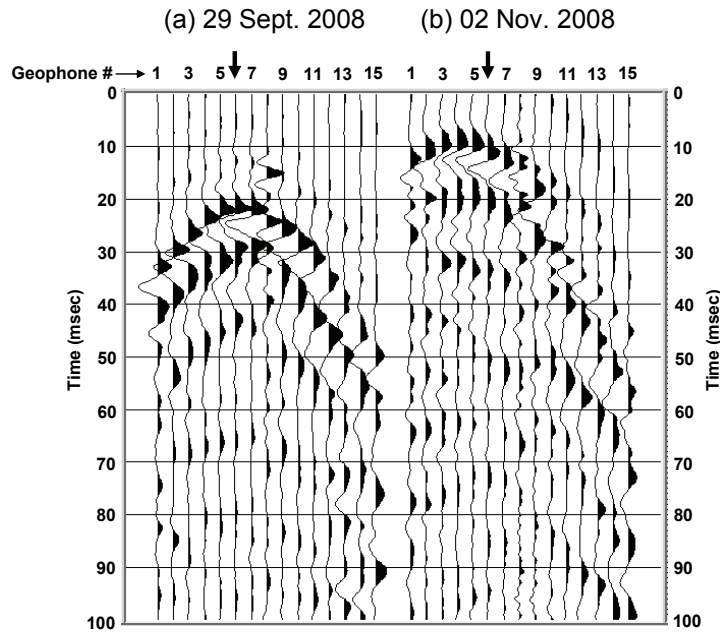

Figure 8 Shear wave data received by an array of 15 geophones located at the bottom of the sand-filled container before Biogrout treatment (left) and after 1 day of flushing with the reagents (right). The seismic shear-wave source was located on top of the sand body (the source location just above geophone no. 6 is shown by the arrow on the top margin). Similar data (not shown here) were recorded for several other source locations on the sand body and on 4 more days measuring the effect of progressive biogrouting.

From the arrival time of the shear wave, the distance between source and receiver, and the transmitted shear-wave arrival move-out seen in the geophone array, the shear wave velocity could be reliably determined. This shear wave velocity is used to calculate the shear modulus G_0:

$$G_0 = \rho V_s^2 \qquad (5)$$

where ρ is the bulk density [kg.m^3] and V_s is the shear wave velocity in [m.s^{-1}]. The G_0 estimated from the measured V_S is an average over the thickness (2.25 m) of the sand body. ρ is determined from the measured values of the bulk liquid density and solid density, which increased in time due to the precipitation of $CaCO_3$. In order to estimate the shear modulus before treatment, after one day and after the entire treatment as presented in Figure 9, we assumed the bulk density as 1850, 1950 and 2200 kg/m^3. ρ was estimated from the estimated values for dry density, porosity and fluid density, which was derived from the biochemical measurements. Possible uncertainties in these estimates of ρ have relatively small effect on G_0, because of the large change in the wave velocity and the dependence of G_0 on the second power of V_S. The in-situ seismic measurements indicate that in the vicinity of the injection well the average shear modulus of the cemented sand increased from less than 20MPa to about 150 MPa only after the first day of injection. After the whole experiment, in which 100 m^3 of reagent solution was flushed in course of 12 days, G_0 increased to 100 MPa near the extraction point and to nearly 350 MPa close to the injection.
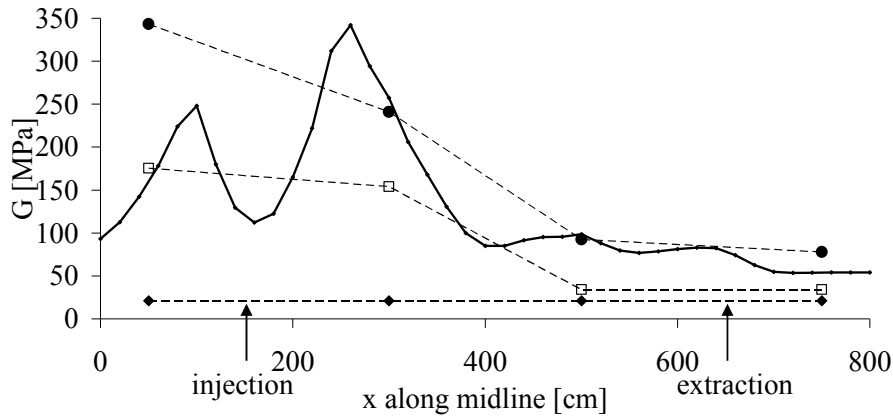
Figure 9 The shear modulus at low strains (G_0) as a function of distance along the middle line through the large-scale Biogrout experimental set-up. The two approaches of determining the G_0, shown here, are (1) based on measurements of elastic stiffness and $CaCO_3$ contents on samples in the laboratory (solid line), and (2) based on direct estimation from measured V_S by in-situ seismic tests and estimated ρ at 4 different source locations (dashed lines). Seismic measurements were done before treatment (♦), after one day (□) and after full treatment (●). The two arrows indicate the locations of injection and extraction wells.

Figure 9 illustrates a comparison of two independent estimates of small strain shear modulus (G_0) of the sand at various distances from the Biogrout injection well along the middle line connecting the central injection and extraction wells (see the arrows in Figure 9). The solid line shows the G_0 estimated from the obtained correlation (Figure 6 and equation 3) between the measured $CaCO_3$ content and the Young's modulus of the unloading-reloading curve (E_{ur}) and using equation 4, assuming a Poisson's ratio of 0. The values at various depths at a given location (see Figure 7) have been averaged to produce this distribution. The 3 dashed/dotted lines in Figure 9 indicate G_0 calculated according to equation 5 from estimated values for ρ and the measured V_S (see Figure 8) for a direct transmission through the sand over a distance of 2.25 m. Measurements were performed at 4 different source locations right above the middle array of geophones (x= 50, 300, 500 and 750 cm) and respectively at 3 different stages of our experiment – before biogrouting (initial), after 1 day of biogrouting (9 m³ of reagent solution), and after the whole Biogrout treatment (100 m³ of reagent solution). Note that these two different estimates are only to be compared for the end values, because the ex-situ lab estimates are only available after the entire experiment.

Remarkably, we notice that although these two estimates are based on different physical principles (empirical relations with large variance using the geotechnical lab test results versus the in-situ seismic measurements), the spatial trend of stiffening of the sand delineated by the two methods is very similar: Between 150 and 650 cm G_0 decreases significantly from 350 to about 100 MPa: the two different approaches show similar values. The low G_0 values calculated from geotechnical measurements close to the injection well (solid line in Figure 9, see the left arrow) were not observed in the in-situ seismic measurements. This is simply because no V_S measurement was possible at the location of injection as the seismic source could not be placed there; (the dashed lines should not be interpreted). Left of the injection well (X = 0-100 cm in Figure 9), the

difference between the two estimates is due to the fact that there were relatively few samples where $CaCO_3$ was measured (Figures 3 and 7), and hence the estimate from $CaCO_3$ content does not represent the entire thickness of the sand, while the seismic velocity offered the stiffness averaged over the entire 2.25 m of sand.

Shear moduli or stiffness derived from geotechnical and seismic measurements are in the same order of magnitude, indicating that both methods, described above, can be used to determine the average mechanical properties of the bulk soil/rock mass. The advantage of the seismic measurements is that the increase of the average stiffness can be followed in time and space and as the method works remotely, one gets in-situ estimates. However, in this case the seismic velocity is an average over a certain thickness or volume. With higher multiplicity of seismic sources and receivers, dense and spatially uniform seismic ray coverage through the investigation volume and inversion of seismic attributes (time, amplitude, various phase arrivals, waveform), it is possible to illuminate the local heterogeneities and can obtain a detailed spatial distribution of the shear modulus from the seismic data. That will require considerable efforts in both acquisition and processing/computation. Such geometry and multiplicity were not available in case of our experiment. It was, therefore, not possible to achieve the spatial details in shear modulus from our seismic data as we could obtain from the geotechnical tests on samples collected at many locations distributed over the entire cemented sand body.

3.4   Requirements and possibilities for railroad stabilization

The large-scale demonstration experiment showed that it was possible to increase the average shear modulus of a semi-confined sand layer more than tenfold from 20 MPa to about 350 MPa. Next question is whether this increase in stiffness is sufficient to mitigate continuous maintenance and risk of failure of the railroads. To evaluate the potential of Biogrout as ground improvement method under railroad tracks and in particular the effect of biogrouting on critical velocity, the situation near Gouda Goverwelle, a train station in the western part of The Netherlands, is used as a case study. The soil underneath the tracks at this location consists of alternate layers of very soft peat and sand and the track does not meet the required Dutch design regulations (Prorail, 2006). According to these regulations the train velocity should be lower than 0.54 times the minimum Rayleigh wave velocity (depending on the required safety factor and design velocity). For instance, with a design speed for trains at 200 km h^{-1} which is the lower limit for high speed trains, the track would only satisfy design requirements when the minimum critical (Rayleigh wave) velocity, $v_{crit,min}$, is higher than 333 km h^{-1}.

A computer program SCATMAT based on the theory of wave propagation in stratified media (Kennett, 1983) was developed and used by Van der Poel (1995) and Hölscher (2001) to calculate wave velocities as a function of load frequency for simplified subsoil profiles consisting of parallel homogeneous horizontal layers. The required parameters here include layer thickness, bulk density, shear modulus (G_0) and bulk modulus (K). From cone penetration tests a subsoil profile was established and average values for cone resistance (q_c), bulk weight (γ_b) and Poisson's ratio (v) were determined for each layer. From these values G_0 and K were determined for each layer using empirical relationships

(Marcon, 2001). The subsoil profile at Gouda Goverwelle and its geotechnical parameters are presented in Table 1.

Table 1 Soil profile for the railroad track at Gouda Goverwelle in The Netherlands, with parameters: layer thickness, D, cone resistance, q_c, bulk weight, γ_b, Poisson's ratio, v, shear modulus, G, and bulk modulus, K.

Material	D [m]	q_c [MPa]	γ_b [kN/m³]	v [-]	G [MPa]	K [MPa]
Sand	2.7	8	18	0.3	77.3	167.4
Peat	0.5	0.4	10	0.4	2.0	9.5
Sand	1.5	8	18	0.3	84.7	183.4
Peat	3.5	0.3	11	0.4	2.7	12.8
Sand	0.8	6	20	0.4	72.6	339.0
Peat	2.2	0.4	12	0.4	3.1	14.7
Sand	2.5	20	21	0.4	156.4	730.0

Using SCATMAT, the minimum critical velocity, $v_{crit,min}$, (i.e. the minimum Rayleigh wave velocity in the velocity-frequency plot) was calculated for the current soil profile. Next to the current soil profile three different ground improvement scenarios were suggested: 1) ground improvement of the top sand layer up to an average shear modulus of 300 MPa (as observed in the experiment discussed here); 2) ground improvement of the top sand layer up to a shear modulus of 500 MPa; and 3) ground improvement of the top sand layer up to a shear modulus of 500 MPa, while reducing its thickness from 2.7 to 2 m. The used input parameters for calculating these scenarios with SCATMAT are presented in *Table 2*. For the other layers same values for the parameters where used as for the current profile (Table 1).

Table 2 Geotechnical parameters for different ground improvement scenarios in which the top sand layer underneath the railroad track at Gouda Goverwelle is treated.

Scenario	D [m]	γ_b [kN/m3]	G [Mpa]	K [MPa]
Current profile	2.7	18	77.3	167.4
1: G_0=300	2.7	20.5	300	650
2: G_0=500	2.7	21	500	1083
3: G_0=500;D=2.0	2.0	21	500	1083

Although an average shear modulus of 500 MPa was not reached in the large-scale experiment, shear modulus exceeding 3000 MPa could be locally obtained (Figure 7). Optimization of the treatment procedure should enable higher stiffness and strength with lower variability. The last scenario was calculated to investigate whether ground improvement could be combined with a thinner layer of sand. Thinner sand layers might be advantageous as soft soil layers compress under the load of the embankment. The current practice to overcome this problem is a periodic raising of the embankments, which is not sustainable. The table below presents the results of the calculations used to determine the minimum required thickness of the embankment for the stiffness G_0=500 MPa.

Table 3 Minimum critical (Rayleigh wave) velocity $v_{crit,min}$ for different scenarios of ground improvement underneath the railroad track near Gouda Goverwelle. This velocity resulted from SCATMAT calculations. According to Dutch regulations the maximum allowable train velocity $v_{train,max}$ is 0.54 times $v_{crit,min}$.

	$v_{crit;min}$ [m s^{-1}]	$v_{crit;min}$ [km h^{-1}]	$v_{train,max}$ [km h^{-1}]
Current profile	86	311	168
1: G_0=300	109	392	212
2: G_0=500	120	434	234
3: G_0=500;D=2.0	104	376	203

Where the current profile allowed a maximum train velocity of 168 km h^{-1}, treatment as performed in the biogrouting experiment reaching an average shear modulus of about 300 MPa, would increase the critical velocity more than 25%, which would be sufficient to satisfy Dutch regulations. Further treatment reaching G_0 of 500 MPa would allow thinner sand layers. As a result of biogrouting treatment the density of the sand layer also increases, which has a negative influence on the long-term settlement of the underlying soft soils. However, this increase in bulk weight is compensated by a decrease in layer thickness when thinner sand layers are considered.

Apart from the effect of biogrouting on the Rayleigh wave velocity the increase in strength also reduces the risk of failure due to liquefaction. The extent of this effect should be further investigated. Secondly the feasibility of biogrouting does not depend on technical factors alone, but involves economical and legislative issues as well. Apart from the technical feasibility, the cost of required substrates (calcium chloride, urea and bacteria) and removal of produced byproducts (ammonium chloride), will affect the commercial potential. To improve feasibility and sustainability of biogrouting, new processes are being investigated, which do not produce byproducts that require subsequent removal, make use of indigenous microbial population and potentially even use waste products of other industries as substrates (Van Paassen et al. 2009).

4 Conclusions

In a large scale demonstration experiment, we showed that biogrouting – ground improvement by microbial induced carbonate precipitation, can be used to significantly improve the stiffness of sand embankments on soft soils. The increase in stiffness allows higher train velocities and reducing required maintenance. The increase in stiffness is proven using two approaches - in-situ time-lapse shear-wave transmission seismics and empirical estimation based on lab experiment data (unconfined compressive strength tests) on excavated samples. Although these two approaches are based on different physical principles, the derived results correspond remarkably well. While the lab measurements provided more local information on small scale heterogeneity of the resulting cementation, the in-situ seismic measurements allowed to monitor the biogrouting progress both in space and time without physically disturbing the ground.

References

British Standard Institution (BSI), 1999. *BS 5930:1999 Code of practice for site investigations* London, British Standard Institution.

De Jong, J.T., Fritzges, M.B. & Nusslein, K. 2006. "Microbially Induced Cementation to Control Sand Response to Undrained Shear." *Journal of Geotechnical and Geoenvironmental Engineering* 132(11): 1381-1392.

De Jong, J.T., Mortensen, B.M., Martinez, B.C. & Nelson, D.C. 2009. "Bio-mediated soil improvement." *Ecological Engineering* In Press, Corrected Proof.

Ghose, R., Brouwer, J., and Nijhof, V., 1996. A portable S-wave vibrator for high-resolution imaging of the shallow subsurface, *Proceedings of the International Conference of the European Association of Geoscientists and Engineers*, M037.

Ghose, R, & Goudswaard, JCM, 2004. Integrating S-wave seismic-reflection data and cone-penetration-test data using multiangle multiscale approach, *Geophysics*, 69, 440-459.

Ghose, R., 2002. High-frequency shear wave reflections from shallow subsoil layers using a vibrator source: sweep cross-correlation versus deconvolution with groundforce derivative, *Proceedings of the International Conference of the Society of Exploration Geophyssicts*, Salt lake City, USA.

Harkes, M.P. Paassen L.A. van, Booster J. L., Whiffin, V. S. and Loosdrecht, M.C.M. van, 2009. Fixation and distribution of bacterial activity in sand to induce carbonate precipitation for ground reinforcement, *Ecological Engineering* In Press.

Hölscher, P, 2002, Simplified models for Critical speed of moving loads on layered halfspace, in: *Learned and Applied, soil mechanics out of Delft*; Barends, F.B.J.; Steijger, P.M. (ed.), Lisse, Balkema

Ivanov, V. & Chu, J. 2008. "Applications of microorganisms to geotechnical engineering for bioclogging and biocementation of soil in situ." *Reviews in Environmental Science and Biotechnology* 7(2): 139-153.

Karol, R.H. 2003. *Chemical grouting and soil stabilization.* New York, Dekker

Kaynia, AM, Madshus, C & Zackrisson, P. 2000. "Ground Vibration from High-Speed Trains: Prediction and Countermeasure." *Journal of Geotechnical and Geoenvironmental Engineering* 126(6): 531-537.

Kennett, BLN 1983, *Seismic Wave Propagation in Stratified Media*, Cambridge University Press.

Marcon, A, 2001, *Prediction of soil the stiffness, CPT or VSP?*, MSc thesis, Institut des Sciences et Techniques de Grenoble and GeoDelft (currently Deltares Geo-Engineering)

ProRail, 2006, *Guideline for design of embankments and geotechnical structures* (In dutch: Ontwerpvoorschrift Baanlichaam en Geotechniek, version 2), OVS00056-7.1

Van Paassen, L.A., Daza, C.M., Staal, M., Sorokin, D.Y., Van der Zon, W. & Van Loosdrecht, M.C.M.. 2008. Potential soil reinforcement by microbial denitrification, *Ecological Engineering* In Press

Van Paassen, L.A., Harkes, M.P., Van Zwieten, G.A., Van der Zon, W.H., Van der Star, W.R.L. & Van Loosdrecht, M.C.M. 2009. Scale up of BioGrout: a biological ground reinforcement method. *17th International Conference on Soil Mechanics & Geotechnical Engineering*, Alexandria, Egypt.

Van Paassen, L.A., Whiffin, V.S. & Harkes, M.P. 2007. *Immobilization of bacteria to a geological material.* Netherlands. Patent assignee: Stichting GeoDelft. EP1798284-A1; WO2007069884-A1.

Van der Poel, T. 1995. *The elastodynamic wavefield in horizontally layered media*, MSc Thesis, Delft University of Technology, The Netherlands

Whiffin, V.S., Van Paassen, L.A. & Harkes, M.P. 2007. "Microbial Carbonate Precipitation as a Soil Improvement Technique." *Geomicrobiology Journal* 24(5): 417-423.

9

Reinforcement of calcarenite room and pillar mines by microbially induced carbonate precipitation

Abstract

In this study the feasibility of using Biogrout – ground improvement by microbially induced carbonate precipitation (MICP) - for the in-situ reinforcement of calcarenite room and pillar mines was investigated. The applied MICP process comprised microbially catalyzed hydrolysis of urea in a solution containing calcium chloride, resulting in precipitation of calcium carbonate. Two small cores were treated in triaxial setup. The amount of calcium carbonate precipitate was estimated during treatment by measuring the ammonium concentration in the effluent and after treatment by the increase in wet and dry density. Unconfined compressive strength tests showed that the strength of the calcarenite doubled after treatment, while permeability was reduced by fifty percent. Using micro- X-ray computerised tomography (micro-CT) scanning, a funnel pattern was observed in a treated core, spreading outwards from the inlet towards the outlet, indicating non-homogeneously distributed precipitation. Failure patterns of unconfined compressive strength (UCS) tests were affected by heterogeneities in the sample, observed with micro-CT. The experimental results make clear that Biogrout can be used to reinforce calcarenite and can be developed to apply as in-situ reinforcement method for the calcarenite mines.

1   Introduction

Massive limestone calcarenite formations of Maastrichtian age (Upper Cretaceous) outcrop in the South of the Netherlands and the North of Belgium near the city of Maastricht. They have been extensively mined for building stones from the Roman times up to the 1950's. Some of the calcarenite mines, which seemed stable for hundreds of years, have collapsed or are on the verge to collapse and need to be reinforced to avoid the formation of large sinkholes at ground surface and the loss of several hectares of underground space.
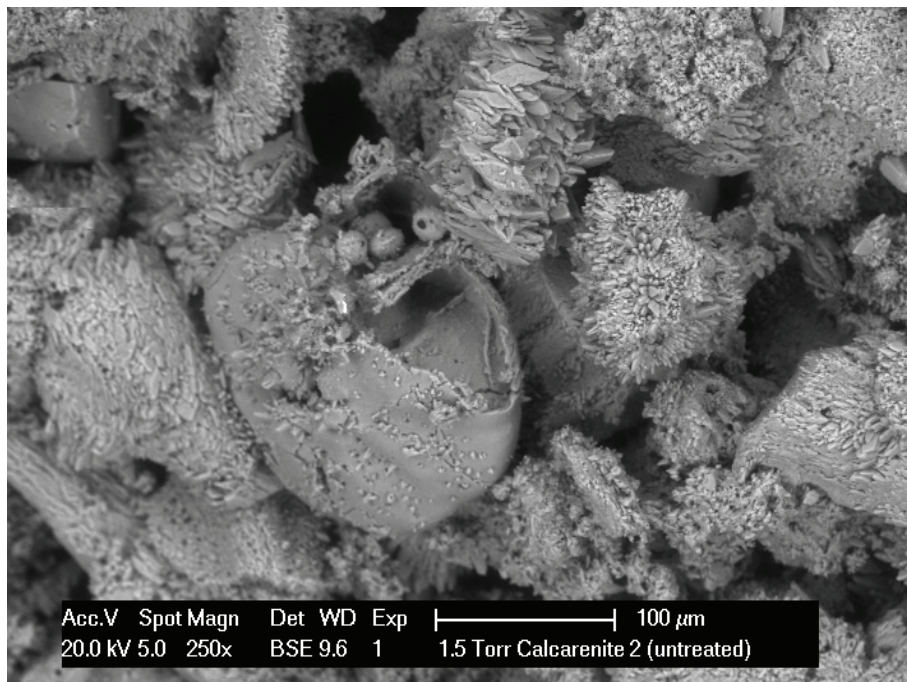
Figure 1. ESEM image of Maastricht calcarenite, showing a nearly intact shell perforated by dogtooth crystals and many fossil fragments fully overgrown by microcrystalline calcium carbonate.

The calcarenite of the Maastricht formation is a weak porous rock with a saturated UCS of 1.5 to 4.5 MPa, a porosity of a 45-50% and a calcium carbonate content rarely less than 96% (Bekendam, 1998). It is a well sorted clastic carbonate rock with sand-sized grains (100 to 400μm), classified as grainstone (Dunham, 1962). The particles are fragmented skeletal components from foraminifera, sponges, bivalves, bryozoa and brachiopods. A few millimetric and centimetric fossils lay subhorizontally in the calcarenite. Many of its grains show a microcrystalline dogtooth cement overgrowth (Figure 1).

Long-term deterioration of the calcareous material, especially at shallow depth, occurs by either dissolution of cementing bonds or formation of micro-cracks, leading to creep (Smith and Rosenbaum, 1993). Creep deformation can eventually lead to spalling of pillars or roof collapse (Figure 2), two of the main failure mechanisms in room and pillar mines (Bekendam, 1998).
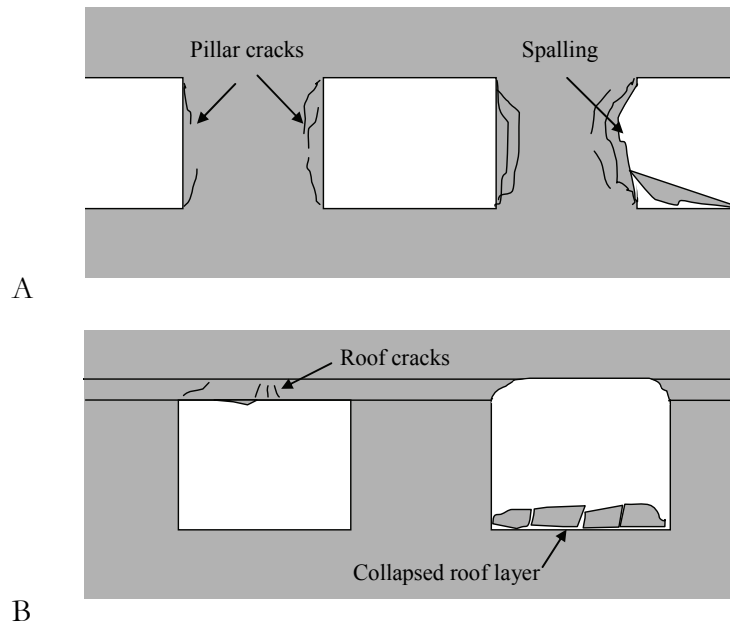
Figure 2. Two of the three main types of local instability for which MICP could be a solution: a) pillar cracking and spalling, b) failure and collapse of roof layers. (after Bekendam, 1998).

The deterioration processes are accelerated by the low confining stresses and high deviatoric stress in the excavation walls. The risk of collapse is highest when the mines are not inundated and groundwater level rises after a period of heavy rainfall.

Currently employed remediation measures consist of back-filling galleries, of reinforcing weak or failed pillars with a concrete or brick-walled casing or installing additional artificial pillars supporting the roof (Van den Eeckhaut et al. 2007). In this paper, the feasibility for using microbially induced carbonate precipitation (MICP) (DeJong et al. 2006; Whiffin et al. 2007) as an alternative elegant and cost-effective technique to strengthen mine roofs or pillars is evaluated.

In the BioGrout process described by Whiffin et al (2007) a broth containing *Sporosarcina pasteurii*, bacteria with a high quantity of the enzyme urease, is injected in the porous material. Part of the bacteria adsorb to the solid surface or get stuck within narrow pores. Afterwards successive batches of reagent solution, containing urea and calcium chloride, are injected and left for some time in which the following chemical reactions take place:

$$CO(NH_2)_2 + 2H_2O \rightarrow 2NH_4^+ + CO_3^{2-}$$

$$Ca^{2+} + CO_3^{2-} \rightarrow CaCO_3(s)$$
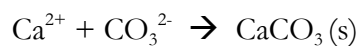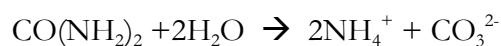
The microbial urease catalyses the hydrolysis of urea and the produced carbonate precipitates with dissolved calcium as calcium carbonate crystals. The remaining ammonium chloride is removed by the next batch of reagent solution. The newly formed calcium carbonate crystals restore or increase the number of intergranular cementation bonds, improving the rock material strength and stiffness. Using this process loose unconsolidated quartz sand has been cemented up to unconfined compressive strength (UCS) of 30 MPa (Whiffin et al. 2007; Harkes et al. 2008). By controlling the rate of hydrolysis and precipitation and the number of treatments, biogrouting can be applied in

such a way that strength increases without significant reduction of the hydraulic conductivity (Harkes et al, 2008).

Laboratory tests have been carried out to quantify the effect of Biogrout treatment on strength, stiffness and permeability of calcarenite from Maastricht formation. The homogeneity of induced cementation has been checked at the core scale with the help of micro-CT scans.

2 Materials and methods

2.1 Treatment

Four 38 mm diameter and 81 mm length cores were used for this preliminary study. The cores were drilled from a 50x50x50 cm³ block of calcarenite from the Emael member of the Maastricht formation excavated in the Sibber groeve, with properties as described above. The block seemed homogeneous and no stratigraphic sequences could be observed. Some larger shells (2-8 mm diameter) could be observed in the material, all of them orientated sub-horizontally.

Core 2 and 4 were left untreated and used as reference. Core 1 and 3 were treated with MICP. They were saturated under vacuum and placed in a triaxial cell under a confining pressure of 40 kPa before being flushed with the bacterial broth and the batches of reagent solution. Inflow and outflow of fluids went through a hole at the centre of the loading caps. Flushing was done from bottom to top at a constant rate of 2.2 mL min⁻¹. Assuming an available porosity of 50%, this corresponded to an average flow velocity of 0.2 m h⁻¹. According to Harkes et al (2008) at this velocity bacteria will not flush out after placement.

First 2 pore volumes of (approximately 45 mL) bacterial broth, containing *Sporosarcina pasteurii* (DSMZ 33), which was cultivated according to Whiffin et al. (2007), were flushed through the water saturated core. After 2 hours, in which the bacteria were left to attach to the solid material, the first batch of 1.5 pore volume (about 75 mL) of reagent solution (1 M ureum $CO(NH_2)_2$ + 1M $CaCl_2$) was flushed through. After the first batch of cementation fluid the cores were left for about 24 hours to react. Then the procedure of flushing a batch of reagent solution followed by a reaction period of 24 hours was repeated twice. Finally a batch of water was flushed through to remove all remaining dissolved products. Between the four flushes, in- and outlet valves were closed so that pore pressure could build up in the sample.

2.2 Monitoring and testing methods

2.2.1 Ammonium measurements

During successive batch flushes, samples of the effluent were taken for ammonium measurements to calculate the amount of precipitated calcium carbonate. Ammonium concentrations were determined by a modified Nessler method (Whiffin et al. 2007).

The relation between ammonium concentration of effluent and amount of precipitated calcium carbonate comes from the reaction stoichiometry; for each 2 moles of ammonium 1 mol of calcium carbonate is formed. The total amount of calcium carbonate can be determined by integrating the ammonium measurements.

2.2.2   Calcium carbonate precipitation in the core

The amount of actually precipitated calcium carbonate in the core is checked by measuring the increase in dry weights due to biogrouting. The mass of the precipitated calcium carbonate is expected to be less than the values derived from the ammonium measurements since part of the precipitate ends up in the system or in the outflow.

2.2.3   Strength and stiffness

To determine changes in strength and stiffness caused by bio-grouting, unconfined compressive strength (UCS) tests were performed on the pairs of untreated and treated cores according to ASTM D2938-95, -D3148 and -D4543 standards. Radial strain was measured at mid-height of the sample using a radial chain extensometer. Axial strain was measured with 2 axial strain transducers over the whole length of the sample. Cores were saturated under vacuum before testing. Oven dried cores would have a higher strength.

2.2.4   Permeability

Falling head permeability tests were carried out after treatment on one treated and two untreated cores. Cores were first saturated under vacuum before being tested.

2.2.5   Micro-CT scanning and image analysis of macro- to micro structure

To get insight into the amount and distribution of calcium carbonate precipitation in the pores, cores were subjected to micro- X-ray computerised tomography before and after treatment. A nanotom-180 of Phoenix X-ray, producing an X-ray cone beam with a maximum voltage of 180 kV, a maximum capacity of 15 W and a sub-micron minimum focal spot was used.

As a trial a 1.5x1x1 cm^3 cube of Maastricht calcarenite was scanned. A part of a constructed 2D cross-section of this 3D scan is shown in Figure 3. The image has a pixel size of 8 μm. Grains are sharp and thin internal walls of hollow shells are clearly visible. The number of intergranular contacts is limited. Submicro-resolution susceptible to reveal microcrystalline 'dogtooth' coating (as shown in Figure 1) can be obtained on millimetric samples only. To penetrate dense or large samples as those subjected to biogrouting, a higher beam energy is required deteriorating spatial resolution and image analysis for density or porosity determination. Scan time can be increased for noise reduction by image integration up to several hours but at the detriment of the stability of the whole system.
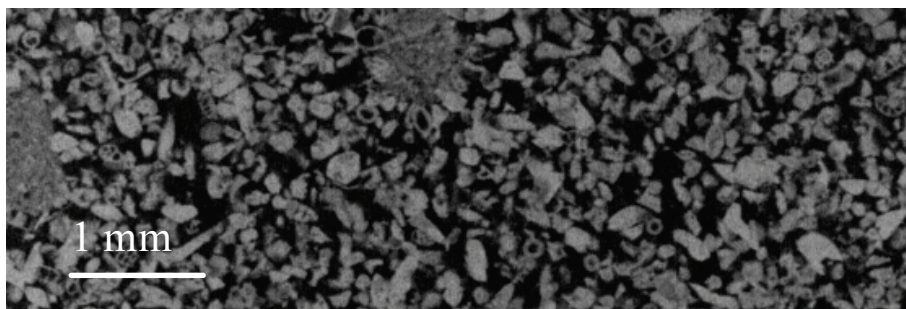
Figure 3. Detail of a constructed 2D cross-section from a micro-CT scan of a 1.5x1x1 cm^3 piece of calcarenite at a resolution of 8μm, showing the high porosity lightly cemented sandstone before treatment..

Since the calcarenite matrix and its artificial cementation are both made of calcium carbonate, they present the same attenuation to X-rays and cannot be directly distinguished on a micro-CT scan. Calcification does not appear as clearly as it would for a calcified siliceous sandstone (De Jong et al. 2006) since quartz attenuates X-rays less than calcite. Instead quantitative analysis of the spatial distribution of newly formed calcium carbonate in the calcarenite was done by substracting images taken before and after biogrouting. The simplified volume registration adopted by Plougonven and Bernard (2006) for quantifying limestone dissolution by acidic water was implemented.

3 Results and discussion

3.1 Ammonium measurements
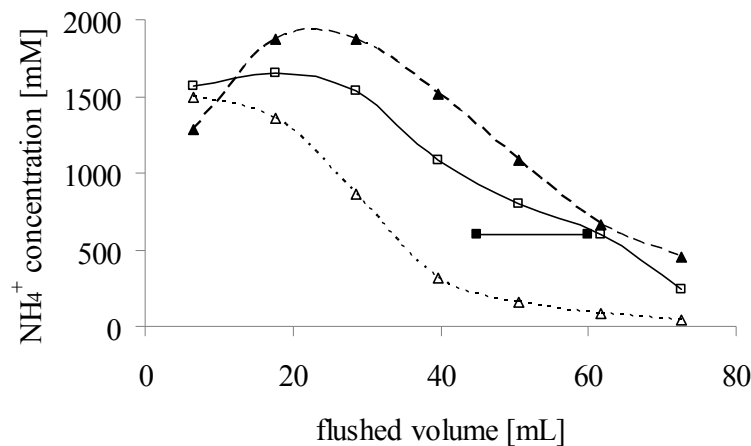
Figure 4. Measured ammonium concentration in the effluent during treatment of core 1 per flush: ■: flush 1, ▲: flush 2, □: flush 3, ⊿: flush 4.

Ammonium measurement during the first flush showed that the effluent leaving the core after 1 pore volume (45 mL) already contained about 600 mM of ammonium, which was produced within the 20 min of flushing (Figure 4). 24 hours later during the second flush the concentration increased from 1200 mM nearly up to the level of full conversion of 1 M urea into 2M of ammonium. After about 40 mL the effluent got diluted by fresh, less reacted reagent solution. Third and fourth flush showed similar patterns, except for a lower maximum conversion level, indicating a decrease of urease activity in time. The total amount of precipitated calcium carbonate could be estimated by integrating the concentration over the flushed volumes. A total of 10.8 g was estimated for core 1 and 11.0 g of $CaCO_3$ for core 3. With a total flushed volume of 225 mL of a 1M reagent solution, the theoretical maximum amount of $CaCO_3$ was 22.5 g.

3.2 Precipitation

Porosity derived from core dimensions and dry and saturated weights was found to be 49 and 53% for treated and untreated calcarenite respectively.
Using values for dry cores, 8.6 and 9.1 grams of calcium carbonate was found to have formed inside core 1 and 3 respectively. The difference between these values and those

derived from ammonium measurement (11.3 resp. 11.0 g) can be attributed to the precipitate that was found outside the core in the system (loading caps and tubes) when dismantling the setup and possible losses of dissolved calcium carbonate in the effluent. Table 1 gives an overview of the measurement of calcium carbonate precipitation.

Table 1. Overview of measurements on amount of precipitated calcium carbonate for treated (1&3) and untreated (2&4) cores.

Core	1	3	2	4
Precipitated $CaCO_3$ (g) from ammonium measurement	11.3	11.0	-	-
Precipitated $CaCO_3$ (g) from dry density measurement	8.6	9.1	-	-
Saturated density (kg m^{-3})	1849	1849	1783	1793
Dry density (kg m^{-3})	1358	1355	1258	1256
$CaCO_3$ dry (kg m^{-3})*	100	99	-	-
Porosity (-)	0.49	0.50	0.53	0.54

*CaCO₃ dry: difference in dry density before and after treatment attributed to the precipitated CaCO₃.

3.3 Permeability

Using the falling head method, a permeability of 13 and 5.5 Darcy was measured on untreated and respectively treated calcarenite cores. Despite a decrease in permeability of about 50%, biogrouted cores remain highly permeable; their pores are not clogged. Clogging is not wanted as it would modify water flow. Water flow could for example be directed to the roof instead of a reinforced pillar and weaken the roof.

3.4 Strength and stiffness

Figure 5 gives an overview on the deformation behaviour exhibited by a grouted and non grouted core during uniaxial compressive loading. Table 2 summarizes the mechanical properties.
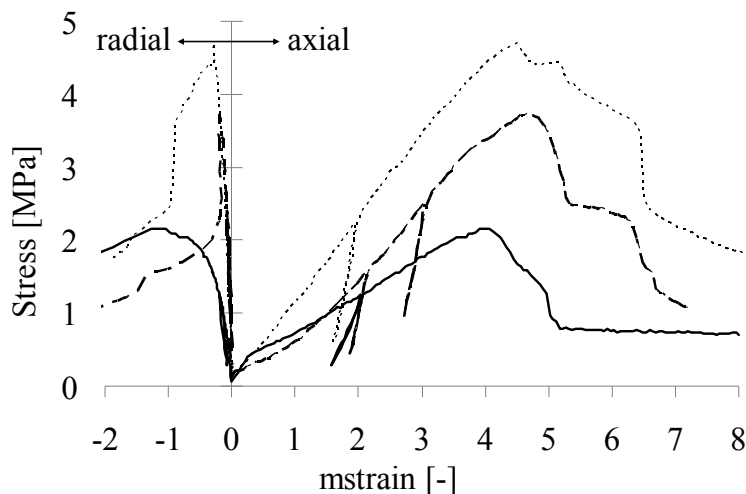
Figure 5. Stress-strain plot (axial: right and radial: left) for determination of mechanical parameters. Elastic loops are at approximately 50% UCS. Core 1:······, core 3: - - - -, core 4: ——

UCS-values were nearly the same for both untreated cores: 2.15 MPa and 2.16 MPa against 3.7 MPa and 4.7 MPa for the treated cores. Residual strengths are all below 2 MPa.

Table 2. Mechanical properties of treated (1&3) and untreated cores (2&4).

Core	1	3	2	4
UCS (MPa)	4.70	3.74	2.15	2.16
Residual strength (MPa)	-	-	1.55	-
Axial strain at peak (mstrain)	4.51	4.67	2.60	4.01
Radial strain at peak (mstrain)	-0,28	-0,19	-0.70	-1.19
E_{50} (GPa)	1.10	1.01	0.76	0.49
ν_{50} (-)	0.07	0.08	0.16	0.12
$E_{un\text{-}reloading\ loop}$ (GPa)	4.44	4.39	2.43	1.87
$\nu_{un\text{-}reloading\ loop}$ (-)	0.13	0.15	0.33	0.20

Axial strains at stress peak tend to be higher for treated cores (around 4.6 mstrain). However, values for untreated cores vary significantly from 2.6 to 4 mstrain. The lower value of 2.6 is probably an artefact due to preloading. Elastic axial stiffness measured in unloading/reloading loops ($E_{un\text{-}reloading}$) was around 4.4 and 2.2 GPa for the treated and untreated cores respectively while their tangent axial stiffness at 50 % of the stress peak was about 1.0 to 1.1 and 0.5 to 0.8 GPa respectively.

 Radial extension is lower for grouted than for non grouted cores. The elastic Poisson's ratio ($\nu_{un\text{-}reloading}$) was in average 0.14 against 0.25 respectively. In brief, both treated and untreated samples exhibit a brittle behaviour with a clear peak strength. Treated cores are twice stronger and stiffer than the untreated cores and they deform less laterally. Failure propagated along inclined shear planes in the non-treated cores. In the treated cores, it occurred under the form of scales surrounding a cone pointed towards the base of the sample from where batches of bacterial broth and reagent solution were injected.

3.5 Micro-CT scanning and image analysis

Core 1 was scanned before and after treatment, resulting in 3D images of both untreated and treated material. Scans of 38 mm diameter cores have a resolution of 20 µm. Due to data processing limitations, only a small part of the sample could be reconstructed at this resolution. As the whole sample was reconstructed, resolution dropped to 40 µm.

Figure 6 and 7 display horizontal and vertical slices respectively of the untreated and biogrouted calcarenite core at a resolution of 40 µm. The scans recorded before grouting illustrate the relative homogeneity of the material at the centimetre scale apart from a few large shells. The scans recorded after grouting show an uneven distribution of precipitated calcium carbonate, with more $CaCO_3$ precipitated in a funnel pattern emerging from the bottom of the core near the injection point and vanishing before the top edge of the core. This funneling pattern is consistent with the failure pattern of the treated cores.
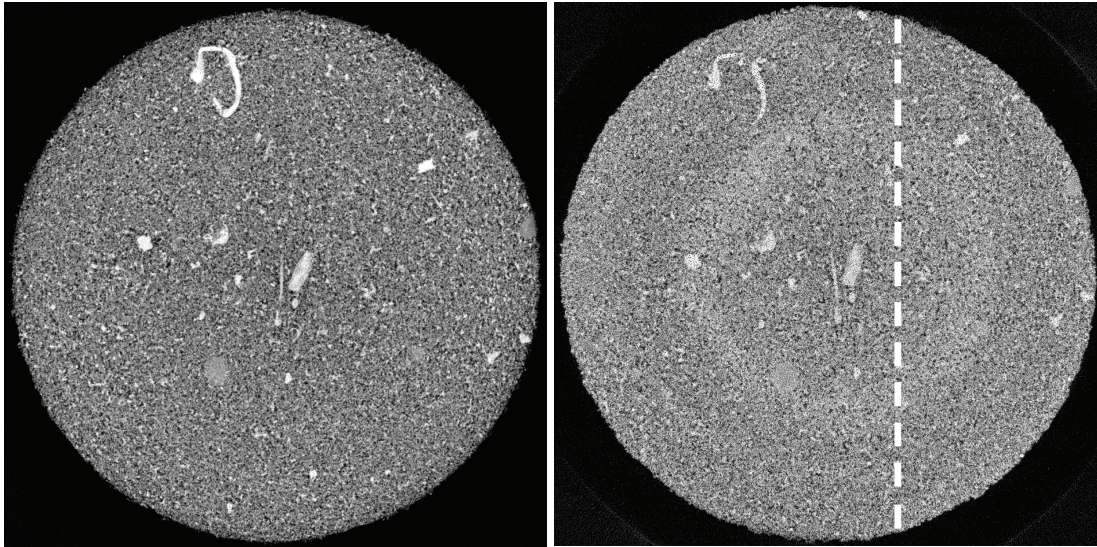
Figure 6. Horizontal slice along the dashed line in Figure 7 at 40 mm from the bottom (inlet) of core 1 before (left) and after (right) bio-treatment. Resolution: 40 μm.
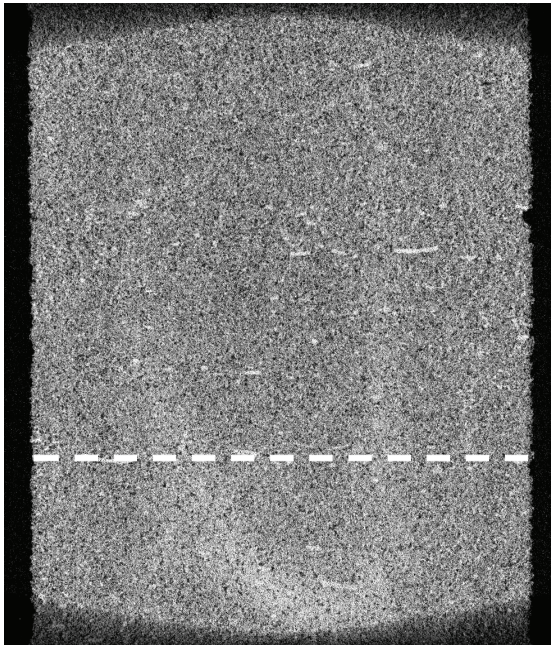
Figure 7. Section between 25 to 75 mm from bottom taken from a vertical slice along the dashed line in Figure 6 *of core 1 after biogrouting, width: 35 mm. The funnelling pattern is clearly visible. Resolution: 40 μm.*

One explanation for this funnelling pattern can be the absence of distribution pads between the core and loading cap in combination with the high permeability of the calcarenite and a short core length. As a result the flow is initially concentrated near the inlet, diverging from the centre flow line due to dispersion and then converging again towards the outlet. Relatively large dead zones with no flow and hence no supply of bacteria and reagents will exist. The reduction in permeability by bacteria or crystals, will divert the flow outwards from the central flow line. Behind a zone of precipitation (or a large shell) another dead zone can emerge, with less precipitation in that zone as a result. Porosity in the funnel and outside can be estimated from grey levels and average core porosity to be approx. 48 and 51 % respectively. The funnel pattern will have affected

strength, deformability and permeability. A more even distribution of precipitate in the core would probably result in different values for permeability, strength and stiffness.

Quantitative analysis of the spatial distribution of newly formed calcium carbonate in the calcarenite by substracting the micro-CT scan images before and after treatment was not yet successful. Due to the increase of density by $CaCO_3$ precipitation, X-rays penetrated less easily in the core after biogrout treatment and scanning settings had to be adjusted to obtain an image of a reasonable quality, resulting in a different colour map of gray scales and rendering image substraction unreliable. Secondly, since biogrouting was not conducted inside the micro-CT scan, some translations and rotations of the core took place between tomographies. 2D image registration obtained by matching remarkable features such as large shells did not work. First, the vertical axis of the core did not keep the same inclination between scans and shells did not remain entirely in the same horizontal slice. Second, large shells were possibly affected by calcification and are therefore not invariant. Instead of 2D image registration volume registration is necessary to quantify and map $CaCO_3$ precipitation. This has not yet been applied onto the images of the trial tests.

4 Conclusions and outlook

First MICP trials at the laboratory scale on the calcarenite of the Maastricht formation are successful. Strength and stiffness of the calcarenite are doubled, while permeability is only reduced by 50%, leaving enough possibilities for further treatment or groundwater flow.
Homogeneity of the flow through the material is important for homogeneous distribution of the precipitated calcium carbonate at centimetre scale. A funnelling pattern observed in the grouted cores is interpreted as a result of a non-homogeneous cementation and has influenced the outcome of the strength and permeability tests. Strength at the more cemented parts of the core might have been higher than the measured value and permeability lower.
Results and experiences gained during the research provide the following suggestions for further laboratory investigation before engaging into large scale testing and application:
- Different treatment procedures should be tested to find the best combination between number and time of batch treatment, flow rate and flushed volume.
- Homogeneous flow through the core should be applied by placing distribution pads on both sides of the core to achieve homogeneity in the precipitated calcium carbonate, probably resulting in even higher strength.

Further image analysis is needed to visualize the distribution of newly formed calcium carbonate. Proper transformation of 3D images to quantitatively compare different scans is essential for this analysis. To do proper quantitative analysis, a smaller sample might be scanned, to achieve a higher spatial and density resolution.

References

Bekendam, R.F. 1998. Pillar stability and large-scale collapse of abandoned room and pillar limestone mines in South-Limburg, the Netherlands, PhD thesis, TU Delft, The Netherlands, 361 pp.

Dunham, R.J. 1962. Classification of carbonate rocks according to depositional texture. Classifcation of carbonate rocks (ed. by W.E. Ham), AAPG, Tulsa, pp. 108-121.

DeJong, J.T., Fritzges, M.B. and Nusslein, K. 2006. Microbially Induced Cementation to Control Sand Response to Undrained Shear. Journal of Geotechnical and Geoenvironmental Engineering, Vol.132, No.11, pp. 1381-1392.

Harkes, M.P., Booster, J.L., Van Paassen, L.A., Van Loosdrecht, M.C.M. and Whiffin, V.S. 2008. Microbial induced carbonate precipitation as ground improvement technique – bacterial fixation and distribution. International conference on BioGeoCivil Engineering, Deltares, Delft.

Plougoven, E. and Bernard, D. 2006. A rigid registration method for the study of microgeometry evolution of limestone during dissolution by acidic water. Advances in x-ray tomography for geomaterials, pp. 349-354.

Smith, G.J. and Rosenbaum, M.S. 1993. Abandoned shallow mineworkings in chalk: a review of the geological aspects leading their destabilisation. Bulletin of the International Association of Engineering Geology , Vol.48, No.1, pp. 101-108.

Van Den Eeckhaut, M., J. Poesen, M. Dusar, V. Martens, and P. Duchateau. 2007. Sinkhole formation above underground limestone quarries: A case study in South Limburg (Belgium). Geomorphology Vol 91, No.1-2, pp. 19-37.

Van der Schrier, J.S. and Gerritsen, R.H. 2004. Cut-and-Cover Tunnel below Boulevard River Meuse, Maastricht, The Netherlands. Engineering Geology for Infrastructure Planning in Europe, LNES Vol.104, pp. 767-776.

Whiffin, V.S., Van Paassen, L.A. and Harkes, M.P. 2007. Microbial Carbonate Precipitation as a Soil Improvement Technique. Geomicrobiology Journal Vol.24, No.5, pp. 417-423.

10

Potential ground reinforcement
by
biological denitrification

Abstract

Currently new ground reinforcement techniques are being developed based on microbially induced carbonate precipitation (MICP). Many studies on MICP use microbially catalyzed hydrolysis of urea to produce carbonate. In the presence of dissolved calcium this process leads to precipitation of calcium carbonate crystals, which form bridges between the sand grains en hence increase strength and stiffness. Next to urea hydrolysis, there are many other microbial processes, which can lead to the precipitation of calcium carbonate. In this study the theoretical feasibility of these alternative MICP processes for ground reinforcement is evaluated. Evaluation factors are substrate solubility, $CaCO_3$ yield, reaction rate and type and amount of side-product. The most suitable candidate as alternative MICP method for sand consolidation turned out to be microbial denitrification of calcium nitrate, using calcium salts of fatty acids as electron donor and carbon source. This process leads to calcium carbonate precipitation, bacterial growth and production of nitrogen gas and some excess carbon dioxide. The feasibility of MICP by denitrification is tested experimentally in liquid batch culture, on agar plate and in sand column experiments. Results of these experiments are presented and discussed.

1 Introduction

In many regions and industrial sites, the mechanical properties of soil are insufficient: Roads and railways undergo settlement, dikes, dunes and slopes can become unstable and slopes, coasts and rivers are subject to erosion. Earthquakes can cause liquefaction of loose sediments. Water and oil production wells in loosely cemented layers often produce sand, which has to be removed. In land reclamation projects the compaction of the recovered land is a major concern.

Stabilization of soil is desirable for all these applications. At the surface, soil stabilization can be achieved using constructive, ecological or combined approaches (Comoss et al. 2002; Jones and Hanna 2004; Fan and Su 2008; Normaniza et al. 2008) to prevent erosion. However, when stabilization of a soil mass is required, surficial techniques are insufficient and in situ strengthening techniques, like chemical grouting are used. However, chemical grouting techniques are often costly and not suitable for treating large volumes, due to a high viscosity or a fast hardening rate of the injected fluids. In addition, these methods significantly reduce the permeability of the strengthened soil, which hinders groundwater flow and limits long distance injection, making large-scale treatment unfeasible. Biological techniques -biogrouting- can provide the solution (Whiffin 2004; DeJong et al. 2006; Ivanov and Chu 2008). By injecting specific groups of micro-organisms into the soil, in combination with substrates, precipitation of inorganic minerals is induced at the desired location. These minerals connect the existing sand grains, thereby increasing the strength of the material. The product has similar properties as natural sandstone and it remains permeable, thereby enabling large-scale applications.

In the currently described biogrouting process, aerobic, heterotrophic micro-organisms containing the enzyme urease are cultivated in the laboratory, introduced in the soil and supplied with a solution of urea and calcium chloride (Nemati and Voordouw 2003; DeJong et al. 2006; Whiffin et al. 2007). The microbial urease catalyzes the hydrolysis of urea into ammonium and carbonate. The produced carbonate ions precipitate in the presence of calcium ions as calcite crystals, which form cementing bridges between the existing sand grains. The remaining ammonium chloride solution is removed. With this method, loose sands are stabilized to a desired strength varying from loosely cemented sand to moderately strong rock (unconfined compressive strengths of 0.2 – 20 MPa) (Whiffin et al. 2007; Harkes et al. 2008). The corresponding amount of precipitated calcium carbonate varies from 30 to 600 kg m^{-3} of soil. Once precipitated the calcium carbonate will only dissolve very slowly, either when continuously flushed by acidic groundwater or as a result of acidifying processes in the pores (e.g. degradation of biomass). When sufficient calcium carbonate is precipitated, durable soil stabilization can be achieved. At present, the principle has been applied successfully on a scale of 1 m^3 and the first tests on demonstration scale (100 m^3) are being executed.

To try to overcome some problems encountered with the urease process, such as production and required removal of ammonium chloride and the use of aerobic organisms with consequent decaying urease activity in time due to a lack of oxygen in the

subsurface (Whiffin et al. 2007), the suitability of other possible MICP processes for ground improvement are evaluated in this study. The feasibility for ground improvement of the best alternative process, is tested experimentally.

2   Materials and methods

2.1   Criteria for evaluation of MICP processes for gound improvement

There are many biological processes, which can lead to precipitation of calcium carbonate (Castanier et al. 1999), but not all are suitable for soil reinforcement. To obtain significant strength improvement in a loose granular material at least 60 kg $CaCO_3$ m^{-3} soil has to be precipitated, which corresponds to approximately 2 mol $CaCO_3$ precipitate per litre of pore space (Whiffin et al. 2007). To induce such an amount of calcium carbonate precipitation homogeneously distributed and over large volume in the underground, substrates have to be injected and transported over a substantial distance into the porous material.

The suitability of different MICP processes for soil reinforcement, i.e. whether sufficient $CaCO_3$ can be homogeneously precipitated over a long distance, has been evaluated based on 4 criteria:
1. solubility of the combination of substrates
2. rate of calcium carbonate formation
3. amount of substrates required
4. amount and type of side-products

For economic reasons high substrate concentrations are preferred (typically molar range). For example, substrate concentrations resulting in 100 mM $CaCO_3$ precipitation already require that the sand is flushed with 20 pore volumes to reach significant reinforcement. Lower concentrations require even more pore volumes and are therefore considered economically unfeasible. In other words, the combination of substrates should be sufficiently soluble in water before it is injected and converted into the poorly soluble calcium carbonate.

The rate of calcium carbonate precipitation is an important process variable. The rate should be low enough to avoid rapid precipitation and consequent clogging near the inlet since that would limit the injection distance. The conversion rate should not be too low, as then it will take too much time to reach the required level of cementation.

The required amount of substrates for $CaCO_3$ precipitation follows from the reaction stoichiometry. In this evaluation only catabolic stoichiometry is taken into account. Substrates required for biomass growth (anabolism) are not included. The amount of substrate required is important as it determines the process efficiency and costs. The choice of organic substrate can be based on the $CaCO_3$ yield. On the other hand if cheap

substrates, like waste streams, can be used, the required amount of substrate might become less important as an economical factor.

The amount and type of side products also follow from reaction stoichiometry. Apart from making the reaction less efficient, side products can affect the suitability of the process by disturbing the cementation process. For example, gas formation might lower the permeability and block the flow towards the desired location. In addition, some side products, but also substrates, might be toxic for the organism, especially at high concentrations, and thereby lowering the metabolic rates. Other products need to be removed, like ammonium chloride in the urease process.

2.2   Medium composition for denitrification experiments

Calcium acetate and calcium nitrate were used as substrates to test the feasibility of denitrification as MICP process for ground improvement. Calcium acetate and calcium nitrate concentrations varied in the different experiments, but acetate-nitrate molar ratios were fixed at 1:1.5 or 1:1.2 ratio for respectively the batch experiments and the sand column experiment. To all media additional nutrients were added to avoid nutrient limitation during growth of the micro-organisms, comprising 0.003 mM $(NH_4)_2SO_4$, 0.0024 mM $MgSO_4.7H_2O$, 0.006 mM KH_2PO_4, 0.014 mM K_2HPO_4 and 1mL L^{-1} trace element solution SL12B (Overmann et al. 1992). At high substrate concentration (>100 mM calcium) precipitation occurred when the additional nutrients were added. The precipitate was assumed to be a precipitate of calcium phosphate. In batch experiments the media were filter sterilized before inoculation. In the sand column experiments the precipitate was left in the media.

2.3   Sand column experiment

To evaluate the potential of denitrification for biogrouting in a sand column an enriched inoculum was generated in medium that selects for denitrifiers. In the first cultivation a 150 mL flask was filled with 100 mL of medium containing 50mM calcium acetate and 60 mM calcium nitrate. The medium was inoculated with 15 g of soil from the botanical garden of Delft University of Technology. After several days of incubation at 30ºC. 100 mL of fresh medium was inoculated with 5 mL of the first incubation. This enrichment culture was used to inoculate the sand column.

The sand column was a PVC tube (length 200 cm, diameter 4.5 cm) filled with quartz sand with an average particle size of 250 μm. The total volume was 3L and the porosity in the column was about 35%. Consequently the pore volume was about 1 L.

After preparation, the column was mounted vertically and inoculated at the top with 100 mL enrichment culture. Thereafter medium containing 100 mM calcium acetate and 120 mM calcium nitrate was flushed through the column from top to bottom at an average flow rate of ~0.14 L day^{-1}. After 15 days, 2 L of new medium containing initially 100 mM calcium acetate and 120 mM calcium nitrate was circulated through the column at a constant hydraulic gradient of approximately 0.5 m m^{-1}. When measurement of the electrical conductivity of the effluent indicated that nearly all the dissolved substrate was converted, the media was refreshed. In this way 3 times 2 L and 1.4 L containing 25 mM calcium acetate and 30 mM calcium nitrate were circulated through the column, followed

by 2 times 0.8 , 1.6 and 2 L containing 100 and 120 mM substrate and another 2L with 25 and 30 mM. Finally 5 L containing 50 mM calcium acetate and 60 mM calcium nitrate was flushed through without recycling. In total 25 L of substrate solutions was used during a period of 100 days. In total about 3 mole of calcium was supplied to the column, which would result theoretically in formation of 300 g $CaCO_3$, which is equivalent with 100 kg m^{-3} soil and would give measurable strength according to chapter 5 (Whiffin et al. 2007) and chapter 7 (Harkes et al. 2008).

During the experiment, electrical conductivity of the effluent and total weight of the effluent were continuously measured to determine the substrate concentration and flow rate and samples were taken at regular intervals to measure the acetate, nitrate and nitrite concentrations and to analyze crystals and micro-organisms observed in the effluent. The conversion rate could be derived from the decrease in measured substrate concentration during a single flush. After the treatment, the column was cut in sections. For each section the $CaCO_3$ content was determined (Whiffin et al. 2007). An estimate of strength was obtained using an empirical correlation between $CaCO_3\%$ and unconfined compressive strength (Whiffin et al. 2007; Harkes et al. 2008).

From the top section samples were taken and analyzed using a Philips XL30 environmental scanning electron microscope (ESEM) equipped with an EDAX X-ray microanalysis system.

2.4   Isolation

A sample was taken from the effluent of the sand column after 60 days of operation, from which a pure culture was isolated. To isolate the already dominant bacterium, the sample was first serial diluted in the medium used to flush the sand column (100 mM calcium acetate/120 mM calcium nitrate) using 10 mL liquid in 15 mL Hungate tubes. The tubes were flushed with argon to generate anaerobic conditions. From the final positive dilution (10^{-9}) the culture solution was plated and the plates were incubated in closed jars filled with argon in presence of oxygen-scavenging catalyser Anaerogen (Oxoid) for a period of 2 weeks. A dominant colony type was picked and grown in the liquid medium at denitrifying conditions. Culture purity was confirmed microscopically and by 16S-rRNA gene sequencing.

2.5   Identification of the dominant bacteria

DGGE analysis (Schafer and Muyzer 2001) was performed to test whether the isolated pure culture represented a dominant phylotype of the denitrifying biomass in the sand column. Genomic DNA was extracted from the cell pellets and further purified using the UltraClean Soil DNA Extraction Kit (MoBio Laboratories, USA). For the DGGE analysis a 550 bp fragment of the 16S rRNA gene was amplified with primers 341f+GC/907r and for the identification of the pure culture, a nearly whole 16S rRNA gene fragment was amplified using general bacterial primers GM3/GM4 (Schafer and Muyzer 2001). The sequences were compared to sequences stored in GenBank using the BLAST algorithm.

2.6   Batch experiments

Using the isolated strain, growth experiments with different substrate concentrations were performed in 30 mL serum bottles filled with 20 mL medium under argon gas atmosphere. The medium contained different concentrations of both calcium acetate and calcium nitrate (table 2) but the ratio acetate:nitrate was always 1:1.5. During the experiments gas, crystal and biomass formation were daily inspected and samples were taken several times until the growth ceased to analyse biomass (OD590), nitrite (spectrophotometry), N_2O (gas chromatography) and pH. Nitrate was detected qualitatively using Merck nitrate test strips (Merckquant) in case when nitrite was absent.

3   Results

3.1   Comparison of MICP processes

Micro-organisms, which are known to induce carbonate precipitation, by either consuming inorganic carbon (i.e. autotrophy), by acting as a crystal nucleus or by actively binding co-precipitating cations, like calcium from solution (i.e. active precipitation similar to shells), require a continuous supply of dissolved inorganic carbon and calcium in solution. As simultaneous injection of slightly oversaturated solution of calcium and inorganic carbon would require enormous amounts of liquid volume to induce sufficient precipitation and as highly concentrated dissolved calcium and inorganic carbon in the subsurface would lead to immediate precipitation and limited injection distance, these processes are considered unsuitable to be used underground.

Due to the limited solubility of calcium and inorganic carbon, a MICP process is only suitable for soil reinforcement when both inorganic carbon and alkalinity are sufficiently produced in situ in presence of a high concentration of dissolved calcium. Respiratory chemoheterotrophic micro-organisms produce inorganic carbon as a result of their metabolism, in which organic carbon is oxidized and an available electron acceptor is reduced. Many compounds can serve as electron acceptor, including oxygen, nitrate or nitrite, sulphate, sulphite, sulfur and oxidised iron or manganese

Table 1 Qualitative comparison of the suitability for biogrouting of several theoretical heterotrophic conversions using calcium acetate as organic substrate and several electron acceptors compared with urea hydrolysis.

Conversion type	Catabolic reaction per mole CaCO₃	solubility	rate	yield	side products
Urea hydrolysis	$1CO(NH_2)_2 + 2H_2O + 1Ca(Cl)_2$ $\rightarrow 1CaCO_3 + 2NH_4Cl$	++	++	-	-
Aerobic oxidation	$1Ca(C_2H_3O_2)_2 + 4O_2$ $\rightarrow 1CaCO_3 + 3CO_2 + 3H_2O$	--	+	--	+
Nitrate reduction	$\frac{1}{2.6}Ca(C_2H_3O_2)_2 + \frac{1.6}{2.6}Ca(NO_3)_2$ $\rightarrow 1CaCO_3 + \frac{1.6}{2.6}N_2 + \frac{1.4}{2.6}CO_2$	+	+	+	+
Sulphate reduction	$\frac{1}{3}Ca(C_2H_3O_2)_2 + \frac{2}{3}CaSO_4$ $\rightarrow 1CaCO_3 + \frac{1}{3}CO_2 + \frac{1}{3}H_2O + \frac{2}{3}H_2S$	-	-	++	-

Table 1 shows the results of a theoretical evaluation of the suitability of three chemoheterotrophic processes with different electron acceptors (oxygen, nitrate and sulfate) and acetate as carbon source and electron donor in comparison with the urease process.

3.1.1 Solubility

Due to the low solubility of oxygen in water (less than 1 mM under ambient conditions) aerobic oxidation is considered unsuitable for ground improvement. Also sulfate is poorly soluble in combination with calcium (less than 15 mM). Ferric iron and oxidized manganese, two other possible electron acceptors omitted in this evaluation are also poorly soluble at neutral pH and therefore considered unsuitable for ground improvement. Substrates for denitrification, in this case calcium acetate and calcium nitrate are reasonably soluble (up to 500 mM), although less than the substrates used for the urea hydrolysis process. Some organic substrates, which can be oxidized by denitrifying organisms, are poorly soluble in combination with calcium, e.g. citrate, succinate and malate (Zabozlaev et al. 2007), and will be unsuitable for inducing MICP in situ.

3.1.2 Rate

The $CaCO_3$ precipitation rate for urea hydrolysis depends on the amount of micro-organisms and the specific urease activity per micro-organism. Reported values for maximum urease activity in soils, using Sporosarcina pasteurii in MICP experiments vary from 100 to 1200 mM $CaCO_3$ h^{-1} (Whiffin et al. 2007; Harkes et al. 2008). However the aerobic bacteria used for urea hydrolysis cannot grow in situ due to lack of oxygen, resulting in a decay of the precipitation rate in time. For the other processes the organisms can grow from the energy provided by the catabolic reaction. Therefore the precipitation rate might increase in time with increasing biomass concentration. Biomass growth rate depends on the amount of energy produced by the catabolic reaction, which is highest for aerobic oxidation and lowest for sulphate reduction (Heijnen 1999). In theory nitrate reduction can reach similar $CaCO_3$ precipitation rates as for urease as long as there is sufficient biomass.

3.1.3 $CaCO_3$ yield

The $CaCO_3$ yield of the catabolic reactions presented in table 1 is not so different for urea hydrolysis (1.7 gram substrate (S) per gram $CaCO_3$ (P)), nitrate reduction (1.6 g-S/g-P) and sulphate reduction (1.4 g-S/g-P). Aerobic respiration has a lower yield due to the lack of produced alkalinity. The biomass yield is higher when the catabolic reaction generates more energy. As a result urea hydrolysis (and aerobic respiration) are expected to produce more biomass and hence less $CaCO_3$ than nitrate and sulphate reduction when biomass grows at maximum rate (Heijnen, 1999). On the other hand, when the biomass growth rate (and hence also the $CaCO_3$ precipitation rate) is limited the $CaCO_3$ yield will increase towards the catabolic yield. In general, more reduced compounds provide higher growth yield on a carbon base and produce less inorganic carbon. More oxidized compounds, like oxalate, acetate or formate, will therefore give relatively higher amounts of $CaCO_3$ then more reduced compounds, like glucose. For all processes holds

when both substrates are provided as calcium salts the yield of $CaCO_3$ is higher compared to other organic substrates, like glucose, which produce less alkalinity.

3.1.4 Side products

While for urea hydrolysis the produced ammonium chloride needs to be removed from the underground, the side products of denitrification, nitrogen gas and CO_2, seem harmless (if no intermediate compounds, like nitrite or nitrous oxide accumulate) and removal of the liquid or treatment of these side products is not required.

Based on this theoretical evaluation of MICP processes, nitrate reduction seems have potential for ground reinforcement

3.2 Batch experiments

It was relatively easy to obtain an enrichment culture at high calcium content in the medium, despite that the inoculum came from an ordinary garden soil, that was not subjected to high salt or calcium conditions. Batch incubation experiments on both the enrichment and the isolated bacterium showed $CaCO_3$ precipitation (Figure 1), gas formation and microbial growth on nitrate and acetate, within several days and up to a calcium concentration of 200 mM. The pH remained within the range 6-8, but decreased with increasing substrate concentration. At the high nitrate concentrations accumulation of nitrite and N_2O was observed (Table 2).
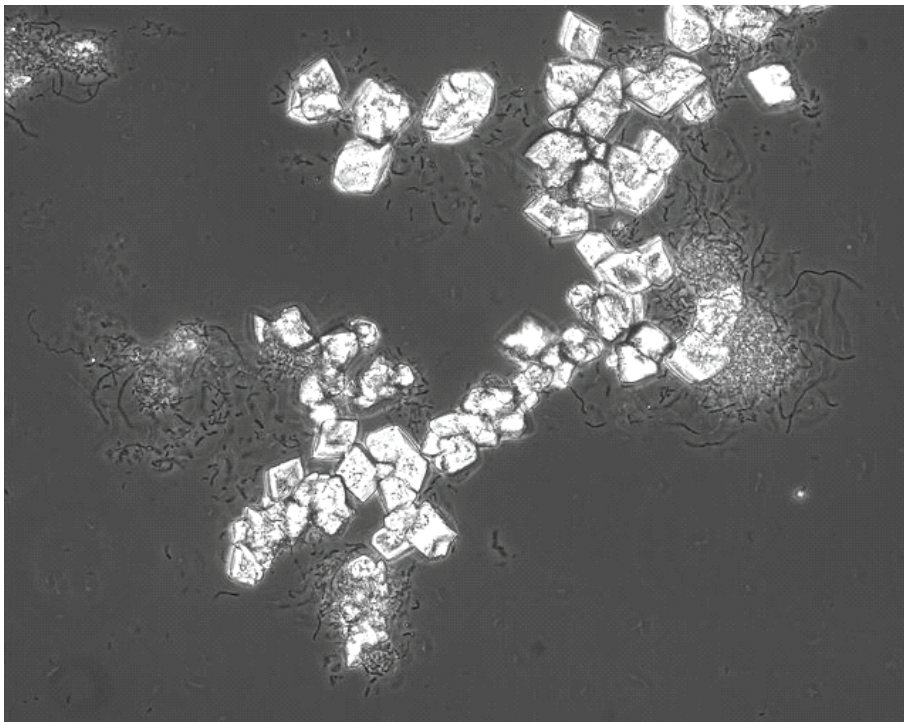
Figure 1 Microscope image (400× magnification) of a liquid enrichment culture with 50 mM calcium acetate and 60 mM calcium nitrate, showing simultaneously growing bacteria and calcium carbonate crystals after 1 week of incubation.

Table 2 Results of batch experiments inoculated with isolated bacteria, Castellaniella denitrificans, after 7 days of incubation at 30ºC.

Medium concentrations			CaCO$_3$ Precipitate	Growth OD590	pH	Gas	NO$_2^-$ mM	N$_2$O	
Ca, mM	Acetate, mM	NO$_3^-$, mM						% gas phase	mM N*
20	16	24	+	0.171	7.14	+	0	0.23	0.2
50	40	60	++	0.174	6.83	+	5.8	1.10	1.1
100	80	120	+++	0.640	6.70	++	22.0	8.02	7.2
200	160	240	+++	0.740	6.35	++	85.0	9.50	8.48

* assuming 1/3 in liquid, 2/3 in the gas phase (k=0.44)

Microscopic analysis of the sand column effluent showed that one bacterial morphotype was dominating. PCR-DGGE on the 16S-RNA genes of both the isolate and the enrichment showed that the dominant organism in the enrichment was the same as the isolated organism. Sequencing of the 16S-RNA gene identified the organism as *Castellaniella denitrificans* (100% similarity), a gram-negative, facultatively anaerobic organism (Kampfer et al. 2006) isolated and enriched under denitrifying conditions from waste water treatment plants in Germany (Denger et al. 1997) and Korea (Baek et al. 2003). Closely related organisms were found in soils, which contained high concentrations of nitrate (>130 mM) and were biostimulated by injection of a biodegradable electron-donor, ethanol (Spain et al. 2007).

Microscopic analysis of the colonies of isolates on agar plates showed that within the colonies single calcite crystals had grown op to a size of 100 to 200 μm, indicating a reaction rate controlled crystal growth.

3.3 Sand column experiment

During 100 days in which the sand column was flushed with a total of 25 L substrate solutions divided in 13 batches containing 25, 50 or 100 mM calcium acetate and 30, 60 or 120 mM calcium nitrate, an estimated amount of 300 g CaCO$_3$ was formed. During the first 10 days, in which a solution of 100 mM calcium acetate was flushed through continuously from top to bottom, the amount of conversion increased until a steady state was reached at which according to the EC measurements 25% of the substrate was consumed within the residence time in the column (Figure 2).

After 15 days of flushing a new batch of 2 L containing 100 mM calcium acetate and 120 mM calcium nitrate was recycled and consumed within 6 days (35 mmol calcium acetate per day). The next 7 flushes were consumed at a similar rate. In the effluent, both crystals and bacterial cells were observed. During the 8th and 9th flush, which started at days 62 and 74, the conversion rate was lower (20 mmol calcium acetate per day).
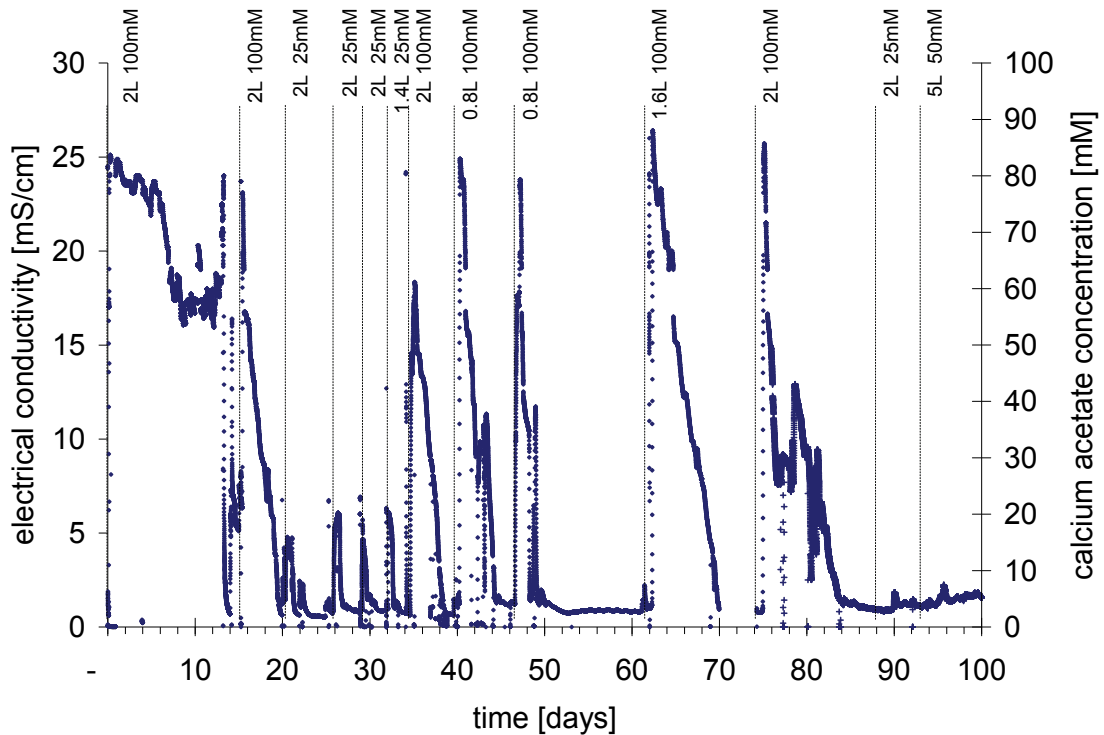
Figure 2 Measured electrical conductivity (EC) of the effluent of a sand column which was flushed during 100 days with 13 solutions containing 25, 50 or 100 mM calcium acetate and 30, 60 or 120 mM calcium nitrate. The dashed lines indicate the start of a new solution with its volume and concentration calcium acetate. The first and the last solution were flushed without recycling, while for the others the effluent was collected and recycled as influent. EC correlates well with the amount of conversion and is in this case a measure of calcium acetate concentration.
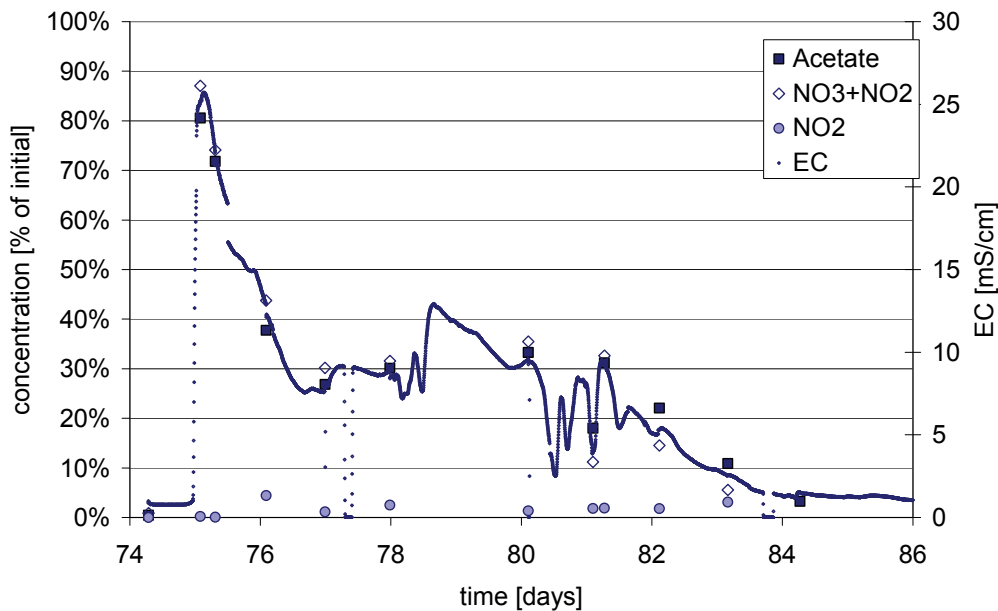
Figure 3 Detail of Figure 2 showing the measurements during a flush of 2 L containing 100 mM calcium acetate and 120 mM calcium nitrate, which was started after 74 days. Measured nitrate, nitrite and acetate concentration are normalized as a percentage of initial acetate or nitrate concentration and correlate well with the electrical conductivity of the effluent. EC correlates well with the normalized substrate concentrations. Nitrite does not accumulate.

The measured electrical conductivity correlated well with the total nitrogen and acetate concentrations (Figure 3). Although the substrate concentration in the effluent had a continuously decreasing trend, the conductivity pattern showed that the concentration fluctuated significantly. These fluctuations were partly attributed to the recycling of the medium: when the depleted media were replaced by fresh medium the influent was initially diluted by the depleted effluent from the column. However, also an irregular flow pattern might have caused concentration fluctuations. For example, during a 7 day period of the final flush (Figure 4), starting at day 92, the average flow rate slowly decreased from 0.5 to 0.25 kg day^{-1} as a result of the gradual decrease in permeability by a combination of entrapped biomass, gas bubble formation and crystal formation.
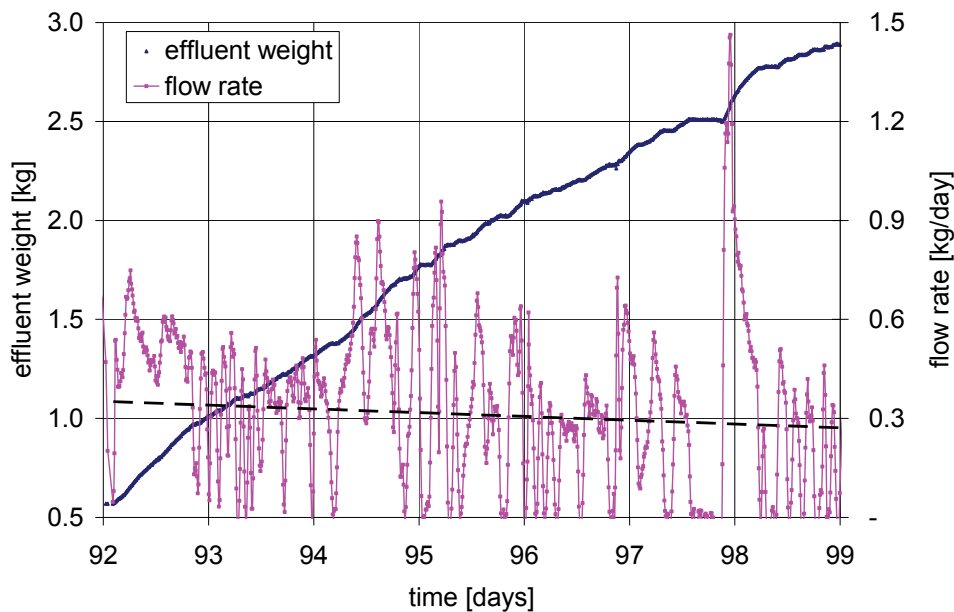
Figure 4 Effluent weight and flow rate during the final flush of 1.8 L solution of 50 mM calcium acetate and 60 mM calcium nitrate, which was flushed continuously from top to bottom at constant head difference between inlet and outlet of approximately 1 m. Although the head difference between inlet and outlet is nearly constant the flow rate is very irregular due to the formation of gas bubbles. The gas bubbles which tend to flow upwards are blocking the fluid flow downwards. Once zones of gas or liquid get connected sudden rapid flows occur. Some of the gas is dragged downwards along with the fluid. Once the gas reaches the outlet the measured fluid flow rate drops to zero.

However, the actual flow rate was highly fluctuating from 0 to 1.4 kg day^{-1}. The irregular flow rate is expected to be a result of the gas production. In periods when the flow rate dropped to zero the gas was observed as being pushed out of the sand column. Near the inlet, gas bubbles were observed, which were agglomerating in the pores. When the agglomerated bubbles formed a network, sudden upward gas bursts were observed, counteracted by a downward fluid flow which filled up the pores again. Apart from causing an irregular flow pattern, these counteracting flows caused sand grains in the upper 10 cm to regularly fluidize and cracks appeared in the sand column in the upper 50 cm.

The final 5 L were not recycled as the effluent did not show significant substrate concentrations. Apparently all substrate was consumed within the hydraulic residence time of the solution.

If all 300 g of $CaCO_3$ which was formed would have precipitated within the column this would correspond to 100 kg $CaCO_3$ m^{-3} soil (6%). The measured $CaCO_3$ content decreased from 10 % of the soil dry weight (155 kg $CaCO_3$ m^{-3} soil) at the top to less than 1% at the bottom (Figure 5).
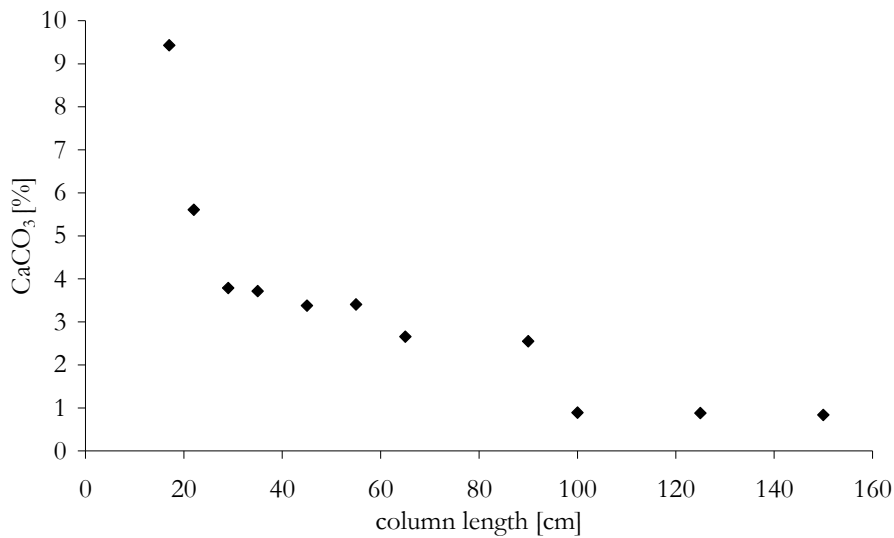
Figure 5 The $CaCO_3$ content in the sand column decreases with distance from the inlet from 9.4% (155 kg m^{-3}) to less than 1% (15 kg m^{-3}).

Using the empirical relationship between $CaCO_3$ content and unconfined compressive strength (UCS) (Van Paassen et al. 2009) the theoretical UCS in the top sections is estimated from the $CaCO_3$ content at 250-500 kPa, neglecting the cracks due to gas formation.
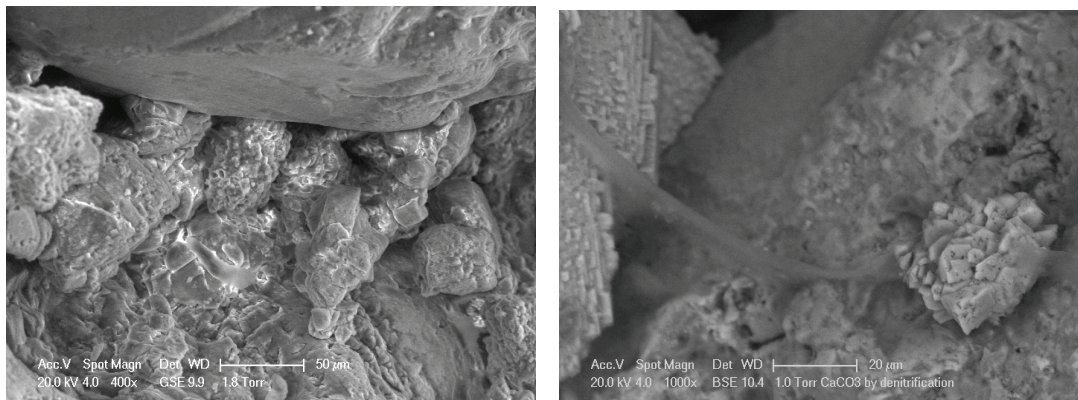
Figure 6 ESEM images from a sample taken from the top part of the sand column, containing 55 kg $CaCO_3$ m^{-3} soil. The left image shows $CaCO_3$ crystals (bottom) precipitated on the surface of a sand grain (top) and filling the pore throats. The right image shows an agglomerate of $CaCO_3$ crystals (right). Black spots on the crystal faces are traces of where bacteria have been encapsulated in the crystal. Some slime threads (left), are another product of bioconversion: extracellular polymeric substance.

Environmental scanning electron microscope analysis of the top part of the column showed that agglomerated calcite crystals filled up the pore throats between the sand grains (Figure 6). On the surface of the crystals, black spots were observed likely to be imprints of encapsulated bacteria. Also slime connected to the crystals and the sand grain surfaces was observed, likely to be some extracellular polysaccharide, a general product associated with microbial growth on surfaces (Wingender et al. 1999).

4 Discussion

Based on the solubility of its potential substrates and lack of side products, nitrate reduction seems the best alternative for urea hydrolysis as MICP process for ground improvement. Although the induced precipitation rate by nitrate reduction might be lower than by urea hydrolysis, it is more stable for denitrification. As the denitrifying organisms gain energy from the catabolic reaction while producing $CaCO_3$, they are able to maintain or increase the in situ precipitation rate over a long time period. Although the performed experiments proved that denitrification is a potential MICP process for ground reinforcement, the results indentified several discrepancies.

Firstly, while the solubility of calcium, fatty acids and nitrate should allow the use of substrate concentrations up to 1 M, experiments have only shown microbial growth, gas and crystal formation at calcium concentrations of up to 200 mM (80 mM calcium acetate and 120 mM calcium nitrate). At calcium concentrations above 100 mM it was found that nitrite and nitrous oxide accumulated. Nitrite (NO_2^-) and nitrous oxide (N_2O) are intermediates in the denitrification process and can accumulate when denitrification takes place under suboptimal conditions. There are four different enzymes involved in the denitrification process. As each enzyme has a different localization, life time, regulatory mechanism, kinetics and sensitivity to inhibitory factors, it might be expected that by such factors as nitrate or calcium overloading inhibition of one of the reduction steps would occur, leading to incomplete denitrification and accumulation of intermediates. Accumulation of intermediates as nitrite and nitrous oxide is undesired as it can be of environmental concern and their toxicity can reduce conversion rates (Glass and Silverstein 1998) and thereby lower $CaCO_3$ precipitation. At similar calcium concentrations, less nitrite accumulated in the sand column experiment than in the batch experiments (e.g. nitrite concentration in Figure 3 is maximum approximately 5% of 240 mM = 12 mM (day 76) and decreasing after that). Possibly, less intermediates were formed in the column due to a lower acetate:nitrate ratio in the feed. Another explanation could be an increased conversion rate by accumulation of biomass attached the large granular surface as observed in particle-based biofilm reactors (Nicolella et al. 2000). Finally, the difference in nitrite and NO_2 accumulation may also be explained by a fundamental difference in how the substrate concentrations change during the process. In batch incubations the substrate concentrations change in time, and all bacteria present in the incubation face the whole range of substrate concentrations. In the sand column the concentration gradients are spatial, and can be expected to be relatively stable in time. These spatial gradients exist at pore scale due to the irregular network of pores, filled with stagnant or flowing gas and liquid and with a heterogeneous distributed microbial activity. As a result substrates and products are badly mixed and transport limited by convection

or diffusion towards the reactive sites. Also over the length of the column gradients exist: different segments in the column will only 'see' a small range of substrate concentrations, and may be expected to optimize its performance within this range, with specific affinities and functional groups per segment, where the segment length is determined by the fall of substrate concentration. Heterogeneous systems such as a sand column, are generally characterized by lower conversion rates due to limiting substrate concentrations, but on the other hand also show lower product inhibition and often have a higher functional stability than a homogenous well mixed liquid culture (Fernandez et al. 2000).

Although the concentration of nitrite in the outlet of the sand column was significantly lower than in the batch experiments, it can still negatively affect the potential of denitrification for soil reinforcement. Firstly, the concentration is well above the maximum contaminant limit for potable water established by e.g. the EU Water Framework Directive. Secondly, at slightly acidic pH, concentrations higher than 10 mM nitrite inhibit denitrification (Almeida et al. 1995; Glass et al. 1997; Glass and Silverstein, 1998).

The observed conversion rate corresponds to 440 mmol of $CaCO_3$ formed within 10 days in a pore volume of approximately 1 L. Assuming the main part of the conversions taking place in the sand column, this would lead to a precipitation rate of 4.5 g $CaCO_3$ L^{-1} day^{-1} or 1.5 kg $CaCO_3$ m^{-3} soil day^{-1}). At this rate approximately 60 days are needed to reach a target amount of 100 kg $CaCO_3$ m^{-3} soil. These observed maximum conversion rate and extrapolated treatment time are still far from their desired values, but this may be improved by e.g. enrichment of (more suitable) denitrifying micro-organisms before using them as inoculum, by optimizing the substrate composition or by injection at high density denitrifying cultures together with the substrate in a mode analogous to the urea-based MICP.

Since the goal of this study was to show the potential of denitrification as a MICP for ground reinforcement, not much effort was put in optimizing the process. It was clearly shown in this study that different media compositions and process conditions had effect on the conversion rates as well as on the production of toxic intermediates. It is expected that in the optimization stage it will be possible to isolate denitrifiers that can stand higher substrate concentrations as well as to create the conditions under which no or very limited amounts of toxic intermediates are produced.

Although $CaCO_3$ was found all over the column, the amount of $CaCO_3$ in the column was much lower than the total converted amount. The low and decreasing $CaCO_3$ content with distance from the inlet might have several explanations. Firstly, the fresh influent did not contain nitrite or any other toxic compounds, that limits the conversion rate. Therefore the top of the column was likely not subjected to high nitrite levels. Further down the column these inhibiting compounds might already have accumulated due to conversion at the top. Secondly, especially at the end of treatment the flow rate dropped, acetate and nitrate were depleted before reaching the end of the column, leaving less precipitate for that part of the column. In practice, when operating at constant flow rate (with increasing pressure), this effect might be limited. Also the observation of crystals in the effluent, which had been flushed out when they were still to small to get stuck in the pores, might explain part of the disappearance of $CaCO_3$. The bacteria observed in the effluent, might also have caused precipitation taking place in the effluent tubes or storage vessels. Finally, the inlet might be slowly clogging by trapping

fine particles –crystals and bacteria- coming from the recycled fluids, indicating that not all the calcium carbonate that had been measured in the top of the column was actually produced in there.

Several experimental results are supporting the feasibility of using denitrification as MICP for ground reinforcement: 1) The permeability remained high enough to allow flow at low pressure injection, even though the flow rate was irregular as nitrogen gas bubbles periodically blocked the liquid flow downwards, 2) The gas bubbles having the tendency of travelling upward and agglomerate to form cracks, did not affect the stability of the sand bed 0.5 m below the top of the sand surface, which corresponds to an overburden pressure of 5 kPa. Due to the horizontal confinement of the sand in the column, vertical cracks to release gas pressure. As in practical applications overburden pressures are often higher than 5 kPa and horizontal deformations are likely to occur, negative effects of gas formation on soil stability are expected to be minimal. 3) The process could be started using garden soil or sludge from a waste water treatment as an inoculum without requiring a specific organism. 4) Separate cultivation and injection of bacteria as performed for the urease process (Whiffin et al. 2007) was not required as bacteria grew in situ on the substrate they also used for inducing calcium carbonate precipitation. And 5) No or low need for removal of side products, which simplifies practical application significantly.

The process costs and environmental impact can be further reduced by obtaining both substrates (calcium nitrate and calcium acetate) through conversion of waste streams. Calcium nitrate can be produced by biological nitrification of ammonium in the presence of calcium carbonate, whereas calcium acetate can be produced through biological acetogenesis: short anaerobic biological treatment of organic matter (also in the presence of calcium carbonate). Both the ammonium and the organic matter which are required for these processes can be obtained from amply available waste streams, i.e. from food industry, tanneries or agriculture or when the denitrification process is used in combination with the urea based MICP process.

5 Conclusions

The potential of denitrification for inducing carbonate precipitation for ground reinforcement applications has been proven by theoretical evaluation with alternative processes and experimental results. In this process organic compounds, like acetate, can be oxidized to produce carbonate ions and alkalinity, which are required for the precipitation of calcite, while nitrate is reduced to nitrogen gas. Using calcium salts of both the electron donor and acceptor results in a high $CaCO_3$ yield. Calcium salts of nitrate and acetate are soluble up to 1M, enabling injection of highly concentrated substrate solutions. The occurrence of inhibitive intermediates (nitrite and nitrous oxide) at high concentrations and the heterogeneous distribution of calcium carbonate in the sand column still negatively affect the potential of denitrification as soil reinforcement method and require further study. As the rate of calcium carbonate formation by denitrification is still far lower than for the urease process, it requires further optimization for practical applications.

References

Almeida JS, Julio SM, Reis MAM & Carrondo MJT, 1995. Nitrite Inhibition of Denitrification by Pseudomonas-Fluorescens. *Biotechnology and Bioengineering* 46(3):194-201.

Baek SH, Kim K-H, Yin C-R, Jeon CO, Im W-T, Kim K-K & Lee S-T. 2003. Isolation and Characterization of Bacteria Capable of Degrading Phenol and Reducing Nitrate Under Low-Oxygen Conditions. *Current Microbiology* 47(6):462-466.

Castanier S, Le Metayer-Levrel G, Perthuisot J-P. 1999. Ca-carbonates precipitation and limestone genesis -- the microbiogeologist point of view. *Sedimentary Geology* 126(1-4):9.

Comoss EJ, Kelly DA, Leslie HZ. 2002. Innovative erosion control involving the beneficial use of dredge material, indigenous vegetation and landscaping along the Lake Erie Shoreline. *Ecological Engineering* 19(3):203-210.

DeJong JT, Fritzges MB, Nusslein K. 2006. Microbially Induced Cementation to Control Sand Response to Undrained Shear. *Journal of Geotechnical and Geoenvironmental Engineering* 132(11):1381-1392.

Denger K, Laue H & Cook AM. 1997. Anaerobic taurine oxidation: a novel reaction by a nitrate-reducing Alcaligenes sp. *Microbiology* 143(6):1919-1924.

Fan C-C & Su C-F. 2008. Role of roots in the shear strength of root-reinforced soils with high moisture content. *Ecological Engineering* 33(2):157-166.

Fernandez AS, Hashsham SA, Dollhopf SL, Raskin L, Glagoleva O, Dazzo FB, Hickey RF, Criddle CS & Tiedje JM. 2000. Flexible Community Structure Correlates with Stable Community Function in Methanogenic Bioreactor Communities Perturbed by Glucose. *Applied and Environmental Microbiology* 66(9):4058-4067.

Glass C & Silverstein J. 1998. Denitrification kinetics of high nitrate concentration water: pH effect on inhibition and nitrite accumulation. *Water Research* 32(3):831-839.

Glass C, Silverstein J & Oh J. 1997. Inhibition of denitrification in activated sludge by nitrite. *Water Environment Research* 69(6):1086-1093.

Harkes MP, Booster JL, Van Paassen LA, Van Loosdrecht MCM & Whiffin VS. 2008. Microbial induced carbonate precipitation as ground improvement method – bacterial fixation and empirical correlation CaCO3 vs strength. *International conference on BioGeoCivil Engineering*, Delft.

Heijnen JJ 1999. Bioenergetics of microbial growth. In: Flickinger MC, Drew SW, editors. *Encyclopedia of bioprocess technology: fermentation, biocatalysis and bioseparation*: John Wiley & Sons, Inc. p 267-291.

Ivanov V & Chu J 2008. Applications of microorganisms to geotechnical engineering for bioclogging and biocementation of soil in situ. *Reviews in Environmental Science and Biotechnology* 7(2):139-153.

Jones K & Hanna E 2004. Design and implementation of an ecological engineering approach to coastal restoration at Loyola Beach, Kleberg County, Texas. *Ecological Engineering* 22(4-5):249-261.

Kampfer P, Denger K, Cook AM, Lee ST, Jackel U, Denner EBM & Busse HJ. 2006. Castellaniella gen. nov., to accommodate the phylogenetic lineage of Alcaligenes defragrans, and proposal of Castellaniella defragrans gen. nov., comb. nov. and Castellaniella denitrificans sp. nov. *International Journal of Systematic and Evolutionary Microbiology* 56(4):815-819.

Nemati M & Voordouw G. 2003. Modification of porous media permeability, using calcium carbonate produced enzymatically in situ. *Enzyme and Microbial Technology* 33(5):635-642.

Nicolella C, Van Loosdrecht MCM & Heijnen JJ. 2000. Particle-based biofilm reactor technology. *Trends in Biotechnology* 18(7):312-320.

Normaniza O, Faisal HA & Barakbah SS. 2008. Engineering properties of Leucaena leucocephala for prevention of slope failure. *Ecological Engineering* 32(3):215-221.

Overmann J, Fischer U & Pfennig N. 1992. A new purple sulfur bacterium from saline littoral sediments, Thiorhodovibrio winogradskyi gen. nov. and sp. nov. *Archives of Microbiology* 157(4):329-335.

Schafer H & Muyzer G. 2001. Denaturing gradient gel electrophoresis in marine microbial ecology. *Methods in Microbiology*, Vol 30. p 425-468.

Spain AM, Peacock AD, Istok JD, Elshahed MS, Najar FZ, Roe BA, White DC & Krumholz LR. 2007. Identification and Isolation of a Castellaniella Species Important during Biostimulation of an Acidic Nitrate- and Uranium-Contaminated Aquifer. *Applied and Environmental Microbiology* 73(15):4892-4904.

Whiffin VS. 2004. *Microbial CaCO3 Precipitation for the production of Biocement* [Ph.D thesis]. Perth, Western Australia: Murdoch University. 154 p.

Whiffin VS, van Paassen LA & Harkes MP. 2007. Microbial Carbonate Precipitation as a Soil Improvement Technique. *Geomicrobiology Journal* 24(5):417-423.

Wingender J, Neu TR & Flemming H-C. 1999. What are bacterial extracellular polymeric substances? In: Wingender J, Neu TR, Flemming H-C, editors. *Microbial Extracellular Polymeric Substances: Characterization, Structure, and Function*: Springer. p 1-15.

Zabozlaev A, Oganesyan É & Pogorelov V. 2007. Solubilization of poorly soluble calcium salts of organic acids with sorbitol. *Pharmaceutical Chemistry Journal* 41(8):430-433.

Summary

The mechanical properties of soils often do not satisfy human demand or expectation. Preventing damage to buildings and infrastructure requires either serious constructive measures or continuous maintenance. Grouting has been used as a ground improvement method in many applications in civil and mining engineering, often as a method to locally stabilize the ground, before, concordant or after construction. Most grouting methods are based on mixing or injecting grout - a mixture of cement, lime or other chemicals with water or air - into the ground. As grout hardens in time, the strength and stiffness of the soil increase. Due to the technical limitations, costs and environmental impact, these methods are often unfeasible for large-scale treatment.

In this study, an alternative ground improvement method based on biologically formed grout –"Biogrout"- is investigated. When supplied with suitable substrates, micro-organisms can catalyze biochemical conversions in the subsurface resulting in precipitation (or dissolution) of inorganic minerals, which change the mechanical soil properties. This study focuses on one of these biochemical conversions: microbially catalyzed hydrolysis of urea, inducing calcium carbonate precipitation in sand.

This Biogrout process comprises the following steps:
1) *Sporosarcina pasteurii*, a bacterial species containing a large amount of the enzyme urease, are cultivated in suspension.
2) The suspension containing the bacteria is injected in the ground and supplied with a solution containing urea and calcium chloride.
3) The urease catalyzes the conversion of urea into ammonium and carbonate and the produced carbonate precipitates with calcium as calcium carbonate crystals. These crystals form bonds between the sand grains increasing the strength and stiffness of the sand.
4) The remaining ammonium chloride is extracted and disposed.

The goal of this study was to develop this process from laboratory experiments to a field scale application, to identify its limitations, and to provide the engineering tools, which are required to design treatment procedures. The engineering tools correlate the operational process variables, like flow rate, pumping time and volume, amount of reagents and bacteria, and injection (and extraction) strategy, to the required process results, such as the engineering parameters strength, stiffness, permeability, porosity and eventually also costs.

The following criteria are considered essential to develop a Biogrout process:
1) The required treatment time and required volume of liquids to be injected (and extracted) must be low, which implies high concentrations of urea and calcium chloride (in the order of moles per liter) and high conversion rates (in the order of moles $CaCO_3$ per liter per day).

2) The injection distance must be high at low injection pressure, which implies that permeability should be maintained, in order to enable multiple treatments and limit the number of required injection wells.
3) The environmental impact and costs must be low;
4) The resulting strength (and stiffness) must be predictable, controllable reproducible and homogeneous.

Process characteristics

In chapter 2 the factors affecting the Biogrout process are evaluated under the intended conditions for field applications (i.e. high conversion rates and high concentrations). The evaluation shows that the initial hydrolysis rate mainly depends on the amount of bacteria and their cultivation and storage conditions. The hydrolysis rate is affected by environmental conditions such as concentration of urea and calcium, temperature and pH, and during the process the hydrolysis rate decreases in time due to cell degradation, encapsulation of bacteria in crystals and/or flush out of bacterial cells. In experiments in which the urea hydrolysis rate was known, the changes in concentrations of the main components (urea, calcium, ammonium and calcium carbonate) could be reasonably monitored by electrical conductivity and reasonably predicted, using a simplified model. More complex models, which include acid-base equilibria and precipitation kinetics, did not predict the concentrations of the main compounds significantly better, but enabled calculation of supersaturation, pH, and the number, size and type of crystals. However, quantitative prediction to a level at which the pH, conductivity and crystal properties are simulated accurately was not yet possible with the developed models.

During the experiments, a wide variety of $CaCO_3$ crystal properties was observed, which is described in chapter 3. The crystal properties (number, size, shape, mineral type and location) were affected by the hydrolysis rate, and the presence and type of nucleation sites (e.g. bacteria or sand grains). At high hydrolysis rates in absence of nucleation sites spherically shaped vaterite crystals were formed (a metastable mineral type of $CaCO_3$), while at low hydrolysis rates or in presence of nucleation sites rhomboidal calcite was dominant. Also layered composite mineral structures were observed, with the least stable mineral phase on the inside and most stable form (calcite) on the outside. The occurrence of metastable mineral precursors and its effect on the engineering behavior are considered limited.

When bacteria, urea and calcium chloride are mixed before injecting them in the ground the Biogrout process would immediately start, resulting in flocculated bacteria and crystals clogging the pores close to the injection well and limiting the injection distance, especially in fine sands. In chapter 4 a method is described in which bacteria and reagents are flushed sequentially through the soil in order to achieve a more efficient use and homogeneous distribution of the bacteria and the resulting precipitation rate over a long distance.

Experimental scale up

After several small sand column experiments the procedure was applied in a five-meter sand column experiment, which is described in chapter 5. This experiment provided the first evidence that significant strength increase could be achieved at low injection pressure, within 6 days of treatment and 5 flushed pore volumes (including placement of bacteria and removing the remaining ammonium chloride), at a long distance and without reducing the permeability significantly.

Further scale up experiments are described in chapter 6, in which equipment, conditions and techniques are used, which are also used in potential applications. First, experiments were performed in a 1 m^3 container set-up simulating a spherical injection from a single point, followed by a 100 m^3 field scale experiment. In this final experiment 40 m^3 of sand was biologically cemented within 12 days and 6 pore volumes, stretching over a length of 5 m between three injection and three extraction points. Although in both scale up experiments significant increase of the average strength was obtained, but distinct spatial variability of the mechanical properties was observed. The heterogeneity is considered to be affected by the induced flow field, the distribution of bacteria, the procedure of supplying reagents (continuous flow or sequential batches) and the crystallization process.

Geotechnical design parameters

Using the measurements of these scale-up experiments, empirical correlations were established which are described in chapter 7. Strength and stiffness correlated well with $CaCO_3$ content, but better with the dry density after treatment due to variations in the initial density. The geotechnical parameters (cohesion, friction angle, and parameters describing the deformation behavior), which are required to design treatment procedures for several emphasized applications were determined for a wide range of initial densities and $CaCO_3$ contents.

Applications

Using the results described in chapter 6 and 7, the feasibility of a typical application was determined in chapter 8: increasing the stiffness of railroad embankments in order to mitigate the continuous maintenance, which is required to counteract the compaction due to dynamic loading of passing trains, and increase the allowable train speed. The risk of compaction increases with increasing train velocity. It was predicted that the obtained increase in stiffness in the field scale experiment will increase the allowable train speed by 20%.

Another potential application is presented in chapter 9: using Biogrout for the in-situ reinforcement of calcarenite room and pillar mines. The investigation showed that Biogrout can be used to increase the strength in lightly cemented porous rocks, which reduces the risk of mine collapse.

Alternative process

Remaining issues in the Biogrout process based on urea hydrolysis include the required removal of ammonium chloride and the use of axenically cultivated aerobic organisms with consequent decaying urease activity in time due to a lack of oxygen in the subsurface. To avoid both these issues the suitability of other possible MICP processes for ground improvement is evaluated in chapter 10. The feasibility of the best alternative, in which calcium acetate (or other calcium salts of fatty acids) and calcium nitrate are converted to induce calcium carbonate precipitation is shown experimentally.

Samenvatting

De mechanische eigenschappen van grond voldoen vaak niet aan de wensen of verwachtingen van de gebruiker. Het beperken van schade aan gebouwen en infrastructuur vereist vaak serieuze constructieve maatregelen of continu onderhoud. Grouting is een grondverbeteringsmethode, die veel wordt gebruikt voor civiel technische en mijnbouwkundige toepassingen, om grond te stabiliseren voor, tijdens of na de bouw. Traditionele groutingtechnieken zijn gebaseerd op het mengen of injecteren van grout - een mengsel van cement of andere chemicaliën met water of lucht - in de bodem. Terwijl de grout uithardt nemen de sterkte en stijfheid van de grond toe. Wegens technische beperkingen, hoge kosten en impact op het milieu zijn deze methoden vaak ongeschikt om op grote schaal te worden toegepast.

In dit proefschrift wordt een alternatieve grondverbeteringsmethode beschreven op basis van biologisch gevormde grout: Biogrout. Voorzien van de juiste voeding kunnen micro-organismen in de bodem biochemische reacties katalyseren, waarbij anorganische mineralen neerslaan en de mechanische eigenschappen van grond worden verbeterd. De focus van dit proefschrift ligt bij de biologisch gekatalyseerde hydrolyse van ureum, wat leidt tot de precipitatie van calciumcarbonaat (kalk) in zand.

Dit Biogrout proces bestaat uit 4 stappen:
1) *Sporosarcina pasteurii*, een bacterie die een grote hoeveelheid van het enzym urease bevat wordt in suspensie gekweekt.
2) De suspensie met bacteriën wordt in de bodem geïnjecteerd en voorzien van een oplossing met ureum en calciumchloride.
3) Urease katalyseert de omzetting van ureum naar ammonium en carbonaat, waarbij het carbonaat neerslaat als calciumcarbonaatkristallen. Deze kristallen vormen verbindingen tussen de korrels, waardoor de sterkte en stijfheid van het zand toenemen;
4) Het resterende ammoniumchloride wordt uit de bodem ontrokken en verwijderd.

Het doel van deze studie was om het Biogrout-proces te ontwikkelen van laboratorium experiment tot praktijk toepassing. Uitvoeringsprocedures moesten worden ontworpen om procesvariabelen, zoals debiet, hoeveelheid grondstoffen en bacteriën en injectieprotocol, te correleren aan de te verwachten grondeigenschappen, zoals sterkte, stijfheid, porositeit en permeabiliteit.

De volgende criteria zijn essentieel voor een succesvolle ontwikkeling van het Biogrout-proces:
1) De hoeveelheid te injecteren vloeistoffen en de uitvoeringstijd moeten beperkt blijven, wat betekent dat hoge concentraties van de grondstoffen (mol per liter) en hoge omzettingssnelheden (mol $CaCO_3$ per liter per dag) moeten worden gebruikt.

2) Een grote injectieafstand is gewenst bij een lage injectie druk en behoud van doorlatendheid, zodat meerdere behandelingen mogelijk zijn en het aantal injectie- (en extractiebronnen) kan worden beperkt;

3) Milieu-impact en kosten moeten beperkt blijven;

4) De resulterende sterkte (en stijfheid) moeten voorspelbaar, controleerbaar, reproduceerbaar en homogeen zijn.

Proces eigenschappen

In hoofdstuk 2 worden de factoren bepaald die het Biogrout proces beïnvloeden onder de veronderstelde condities voor praktijktoepassingen (hoge omzettingssnelheid en hoge concentraties). Hierbij werd aangetoond dat the initiële hydrolysesnelheid met name afhangt van de hoeveelheid bacteriën en de condities waarbij deze worden gekweekt en opgeslagen voor gebruik. De hydrolysesnelheid wordt verder beïnvloed door omgevingscondities, zoals de concentraties van ureum en calcium, temperatuur, en pH en gedurende het proces neemt de snelheid af doordat de bacteriën geleidelijk sterven, uitspoelen of ingekapseld worden in de kristallen. Wanneer de hydrolyse snelheid bekend is kan de verandering in concentraties van de belangrijkste componenten (ureum, calcium, ammonium en calciumcarbonaat) redelijk nauwkeurig worden gemeten met de elektrische geleidbaarheid en worden voorspeld met een relatief eenvoudig rekenmodel op basis van een enkele chemische reactievergelijking. Complexere rekenmodellen, die rekening houden met zuur-base-evenwichten en precipitatiekinetiek, leiden niet tot een significant nauwkeuriger voorspelling, maar maken het wel mogelijk andere proces parameters te berekenen, zoals de oververzadiging, pH en aantal, vorm en type kristallen. Nauwkeurige voorspellingen van pH, geleidbaarheid en kristaleigenschappen lijken met deze modellen echter nog niet mogelijk.

Tijdens verschillende experimenten is een scala aan kristaleigenschappen waargenomen, welke in hoofdstuk 3 worden beschreven. De kristaleigenschappen (aantal, grootte, vorm, mineraal type en locatie) zijn sterk afhankelijk van de hydrolysesnelheid en de aanwezigheid en type nucleatie-oppervlak (bijvoorbeeld zandkorrels of bacteriën). Bij hoge snelheid in afwezigheid van nucleatiekernen worden bolvormige vateriet kristallen gevormd (een metastabiel mineraal type van $CaCO_3$), terwijl bij lage snelheid of de aanwezigheid van veel kristaloppervlak (zoals in kalkzand of kalksteen) rhomboïdaal calciet dominant is. Ook zijn gelaagde composiet schilstructuren waargenomen, met het minst stabiele mineraal in het centrum en de meest stabiele vorm (calciet) aan de buitenkant. Het voorkomen van metastabiele mineralen in de praktijk en het effect ervan op de geotechnische eigenschappen worden beperkt verondersteld.

Wanneer bacteriën met ureum en calciumchloride worden gemengd, voordat zij in de bodem worden geïnjecteerd kunnen de poriën rondom een injectiebron verstopt raken doordat de bacteriën flocculeren en het kristallisatieproces direct begint. Hierdoor wordt de injectieafstand beperkt, voornamelijk in fijne zanden. In hoofdstuk 4 wordt een methode beschrijven waarbij de bacteriën en reagens sequentieel worden geïnjecteerd, met eventueel een fixatievloeistof er tussen in. Hierdoor is een efficiënter gebruik van de bacteriën mogelijk en wordt een homogenere verdeling van bacteriën en resulterende hoeveelheid $CaCO_3$ bereikt over grotere afstand.

Experimentele opschaling

Hoofdstuk 5 beschrijft een experiment waarin de ontwikkelde Biogrout-procedure is toegepast op een vijf meter lange zandkolom. Dit experiment leverde het eerste bewijs dat significante sterkte kan worden bereikt bij lage injectiedruk, binnen 6 dagen waarin de kolom in totaal 5 keer was doorspoeld (inclusief bacteriën, fixatievloeistof, reagents en naspoelen met water om de resterende amoniumchloride te verwijderen) over grote afstand (5 m), waarbij de doorlatendheid grotendeels behouden blijft.

In hoofdstuk 6 worden twee verdere opschalingsstappen beschreven, waarbij gebruik gemaakt is van condities en technieken, die ook bij potentiële toepassingen worden gebruikt. Eerst zijn experimenten uitgevoerd in een container van 1 m^3, waarin een bolvormige injectie vanuit één punt is gerealiseerd, gevolgd door een experiment op een schaal van 100 m^3. In dit laatste experiment werd 40 m^3 zand biologisch verstevigd binnen 12 dagen, waarin het zandlichaam 6 keer was doorspoeld over een afstand van 5 m tussen 3 injectie- en 3 extractiebronnen. In beide opschalingsexperimenten was de gemiddelde sterkte significant toegenomen, maar was de ruimtelijke variatie in mechanische eigenschappen erg groot. Deze heterogeniteit is toegeschreven aan het stromingsregime in het zandpakket, de verdeling van bacteriën, de manier van injecteren van de reagensoplossing (continu of in pulsen) en het kristallisatieproces.

Geotechnische ontwerpparameters

Met het materiaal uit de opschalingsexperimenten konden empirische correlaties worden opgesteld, die zijn beschreven in hoofdstuk 7. Sterkte en stijfheid correleren redelijk met het kalkgehalte, maar nog beter met de droge dichtheid na grondverbetering. Het verschil in correlatie werd veroorzaakt door variaties in de initiële droge dichtheid voor Biogrout-behandeling. De geotechnische parameters (cohesie, wrijvingshoek en eigenschappen die het vervormingsgedrag beschrijven), die nodig zijn voor het ontwerp van uitvoeringsprocedures zijn bepaald voor verschillende kalkgehaltes en initiële droge dichtheden.

Toepassingen

Met de resultaten uit hoofdstuk 6 en 7 is in hoofdstuk 8 de haalbaarheid bepaald van een typische toepassing van het Biogrout-proces: het verhogen van de stijfheid onder een spoorbaanlichaam. Hiermee kan het continue onderhoud worden verminderd, dat nodig is om de verzakking te compenseren die wordt veroorzaakt door de dynamische belasting van passerende treinen. Ook kunnen treinen met hogere snelheid op het traject worden toegelaten. Het kans op verzakkingen neemt namelijk toe bij toenemende treinsnelheid. Op basis van de aangetoonde stijfheid in het 100 m^3 experiment is voorspeld dat een toename van de maximaal toelaatbare treinsnelheid van 20% mogelijk is.

Een andere potentiële toepassing is beschreven in hoofdstuk 9: het verstevigen van zwakke pilaren in mergel (kalksteen) groeves. Experimenteel is aangetoond dat met Biogrout ook in poreuze, licht-gecementeerde, gesteenten de sterkte kan worden verdubbeld, waardoor het instortingsgevaar in de mergelgroeves kan worden verminderd.

Alternatief proces

De verwijdering van het ammoniumchloride, het gebruik van specifieke bacteriën die worden gekweekt onder speciale groeicondities, en de afname van de urease-activiteit in de tijd blijven nog aandachtspunten van het Biogrout-proces op basis van hydrolyse van ureum. Om deze aspecten te omzeilen is in hoofdstuk 10 een inventarisatie gedaan naar alternatieve microbiële conversies die leiden tot kalkneerslag. Het potentieel van het beste alternatief, waarbij calciumacetaat (of andere calciumzouten van vetzuren) en calciumnitraat worden omgezet naar calciumcarbonaat en stikstofgas is experimenteel aangetoond.

Acknowledgements

Curriculum Vitae

Leon Andreas van Paassen was born on January 28, 1976 in Rijswijk, The Netherlands. In 1994 he obtained his Gymnasium diploma at the Sint Stanislas College in Delft. Subsequently, he studied Applied Earth Sciences at Delft University of Technology. He graduated at the department of Engineering Geology in 2002 with a MSc thesis entitled 'The influence of pore fluid salinity on consolidation behaviour and undrained shear strength development of clayey soils'. During his study Leon worked as graduate-assistant for the courses 'Geological mapping and Geological constructions' (1996-1998) and 'Site Investigation' (1998-2000). He also worked in the kitchen of Kleyweg's Stadskoffyhuis, preparing salads, pancakes and Kleyweg's famous sandwiches 'Lekkerste broodje van Nederland' (1995-2000). Meanwhile, he was captain of the rugby team and treasurer for the rugby club SRC THOR. In 2001-2002 he worked as junior geotechnical engineer at IFCO Foundation Expertise BV, where he did projects on acoustic pile integrity testing, vibration monitoring and a damage investigation on a dike failure. After completing his MSc, Leon was appointed as geotechnical consultant at GeoDelft, now named Deltares, at the department of Foundations and Underground Constructions, where he advised on a variety of projects, including the design of dikes, foundations, sheetpiles, building pits and pipelines. In 2003-2007 he was treasurer for the Dutch Society of Engineering Geologist, Ingeokring. In 2004 he contributed to a research proposal on Biogrout, which was granted (2 M€). Subsequently, after supervising a geotechnical site investigation for a pipeline construction in the Caspian Sea, Kazakhstan, he started in 2005 as PhD-student within the Biogrout-project at the Department of Biotechnology at Delft University of Technology, while at the same time he kept a small position at Deltares. Three months of his PhD research he spent at Murdoch University, Perth, Australia. He contributed to several publications, patents and presentations, including the winning idea for the B-Basic Leo Petrus Innovation Trophy 2008 (100 k€): 'Sand to sandstone using waste as cement' and the prize-winning paper for the Young Member Award 2009 of the International Society for Soil Mechanics and Geo-Engineering. The research culminated in this thesis entitled 'Biogrout: ground improvement by microbially induced carbonate precipitation'. In 2008 he co-organised the first international conference on BioGeoCivil Engineering. After four years at the university he got back at Deltares, where he was responsible for part of the research program on Smartsoils®. Recently, he went back to his MSc-roots as he was appointed Assistant Professor in the section of Environmental Engineering Geology of Delft University of Technology. In 2005 Leon married Marja Bakker, with whom he got a daughter, Naima, in 2007 and is expecting another daughter in November 2009.

Publications

Journal contributions

Harkes, MP, Van Paassen LA, Booster, JL, Whiffin, VS & Van Loosdrecht, MCM, 2009. Fixation and distribution of bacterial activity in sand to induce carbonate precipitation for ground reinforcement, Ecological Engineering Published online, doi: 10.1016/j.ecoleng.2009.01.004.

Van Paassen, LA, Daza, CM, Staal, M, Sorokin, DY, Van der Zon, W. & Van Loosdrecht, MCM, 2009. Potential soil reinforcement by microbial denitrification, Ecological Engineering, published online, doi: 10.1016/j.ecoleng.2009.03.026.

Whiffin, VS, Paassen, LA van, Harkes, MP (2007). Microbial Carbonate Precipitation as a Soil Improvement Technique. Geomicrobiology Journal. 24 (5), 417 - 423.

Conference proceedings

Blauw, M, Harkes, M, Loosdrecht, MCM van, Paassen, LA van, Van, M.A. & Ruyt, M van der. (2008), Climate Change Resistant Coastline by biological In-situ reinforcement of Sand, In 11th Baltic Sea Geotechnical Conference, Geotechnics in Maritime Engineering, 15-18 september 2008, Gdansk, Poland, edited by Z. Mlynarek , Z. Sikora and E. Dembicki, ISBN 978-83-602610-7-1, Vol 2, pp 585-589.

Booster, JL, Meurs, GAM van, Pruiksma, JP, Van Paassen, LA, Harkes, MP & Whiffin, VS (2008). 1D-modelling of microbially induced calcite precipitation for geotechnical applications. In Henk Jonkers, Jacco Booster, Leon van Paassen & Mark van Loodrecht (Eds.), BGCE 2008, 1st International conference BioGeoCivil Engineering, 23-25 June 2008, The Netherlands (pp. 19-28). Delft: TU Delft en Deltares.

Ghose, R., Van Paassen, L.A., Van der Star, W.R.L., Van der Linden, T.J.M. & Van Zwieten, G.A. 2009. Monitoring progressive cementation of sand by biogrouting through time-lapse shearwave seismics. Near Surface 2009 – 15th European Meeting of Environmental and Engineering Geophysics, Dublin, Ireland.

Harkes, MP, Booster, JL, Van Paassen, LA, Van Loosdrecht, MCM & Whiffin, VS (2008). Microbial induced carbonate precipitation as ground improvement method - bacterial fixation and empirical correlation CaCO3 vs strength. In Henk Jonkers, Jacco Booster, Leon van Paassen & Mark van Loosdrecht (Eds.), BGCE 2008, 1st International conference BioGeoCivil Engineering, 23-25 June 2008, The Netherlands (pp. 37-44). Delft: TU Delft en Deltares.

Ngan-Tillard, D.J.M., Verwaal, W., Maurenbrecher, P.M. & Van Paassen, L.A. 2009. Microstructural degradation of Maastrichtian limestones. ISRM Regional conference EUROCK 2009 – Rock engineering in difficult ground conditions – Soft rocks and karst, Dubrovnik, Croatia

Staal, MJ, Van Paassen, LA, Brasser, HJ, Krijger, GC and Loosdrecht, MCM van. (2008). Can biological mediated silicate binding in biofilms be used for biogrouting?, In Henk Jonkers, Jacco Booster, Leon van Paassen & Mark van Loosdrecht (Eds.), BGCE 2008, 1st International conference BioGeoCivil Engineering, 23-25 June 2008, The Netherlands (pp. 124-133). Delft: TU Delft en Deltares.

Van der Star, W.R.L., Taher, E., Harkes, M.P., Van Loosdrecht, M.C.M. & Van Paassen, L.A. 2009. Use of waste streams and microbes for in situ transformation of sand into sandstone. International Symposium on Ground Improvement Technologies and Case Histories (ISGI2009), Singapore.

Van Paassen, LA, Harkes, MP, Van Zwieten, GA, Van der Zon, WH, Van der Star, WRL & Van Loosdrecht, MCM, 2009, Scale up of BioGrout: a biological ground reinforcement method, Proceedings of the 17th international conference on soil mechanics and geotechnical engineering, 5-9 october 2009, Alexandria, Egypt

Van Paassen, LA, Pieron, M, Mulder, A, Van der Linden TJM, Van Loosdrecht, MCM & Ngan-Tillard, DJM, 2009, Strength and deformation of biologically cemented sandstone, Proceedings of the ISRM Regional conference EUROCK 2009 – Rock engineering in difficult ground conditions – Soft rocks and karst, 29-31 October 2009, Dubrovnik, Croatia

Van Paassen, L.A. 2009. Microbes turning sand into sandstone, using waste as cement. Presented at 4th International Young Geotechnical Engineering Conference Alexandria, Egypt.

Van Paassen, LA, Isimite, J, Picioreanu, C & Loosdrecht, MCM van (2008). Computational model to study microbial carbonate precipitation in porous media at micro-scale. In Henk Jonkers, Jacco Booster, Leon van Paassen & Mark van Loosdrecht (Eds.), BGCE 2008, 1st International conference BioGeoCivel Engineering, 23-25 June 2008, The Netherlands (pp. 45-50). Delft: TU Delft en Deltares.

Van Paassen, LA, Daza, CM, Staal, MJ, Sorokin, DY & Loosdrecht, MCM van (2008). In situ soil reinforcement by microbial denitrification. In Henk Jonkers, Jacco Booster, Leon van Paassen & Mark van Loosdrecht (Eds.), BGCE 2008, 1st International conference BioGeoCivel Engineering, 23-25 June 2008, The Netherlands (pp. 124-133). Delft: TU Delft en Deltares.

Van Paassen, LA, Loosdrecht, MCM van, Eijnden, AP van den, Mulder, A, Verwaal, W, Ngan-Tillard, DJM, Harkes, MP & Bekendam, RF (2008). Reinforcement of calcarenite room and pillar mines by microbially induced carbonate precipitation. In EuroEngeo 2008 (pp. 1-6). Madrid: Escuela de Ingenieria de Obras Publicas Madrid.

Patents

Paassen, LA van, C. M. Daza, M. C. M. Van Loosdrecht, R. Kleerebezem, W. Van der Star, and W. Van der Zon. (2008). Microbially induced carbonate precipitation as ground improvement technique, patent applicant: Stichting Deltares, EP1798284-A1 (8 October 2008); WO2007069884-A1 (9 October 2008).

Paassen, L. A. van, V. S. Whiffin, and M. P. Harkes. (2007). Immobilization of bacteria to a geological material, patent applicant: Stichting Deltares, EP1798284-A1 (20 Jun 2007); WO2007069884-A1 (21 Jun 2007); EP1974031-A1 (01 Oct 2008).

Other results

Van Paassen, LA, Harkes, MP, Van der Linden, TJM & Dura H (2009), "Hoe komt dit zandsteen zo stevig?", in *HoeZo!* (dutch television science quiz), aflevering 7 (11 august 2009), seizoen 2009, www.teleac.nl/hoezo

Van Paassen, LA & Kleerebezem, R (2007). Imagine schoolproject finalists 2006-2007: Verest, T, Meer, S van der, Schepers, I, Penterman, R, Rijkers, E "Dijken bouwen met bacteriën voor Bam in Afrika - slimme grond maakt dijk sterker".

www.watisgenomics.nl/genomics/genomics/milieu.html   Author: Maartje   de Gruyter

Van Paassen, LA (2008, 8 January) Radio interview for Microbe World radio (www.microbeworld.org/look/radio.aspx)

Van Paassen, LA (2009) 9 prikkelende en intrigerende kwesties (7 jan; 26 mei, 2,3,4,6 jul, 3 aug, 21 okt, 19 nov) *NWT Scheurkalender 2009*

Van der Star, WRL, Van Paassen, LA, Molendijk, WO & Van Loosdrecht, MCM, (2008) From sand to sandstone, using waste as cement, Winner BBasic Leo Petrus Innovation Trophy 2008 (100 k€ research funding)

Van Paassen, LA & Van der Star, WRL. Interview by AA van de Graaf. Prijswinnend idee: innovatieve zandfixatie, in *Civiele techniek*, volume 63, issue 5/6, p27-28

Van Paassen, LA, Lambert, J, Hamer D den, (2008) Bacteriën zijn veelzijdige bouwers in de bodem, *Land+Water*, volume 48, issue 12, p20-21